

R-06-39

Geological characteristics of deformation zones and a strategy for their detection in a repository

John Cosgrove, Imperial College of Science and Technology London

Roy Stanfors, RS Consulting

Kennert Röshoff, BergByggKonsult AB

September 2006

Svensk Kärnbränslehantering AB

Swedish Nuclear Fuel
and Waste Management Co
Box 5864
SE-102 40 Stockholm Sweden
Tel 08-459 84 00
+46 8 459 84 00
Fax 08-661 57 19
+46 8 661 57 19



ISSN 1402-3091

SKB Rapport R-06-39

Geological characteristics of deformation zones and a strategy for their detection in a repository

John Cosgrove, Imperial College of Science and
Technology London

Roy Stanfors, RS Consulting

Kennert Röshoff, BergByggKonsult AB

September 2006

Keywords: Post-glacial faulting, Deformation zone, Fracture reactivation, Repository integrity.

This report concerns a study which was conducted for SKB. The conclusions and viewpoints presented in the report are those of the authors and do not necessarily coincide with those of the client.

A pdf version of this document can be downloaded from www.skb.se

Summary

Field observations in parts of the Scandinavian Precambrian shield show that some large faults have been seismically active since the last glaciation and this activity is thought to be the result of the retreat of the ice cap. The question therefore arises as to whether during subsequent glaciations, glacially stimulated seismicity might cause displacements along fractures and other planar and sub-planar zones of weakness (known collectively as deformation zones) cutting a repository site, and if so, whether these displacements represent a threat to the integrity of the repository.

Repository design is such that movements of up to 10 cm on such deformation zones can be tolerated and the task is therefore to identify any deformation zone within the repository site along which there is a possibility of movement greater than 10 cm occurring. The established relationship between the length of a deformation zone and the maximum displacement that can occur along it is such that only zones longer than ~ 50 m need to be identified.

This report, in conjunction with the companion report /Munier 2006/, addresses the problem of identifying deformation zones longer than 50 m within a proposed repository site using the data provided by surface and tunnel mapping, borehole analysis and other geophysical techniques. In order to achieve this objective three tasks have been identified. These are 1) to summarise the current state of knowledge on the geological characteristics of deformation zones in the size range $50 \text{ m} < r < 250 \text{ m}$. 2) to propose suitable investigation methods for identifying and localising deformation zones in tunnels and boreholes and to give examples of their application and 3) to examine the extent of the intersection of these zones with the repository tunnels and deposition holes, specifically to determine whether the structure intersects the full perimeter of the hole, and to use the Full Perimeter Intersection (FPI) criterion to quantify the chances of a repository tunnel or deposition hole being intersected by a deformation zone in the size range $50 \text{ m} < r < 250 \text{ m}$. This quantification is achieved by DFN numerical modelling. The present report presents the results of the first two studies and involves a detailed discussion of the theories that relate to the formation of deformation zones and of the second order features that are associated with them and of the parameters that can be used to indicate their length (e.g. aperture, displacement, width, conductivity etc). This is followed by a discussion of the available methods for determining the location, orientation and length of deformation zones during the various stages in the construction of the repository. Specific examples of the use of some of these methods for the detection and characterisation of deformation zones at Aspö are also described.

The procedures and methodologies described in this report can then be used to provide the best available site specific 3D geological data base, which is focused on describing the size, type, orientation, location etc of deformation zones within a proposed repository site. These data provide the input for the DFN modelling (presented in an accompanying report /Munier 2006/ that can be used to quantify the probability of a deposition tunnel or deposition hole being intersected by a deformation zone in the size range $50 \text{ m} < r < 250 \text{ m}$.

Abstract

Evidence of post-glacial faulting and associated seismic activity in the Scandinavian shield has lead to an investigation of the potential impact such seismicity might have on the stability of deformation zones (fractures, fracture zones, shear zones i.e. any planar or sub-planar zone of weakness along which slip might occur) cutting a potential repository site.

Slip on such deformation zones in excess of 10 cm threatens the integrity of the repository and slip of this magnitude can occur on zones greater than 50 m in length. It is therefore essential to identify zones longer than this i.e. along which such slip magnitudes can occur. In this report the current understanding on the parameters that control the formation of the various types of deformation are reviewed and the parameters that can be used to indicate their length identified. A methodology is proposed for detecting these zones at different stages of the construction of the repository. The 3D geological model established during the construction can then be used to provide the input data for the numerical modelling of the site (discussed in a companion report /Munier 2006/) and the quantification of the probability that a deformation zone will cut a repository tunnel or deposition hole.

Contents

1	Introduction	9
1.1	Background	9
1.2	Objective	10
1.3	Structure of this report	11
1.4	Terminology	11
1.5	Acknowledgements	14
2	The identification of deformation zones larger than $r = 50$ m in tunnels and deposition holes	15
2.1	Introduction	15
2.2	Missing data	16
2.3	Stress and fracturing	18
2.3.1	Stress state in the Earth's crust	18
2.3.2	Brittle failure; the formation of joints and faults	18
2.3.3	Factors that can modify the regional stress field	20
2.3.4	The effect of pre-existing fractures on stress orientation	20
2.3.5	Residual stress	20
2.3.6	Conclusions	23
2.4	Extensional and shear fractures	23
2.4.1	Types of fractures	23
2.4.2	Extensional fractures	23
2.4.3	Shear fractures	28
2.4.4	Fibrous minerals and other second-order structures	29
2.4.5	Conclusions	30
2.5	Discrete and diffuse fractures and brittle deformation zones	30
2.5.1	Detailed fracture geometry	30
2.5.2	Factors determining fracture geometry	32
2.5.3	Evolution of fault zones	36
2.5.4	The brittle – ductile transition	39
2.5.5	The concept of the integrity of fractures and fracture size	40
2.5.6	Conclusions	43
2.6	Small scale processes linked to fracturing and the process of fracture propagation	43
2.6.1	Small-scale processes linked to fracturing	43
2.6.2	The process of fracture propagation	46
2.6.3	The influence of fault linkage on the displacement profile of a fracture	56
2.6.4	Conclusions	56
2.7	Spacing distribution and the evolution of fracture sets and networks	56
2.7.1	Fracture spacing	56
2.7.2	Distribution laws of fracture spacing	59
2.7.3	Experimental study of fracture spacing	59
2.7.4	Clustering versus uniform distribution of fractures	61
2.7.5	Conclusions	64
2.8	Frequency/size distribution patterns – issues of scale dependency and self similarity	64
2.8.1	Range of fracture size	64
2.8.2	Regional studies of fracture length/frequency	65
2.8.3	Fracture length/frequency plots from numerical models	66
2.8.4	Direct observations of critical fractures in the study areas	69
2.8.5	Conclusions	70

2.9	Second-order structures linked to larger fractures – kinematic indicators	71
2.9.1	Second order structures	71
2.9.2	Kinematic indicators	71
2.9.3	Conclusions	77
2.10	Conductivity	77
2.10.1	Impact of fracture geometry on conductivity	78
2.10.2	Variation of fracture conductivity over geological time	79
2.10.3	Fracture continuity, connectivity and conductivity	79
2.10.4	Influence of current stress regime on fracture conductivity	83
2.10.5	Conclusions	83
2.11	Site specific data	87
2.11.1	Geological setting of the shield	87
2.11.2	Process of glacial loading	87
2.11.3	Dynamic versus static glacial loading model	89
2.11.4	Conclusions	89
2.12	Discussion and conclusions	89
2.12.1	The significance of conductivity as an indicator of fracture length	90
2.12.2	General versus site specific studies	90
2.12.3	Fracture thickness and displacement	91
2.12.4	Further constraints on critical fractures	93
2.12.5	Other techniques for determining the size of a critical structure	94
2.12.6	Identification of deformation zones using two or more boreholes	94
2.12.7	Conclusions	95
3	Investigation methods for the detection of deformation zones	97
3.1	Introduction	97
3.2	Sources of information	98
3.3	Strategies for investigations	99
3.3.1	Correlation and identification of deformation zones	101
3.3.2	Implementation and training	101
3.3.3	Investigations of a deposition area	104
3.3.4	Investigations for the positioning of the deposition tunnels	104
3.3.5	Investigations for the placement of the deposition holes	105
3.3.6	Acceptance of deposition holes	106
3.4	Overview of available methods	107
3.4.1	Tunnel mapping	108
3.4.2	Borehole methods	109
3.4.3	The use of geophysical techniques in tunnels	111
3.5	The recognition of deformation zones in boreholes and tunnels – case studies from Äspö	114
3.6	Modelling updates	116
3.7	Discussion and summary	118
3.7.1	The learning and application process	118
3.7.2	Risk evaluation	119
3.8	Conclusions	120
4	Method for the detection of minor deformation zones using new characterization data	125
4.1	Introduction	125
4.2	Field investigations	125
4.3	Conclusions	131
5	Summary and conclusions	133
5.1	Project Findings	134
5.1.1	Geological indicators of deformation zone (fracture) size	134
5.1.2	Experience from the SKB sites	134
5.1.3	Suitable investigation methods	135
5.2	Implications for the site characterisation programme	136

5.3	Quantification of the probability of missing a critical deformation zone in a deposition hole	137
6	References	139
Appendix A1	Example of minor deformation zone characteristics from Äspö HRL and their cross correlation between boreholes and tunnels	145
Appendix A2	Identification of minor deformation zones by the analysis of borehole data including radar images	155

1 Introduction

1.1 Background

The observed displacement of glacially striated surfaces along large-scale fractures in the Fennoscandian Shield confirms that post-glacial reactivation of large fault zones or smaller planar zones of weakness has occurred. One of the most impressive examples is provided by the Pärvie fault (Figure 1-1) which can be traced for 200 km along strike. The fault has a maximum offset of around 10 m. From the point of view of the potential for post-glacial faulting to reactivate other fractures it is important to establish whether this displacement occurred as one major movement event associated with a major earthquake or in numerous, small increments linked to creep and the minimal release of seismic energy. /Lagerbäck 1991, Mörner 1996, 2004, Mörner et al. 2000/ all argue that the spatial association of known post-glacial faults with extensive liquefaction of fine grained glacial varve deposits, demonstrates that fault movement was seismic. This conclusion is further supported by /Arvidsson 1996/ who points out a strong correlation between the spatial distribution of recent seismicity and the post-glacial faults.

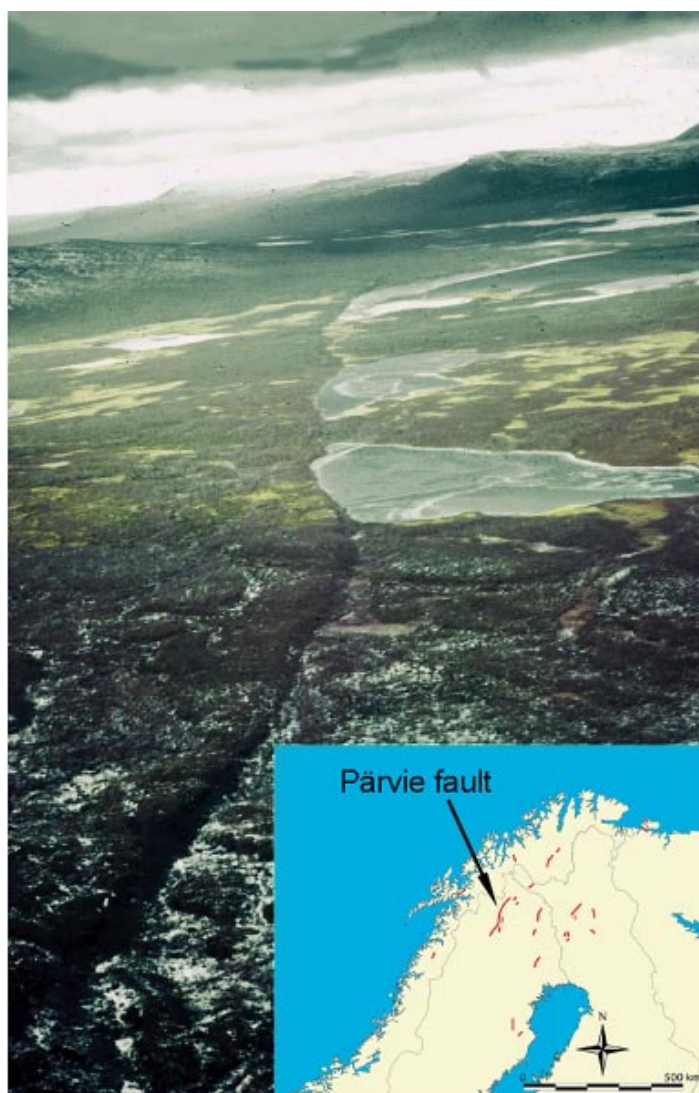


Figure 1-1. An oblique aerial view of the Pärvie Fault, looking NE offsetting the smooth, glaciated, Quaternary surface. /From Munier and Hökmark 2004/.

Although the Fennoscandian Shield is currently one of the most tectonically stable areas in the world, there remains the possibility of earthquakes linked to the reactivation of large planar zones of weakness as a result of the present day geological stress regime or modifications to it linked to the advance and retreat of future glaciers. Consequently a worst case scenario must be assumed, namely that glacially stimulated faulting can occur seismically. Thus the possibility of these earthquakes causing sufficient movement along fractures which intersect a deposition hole to jeopardise the integrity of the canister needs to be considered.

Attempts have been made to quantify the effect of earthquakes linked to the stress release due to slip on large fault zones, on smaller, pre-existing fractures in the vicinity of an excavation, either directly by geological field work or by the use of numerical modelling. /La Pointe et al. 1997, 2000, 2002, La Pointe and Caldouhos 1999/. Further studies of this problem /Munier and Hökmark 2004/, and references there in have demonstrated that the maximum displacement that can occur along a fault is related directly to its length. On the basis of this study and by using the canister/buffer failure criteria proposed in /Börgesson et al. 2003/, it was concluded that only fractures with a radius greater than 50 m can experience sufficient slip (i.e. > 10 cm) to constitute a hazard to the integrity of the canisters. The probability of a deposition hole to be intersected by a potentially damaging fracture can be calculated by a method developed by /Hedin 2005/.

It is assumed that the large-scale fracture zones, along which earthquakes can be generated, (see e.g. Figure 1-1, will be identified during the site investigations. Their presence is therefore taken into account in the planning and positioning of repository areas. The same cannot be said for most of the smaller scale fractures. Consequently it will be necessary to identify fractures greater than this **critical** radius during the construction of a repository to ensure that deposition holes are positioned so that they are not adversely affected by any fracture reactivation. The challenge is to identify these fractures during excavation by both the direct observation and the recognition of specific geometric and geological fracture characteristics within the tunnel or deposition hole, or remotely, using geophysical and other techniques.

1.2 Objective

The overall objective of the EXPECT project is:

To quantitatively estimate the likelihood of a deformation zone in the size range $50\text{ m} < r < 250\text{ m}$ intersecting a deposition tunnel or deposition hole, where r is the radius of the zone.

In an attempt to achieve this objective three tasks have been identified namely:

- To summarize the current state of knowledge on geological characteristics of deformation zones in the size range $50\text{ m} < r < 250\text{ m}$.
- To propose suitable investigation methods for identifying and localizing deformation zones in tunnels and boreholes and to give examples of their application. (The scope of work should mainly encompass investigative methods known to and used by SKB.)
- To examine the extent of the intersection of these zones with the repository tunnels and deposition holes, specifically to determine whether the zones intersect the full perimeter of the hole and to use the Full Perimeter Intersection (FPI) criterion to quantify the chances of a repository tunnel or deposition hole being intersected by a deformation zone in the size range $50\text{ m} < r < 250\text{ m}$. This quantification is achieved by DFN numerical modelling.

The present report presents the results of work carried out on the first two tasks. These are essentially qualitative studies which compliment the third task which is a quantitative numerical modelling of the problem and which enables statistical predictions to be made relating to the intersection of deformation zones and the repository tunnels. The results of this study are presented in an accompanying report /Munier 2006/.

The present report represents the first step in the learning procedure for the site construction phase of a repository and is used to provide the best possible data base to provide the parameters needed for the numerical model. These data control and constrain the model and thereby reduce the uncertainties linked to its predictions.

1.3 Structure of this report

This report is a result of collaboration between members of a “project team” which included members from SKB, RS Consulting, JA Streamflow, Posiva OY, BergByggKonsult AB and Imperial College of Science and Technology, London. We point out that although each member had responsibility for individual chapters of this report, as clarified below, each major conclusion has been agreed upon within the team. The report, jointly edited by Raymond Munier and John Cosgrove, is structured as follows:

Chapter 1, the introduction to the report, presents the factors that prompted this study which sets out to determine how fractures above a critical length (radius > 50 m) can be detected in tunnels and boreholes.

This introductory chapter is followed by a synthesis of published literature on fracture development and morphology (Chapter 2, John Cosgrove) with the aim of seeking parameters that will characterize fracture size and of establishing whether these parameters can be used in tunnels and boreholes to identify fractures in the size range fracture radius $r = 50\text{--}250$ m.

Chapter 3 (Kennert Röshoff) focuses on the various techniques (tunnel and borehole mapping, geophysical techniques etc) that can be used to locate critical fractures in boreholes and tunnels and to determine their orientation and extent. The suitability of these techniques for detecting these fractures at various stages in the repository construction, from the initiation of the access tunnel to the excavation of the deposition holes, is assessed. After establishing a general strategy for fracture detection at all stages of construction, specific studies at Äspö on cross correlation between tunnels and boreholes and on the use of radar techniques to determine the extent of fractures located in boreholes are discussed (Roy Stanfors).

These studies are discussed further in the appendices where an attempt is made to define and quantify the relationship between fracture zone size, width, hydraulic conductivity and other properties with reference to fracture radii in the range 50–250 m. This work draws extensively on the mapping program and other studies carried out in and around the Äspö HRL.

In Chapter 4 (Roy Stanfors) a description is given of an investigation technique using LIDAR to detect minor fracture zones at the surface in the Laxemar study site. Their extension at depth is investigated using boreholes.

The summary and conclusions of the report are presented in Chapter 5.

1.4 Terminology

Terminology is a constant issue of controversy within the Earth sciences. As the Earth sciences encompass a large number of quite disparate disciplines, each with its own traditions and needs, it is naïve to expect any proposed terminology to be accepted by all parties. Nevertheless, being a multidisciplinary organisation, SKB has been required to synchronise its terminology to ensure coherent reporting and to promote understanding. In addition, work has begun to synchronise the terminology of some critical topics between SKB and Posiva, in an attempt to facilitate international collaboration.

Key references that have gained general acceptance within SKB are used in an attempt to ensure a consistent use of terminology. For example, the terminology outlined in /Strähle 2001/ is used for issues related to mapping of outcrops and boreholes and a terminology regarding geological modelling is given in /Munier et al. 2003/. DFN modelling requires its own terminology which is outlined in /Munier 2004/.

The focus of this study is to detect any approximately planar zone of weakness greater than a critical size (radius $r = 50$ m) as there is the possibility that seismically stimulated movement along these zones, linked to glacially stimulated faulting, might damage a canister if it intersects the deposition hole. These planar zones of weakness are often fractures or fracture zones but can be ductile shear zones along which continuity has not been lost and which are therefore not fractures. Nevertheless they may be reactivated in a brittle manner by seismicity linked to glacially induced faulting.

There is a complete spectrum of behaviour observed in rock between totally brittle and totally ductile deformation. Brittle deformation is defined as any deformation that results in the loss of continuity of a material and ductile deformation as any deformation that does not involve any loss of continuity.

One of the characteristics of brittle deformation is that it is highly localised affecting a very small proportion of the material and leaving the majority of the material between adjacent fractures, unstrained. Strain localization decreases as the deformation becomes progressively more ductile and in the extreme case of homogeneous flattening, the ductile deformation is perfectly uniformly distributed throughout the material. Between these two end member deformation states lies a large range of structures which although ductile (i.e. do not represent a loss of continuity in the material) do represent planar zones of intense deformation along which an important planar fabric develops. This process is illustrated Figure 2-48 and discussed in the associated text. Such structures fall under the general heading of ductile deformation zones and there are two main mechanisms by which these structures can form. The first is that they can form in the same way as a shear fracture. These zones are the expression of shear failure in rocks that are in a higher temperature and pressure environment than that in which brittle shear fractures form but they have the same conjugate relationship to their formative stress field as do their brittle equivalents. The maximum principal compression bisects the acute angle between them and the minimum principal compression the obtuse angle. The transition from discrete, brittle shear fractures through brittle deformation zones and ductile deformation zones to a state of homogeneous flattening is shown in Figure 1-2 (upper part). The second mechanism by which ductile shear zones can form is summarised in Figure 1-2 (lower part) which shows a large suit of structures that can form in an anisotropic material depending upon the orientation of the applied stress with respect to the material anisotropy and on the intensity of the anisotropy. Of particular interest to the present discussion are the structures illustrated in Figure 1-2(ii) d, e, h and i. These planar zones would appear as ductile deformation zones in the rock.

The importance of the various types of ductile shear zones in this discussion lies in the fact that although they do not represent fractures as continuity is maintained across them, they do however represent planar zones of weakness which are likely to slip if subjected to a suitably oriented later stress field. As such they must be considered in the current study which relates to the detection of any planar feature along which slip of a critical magnitude (10 cm) might occur in response to a seismic event on a nearby fault.

Thus a general term is needed to include all planar features that might be reactivated by glacial faulting.

A possible term is deformation zone. This has been defined by /Munier et al. 2003/ as follows.

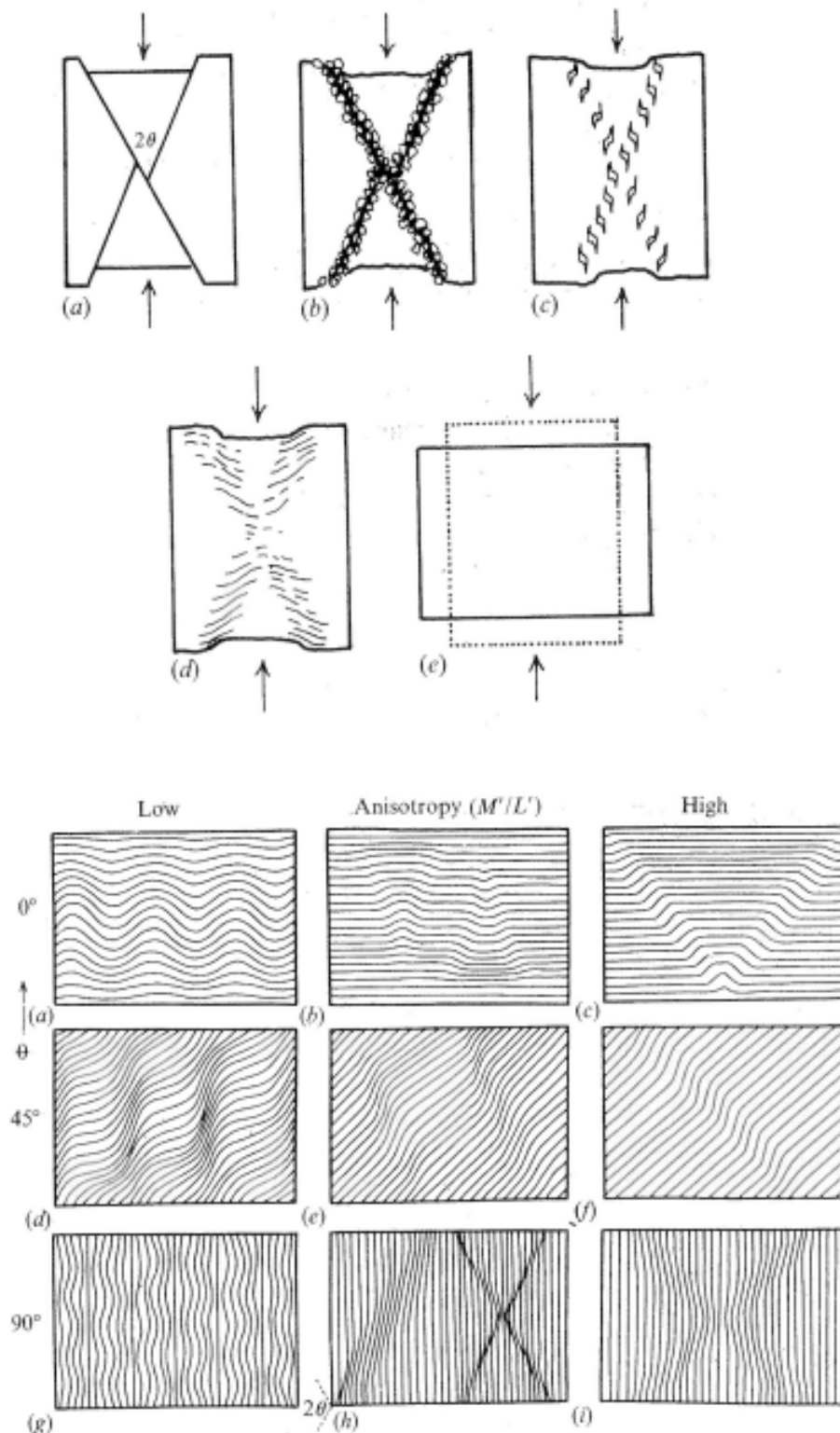


Figure 1-2. Upper diagram shows a) Single brittle fractures, b) and c) brittle deformation zones and d) ductile deformation zones, all expressions of Andersonian shear failure. e) Homogeneous flattening /from Price and Cosgrove 1990/. Lower diagram shows some possible modes of deformation in materials with different intensities of anisotropy (M/L) with the anisotropy inclined at different angles (θ) to the maximum principal compression which is acting in a horizontal direction /from Cosgrove 1976/.

“The term *deformation zone* is used to designate an essentially 2-dimensional structure (a sub-planar structure with a small thickness relative to its lateral extent) in which deformation has been concentrated (or is being concentrated, in the case of active faults). If there is sufficient geological information, deformation zones can be further qualified as brittle, ductile or composite. The term *composite* is applied to deformation zones which show evidence of both brittle and ductile deformation. Composite deformation zones commonly show evidence of *brittle reactivation*, i.e. brittle deformation of a zone already deformed in a ductile manner. The commonly used term “fracture zone” can be used to denote a *brittle deformation zone* or the *brittle part* of a composite deformation zone. The commonly used term “ductile shear zone” can be used to denote a *ductile deformation zone* or the *ductile part* of the composite deformation zone...”

In the Äspö project the following definitions concerning brittle structures were applied during preliminary investigations and tunnel documentation /Bäckblom 1989/. Current terminology /Andersson et al. 2000/ is used in pre-investigations at Laxemar, in brackets below.

Major fracture zone

The term “major fracture zone” was used for a feature > 5 m thick and extending for more than c 1,000 m, with the characteristics that the intensity of natural fractures is at least twice as high as for the surrounding rock. Completely disintegrated and/or chemically altered rock is included in the definition of a fracture zone as well as any kinematic marker. (Regional deformation zone and local major deformation zone according to current terminology at Laxemar).

Minor fracture zone

The term “minor fracture zone” was used for a feature < 5 m thick and extending for c 100–1,000 m. (Local minor zone according to current terminology at Laxemar).

Single open fracture

Persistent, several metres (10–100 m) long fractures, less than 0.1 m thick, mostly steep and estimated to be significant hydraulic conductors were called “single open fractures”. (Local minor zone – except for discrete fracture – according to current terminology at Laxemar).

Thus, in this report, “deformation zone” is the term used to encompass joints and faults (i.e. fractures), fault zones and ductile shear zones i.e. all structures that impose a potential hazard to the integrity of the canister should they reactivate.

1.5 Acknowledgements

The authors would like to thank the members of the EXPECT reference group, A.G. Milnes, O. Olsson, M. Stephens and A. Winberg, for their rigorous and constructive reviews. These have been most valuable and have had a significant impact on the structure and content of the report. Johan Andersson of JAStreamflow is also thanked for his contribution to the conclusions of this report.

2 The identification of deformation zones larger than $r = 50$ m in tunnels and deposition holes

2.1 Introduction

The aim of this chapter is to attempt to identify some characteristic feature or features of a “deformation zone” that can be used to determine whether or not it is equal to or greater than a critical size, (radius > 50 m) and that can be recognised in a tunnel, deposition hole or borehole during excavation.

Before attempting to identify such features it is important to recognise that, as discussed in Chapter 1, the term “deformation zone” used in the above statement includes a variety of structures which have fundamentally different modes of origin. The term embraces any planar or sub-planar feature along which slip of a critical magnitude (10 cm) might occur in response to a seismic event on a nearby fault. These will include:

- Discrete shear fractures (faults).
- Discrete extensional fractures (joints).
- Brittle deformation zones which include fracture zones of both types of fractures.
- Ductile deformation zones often referred to in the literature as “ductile shear zones”.

It is therefore naive to expect there to be a single, second-order feature characteristic of them all. They are more likely to have different features associated with them. In addition, as discussed later in this report, the geometry of any critical structure and the presence or absence of any second-order structures can be markedly influenced by a number of parameters including:

- Rock type.
- Temperature at the time of formation.
- Rate of structure propagation (i.e. strain rate).
- Magnitude of the differential stress.

Unless the concepts outlined above are clearly understood the challenging question of how to identify “critical structures” from the limited data available from tunnels and boreholes, cannot be rigorously addressed.

In order to achieve the overall aim of this work, it is necessary to consider a number of topics, concepts and processes that impact on the geometry, distribution and spatial organisation of fractures, which are the major components of the majority of “critical structures”. These include:

- The link between stress and fracturing (i.e. the link between fracture type, orientation, regularity etc and stress).
- The types of fractures (extensional and shear).
- The relationship between discrete fractures, diffuse fractures and fracture zones.
- The small-scale processes linked to fracturing (e.g. process zone development).
- Fracture propagation and linkage.
- The evolution of fracture sets (the concepts of under saturation, saturation and super saturation).
- Work on fracture distribution (on one scale, i.e. controls on fracture clustering).

- Fracture distribution (across all scales, i.e. fracture frequency/size distribution, scale dependency and self similarity).
- Second-order structures linked to larger fractures (kinematic indicators).

Such a study needs to draw on the literature and understanding from a number of disciplines that relate to fracture development in rocks including:

- Structural Geology.
- Tectonics.
- Rock Mechanics.
- Fracture Mechanics.
- Engineering Geology.
- Fracture mineralogy.
- Hydrology.
- Hydrocarbon Geology.

The hydrocarbon industry have decades of experience in obtaining information about fractures including their geometry, orientation, frequency, length, aperture, distribution, conductivity etc from boreholes using cores, borehole scans and a variety of geophysical investigative techniques. Of particular concern to the industry is the conductivity of individual fractures, fracture sets and of the total fracture network that characterises the rock mass. We are faced with a similar problem, i.e. that of determining the likely geometric properties of fractures from large, long boreholes (tunnels), shorter, narrower boreholes (deposition holes) and conventional boreholes, and it is therefore appropriate to exploit this corpus of work to establish what techniques are available to determine fracture length from the limited data available.

It is relevant to note that the geological setting of oil exploration is usually within bedded sedimentary successions whereas the geological setting of the potential SKB repository sites is in the crystalline rocks of the Fennoscandian Shield. Clearly the organization, distribution and continuity of the various fracture sets in these two different settings are likely to be very different. Nevertheless the techniques developed by the hydrocarbon industry to obtain information about fractures from boreholes is relevant regardless of the geological terrain being investigated.

2.2 Missing data

The principal task being addressed by the present study is that of establishing a methodology for the detection of critical structures from their outcrops in tunnels, and deposition holes. An important part of such a study is to establish the range of fracture sizes that characterize the two study areas of Oskarshamn and Forsmark. These data have been collected for these areas using:

- Outcrop data of individual fractures.
- Interpretation of lineaments from the site scale.
- Intersections of fractures in cored and un-cored boreholes.

There is a lack of data in the size range of some 10s of metres to 100s of metres as can be seen from Figure 2-1. This range contains the critical fractures which are the focus of the present study and it is therefore important to establish their likely density in the study areas.

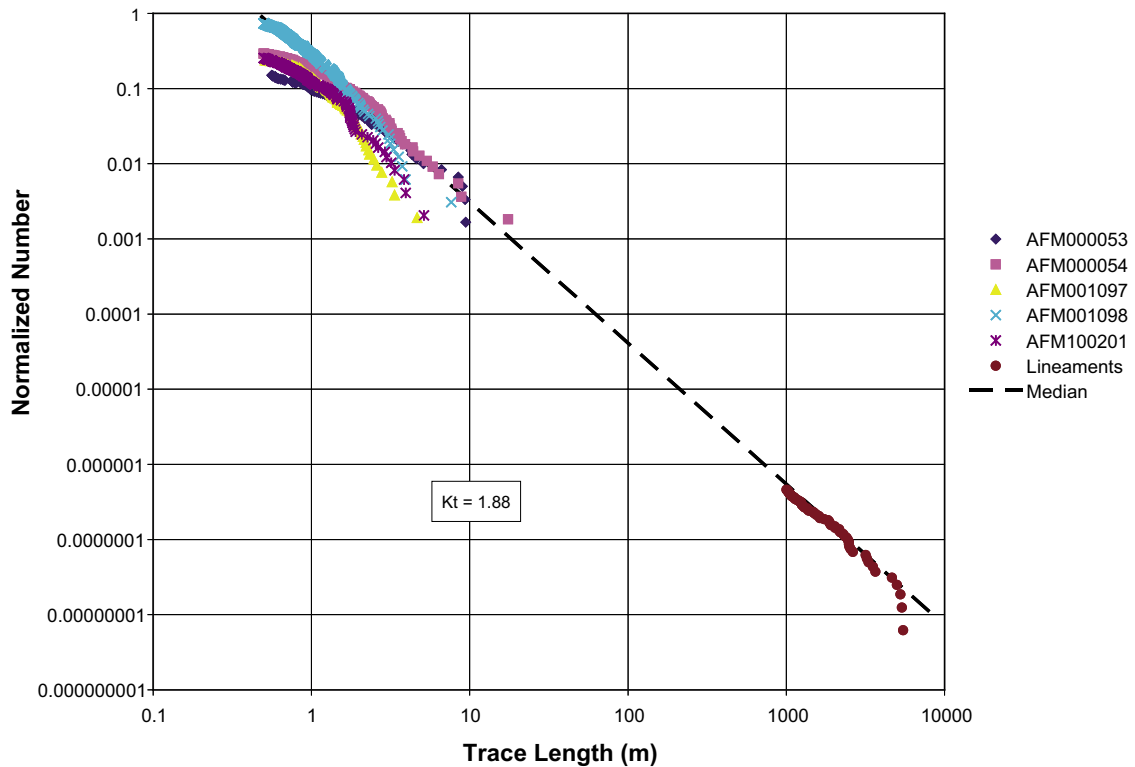


Figure 2-1. Normalized number against trace length of fractures from the Forsmark area. A gap in the data covering fractures from 10s to 1,000 m occurs reflecting the limited outcrop of the region /from La Pointe et al. 2005, Figure 5-6/.

A likely reason for the missing data in Figure 2-1 relates to the size of typical outcrops in the study areas. These rarely exceed 50 m and put an upper limit on the size of structures that can be detected from field studies. A study of aerial and satellite images provides length data for deformation zone traces of a km length and over but little data are available for fractures in the range 10s to 100s of metres. Because these are the fractures that need to be detected during the construction of the repository it is important to establish whether these are missing from the study areas or whether their absence on the graph of Figure 2-1 simply reflects the limitations of outcrop.

There are several ways of achieving this. These include a study of the few outcrops larger than 50 m in the study area and the study of fracture length/frequency data from other regions where data collection is not hindered by lack of suitable sized outcrops. This problem is discussed further in Section 2.8.

Structure of this chapter

As noted earlier in this chapter, this report addresses several geological features, all referred to under the general term “deformation zone”. However, the focus of this chapter is on brittle deformational structures which are referred to as fractures. In the following section a brief review of the literature on the fracture development in rocks is presented with the aim of identifying features that might be used in determining their length from the limited outcrop available in tunnels and outcrops. The chapter is divided into a series of short sections. Sections 2.3 and 2.4 summarise the link between stress, fracture type and fracture orientation and in Section 2.5 the factors that control the expression of brittle failure are discussed. In Section 2.6 the small-scale processes linked to fracturing and the processes of fracture propagation are reviewed and in Section 2.7 the evolution of fracture sets and networks is described and the parameters

controlling fracture spacing distribution considered. Fracture frequency/size distribution patterns in the study areas and from other areas are examined in Section 2.8 and second-order structures linked to larger fractures are described in Section 2.9. The link between conductivity and fracture size is discussed in Section 2.10. In Section 2.11 site-specific data from two potential repository sites at Oskarshamn and Forsmark are examined. The conclusions drawn from these various considerations and their impacts on the problem of recognising critical deformation zones are outlined in the discussion Section 2.12.

2.3 Stress and fracturing

2.3.1 Stress state in the Earth's crust

The stress state in the crust is determined mainly by the vertical overburden stress and any tectonic stress resulting from plate tectonics. These latter stresses tend to be horizontal and may be compressive or extensional depending on the relative motion of the plates. The magnitude of the vertical and horizontal stresses (σ_v and σ_h) generated by the overburden are given by:

$$\sigma_v = z\rho g \quad \text{Equation 2-1}$$

$$\sigma_h = \frac{\sigma_v}{m-1} \quad \text{Equation 2-2}$$

where z is the depth, ρ is the average density of the overburden, g the acceleration due to gravity and m Poisson's number, the reciprocal of Poisson's ratio.

As discussed in the following section the type and orientation of fractures in the Earth's crust are determined by the magnitude and orientation of the stress field.

2.3.2 Brittle failure; the formation of joints and faults

Field observations show that two fundamentally different types of brittle failure occur in rocks. One is the result of shear failure and the other of extensional failure. Displacements on shear fractures are parallel to the fracture walls, and displacements on extensional fractures are normal to the fracture walls. The fractures are termed faults and joints respectively, Figure 2-2 and Figure 2-3.



Figure 2-2. An example of shear failure (faulting) from Northcote Mouth, Bude, England



Figure 2-3. Extensional failure (jointing) from Lilstock, SW England.

The theory of brittle failure considers these two types of fractures, and failure criteria have been developed for both. The Navier-Coulomb criterion of shear failure states that shear failure will occur along a plane in the material along which the shear stress (τ) has sufficient magnitude to overcome the cohesion (C) and the frictional resistance to sliding, i.e.

$$\tau = C + \mu\sigma \quad \text{Equation 2-3}$$

where μ is the coefficient of friction ($\mu = \tan \phi$ where ϕ is the angle of sliding friction) and σ is the normal stress acting across the plane. This criterion is shown graphically on the right hand side (i.e. the region where the normal stresses are compressive) of the graph in Figure 2-4. The criterion of extensional failure was developed by /Griffith 1925/ and is based on the concept that failure is initiated at the tips of suitably oriented micro-fractures within the material as a result of stress magnification in these localities. The criterion he derived can be expressed as:

$$\tau^2 + 4T\sigma - 4T = 0 \quad \text{Equation 2-4}$$

where T is the tensile strength of the material. This parabolic relationship is shown graphically on the left hand side (i.e. the region where the normal stresses are extensional) of the graph in Figure 2-4. The complete brittle failure criterion for both extensional and shear failure can be obtained by joining the two criteria at the point where their slopes are the same.

The intimate link between the orientation of the principal stresses and the two types of fracture planes is apparent from Figure 2-4, and this provides the basis for “fracture analysis” a technique used to determine the chronology and orientation of the various stress fields that have affected the rock over geological time. It can be seen from this figure that shear failure requires a large differential stress ($\sigma_1 - \sigma_3$) i.e. the diameter of the stress circle associated with shear failure is large and for extensional failure is small (less than $2C$ i.e. $\sim 4T$).

Because both types of fractures can be reactivated in shear by a seismic event it is important to be able to recognise critical length fractures of them both.

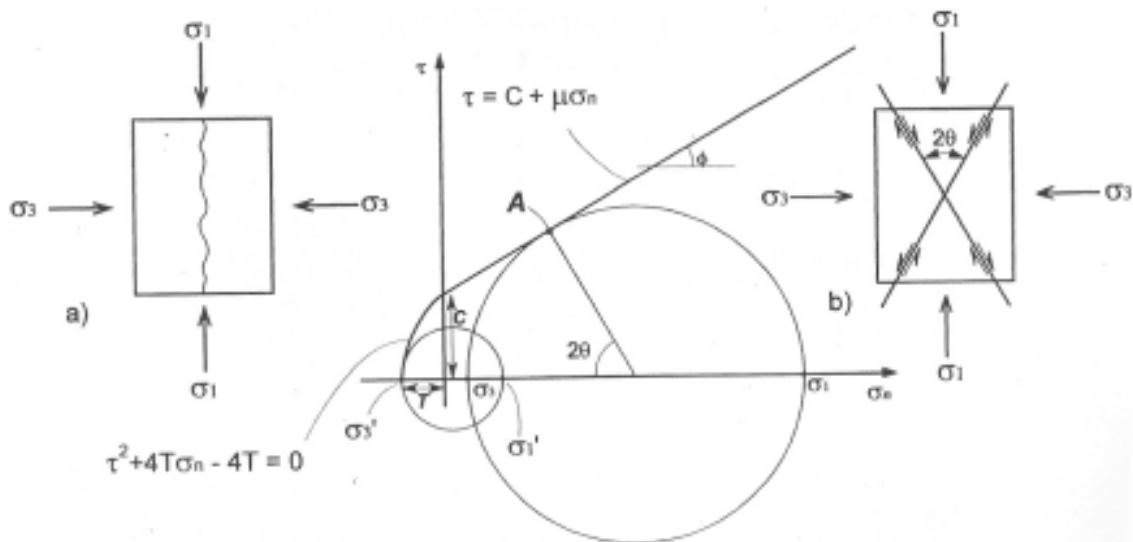


Figure 2-4. The graphical expression of the two brittle failure criteria and two stress states, represented as Mohr stress circles, capable of causing (a) extensional and (b) shear failure.

2.3.3 Factors that can modify the regional stress field

There are a variety of factors that can disturb the magnitude and orientation of the regional stress field generated by the combined effect of overburden and plate tectonics. These include the proximity of fractures, local changes in rock type and the existence of residual stress. Because of these effects local stresses can differ significantly from the regional stress field as discussed below.

2.3.4 The effect of pre-existing fractures on stress orientation

When an open fracture exists in a rock it impacts on the regional stress field. Because the fracture sides are free surfaces they cannot support a shear stress and consequently the stress field in the rock must reorient itself in the vicinity of the fracture so that the principal stresses are either parallel to or normal to the fracture. This deflection can be seen by its effect on subsequent fractures which will swing into an orientation either parallel to or normal to the fracture wall. This is shown on two scales in Figure 2-5. In the upper diagram a small-scale fracture to the SW of the coin, is rotated through an angle of $\sim 40^\circ$ as it approaches an early open fracture which is parallel to the upper and lower edges of the photograph, so that it intersects this fracture at 90° . Similarly as the fracture approaches the fracture on the left hand side of the photograph which is parallel to the edge of the image, a similar rotation occurs so that the fractures meet at 90° . It is apparent from this figure that the early fractures also act as barriers which prevent the propagation of later fractures. Thus an early set of fractures will tend to deflect and impede the propagation of later fractures. In Figure 2-5b a set of extensional, fractures in a Liassic carbonate bed at Lilstock on the Bristol Channel coast is shown, curving towards a large-scale normal fault situated behind the photographer.

2.3.5 Residual stress

The deflection of the regional stress field by fractures, discussed above, can occur on a large range of scales ranging from hand specimen size, Figure 2-5a, through intermediate scale, Figure 2-5b, to deflections that are apparent on satellite images. The fractures shown in Figure 2-5 are all extensional fractures developed in the Liassic limestones of the Bristol Channel, SW England. In addition to these macroscopic deflections of the stress field, when the stress state of a rock is examined on a grain scale, the concept of a regional uniform stress field

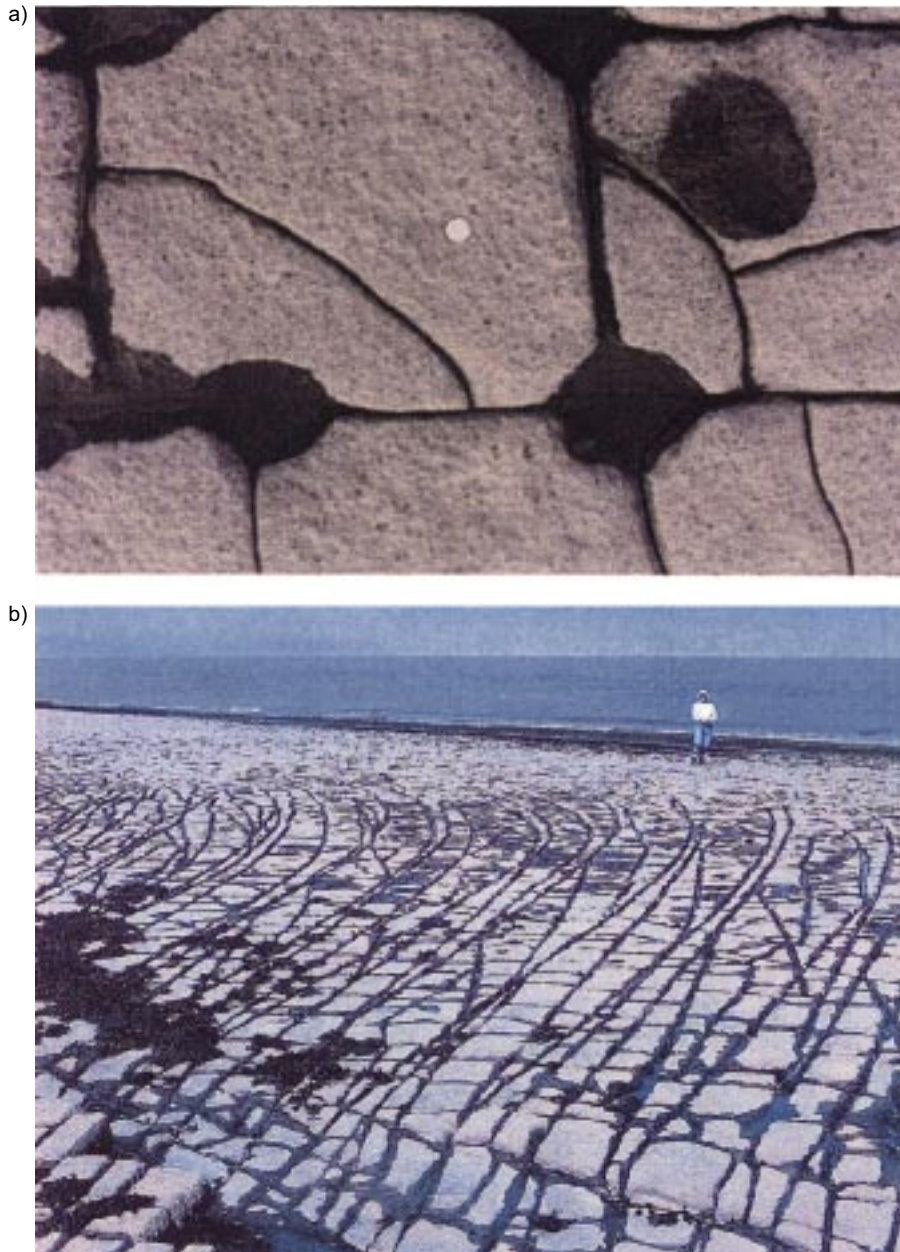


Figure 2-5. (a) The deflection of later fractures by early (horizontal and vertical) fractures. The change in stress orientation caused by the early open fracture is recorded by the curving of the later fractures as they approach and eventually cut the early fractures. See text for discussion. (b) Stress and fracture deflection on a larger-scale than in a). All the fractures shown are extensional fractures. Both images from Lilstock, Bristol Channel coast, SW England.

breaks down, Figure 2-6. The interaction of grains at their point contacts gives rise to a complex and heterogeneous distribution of stress. Cementation of a sediment subjected to an overburden stress results in the stress concentrations shown in Figure 2-6, being locked into the rock. These stresses will remain even when the rock is exhumed and the overburden and lateral confinement considerably reduced. These locked in stresses are termed residual stresses and they can result in the fracturing of rocks during exhumation. For example, within the Oskarshamn area, large, (i.e. critical in length) sub-horizontal exfoliation fractures occur in the upper 100–150 m of the crust and these are the result of the release of residual stresses. Exfoliation fractures are extensional fractures i.e. fractures which form normal to the least principal stress σ_3 . Near the Earth's surface σ_3 is vertical (at the surface it is zero) and consequently the resulting fractures are horizontal.

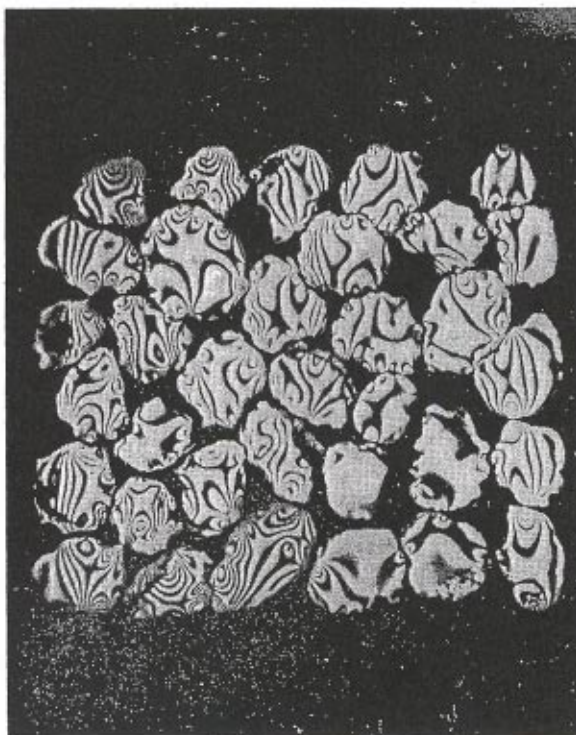
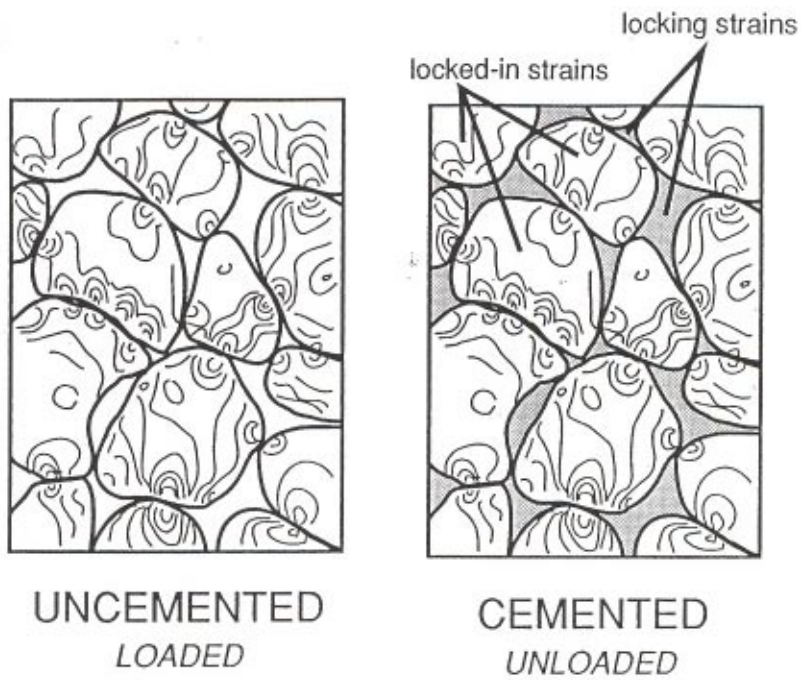


Figure 2-6. Upper diagrams show /Friedman's 1972/ grain-cement model for residual stress in a sandstone. Lower diagram shows the heterogeneous distribution of stress in a gelatine model of a granular material caused by point loading /from Price 1966/.

It should be pointed out that in addition to the formation of new, sub-horizontal fractures, the process of stress release can also lead to the reactivation of geologically ancient fractures, both gently and steeply dipping. Small block rotation linked to this process could lead to the reactivation of ancient, steeply dipping structures.

2.3.6 Conclusions

The fracture network in a rock reflects its stress history over geological time. Each episode of stress can result in the formation of a fracture set and the superposition of these sets leads to the fracture network that now characterizes the fractured rock mass. In an ancient shield area such as the Scandinavian (Fennoscandian) basement this network can contain numerous fracture sets.

It is clear from the above discussion that the orientation and type of fractures making up a fracture set will be determined by the orientation and magnitude of the causative stress field. In addition, early fractures will degrade later regional stress fields resulting in the associated fracture sets becoming progressively more deflected and less continuous.

This understanding of the processes involved in building up a fracture network provides an insight into the likely continuity of the various fracture sets within the rock and as discussed later in the report (Section 2.10) continuity has a major impact on conductivity, one of the key parameters available for the recognition of long fractures.

2.4 Extensional and shear fractures

2.4.1 Types of fractures

As noted in the previous section in the discussion of brittle failure there are two types of brittle fractures namely shear and extensional fractures. These modes of failure are fundamentally different each having a different failure criteria, a different orientation with respect to the principal stresses and a different sense of movement on them. It is therefore not surprising that some very different and characteristic features are found associated with these two types of fractures.

2.4.2 Extensional fractures

Figure 2-5b shows natural examples of extensional fractures forming a network of fractures cutting the Liassic limestone of the Bristol Channel coast in North Somerset, England. The network is made up of several sets of fractures each the result of a separate stress regime. They therefore record the evolution of stress over geological time and as discussed in Section 2.3 the later sets are affected by the earlier set with the result that they are more irregular and less continuous.

Because of the different modes of origin of shear fractures and extensional fractures the second order structures associated with them are different. Extensional fractures often display:

- Plumose structures, Figures 2-7 to 2-9.
- Fibrous minerals infilling these fractures at the time of their formation will grow with the fibres at right angles to the fracture wall, i.e. indicating opening of the fracture, Figure 2-10a.

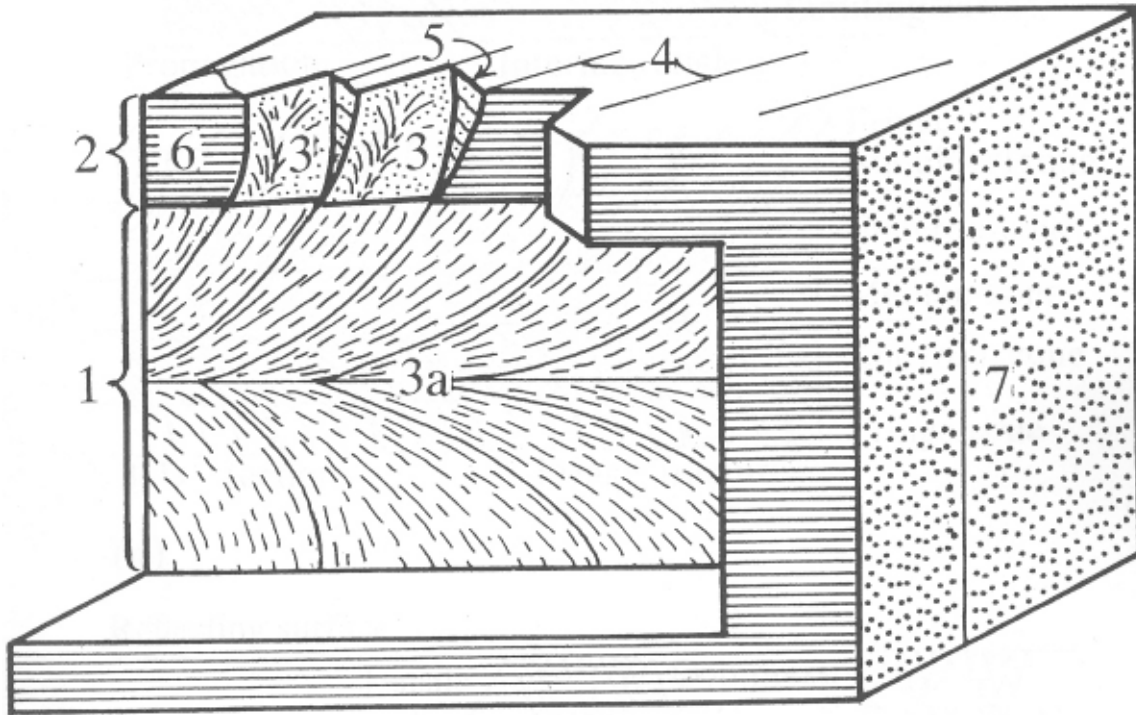


Figure 2-7. Block diagram showing details of surface features on a fracture plane. 1) Main surface, 2) Fringe, 3) Primary plumose or hackle structures, 3a) Secondary plumose structures, 4) En echelon fractures 5) Minor cross fractures joining members of 4, 6) shoulder and 7) Trace of main fracture face /from Hodgson 1961/.

The feather-like markings that constitute the plumose structures (Figures 2-7 to 2-9) can indicate the site of origin of the fracture, i.e. the point where the plumes converge, and concentric arrest lines (Figure 2-9) the position where the fracture propagation was temporarily arrested. In layered rocks the fractures are often layer-bound and have the geometry shown in Figure 2-7 and Figure 2-8. In more massive rocks the fractures approximate more to circular fractures as indicated in Figure 2-9. Because of the relatively unlayered nature of the Fennoscandian Shield, the fractures that develop in the crystalline basement rocks of the potential repository areas are assumed to be approximately circular.

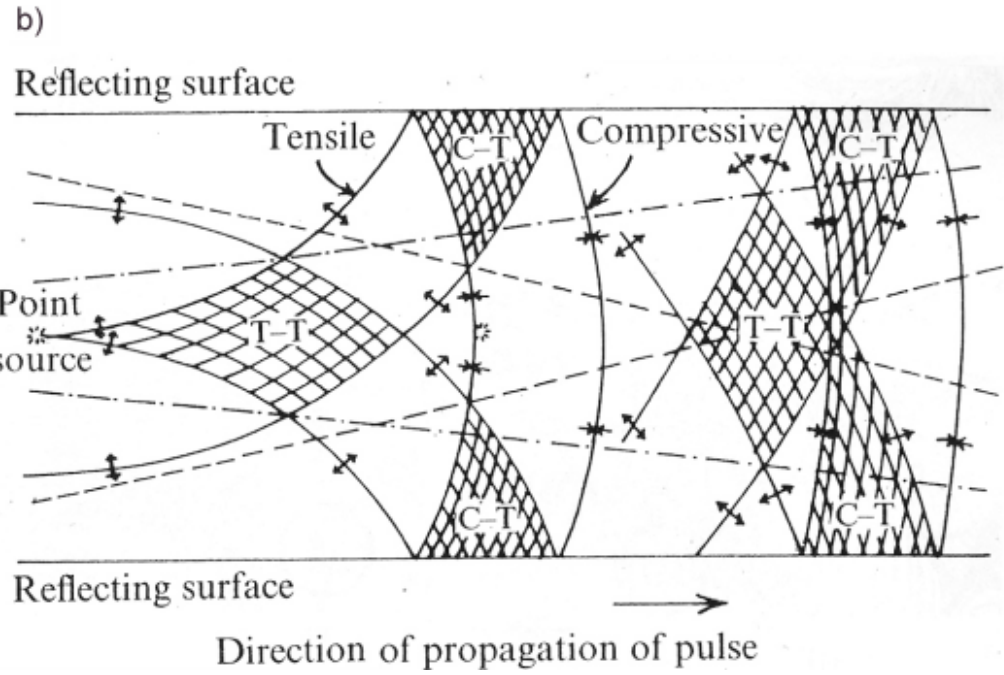
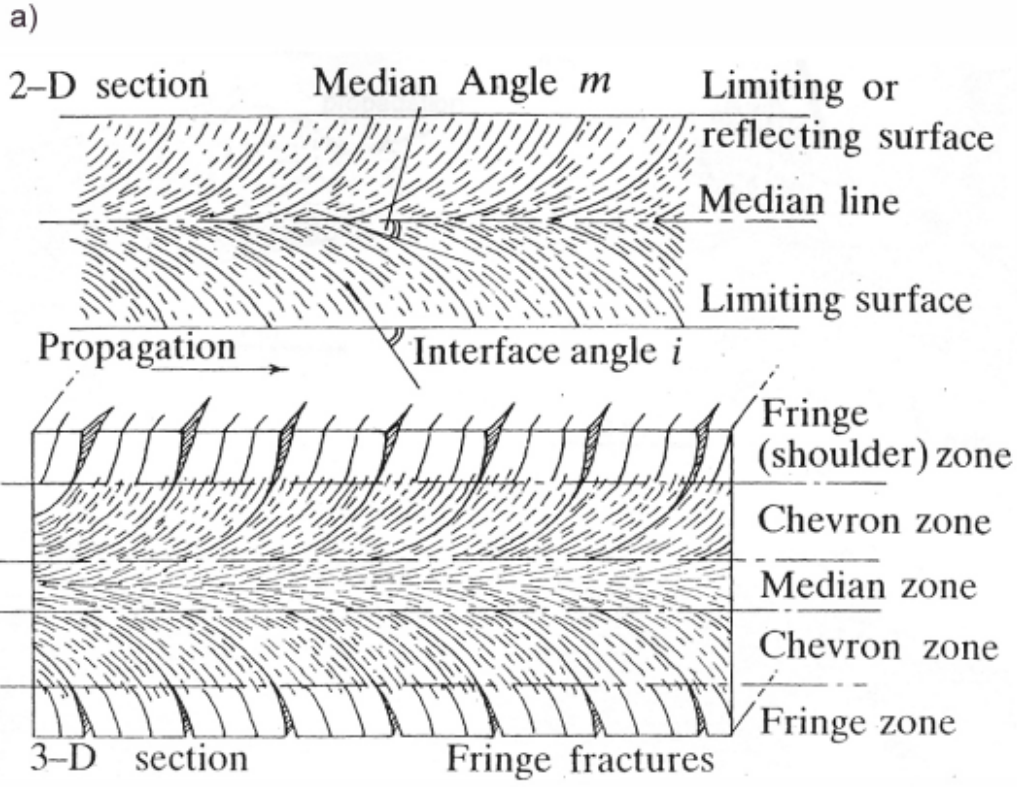


Figure 2-8. a) Hackle (or Chevron) mark geometries and descriptive terms. b) Illustrating a pulse mechanism of direct and reflecting elastic waves which interact to form hackle of plumose structures. The diagram represents the form of an advancing compressive pulse with reflected tensile pulses in its wake [from Gash 1971].

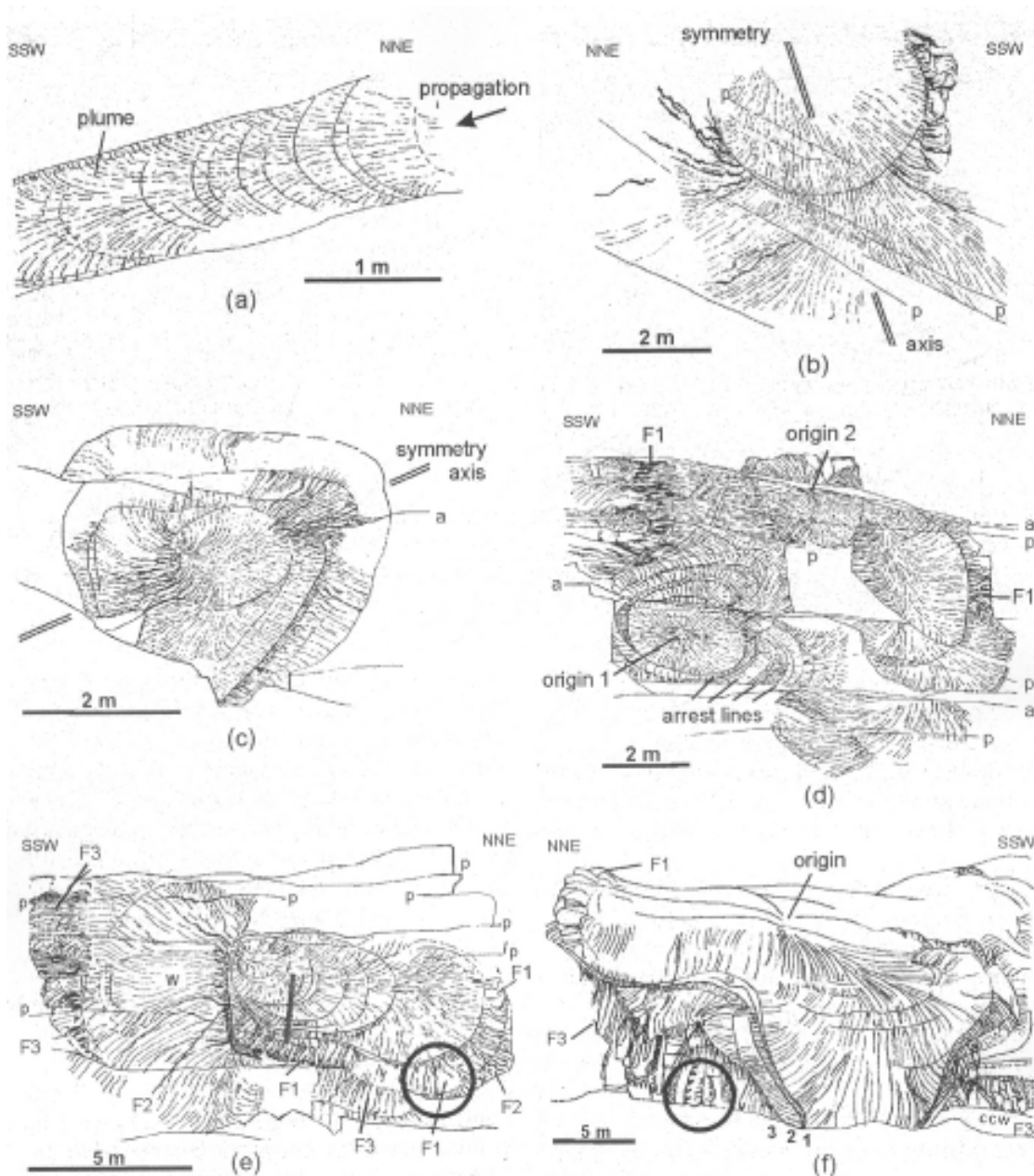


Figure 2-9. Joints in granite with disc-shaped fractures (size between 2 and 30 m) and undulations (rib marks). a) –c) Undulations covered with a plume. d) Two circular fractures that interacted during propagation to form a joint plume on the left-hand side. e) Fracture initiation started in the central circular fracture, then the joint propagated laterally, only to the right. After reaching fringe 2 (F2), the joint propagated only towards the left (overall length 15 m). f) Large, “amoeboid” central parent joint with tongue-like propagation in each direction, the upper part of the joint is erased (from Bankwitz et al. 2004/).

a)



b)



Figure 2-10. (a) A bedding parallel extensional fracture containing fibrous calcite (beef) at right angles to the fracture wall. The fibres indicate the direction of fracture opening. (b) Calcite fibres that grew sub-parallel to the fracture wall indicating opening by movement parallel to the fracture wall. This is clearly a shear fracture.

2.4.3 Shear fractures

In Figure 2-2 conjugate shear fractures are shown cutting Carboniferous turbidites from Bude in SW England. Interestingly the two faults differ. The right hand fracture is a discrete, narrow fracture whereas the left hand fracture is a fracture zone. This aspect of fracturing, namely the factors that determine whether a discrete fracture or a more diffuse brittle deformation zone develops, is discussed in Section 2.5.

Shear fractures and deformation zones often show:

- Slickensides, i.e. mechanically induced striations generated on the walls of a shear fracture as they move past each other.
- Fibrous minerals, which grow at the time of fracture formation and form sub-parallel to the fracture wall, i.e. parallel to the direction of movement, Figure 2-10b.
- Second order extensional fractures, in the form of en echelon tension gashes (Figure 2-11).
- Second order shear fractures, in the form of Riedel Shears (see Section 2.9).
- Ductile deformation fabrics, such as a shear induced cleavage (Figure 2-12).

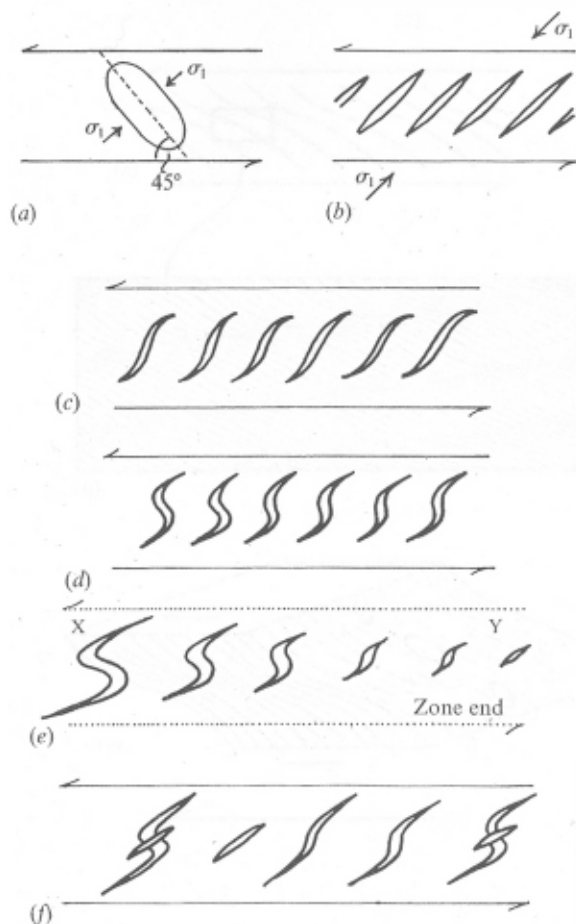


Figure 2-11. The formation of en-echelon tension gashes and their relevance as a kinematic indicator. (a) Shows the orientation of the maximum principal compressive stress with respect to the ductile shear zone or fracture and that of the strain ellipse associated with the first increment of shear deformation. (b)–(f) show the formation and evolution of en-echelon tension gashes in response to this stress /from Price and Cosgrove 1990/.

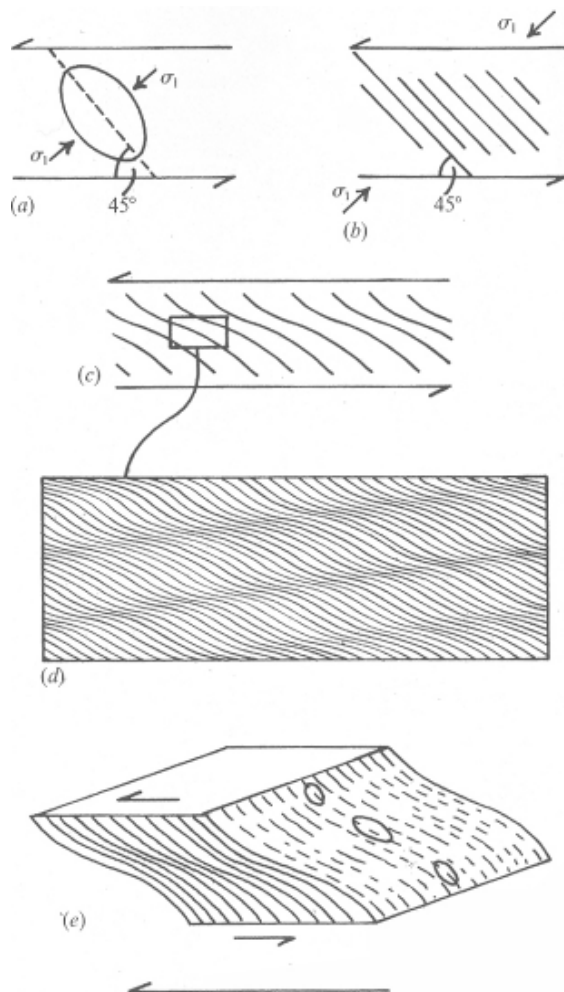


Figure 2-12. (a) The orientation of the maximum principal compressive stress associated with the first increment of shear deformation. (b) The tectonic fabric induced by this compressive stress if the PT conditions and material properties are conducive to ductile, rather than brittle deformation. (c) The rotation of the fabric as shear deformation continues. Note that the new fabric developed at the margins continues to grow at 45° to the shear direction. Continued deformation results in the deformation of the fabric and the production of deformation bands (d). Both the deformation bands and the shear induced fabric can be used as kinematic indicators (e) a 3D view of (c) showing the orientation of the strain ellipse and the lineation on the shear induced fabric [from Price and Cosgrove 1990/.

2.4.4 Fibrous minerals and other second-order structures

Minerals often grow in a fibrous habit when being precipitated into a developing fracture and it has been established that the fibres grow in the direction of fracture opening, /see e.g. Ramsay and Graham 1970/. Consequently fibres form normal to extensional fractures and sub-parallel to shear fractures, Figures 2-10a and b respectively. Other second-order features that form in association with shear fractures include en-echelon tension gashes, Figure 2-11, Riedel Shears and ductile shear zone fabrics, Figure 2-12.

Thus it is often possible to distinguish between the two types of fractures using the various characteristic features listed above. Some of these features, specifically the amount of opening of the extensional fractures and the amount of displacement along shear fractures, are related to fracture size. These size dependant features are particularly important as they can be readily observed in the access tunnels and deposition holes. However, it is noted that the magnitude of the displacements varies along the fractures and this is discussed further in Sections 2.5, 2.7 and 2.8.

2.4.5 Conclusions

Two fundamentally different types of fractures are recognised in rocks, namely shear fractures (faults) and extensional fractures (joints). They have different orientations with respect to the stress fields generating them and different types of displacement, i.e. displacement parallel to and normal to the fracture respectively. Different types of second order structures form in association with each type (plumose structures on extensional fractures, slickensides on shear fractures, see this section and Section 2.9). Both types are susceptible to re-shear in response to seismic impulses linked to post-glacial faulting and consequently critical fractures of both types need to be identified.

2.5 Discrete and diffuse fractures and brittle deformation zones

2.5.1 Detailed fracture geometry

It has been noted that two types of brittle fractures exist, Extensional and Shear. However, the detailed geometry of these fractures can be extremely varied ranging from:

- Single, relatively straight fractures to.
- More diffuse fracture arrays of deformation zones.

In the latter the “fracture” is made up of numerous short fractures which together make up a longer fracture zone (brittle deformation zone) which represents a planar zone of weakness cutting the rock. It is necessary to understand what controls the integrity of a fracture and determines whether a single, discrete fracture or a brittle deformation zone forms in a rock, as this impacts directly on the concept of fracture length, the topic at the centre of this study.

These two types of fracturing are illustrated in Figure 2-13, which shows an idealised normal fault and a fault zone of approximately the same size. The isolated normal fault has an elliptical tip line, with contours of equal displacement occurring around a central displacement maximum. The model for the fault zone shows segmentation occurring in both cross-section and map view with interaction between segments causing deviation from the model of the elliptical tip line. Clearly although the two planar zones of weakness in this figure are approximately the same size, the group of fractures that make up the brittle deformation zone (fracture zone) are shorter than the individual fracture and are therefore likely to slip less when subjected to seismic events.

Clearly a complete spectrum of structures exists between the single fault and the fault zone illustrated in Figure 2-13. With progressive movement on the fault zone (Figure 2-13b) the individual fractures extend and link to produce an anastomosing network of shear fractures bounded by lines of intersection which develop into shear lenses in a gouge and/or breccia matrix. Similarly the propagation of a single fault plane (Figure 2-13a) can also generate fault gouge and breccia and associated small-scale fractures which can lead to the formation of shear lenses. Many faults are characterised by these features and it is clear that for a particular fault zone length, the greater the continuity of the individual fault planes, the greater the potential slip. Depending on the rock type, the magnitude of the slip and the physical conditions (P, T, strain rate) under which the deformation is occurring, the resulting structure can range between a clearly brittle structure made up of numerous interlinking fractures and a ductile shear zone that contains a marked deformation induced fabric which can render the zone relatively weak with respect to the surrounding rock and therefore susceptible to brittle failure and slip if subjected to a later stress field.

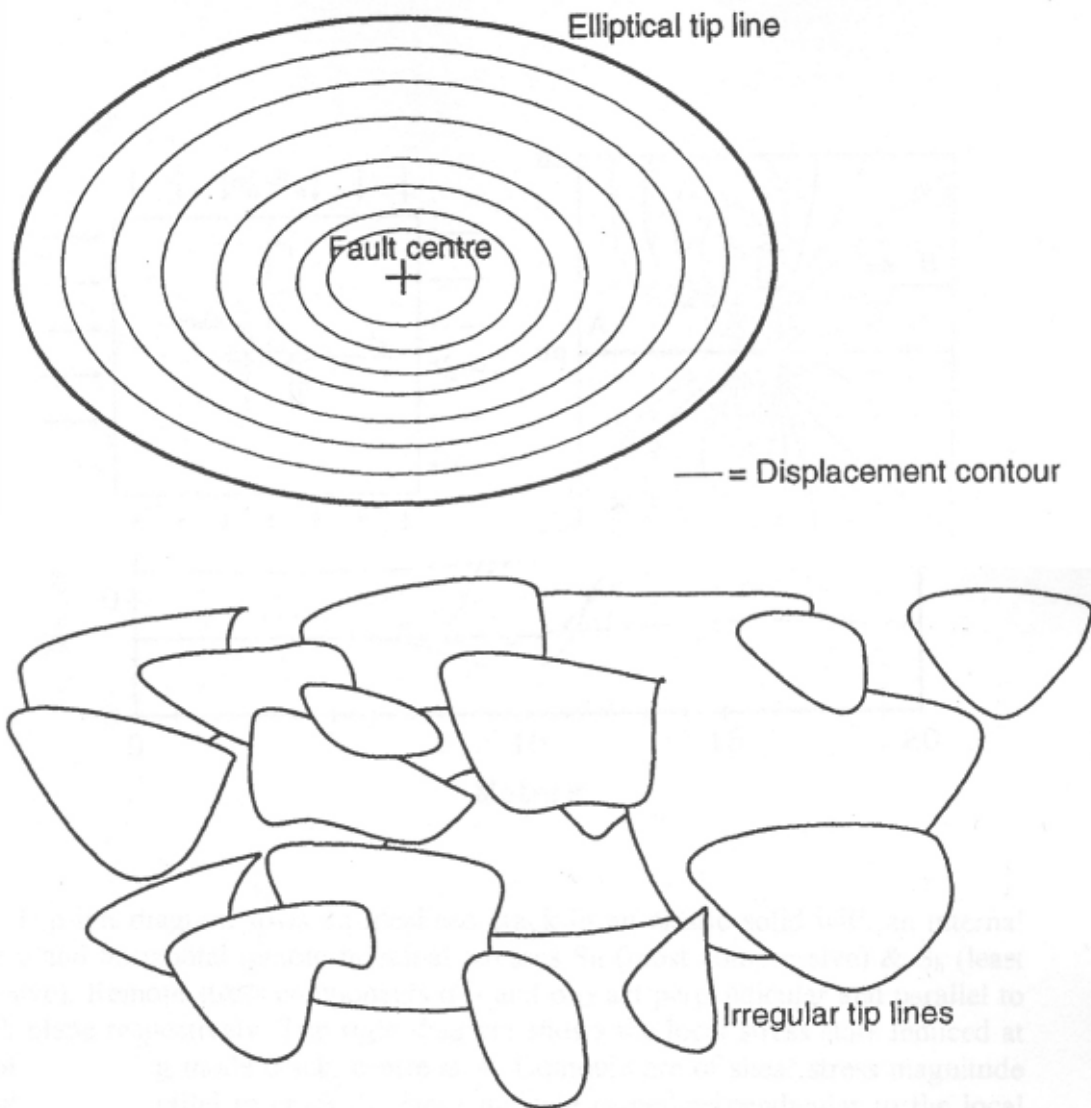


Figure 2-13. (a) Model for an isolated normal fault. The tip line is elliptical, with contours of equal displacement being around a central displacement maximum. (b) Model for the three-dimensional geometry of a fault zone. Segmentation occurs in both cross-section and map view with interaction between segments causing deviation from the model of the elliptical tip line /Peacock and Sanderson 1997/.

Before continuing to discuss the factors that determine whether discrete fractures or fracture zones develop in a rock it is important to recognise that in addition to the process described in the preceding paragraph which relates to the development of a brittle deformation zone linked to the continued movement on a shear fracture and the development of more and more second-order fractures as a result of progressive deformation, there is another mechanism by which closely spaced groups of sub-parallel fractures can form. This mechanism relates to the formation of fracture clusters during the formation of extensional fractures, and is discussed in Section 2.7. Here all the fractures in the cluster are generated at approximately the same time.

2.5.2 Factors determining fracture geometry

There are several parameters that determine the expression of fracturing i.e. control whether a discrete fracture or brittle deformation zone occurs. These include:

- Lithology (i.e. the intrinsic properties of the rock at the time of failure.)
- Strain rate (which in part is a function of the absolute values of the stresses i.e. the fracture driving force, and the PT conditions)
- Differential stress (which controls fracture regularity i.e. whether the fractures are straight or more irregular).
- Affect of other fractures (see Section 2.4)
- P (specifically confining stress) and T conditions at the time of fracturing
- The rock fabric (any pervasive foliation or local, shear induced fabric).

The influence of lithology and rock fabric

The influence of lithology and rock fabric on the expression of brittle failure is well illustrated in the rocks of the Oskarshamn area. The different expressions of brittle failure in these rocks probably reflects rock type as the conditions of PT and strain rate were most likely the same for the majority of fractures which post date the “young” granites. In the more deformed, older rock which contains fracture zones, ductile shear zones and a pervasive mineral fabric, the later failure is likely to be influenced by the existing planar zones of weakness and may exploit them. They are therefore less likely to be expressed as focused, clean fractures of the type that characterise the younger homogeneous granites. It is interesting to consider the expression of exfoliation fractures in the old rock of the younger granites. If there are no suitably oriented (i.e. sub-horizontal fracture zones) then one might expect relatively localized fractures as the PT conditions would favour this. This is what is observed.

Effect of the differential stress on the expression of brittle failure

The effect of the differential stress on the expression of brittle failure has been discussed by a number of authors including /Olson and Pollard 1988, 1989, Renshaw and Pollard 1994a/. The local stress field around the fracture tip is shown in Figure 2-14 (the dashes in the top right hand diagram are parallel to the minimum compressive stress and are therefore parallel to the direction of propagation of an extensional fracture). As can be seen from this figure, this stress field will tend to cause another fracture B parallel to but offset from A, to rotate into an orientation normal to A as the two fractures overlap. This would produce the well known hook relationship and the two fractures would link and meet each other at right angles (see also Figure 2-5a).

/Cotterell and Rice 1980/ have suggested on theoretical grounds that the propagation direction of open mode cracks (extensional fractures) should be sensitive to the remote stress, S_H , acting parallel to the initial crack plane, if they stray from the symmetric situation shown in the top two diagrams in Figure 2-14. For example, in the stress field shown in these diagrams, there is a remote differential stress, $\sigma_{22}^r - \sigma_{11}^r$ which is compressional, aligned with crack A (N.B. in this diagram the maximum principal compression is termed σ_2). /Olson and Pollard 1988, 1989/ point out that if crack B begins to curve away from A as the two fractures begin to overlap, a left lateral shear is resolved across its tip by the remote stresses. If B were to curve towards A, a right lateral shear would be resolved. In both cases the remotely induced shear stress works against the locally induced shear stress and promotes a straighter crack path. Conversely, if the differential stress is tensile, the remote stresses induce the opposite sense of shear and enhance crack path curving. The influence of the remote stress field on the crack propagation path is illustrated quantitatively in the lower diagram in Figure 2-14. Here the effects of four remote stress fields, oriented with respect to the fracture as shown in the upper diagrams, on the fracture path are shown. The fields have differential stresses of -0.5 Mpa, 0 MPa, 1 Mpa and 5 MPa.

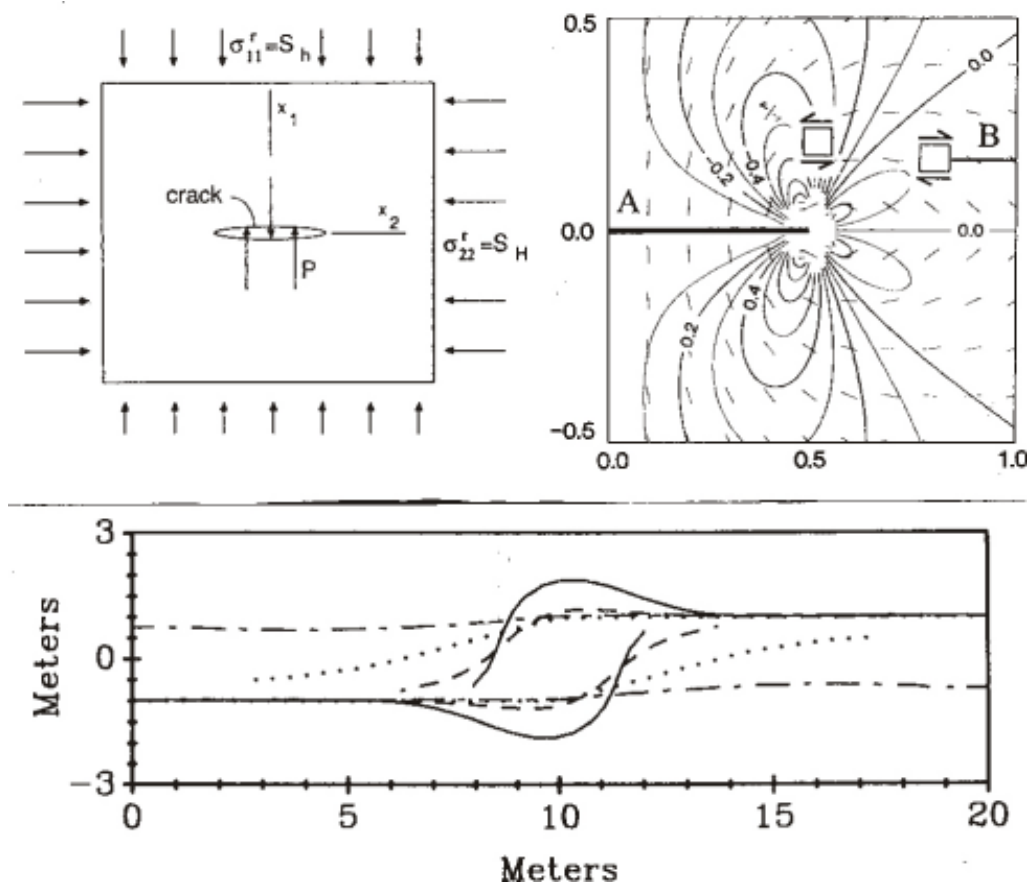


Figure 2-14. Top left diagram shows an idealised crack in an elastic solid with an internal pressure p and horizontal remote principal stresses S_H (most compressive) and S_h (least compressive). Remote stress components σ_{11} and σ_{22} act perpendicular and parallel to the crack plane respectively. Top right diagram shows the local stress state induced at the tip of an opening mode crack, centre at A. Contours are of shear stress magnitude acting on planes parallel to crack A. Dashes indicate planes perpendicular to the local maximum tensile stress and show the possible path of crack B. Bottom diagram graphs of the theoretical crack paths under four different differential remote stress fields. Solid line, -0.5 MPa, dashed, 0 MPa, dotted, 1 MPa and dot-dash, 5 MPa. /from Olson and Pollard 1989/.

For the -0.5 Mpa example (solid line) the remote and fracture tip stresses act together and produce the maximum curving of the fractures. As the remote differential stress becomes progressively more compressive the propagating fracture paths become progressively straighter.

/Olson and Pollard 1989/, suggested that this relationship between fracture straightness and the differential stress at the time of fracturing could be used in palaeo-stress analysis. They introduce a method to infer the remote differential stress magnitude from the curvature of overlapping fracture traces. Curving paths imply the predominance of local crack-induced stresses over the remote stresses during propagation.

They discuss a fracture network in an outcrop from south eastern Utah containing two fracture sets, Figure 2-15 /Olsen and Pollard 1988/. They are shown individually in Figures 2-15b and 2-15c and it can be seen that although the two sets are produced in the same bed the trace patterns are fundamentally different. The NE-SW traces are regularly spaced and uniformly abundant throughout the outcrop, Figure 2-15b. They exhibit an anastomosing geometry with numerous curving overlaps and crack intersections. This is taken to indicate that the remote differential stress was very low and exceeded by the fracture propagating driving pressure (assumed to be provided by the water pressure inside the fractures). In contrast the NW-SE trending joints occur in clusters and display little curving. The linearity of this set is taken to indicate a larger differential stress.

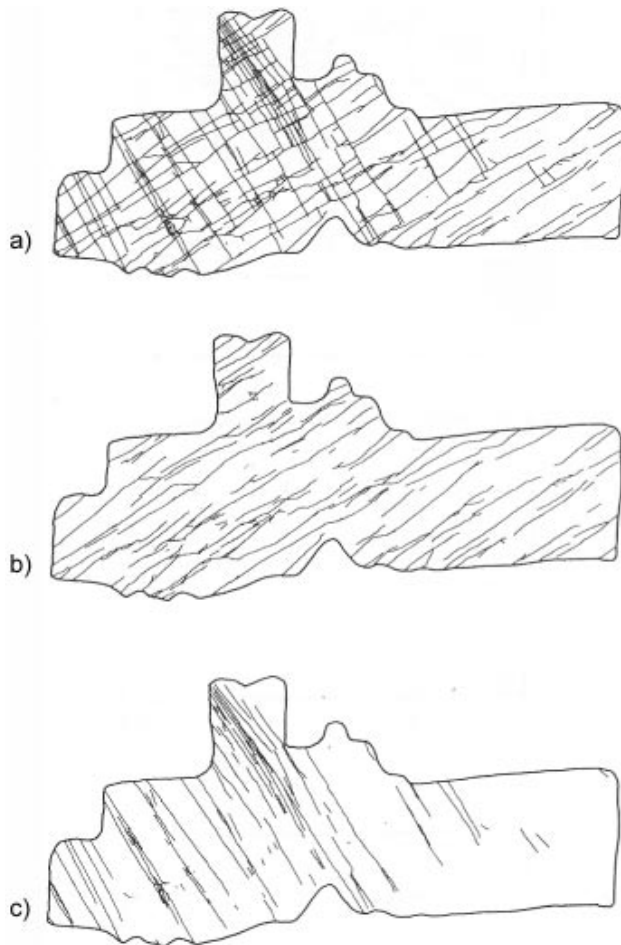


Figure 2-15. (a) Map of joint traces exposed on a bedding plane surface. b) The older joint set formed under near isotropic remote stress. c) The younger set formed under strongly deviatoric remote stress /from Olson and Pollard 1988/. (The outcrop measures 5.5 m by 2.5 m.).

Impact of heterogeneities on the propagation pattern of fractures

/Renshaw and Pollard 1994a/ studied the impact of heterogeneities on the propagation pattern of fractures, Figure 2-16, and conclude that the dominant factor controlling fracture straightness is the magnitude of the far field differential stress. As the differential stress increases, i.e. as the stress ratio R increases, see caption Figure 2-16, so the effect of local fractures on the fracture propagation path becomes progressively weaker, Figure 2-16, bottom 4 diagrams.

The “driving force” available to propagate a fracture, which controls the propagation rate and therefore the straightness of the fractures, is determined by the magnitude of the differential stress ($\sigma_1 - \sigma_3$). Where σ_3 is horizontal, this determines the regularity of the strike of the fractures. Their regularity in the vertical plane is determined by the value of ($\sigma_2 - \sigma_3$), as illustrated in Figure 2-17.

Affect of other fractures

In addition to the control of the fracture tip stresses and the remote differential stress on fracture straightness and length discussed above, the cohesive strength of pre-existing fractures can also have a dramatic effect on these parameters. As discussed in Section 2.5, early open fractures can exert a major influence on the regularity and continuity of later fractures (see e.g. Figure 2-4). When attempting to understand the irregularity of fractures and fracture zones, it is important to recall all the parameters that influence this.

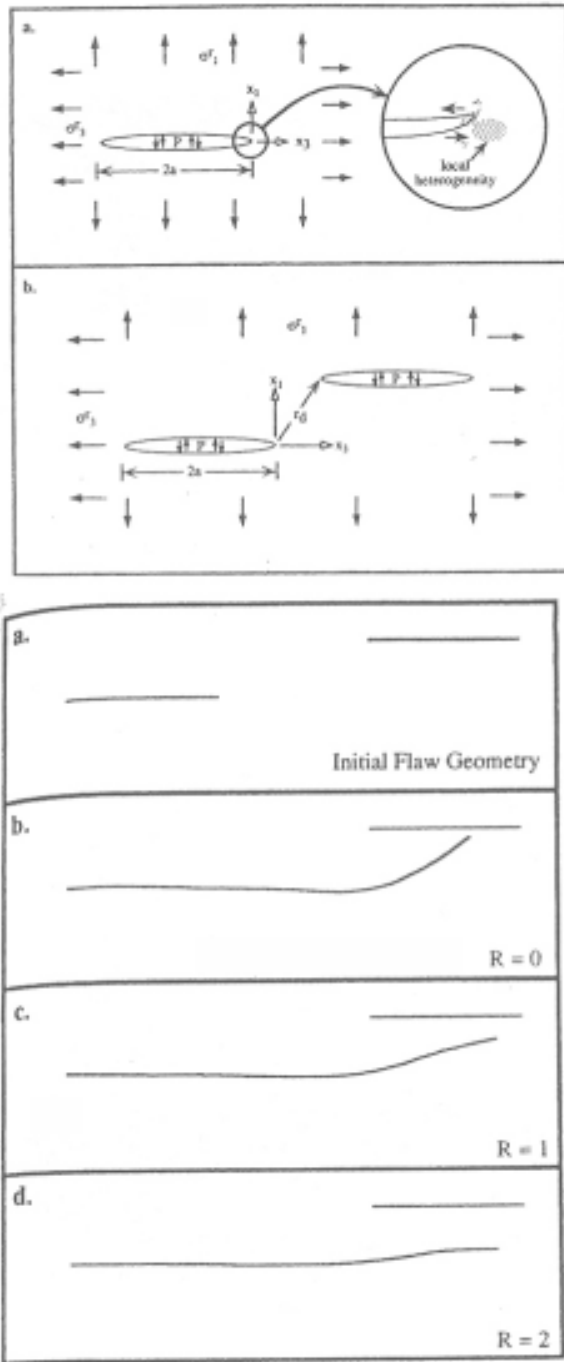


Figure 2-16. Top diagram. a) Co-ordinate system used to define the transverse stress $T = (\sigma_3 - \sigma_1)$ where σ_3 and σ_1 are the maximum and minimum compressive remote stresses respectively. The inset demonstrates how a local heterogeneity can alter the propagation path. b) Co-ordinate system used to describe the interaction between two fractures with an internal fluid pressure P arranged in an echelon geometry. The lower diagram shows the sensitivity of fracture paths to the stress ratio R ($= [(\sigma_3 - \sigma_1) / (\sigma_1 + P)]$). a) shows the two initial flaws, only the left hand one was allowed to propagate /from Renshaw and Pollard 1994b/.

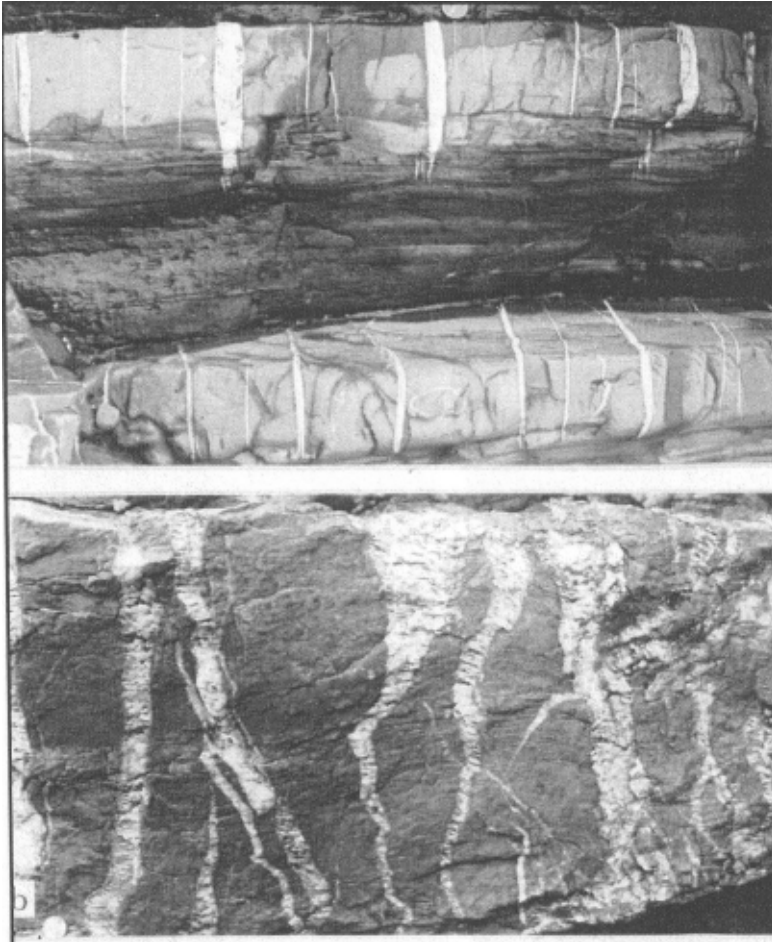
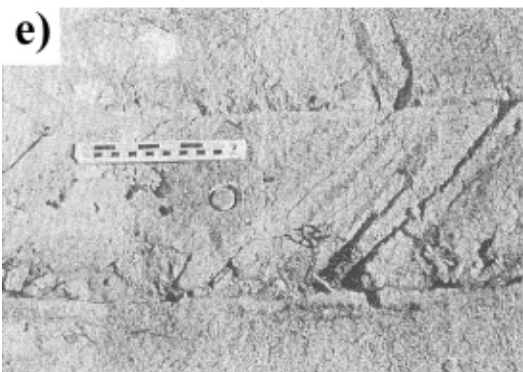
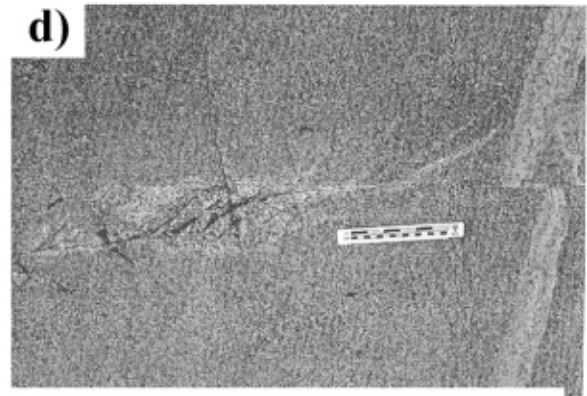
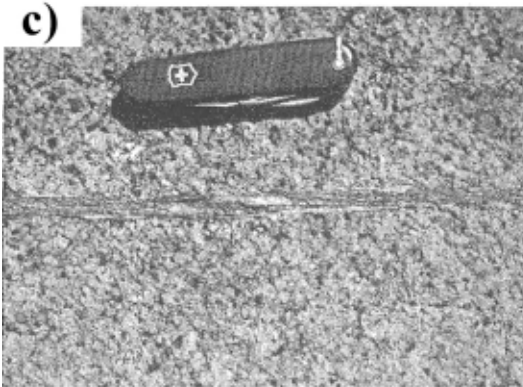
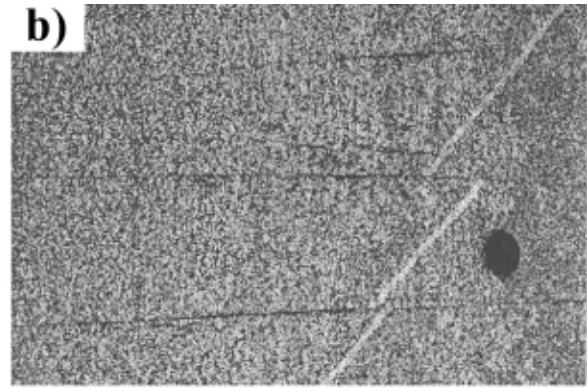
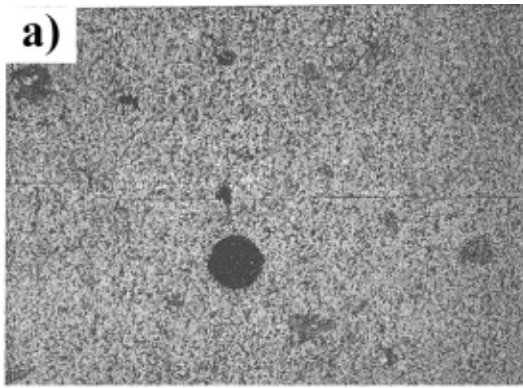


Figure 2-17. Quartz veins infilling extensional fractures. In the upper two layers from the Carboniferous turbidites from Bude SW England, the fractures are well orientated both in their strike and in their profile section indicating that both $(\sigma_1 - \sigma_3)$ and $(\sigma_2 - \sigma_3)$ were large during fracture formation. In the lower layer from St Anne's Head SW Wales, the value of $(\sigma_2 - \sigma_3)$ was smaller and the constraints on the regularity of the profile section through the fractures, considerably less.

2.5.3 Evolution of fault zones

In this section it has been argued that the expression of brittle failure i.e. whether it occurs as localized fractures or as a more diffuse fracture zone, is controlled by parameters such as lithology, stress state (both fracture tip stresses and regional differential stress), strain rate, temperature, pre-existing fractures or rock fabrics. In addition the expression of brittle failure also changes with time as a particular episode of brittle failure develops. This evolution from discrete fracture to complex brittle deformation zone is illustrated in Figure 2-18, which shows photographs of the various stages in the growth of faults in a granitic rock. As the fault develops the fractures evolve from (a) joints sealed with epidote, chlorite and quartz, (b) left lateral shearing of the joints, (c) hydrothermal minerals in the joints have a mylonitic fabric, (d) extensional steps between two fault segments, (e) "Fault zone" between adjacent left lateral faults, (f) Compound fault zone with ~ 100 m left lateral displacement. The bottom illustration in Figure 2-18 is a schematic representation of the evolution of the fault zone.



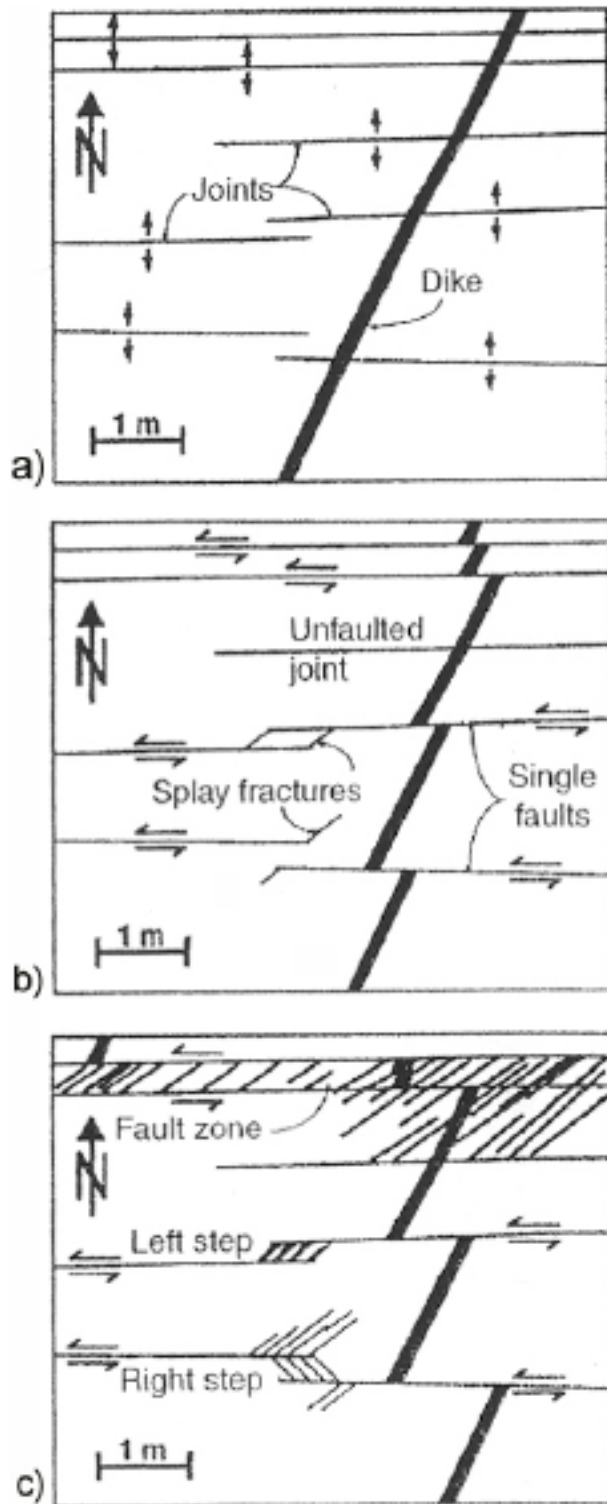


Figure 2-18. Photographs a–c) depicting various stages in the evolution of a fault zone from discrete fractures, in granitic rock /from Pollard and Fletcher 2005/ see text. The lower diagram is a schematic illustration of the development of a fault in granitic rocks of the Sierra Nevada. a) Joints propagate to form one set of open fractures, b) some joints slip to form left-lateral faults with wing cracks near tips linking to neighbouring faults. c) Adjacent left-lateral faults form the boundaries of fault zones /after Buergermann et al. 1994/.

2.5.4 The brittle – ductile transition

The terms brittle and ductile, used to describe the rheological behaviour of the Earth's crust are general terms indicating whether or not discontinuities have developed during deformation. A complete spectrum of deformation behaviour exists, ranging from ideal brittle deformation where the strain is highly localised along planar discontinuities to uniformly distributed strain as for examples occurs during homogeneous flattening (see Figure 1-2). The expression of brittle failure in triaxial test specimens deformed under different confining stresses is shown in Figure 2-19. In the upper diagrams the range of behaviour is represented schematically and

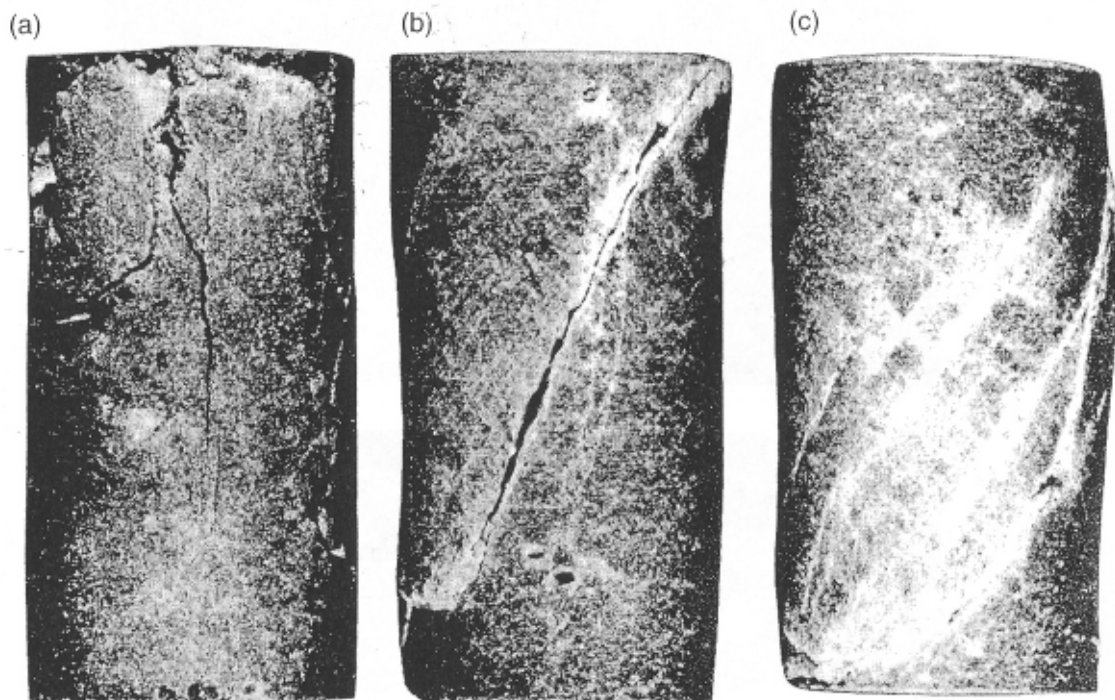
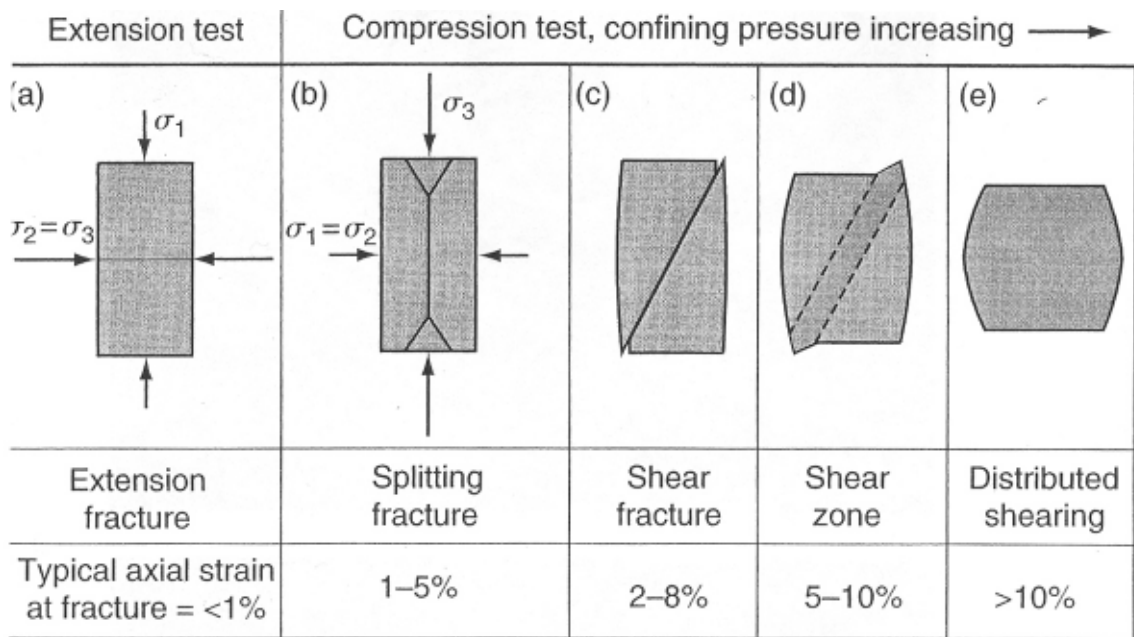


Figure 2-19. Top diagrams show schematic representations of brittle failure styles in triaxial tests. a) Extension test. b)–e) Compression tests with confining pressure increasing to the right /from Griggs and Handin 1960/. Bottom diagrams show examples of brittle failure in triaxial test specimens of Ottawa basalt. a) 0.1 Mpa confining pressure, b) 49 Mpa confining pressure, c) 98 Mpa confining pressure /from Hoshino et al. 1972/.

in the lower photographs the effect of different values of confining stress on the deformation behaviour of samples of basalt can be seen. Increasing confinement favours the formation of a more diffuse fracture zone. This gradation of deformation between discrete fractures and fracture zones also occurs in Nature as can be seen from Figure 2-20 which shows three examples of shear failure in rock. The upper example of well developed granulation seams is the most diffuse example of brittle failure and the lower example of normal faults in turbidites, is the most discrete.

As noted above, there are a several parameters which influence the expression of brittle failure and determine whether a few, continuous, straight fractures form, whether a brittle deformation zone made up of a more diffuse zone of shorter, more irregular fractures forms or whether a continuous, ductile deformation zone (a shear zone) develops which technically is not an example of brittle failure because the rock has not lost its continuity. However, as noted earlier, such a deformation zone may represent a planar or sub-planar zone of weakness along which there is the possibility of seismically induced slip.

The rocks in the Oskarshamn area have undergone a long and complex deformation history over the last 1,800 million years and during this time they have undergone “brittle” deformation under a variety of conditions. Consequently the rocks now possess a suite of fractures and fracture zones that indicate that the rock’s response to brittle deformation at different time during its history was different. As the different sets of brittle structures are superimposed onto each other a progressively more and more complex “fracture” network is built up. Later stress fields may generate new fractures, or, if appropriately oriented with respect to earlier fractures, may cause slip on old fractures. In addition, even during episodes of ductile deformation when continuity of the rock mass is not lost, ductile shear zones formed in the rock which now represent planar zones of mechanical weakness which must be considered as potential planar zones along which movement could occur in response to seismicity linked to post-glacial faulting. The block diagrams in Figure 2-21 indicate the range of planar zones of weakness that cut the rocks at the repository site. It is important to recognise that the task that is being addressed in the current study is that of recognising any of these planar structures that are greater than the critical fracture size.

2.5.5 The concept of the integrity of fractures and fracture size

Relating to the integrity of the fractures, it might be argued that the worse case scenario is the discrete continuous fracture. In any more diffuse array of fractures (i.e. in a fracture zone) it can be argued that;

- i The displacement is likely to be partitioned between several fractures with the result that the displacement on any strand of the brittle deformation zone is likely to be less than along a continuous fracture with the same length as the deformation zone.
- ii The individual fractures making up a brittle deformation zone that is 100 m in diameter, will be considerably less than the critical size (see Figure 2-13) and therefore, because of the empirically established relationship between the length of a fracture and the maximum slip that can occur along it (see Sections 2.8 and 2.12), will not be able to slip sufficiently to pose a threat.

Brittle deformation zones will develop and grow by the process of growth of their individual fractures and by the linkage of fractures in close proximity, (see discussion in Section 2.6 on “Fracture Propagation”). We therefore need to consider the possibility of fractures within the brittle deformation zone linking in response to a seismic pulse stimulated by glacial activity. A worse case scenario can be envisaged in which two sub-critical fractures link to produce a critical fracture and that this composite fracture had a displacement profile similar to that which is associated with a single fracture where the maximum displacement occurs in the centre of the fracture and the displacements die out to zero at the fracture tips, see Figure 2-31. However, as will be seen in Section 2.6, the displacement on a composite fracture formed by fracture linking is generally different (significantly less see Figure 2-32 and Figure 2-33c) to that on a

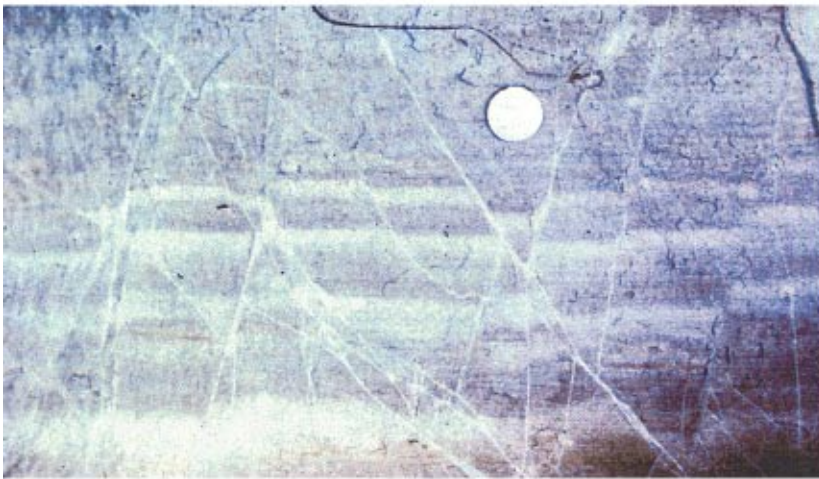
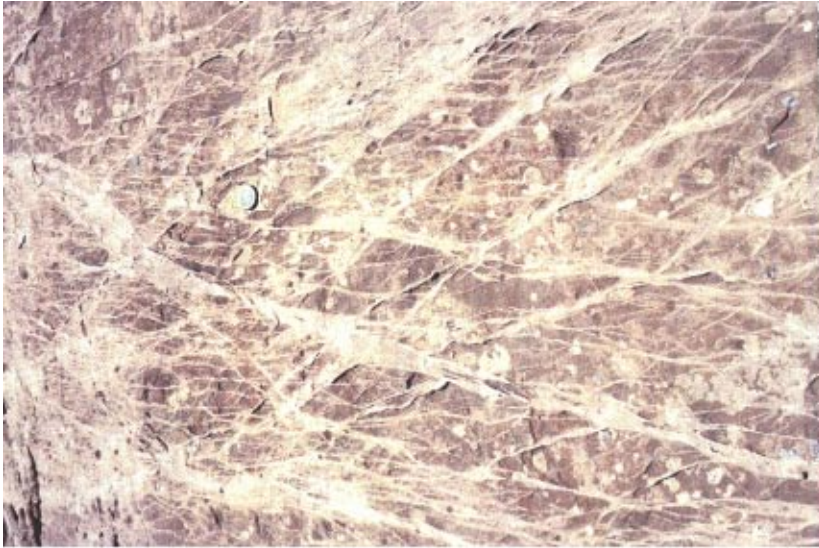
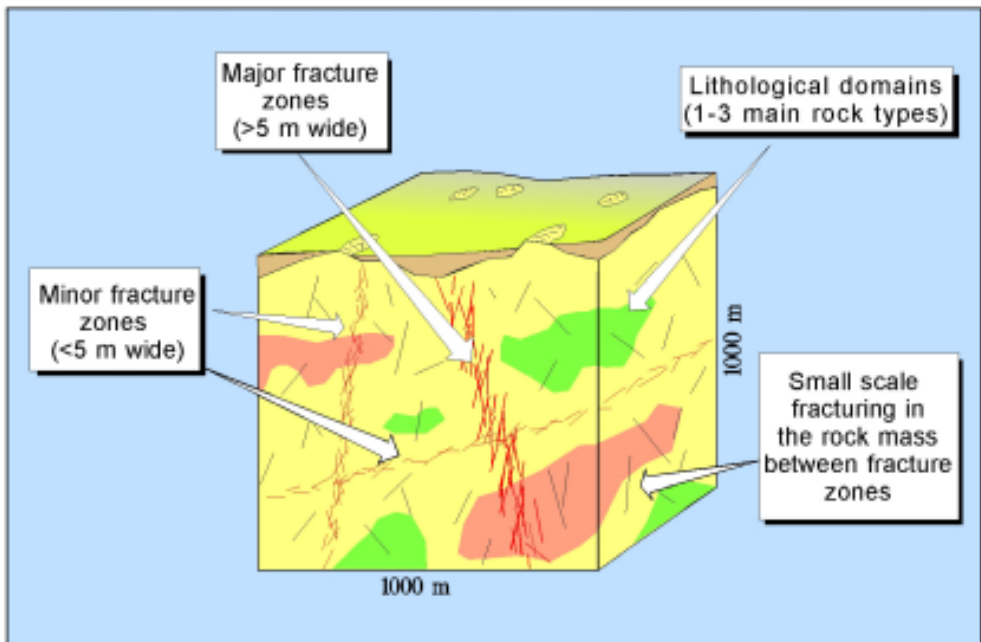


Figure 2-20. Examples of brittle shear failure in which the failure planes become increasingly more and more discrete. Top, shows “granulation seams” in a porous sandstone, Middle more localized shear planes. Bottom, the shear failure is defined by a single fracture plane.



Single open fractures
 Mylonite
 Minor fracture zones (<5m)

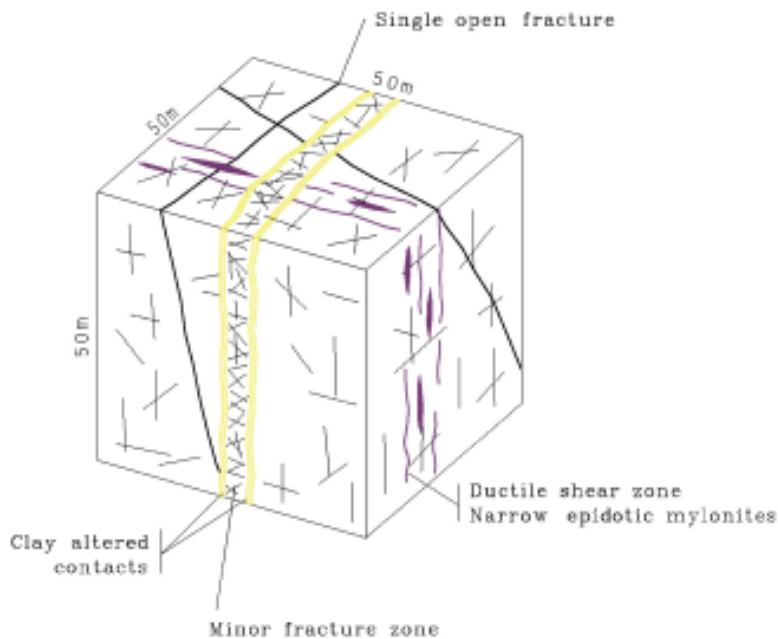


Figure 2-21. The top diagram shows the schematic description of the lithologies and discontinuities, (fracture zones and fractures), at Åspö /from Rhén et al. 1997/. Lower diagram is a block-scale structural model showing the main fracture types encountered at Åspö. These include single open fractures, mylonite zones, minor fracture zones and rock boundaries associated with changes in lithology /from Rhén et al. 1997/.

single fracture. It follows that even if the composite fracture is greater than the critical length, the displacements along it caused by the seismic event that linked the two fractures, would be unlikely to exceed the permitted maximum of 10 cm.

2.5.6 Conclusions

A variety of features impact on the expression of brittle failure in rocks. These include rock type, strain-rate, differential stress and the PT conditions at the time of fracture formation and, as discussed in Section 2.3, the existence or absence of previous fractures. Thus within an ancient crystalline rock mass such as the Fennoscandian Shield, a variety of planar zones of weakness, along which slip might occur in response to seismicity linked to post-glacial faulting, are likely to exist.

These range from discrete, single fractures to more diffuse zones containing numerous smaller fractures. The magnitude of the slip likely to occur along discrete fractures and fracture zones of the same length is the same even though the magnitude of slip on the individual fractures making up the fracture zone will be less than that on the discrete fracture. Thus if a complete fracture zone cuts the repository tunnel or deposition hole the potential slip along it should be assumed to be equal to that which might occur along an individual fracture of the same length.

If individual fractures from a fracture zone cut the excavation then they can be treated as discrete fractures and the magnitude of slip likely to occur along them can be determined from their length.

2.6 Small scale processes linked to fracturing and the process of fracture propagation

2.6.1 Small-scale processes linked to fracturing

A study of fracture development on a microscopic scale has shown that a zone of deformation is generated in front of the advancing fracture tip, often called the “process zone”. This process zone is often represented as a zone of micro-fracturing which has been linked directly to the zone of stress concentration that forms around a fracture tip in a stress field.

The zone of stress concentration around the tip of an extensional fracture subjected to a far-field stress in which the greatest tensile stress is normal to the fracture is shown in Figure 2-22. It can be seen that concentrations of both shear and normal stresses occur in the vicinity of the tip. A similar stress concentration can result from a build up of fluid pressure in the fractures without the need for the far field stress, Figure 2-23, upper diagram. This zone of stress concentration in which the fracture propagation occurs is often referred to as a “plastic” zone in which non-linear deformation occurs. It is also known as the “decohesion” region, Figure 2-24.

Experimental work has indicated that the process zone is characterized by a cloud of micro-fractures, some of which link to allow the main fracture to propagate, Figure 2-25. The diagrams in this figure are scale independent and the size of the process zone will be proportional to the size of the fracture. It might be argued that as the fracture develops and passes through the process zone, evidence of this zone would be left along the margins of the fractures and that the thickness of this zone of micro-fracturing would reflect the size of the fracture. Field studies show that there is often a zone of macroscopic fracturing on either side of major fractures in rocks, particularly shear fractures and that the thickness of this “damage zone” is related to the size of the major fracture with which it is associated. Because of the probable link between the thickness of the “damage zone” and fracture size, this is a topic of direct relevance to the problem of determining fracture length from borehole and other excavation data and warrants further research. Because of the use of “damage zone” in SKB protocol used to discuss blast induced damage, it should be noted that the term “damage zone” as used in this report relates to damage caused to the area adjacent to the main fracture during the natural development of the fracture and is in no way linked to blasting.

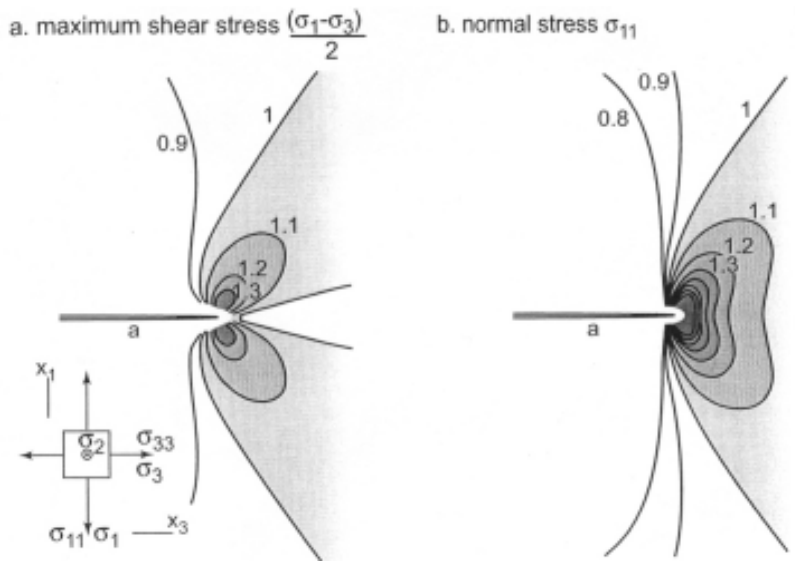


Figure 2-22. Contours of a) normalized maximum shear stress and b) of normalized normal stress acting on planes parallel to the fracture. Shear stress is contoured in two distinct lobes that are oblique to the fracture tips and that are separated by a distinct local minimum along the fracture axis. Normal stress is characterized by a single concentration ahead of the fracture tip with two maxima at 60° with respect to the fracture axis. N.B. Tension is taken as positive and the greatest tensile stress is normal to the fracture /from Eichhubl 2004/.

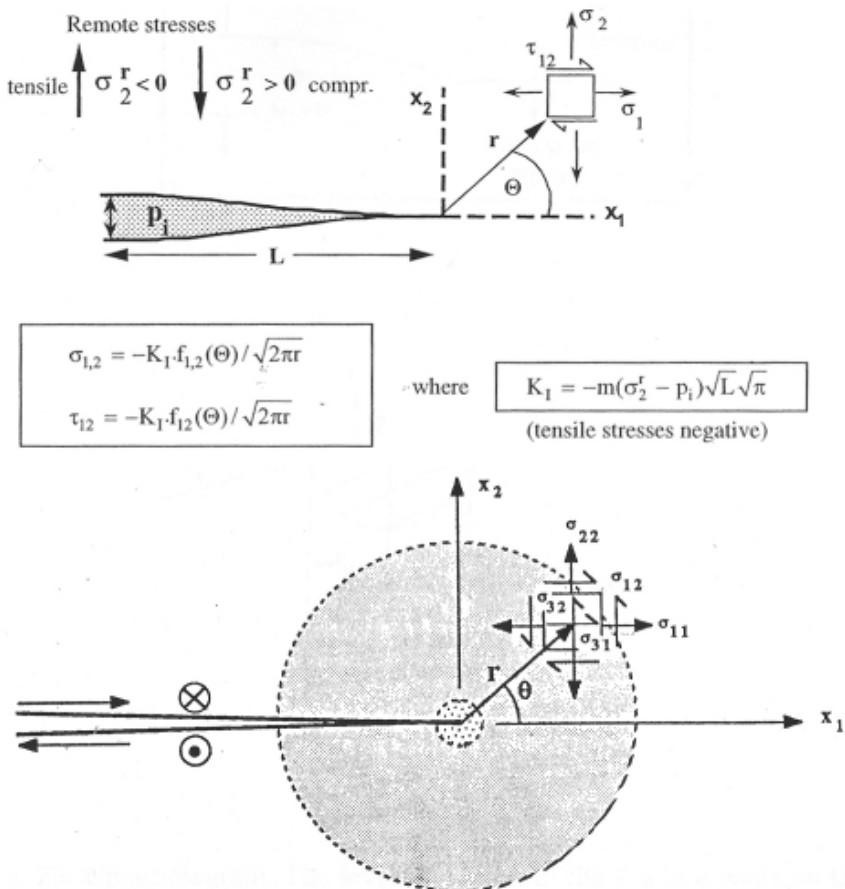


Figure 2-23. Upper figure shows the Stress concentration in the near-tip region of a tensile fracture with internal fluid pressure. /From Mandl 2005/. Lower figure shows the tip of a shear crack. The shaded area shows the region in which the crack tip stress fields are valid /from Li 1987/.

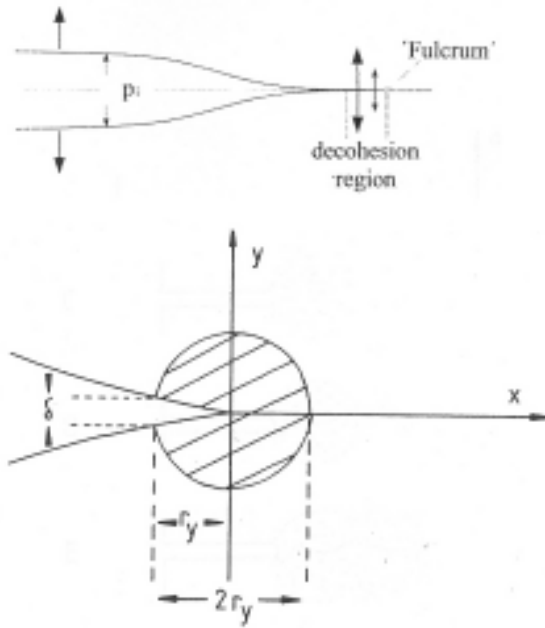


Figure 2-24. Upper diagram. The leverage action of the fracture walls on the near tip region /from Mandl 2005/. Lower diagram. Schematic drawing of the nominal plastic zone, non-linear zone or process zone. For simplicity, it is assumed that this zone is circular in the xy plane, although in practice this will depend upon the state of stress. The intersection of the zone with the crack surface defines the point at which the crack tip opening displacement δ is measured. The drawing shows simple tension deformation where the principal tensional stress is parallel to the y axis /from Atkinson 1987/.

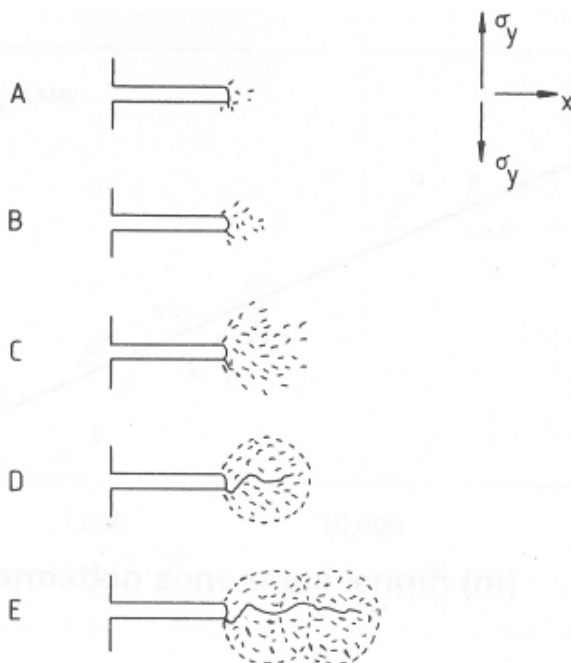


Figure 2-25. Schematic drawing illustrating the development of a process zone and its influence on macrocrack growth. Tensile deformation across the plane $y = 0$ increases through drawings A to E. B) Microcracks mostly isolated and linear elastic behaviour is still observed. C) Microcracking becomes more intense. Some microcracks link up. Non-linear behaviour is observed. D) Within the now fully developed zone of non-linear elasticity of the process zone the macrocrack extends by the linking of microcracks. E) Further macrocrack extension occurs by migration of the process zone through the material ahead of the microcrack tip. The "cloud" of microcracks allows macrocrack extension as described above /from Atkinson 1987/.

2.6.2 The process of fracture propagation

Two mechanisms have been proposed to explain the process of Fracture propagation, Figure 2-26, namely:

- Growth through a process zone.
- Growth by fracture linkage.

Growth of a fracture by propagation through a process zone.

The propagation of a fracture by the mechanism of developing a process zone and propagating into it has been studied experimentally. This work has indicated that the process zone (discussed in the previous section) is characterized by a cloud of micro-fractures some of which link to allow the main fracture to propagate. The influence of the process zone on macro-crack growth is shown schematically in Figure 2-25. Tensile deformation across the plane $y = 0$ increases through drawings A to E. In B) the micro-cracks are mostly isolated and linear elastic behaviour is still observed. In C) micro-cracking becomes more intense and some micro-cracks link up. Non-linear behaviour is observed. In D), within the now fully developed zone of non-linear elasticity of the process zone, the macro-crack extends by linking of micro-cracks. In E) further macro-crack extension occurs by migration of the process zone through the material ahead of the micro-crack tip. The experimentally observed evolution of a process zone in a limestone and the subsequent propagation of the fracture through this zone, is shown in Figure 2-27.

A study of the process zone around the tips of stressed fractures by /Evans and Blumenthal 1984, Eichhubl 2004/, Figure 2-28, shows that damage is sometimes concentrated in side lobes, Figure 2-28a, and sometimes as frontal damage, Figure 2-28b. These observations are clearly relevant to the formation of shear and extensional fractures, the two types of brittle failure. It is argued that under low differential stress the frontal damage pattern is the more efficient, encouraging the formation of extensional fractures and under high differential stress the side lobe pattern is more efficient, encouraging the formation of shear fractures.

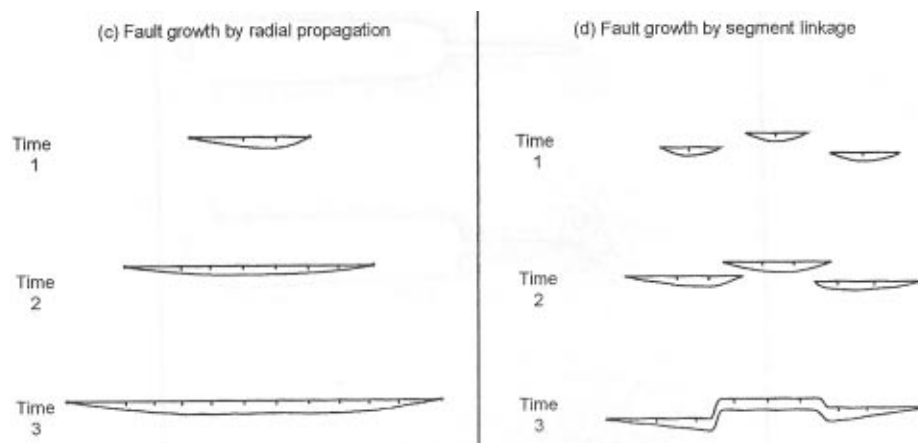


Figure 2-26. Two modes of fracture growth: radial fault propagation, and fault segment linkage.

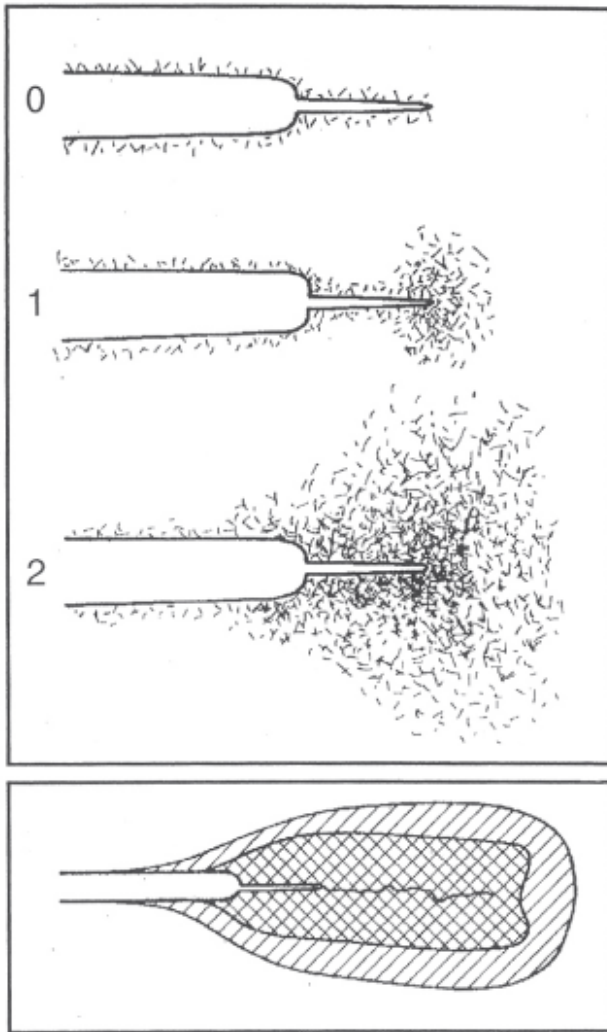


Figure 2-27. Double cantilever beam testing procedure for opening fracture propagation in Salem Limestone. Drawings 0), 1) and 2) show different stages in fracture propagation and the development of the microcrack damage zone. The lower diagram is a schematic illustration of steady state fracture propagation and the evolving damage zone /from Hoagland et al. 1973/.

Various possible modes of microscopic deformation which are likely to occur at a grain-scale during the compressional and extensional deformation of a granular material, are illustrated schematically in Figure 2-29. These processes are thought to operate in the process zone which develops in front of and around an advancing fracture tip during the formation of shear and extensional fractures.

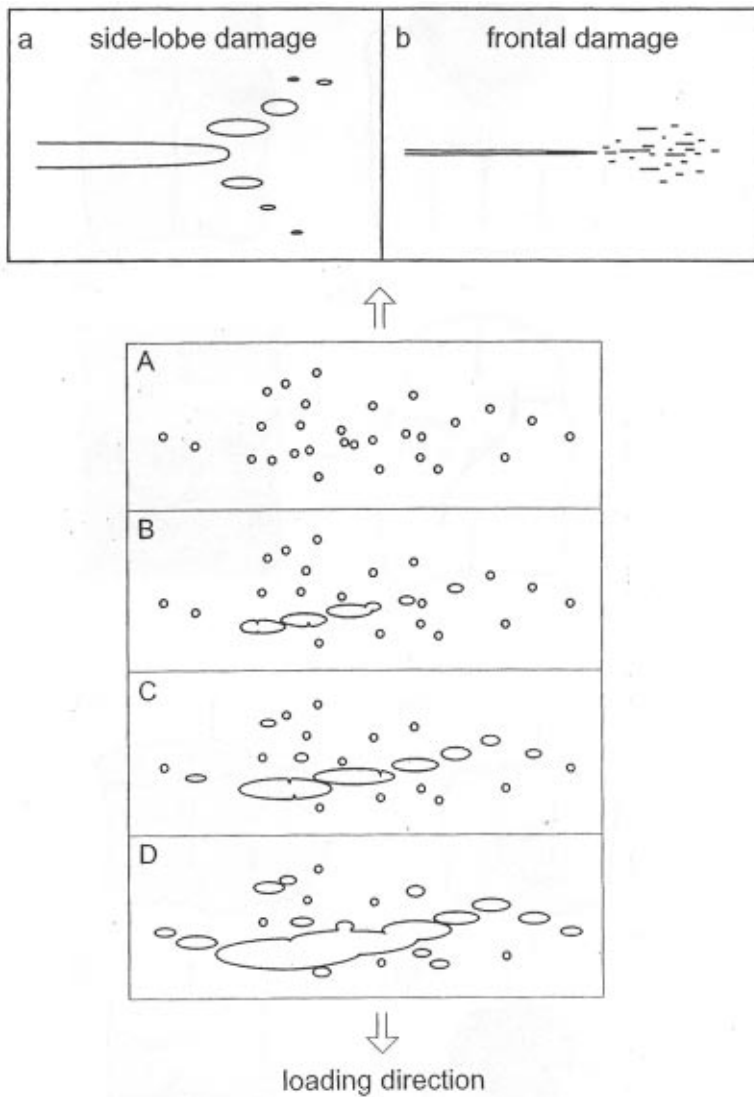


Figure 2-28. Upper diagram showing damage distribution at fracture tips, loaded in tension perpendicular to the fracture: a) Side-lobe damage /after Evans and Blumenthal 1984/, b) frontal damage /from Eichhubl 2004/. Lower diagrams show a sequence of fracture growth by pore growth and coalescence. Fractures are inferred to grow with their long axis perpendicular to the maximum principal tensile or least principal effective compressive stress, σ_3 /from Eichhubl 2004/.

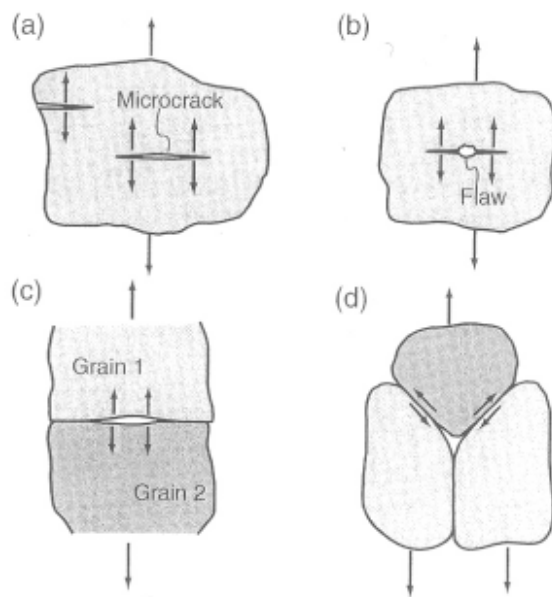
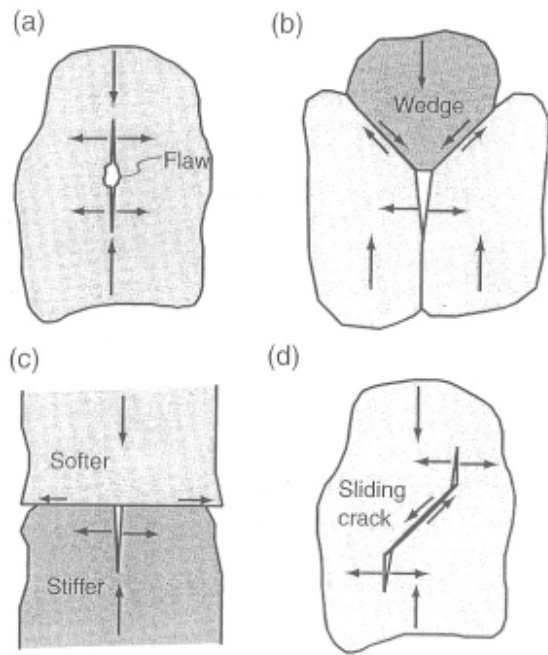


Figure 2-29. Top figure. Schematic examples of microscopic mechanisms of deformation at the grain scale in rock during strength tests. a) Microcrack growth from flaws within mineral grains. b) Wedging of one grain between neighbours with grain boundary sliding. c) Lateral extension of soft grain promotes crack growth in an adjacent stiff grain. d) Slip of inclined flaw induces wing cracks. Bottom figure. Schematic examples of microscopic deformation mechanisms in a damage zone during open fracture propagation. a) Microcrack growth within a mineral grain. b) Growth of crack from flaws. c) Opening of grain boundaries. d) Shearing of grain boundaries as grains pull apart /Pollard and Fletcher 2005/.

Growth of a fracture by fracture linkage

/Trudgill and Cartwright 1994, Cartwright et al. 1995, Cartwright et al. 1996, Walsh et al. 2002/, propose that fault growth consists of propagation, interaction and linkage of fault segments, following a step-like growth. This is in contrast to the accepted model of lateral fault growth where faults were thought to have grown as a result of radial propagation where growth followed a path imposed by a scaling law, /Watterson 1986/. These two processes are represented schematically in Figure 2-26.

Analogue models designed to study the growth of normal faults arrays such as those commonly found at the margins of rift valleys, show clearly that major faults are formed by the linking of a series of smaller faults, Figure 2-30.

Fracture size and fracture displacement

The displacement along any fracture whether it is an extensional fracture or a shear fracture, varies in a predictable way and the concept of displacement gradients along fractures is well established for both mode I and II (extensional and shear) fractures. The maximum displacements usually occur in the central portion of the fracture and displacements die out to zero at the fracture tips. This is illustrated in Figure 2-31, which shows the slip-rate data for a 200 km slipped portion of the San Andreas Fault in Central California. The slip data lies symmetrically around Monarch Peak, the centre of the slipped segment and, despite some “noise” in the geodolite measurements they show a remarkable correlation to the theoretical slip profile for an elastic crack model.

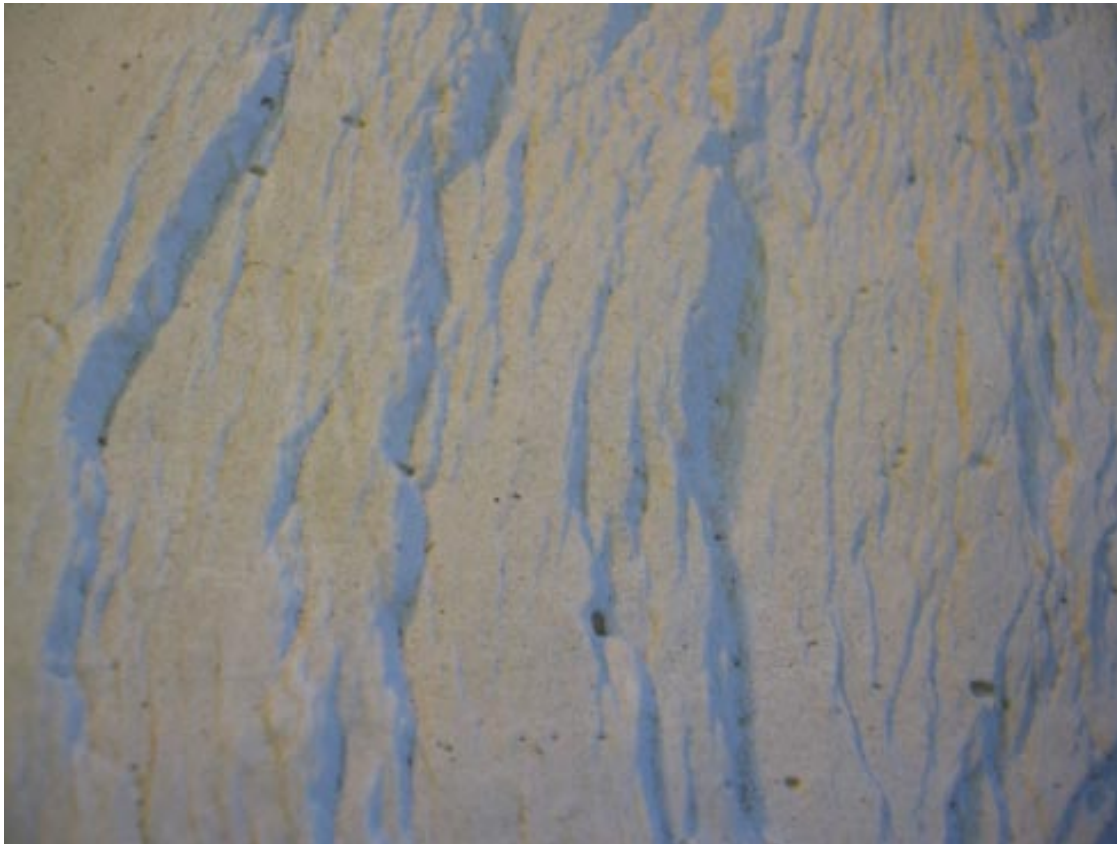


Figure 2-30. A swarm of small-scale normal faults down-stepping to the right, at various stages in their linkage to form longer faults. Plaster of Paris analogue model.

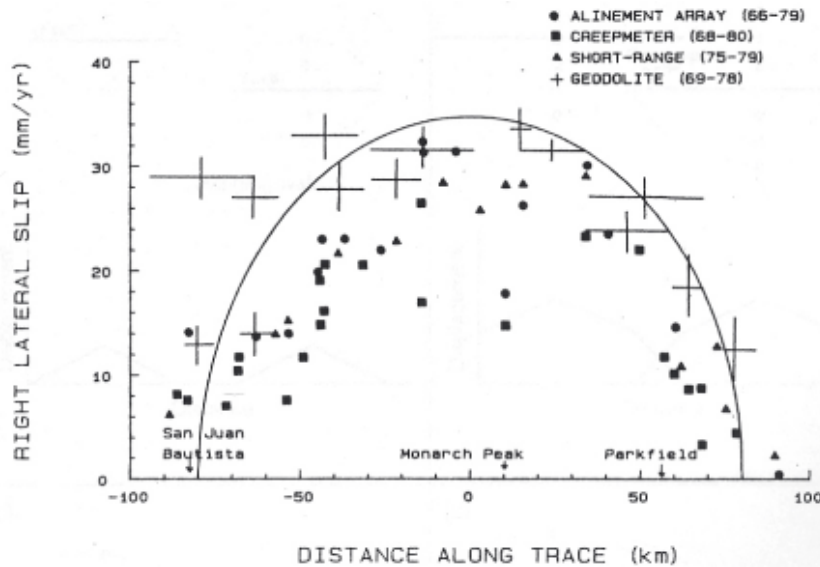


Figure 2-31. Slip rate data from a 200 km trace of the San Andreas fault in central California After /Burford and Harsh 1980, Savage et al. 1981, Schultz et al. 1982/. The curve fit is from the elastic-brittle centre-crack model /from Li 1987/.

However, if two fault segments meet, then the displacement profile will be dramatically altered as indicated by Figure 2-32. This figure shows different stages in the linking of two offset fractures the upper part of each diagram shows the plan view of the faults and the lower part the distribution of displacement. Displacement profiles for a variety of natural faults are shown in Figure 2-33. It can be seen that in some faults the maximum displacement does not occur in the central region of the fault, Figure 2-33a, and that the displacement profiles often indicate clearly that the fault is the result of fault linkage, Figure 2-33d.

The link between the maximum slip on a fracture and the fracture length outlined above applies equally to re-shear on a fracture regardless of its mode of origin. This is illustrated in the results of a numerical simulation, Figure 2-34 which shows the maximum shear displacements induced on a population of fractures 2 km away from a fault generating a Magnitude 6.1 earthquake. It can be seen that despite the scatter of data a clear relationship exists between fracture length and maximum displacement. The maximum possible displacements that can occur on a fracture with a radius of 100 m in response to this seismic event are shown in the lower diagram of Figure 2-34.

The relationship between fracture size and maximum displacement for naturally occurring faults has been studied by a number of authors including /Peacock and Sanderson 1994, 1997/. These authors studied a variety of faults within the United Kingdom and their study included both normal and strike-slip faults, Figure 2-35. It was found that the different types of faults had different size/displacement ratios (r/d_{max} where r is the radius of the fracture and d_{max} the maximum displacement). The strike-slip fault segments have a mean r/d_{max} ratio of 24.2 (range 1.34 to 109), while the normal fault segments at Kilve have a mean r/d_{max} ratio of 65.3 (range of 10 to 307). This is much lower than the mean ratio of 143 found for the isolated British coalfield normal faults and the authors suggest that this is probable because of fault interaction at Kilve which would tend to reduce the ratio.

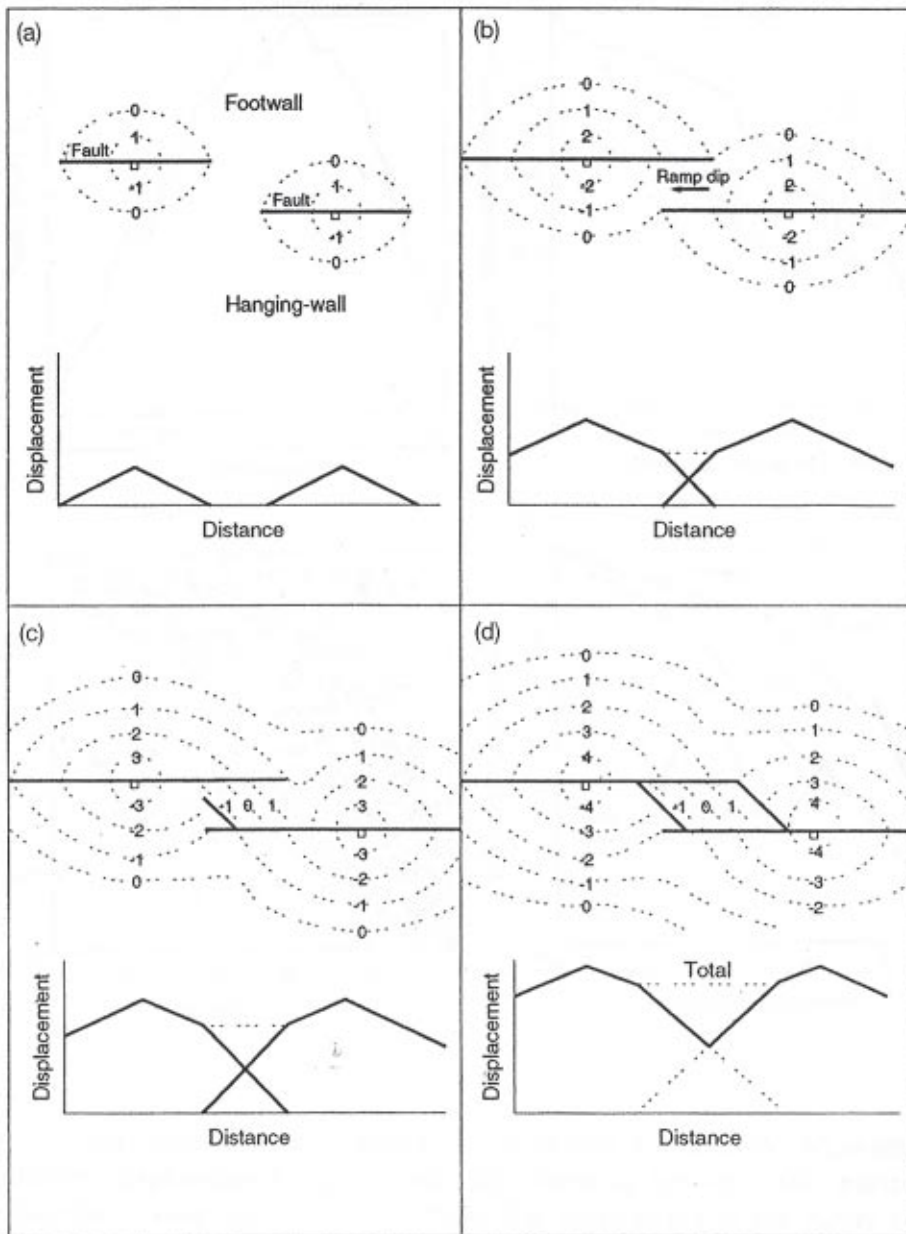


Figure 2-32. Structure contour patterns and displacement (d)/distance (x) graphs at four stages in relay ramp development. The ticks are on the down-throw side of the faults. Half-basin type down-folding occurs in the hanging-wall, and up-folding occurs in the footwall. At stage a) the faults do not interact, so the isolated segments have approximately linear d/x graphs. At stage b) the faults begin to interact, so displacement is transferred between the faults by rotation of the intervening rock block, producing a ramp. At stage c) connecting fractures start to link the overstepping segments and at stage d) the ramp is destroyed, producing a fault bend in map view /from Peacock and Sanderson 1997/.

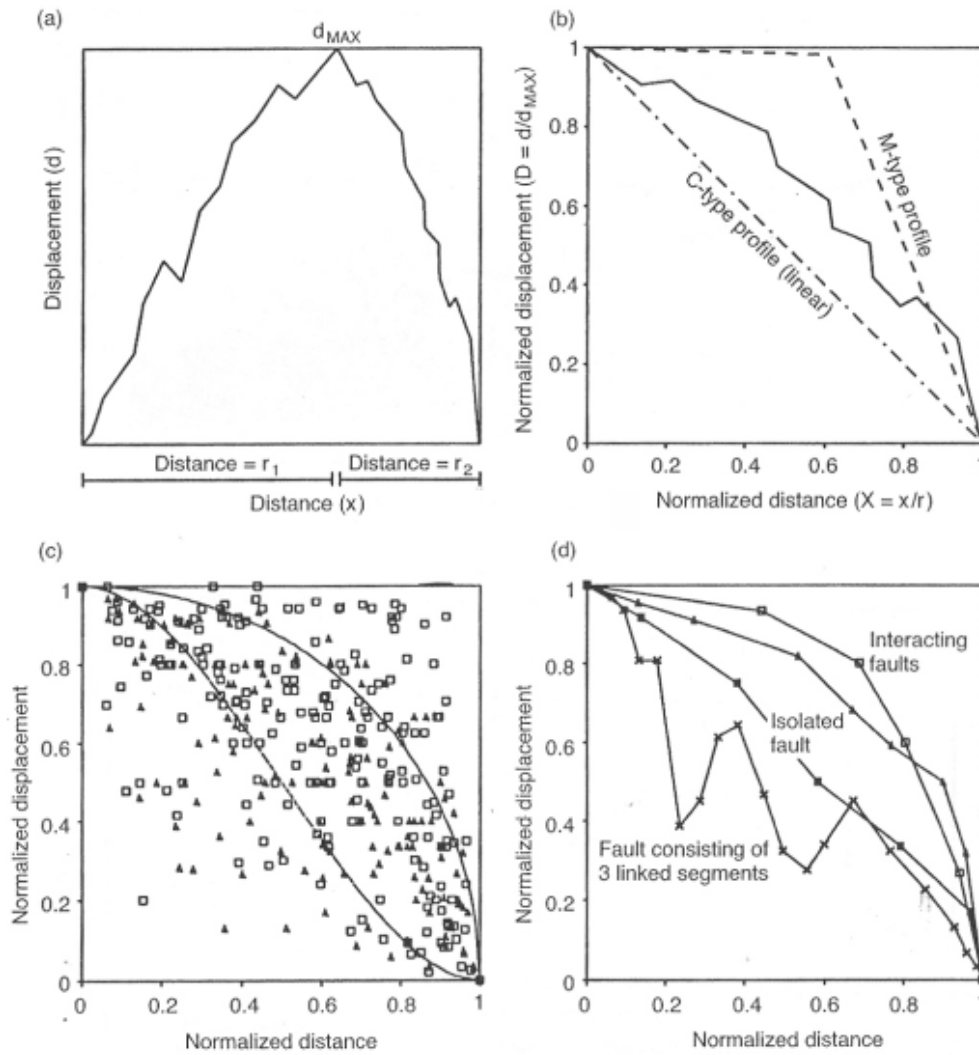


Figure 2-33. (a) Displacement-distance ($d-x$) profile for a fault, showing the maximum displacement (d_{MAX}) and the distance between the maximum displacement point and the tip (r). Note that d_{MAX} is not at the centre of the trace. (b) Normalized displacement-distance ($D-X$) graph for the right hand part of the fault in (a). (c) $D-X$ data for strike-slip faults from Kirkcudbright, SW Scotland (open squares) and for normal faults at Kilve, Somerset (triangles). The $D-X$ profile for a single slip event in an elastic material (solid line) and for a Walsh and Waterson 1987 model (dashed line) are also shown. (d) Examples of $D-X$ profiles for individual fault segments in a fault zone at Kilve. Differences in the profiles can be related to their linkage characteristics. [from Peacock and Sanderson 1997].

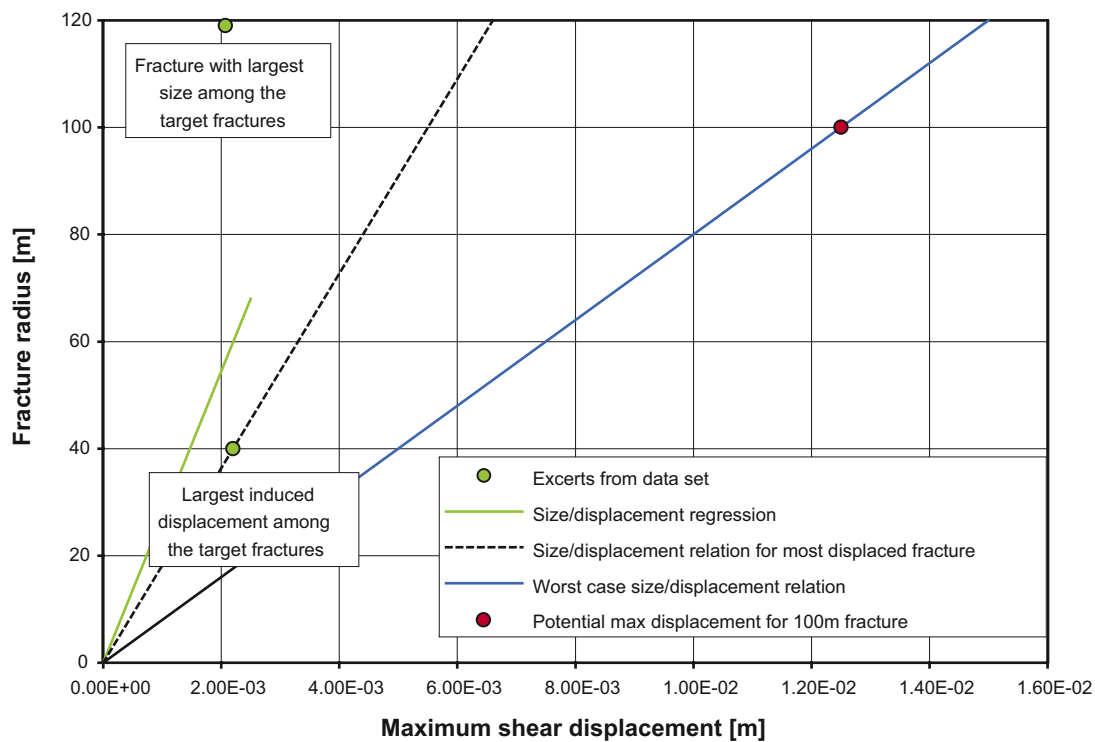
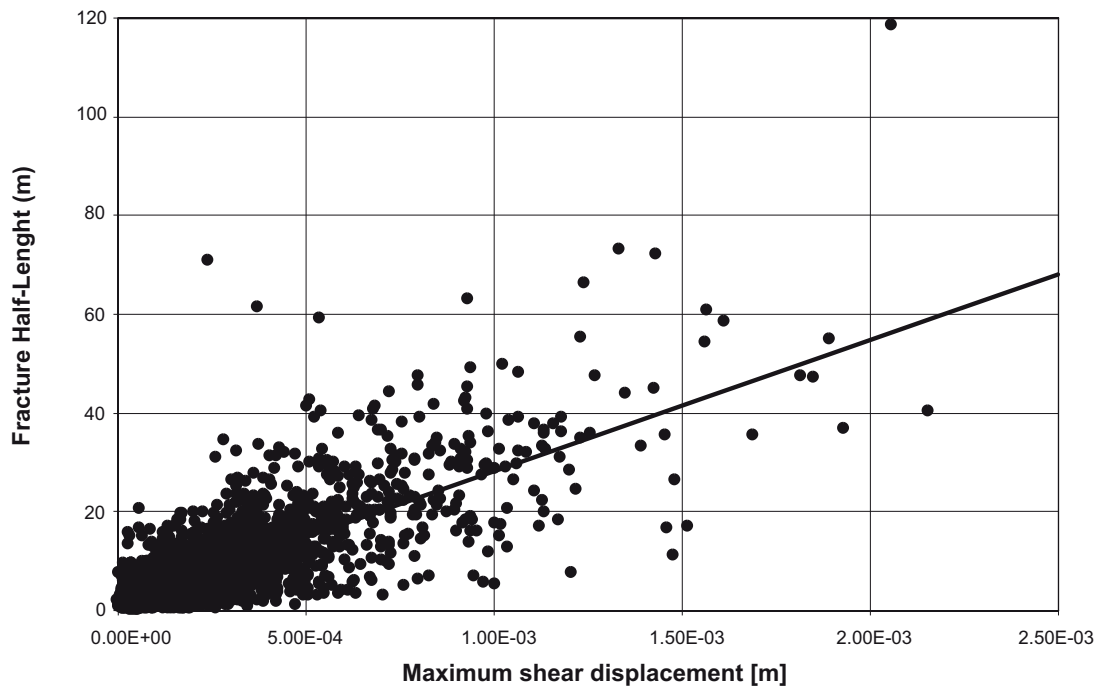


Figure 2-34. Upper graph showing the induced shear displacements on a population of target fractures within a box-shaped rock volume 2 km away from a fault generating a Magnitude 6.1 earthquake. Numerical simulation from /La Pointe et al. 1997/. Lower graph showing the maximum possible displacements of a fracture with 100 m radius. The worst case size/displacement relation is assumed to apply to fractures at closest possible distance from the earthquake fault (i.e. 2 km) /from Munier and Hökmark 2004/.

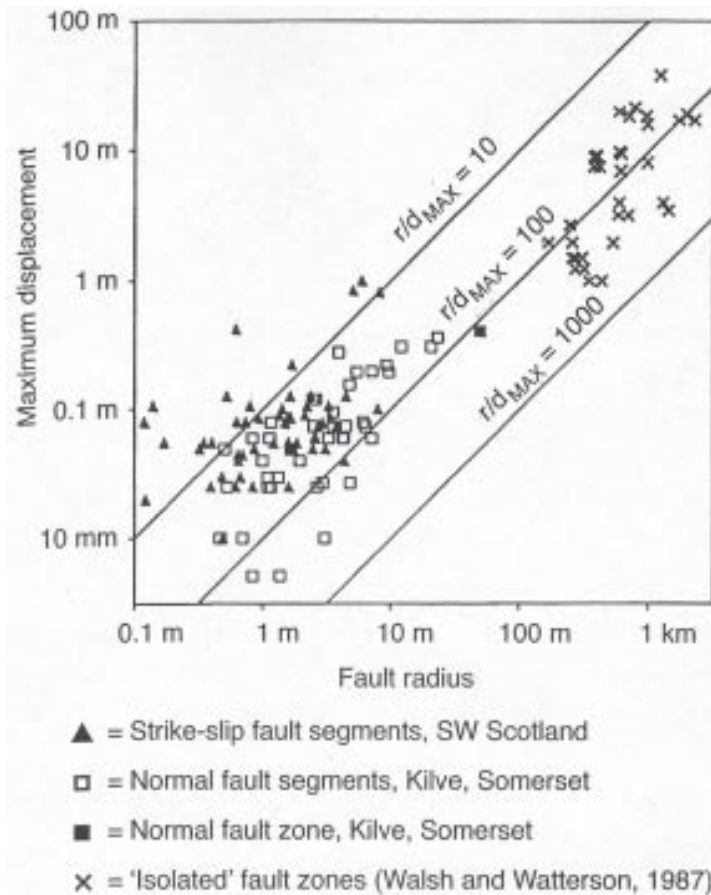


Figure 2-35. Graph of r (distance between the point of maximum displacement and the fault tip) and d_{MAX} (the maximum displacement). Because the displacement profiles are asymmetric (see e.g. Figure 2-32a), each fault can have two points on this graph, each point representing one side of the fault trace from the maximum displacement point. The scatter of points illustrates the variability of r/d_{MAX} data. /from Peacock and Sanderson 1994/.

Although two processes of fracture propagation have been discussed, namely “Growth through a process zone” and “Growth by fracture linkage” it is pertinent to enquire whether they are unrelated processes or whether the latter is simply an up-scaled version of the former. However, this point is not relevant to the problem under consideration, namely that of establishing criteria that indicate the size of a fractures and will therefore not be discussed further here.

Although the above discussion of the relationship between fracture length and displacement has focused on shear fractures and shear displacement, it applies equally to extensional fractures where the displacement is normal to rather than parallel to the fracture walls.

There is therefore an established link between fracture size and displacement for both shear and extensional fractures and it follows that, in theory, displacement can be used an indication of fracture size.

2.6.3 The influence of fault linkage on the displacement profile of a fracture

As pointed out above, Figure 2-32, the process of fault linkage can dramatically influence the displacement profile demonstrating that displacement is not always a direct indication of fracture size. In addition, it has been shown above that displacements vary along a fracture's length and that the amount of shear (or dilation) is determined by both the

- Fracture size.
- Position along the fracture.

It follows therefore that even if a 100 m fracture (i.e. a critical fracture) cuts a deposition hole, unless the intersection is in the central portion of the fracture where the displacement can reach 10 cm, the displacements associated with its re-shear in response to post-glacial fault seismicity will not be of sufficient magnitude to rupture the canister.

2.6.4 Conclusions

Two processes of fracture propagation have been recognised in rocks, (i) the propagation of a fracture through its own process zone by the linking of micro-cracks and (ii) the linking of macro-fractures. The displacement profiles associated with the two processes when linked to shear fracturing are likely to be very different. In the former, maximum displacement generally occurs in the central region of the fracture and dies to zero at the fracture tips. In the latter, composite fracture, the displacement profiles of the two fractures combine and the net displacement is generally less along the composite fracture than along a single fracture of the same size. In addition, the maximum displacement does not usually occur in the middle of the fracture.

Regardless of the different displacement profiles, displacement is one of the parameters that links most directly to fracture size. However, because it varies along a fracture becoming progressively smaller as the fracture tip is approached, it follows that the identification of a small displacement along a fracture CANNOT be taken to indicate that the fracture is small.

2.7 Spacing distribution and the evolution of fracture sets and networks

2.7.1 Fracture spacing

Although the specific remit of this report is to consider the methods that can be used to detect critical deformation zones in boreholes and underground excavations, the authors point out that the task of doing so is aided considerably if the investigator has a good understanding of the processes by which the different deformation zones are generated and the parameters that determine the distribution of the zones within the rock. This section addresses the latter of these two points. It is argued that a clear understanding of this fundamental problem and of the parameters that influence the distribution of deformation within a rock mass will be of great help when faced with the task of determining the location of deformation zones within a proposed repository site.

There has been considerable work carried out on the study of fracture spacing and of the parameters that control this, using a variety of techniques including field observations, theoretical studies, and analogue and numerical modelling /see e.g. Bogdanov 1947, Price 1966, Rives et al. 1992, Wu and Pollard 1995, Bai and Pollard 2000ab, Renshaw and Pollard 1994b, Olson 1993/.

Different patterns of fracture spacing have been reported including negative exponential, power law, log normal and normal, and the mechanism behind these different distributions has been discussed by /Rives et al. 1992/ who suggest that they represent different stages in the evolution of a fracture set.

They argue that the fractures are initiated at randomly distributed irregularities within the material and that consequently initially, the histogram of fracture spacing plots on a negative exponential curve, reflecting the random spacing of the flaws. As the fracture set develops and the fractures become larger, they begin to sense each others presence and consequently begin to interact. At this stage they begin to influence fracture spacing and the histogram changes from negative exponential to “log normal”. As the fracture set continues to develop the histogram begins to display a “normal” distribution. This trend is clearly seen in Figure 2-36, which shows the ideal distribution patterns in the top three diagrams and the gradual change from negative exponential to normal distribution observed as a fracture set evolves in an analogue model from 65, though 109 to 140 fractures (bottom three diagrams in the left hand column). The differences between the histograms linked to a random process and those linked to a process where feedback from pre-existing fractures impacts on the generation of new fractures, is shown in Figure 2-37.

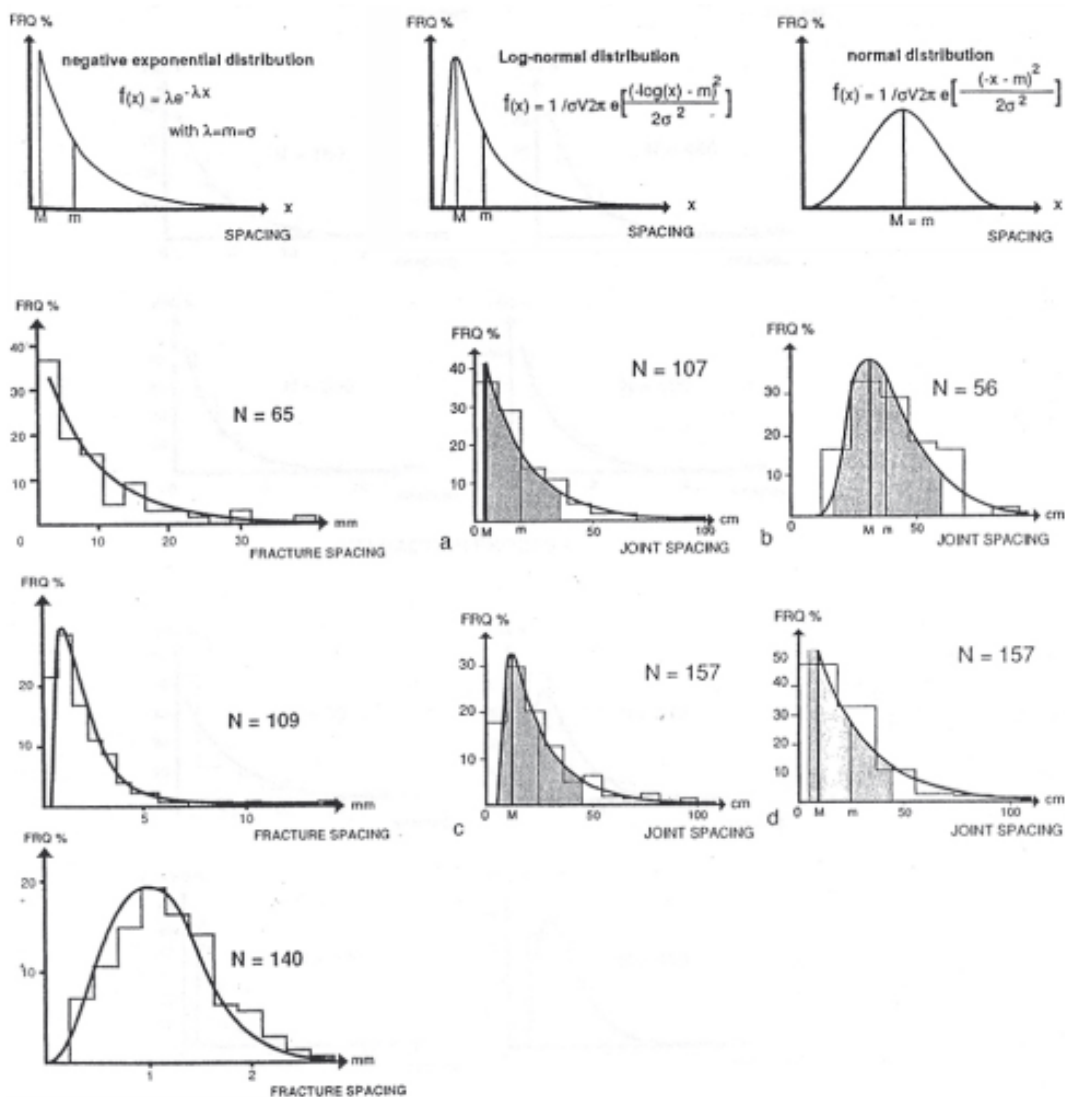
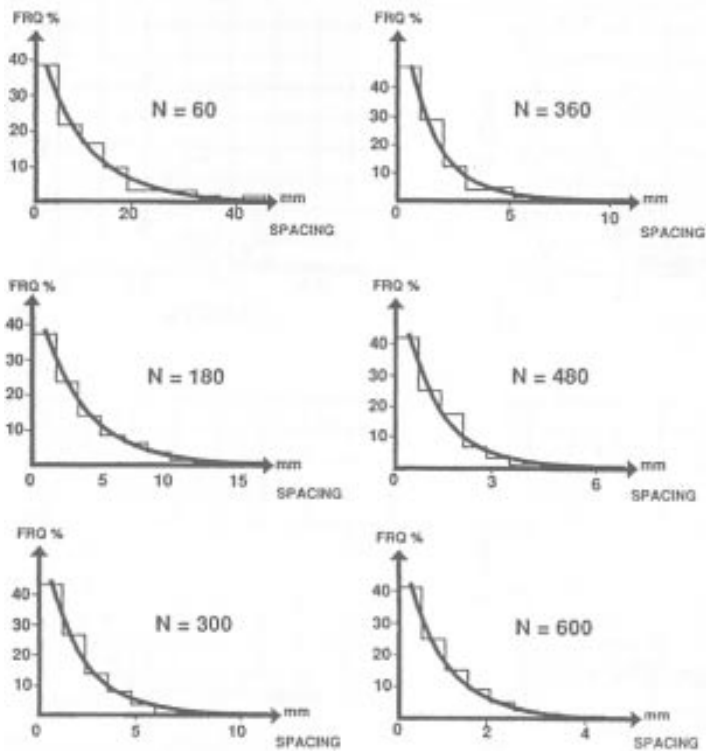


Figure 2-36. Top three graphs show the different types of distribution laws found for natural fractures. M = mode, m = mean and σ = standard deviation. Lower three left hand diagrams show histograms and fitted distribution laws of the spacing observed at different stages of the generation of fractures in an analogue model, i.e. after a few fractures, ($N = 65$), at an intermediate fracture density, ($N = 109$, and at a high fracture density ($n = 140$). Four shaded histograms and fitted distribution laws for joint spacing values sampled in three areas around the U.K.: N = number of values, shaded zones represent the standard deviation. a) a negative exponential distribution, b) a log normal fit, c) log normal and d) negative exponential /from Rives et al. 1992/.



INTERACTION PROCESS

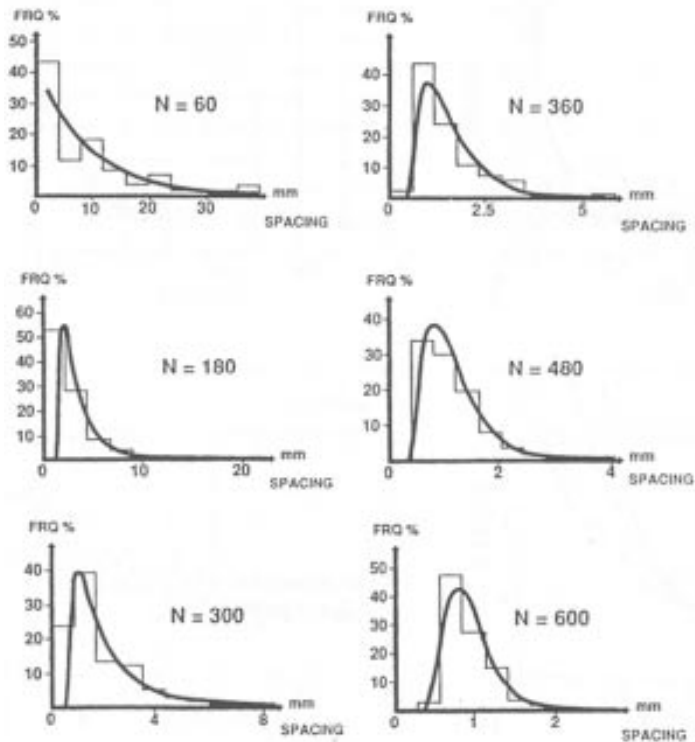


Figure 2-37. The top six diagrams show histograms plus fitted distribution laws at different stages in the generation of a fracture set in an analogue model, with a RANDOM process. With increasing fracture density (increasing N) the type of distribution law (negative exponential) stays the same. The bottom 6 diagrams show histograms plus fitted distribution laws at different stages in the generation of a fracture set in an analogue model, with an INTERACTION process. With increasing fracture density (increasing N) the type of distribution law varies from negative exponential, to log normal to almost normal after 600 fractures have formed /from Rives et al. 1992/.

2.7.2 Distribution laws of fracture spacing

In their paper, /Rives et al. 1992/ introduce some fundamental concepts relating to the different distribution laws of fracture spacing and their implication regarding the process of fracture development. To summarize,

- i They point out that if the process of fracture initiation remains a random process during the propagation of all the fractures during the evolution of the complete fracture set, i.e. if at all stages in the evolution of the fracture set the system remains uninfluenced by the generation of the fractures, the fracture spacing distribution will always plot as a negative exponential distribution.
- ii However, they note that this does not occur and that at some point in the evolution of the fracture set, the influence of earlier formed fractures is “felt” by the new fractures and consequently begins to influence the location of fracture initiation. This point in the evolution of the fracture set is marked by a change in the spacing distribution from negative exponential to log-normal and eventually normal.
- iii These authors introduce the concept of saturation to describe the evolution of the fracture set from an initial random distribution of a few early fractures to a system where the material is saturated with fractures and the formation of new fractures ceases.

One of the most convincing explanations for the linear relationship between layer thickness and fracture spacing first recorded by /Bogdanov 1947/, working in coal in the USSR, is provided by /Bai and Pollard 2000b/. They examined the stress distribution between two adjacent opening mode fractures as a function of the fracture spacing to layer thickness ratio. The results show that when the fracture spacing to layer thickness changes from greater than to less than a “critical value” (approximately 1.0) the normal stress acting perpendicular to the fractures changes from tensile to compressive. This stress state transition precludes further infilling of fractures unless there are existing flaws and/or the fractures are driven by an internal fluid pressure or other mechanism. Hence, for fractures driven by tectonic extension, the critical fracture spacing to layer thickness ratio defines a lower limit, which also defines the condition of “fracture saturation”.

Bai and Pollard (op. cit.) found that the critical value of fracture spacing to layer thickness increases with increasing ratio of Young’s modulus of the fractured layer to the neighbouring layers and with increasing overburden stress (depth) but it decreases with increasing Poisson’s ratio of the adjacent layers. They note that for geologically realistic values of the elastic constants and depths the critical fracture spacing to layer thickness ratio varies between 0.8 and 1.2, a range which encompasses the often cited ratio of 1.0 in the literature for well-developed fracture sets.

2.7.3 Experimental study of fracture spacing

In an experimental study of fracturing /Wu and Pollard 1995/ provided examples which showed the evolution of a fracture set and the onset of “fracture saturation”. They found that when the applied strain reached a certain value, fracture spacing stopped evolving and remained nearly constant. At this stage in the deformation, the fracture sets were well-developed. They found that the spacing at saturation was a function of layer thickness but was independent of strain whereas spacing before saturation varies strongly with applied strain. The onset of fracture saturation is apparent from the plot of fracture spacing against strain for these experiments, shown in Figure 2-38. It can be seen that after a certain amount of strain the fracture separation (S) stabilises at a value of $S/T = 1.0$ where T is the layer thickness.

It can also be argued that in addition to the distribution patterns of the fracture spacing changing with time, the distribution of fracture apertures also changes. I.e. both can be used to indicate the stage of evolution of the fracture set from initiation to saturation.

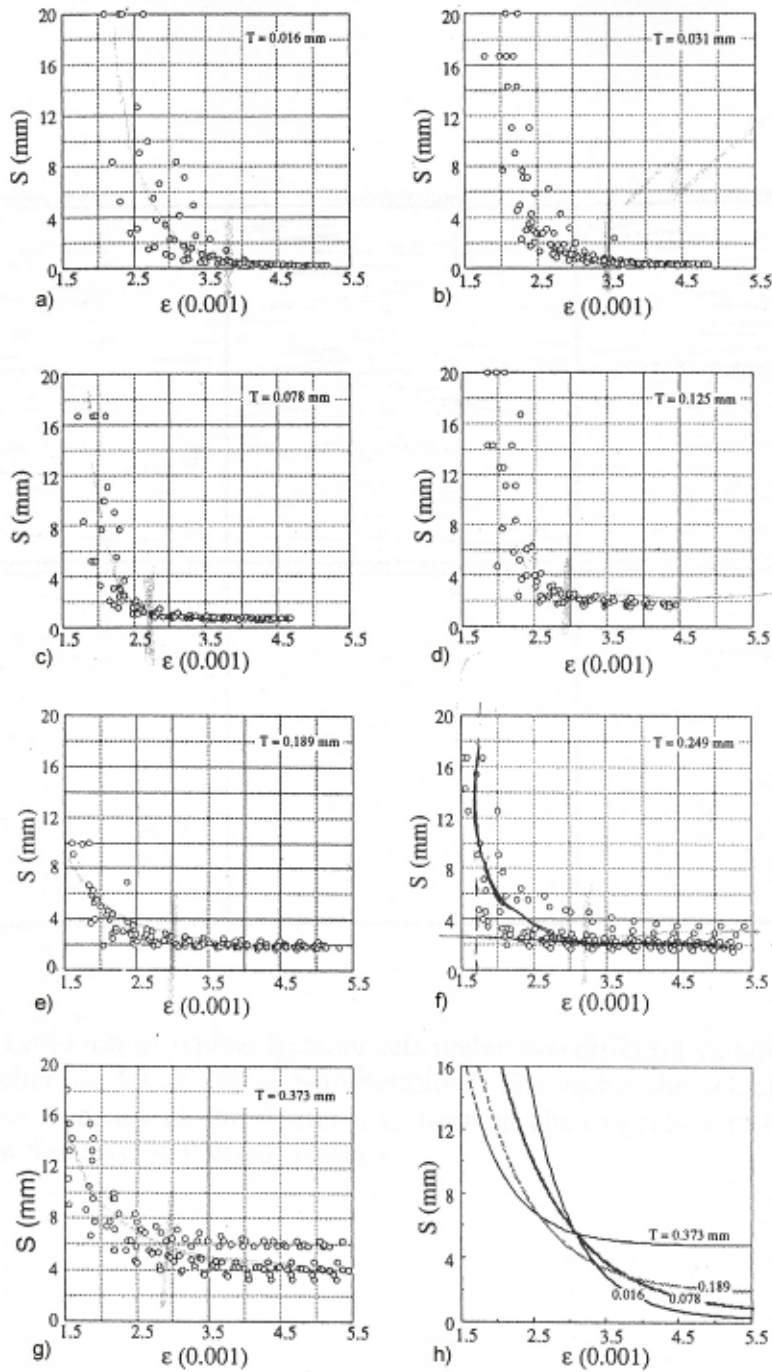


Figure 2-38. a)–g) Plots of fracture spacing against applied strain for a series of experiments on layers of different thickness T . h) curve s fitted to the experimental data. The spacing at saturation is directly proportional to the layer thickness [from Wu and Pollard 1995].

The occurrence of anomalously close fracture spacing.

Despite the numerous examples of a direct relationship between fracture spacing and bed thickness described in the literature and the various explanations for this phenomenon, examples occur in nature where the spacing of fractures is significantly lower than that normally observed in saturated fracture sets. Theoretically, as noted above, saturation is marked by a range of spacing thickness ratios (S/T) between 0.8 and 1.2. Values greater than 1.2 are explained by arguing that the fracturing process has not yet reached saturation level. In an attempt to explain ratios of < 0.8, /Bai and Pollard 2000a/ studied the possibility of “further fracture infilling” by considering flaw distributions between adjacent fractures loaded by extension of the layer. It was found that depending on their position with respect to the existing fractures, some of these flaws could grow into fractures cutting across the layer. For example, if the elastic constants are the same for the fractured and neighbouring layers, then if the new fracture has an S/T ratio of greater than 0.55 it can grow and completely cut the layer.

2.7.4 Clustering versus uniform distribution of fractures

A fracture zone is a general term used by geologists to describe a planar or sub-planar concentration of fractures in a rock. They can be either shear fractures or extensional fractures.

Shear fracture zones have the same spatial relationship to their formative stress field as do discrete shear fractures, cf Figure 2-2a and Figure 2-19b and c bottom diagram. As noted in Section 2.5, the formation of a “shear fracture zone” can occur as a result of continued movement on a shear fracture and the development of more and more second-order fractures.

Extensional fracture zones also occur in rocks and one of the characteristic features of many extensional fracture sets observed in nature and produced either in analogue and numerical models is that of “fracture clustering”. Instead of uniform fracture spacing, clusters of closely spaced fractures develop separated by areas of uniform fracture spacing. The process by which these “fracture clusters” are generated is discussed in the following paragraphs

Two numerical model studies of fracture distribution /Renshaw and Pollard 1994b, Olson 2004/ illustrate the phenomenon of fracture clustering well and offer an explanation as to why such a distribution might develop. The numerical modelling used in this study simulates the mechanical interaction between fractures and the results compare well with experimentally generated fracture sets in analogue models. Renshaw and Pollard found that in their numerical models, once the flaw geometry is specified only one parameter, the velocity exponent, α (which relates the fracture propagation velocity, v , to the stress intensity factor at the fracture tip, K_I), controls the geometric evolution of the fracture set. Sensitivity analysis shows that this parameter also controls the extent to which fracture growth is concentrated within zones or clusters. The amount each fracture tip is advanced for each increment of deformation is given by;

$$l_{adv} = 2a_0 \left(\frac{G}{G_{max}} \right)^\alpha \quad \text{Equation 2-5}$$

where l_{adv} the amount each fracture tip is advanced during an increment of extension, $2a_0$ is the flaw length, G is the elastic energy release rate for the fracture tip, G_{max} is the maximum energy release rate in the fracture set at the current growth iteration and α the velocity exponent.

Figure 2-39 shows the development of typical fracture sets in two models which only differ in the values of their velocity exponents. The initial distribution of flaws in both experiments is the same. As α is decreased the growth rate of the fractures becomes less dependant on the stress intensity factor (i.e. the stress concentration at the fracture tips) distribution across the network, Equation 2-5, and all the fractures tend to grow at a similar rate regardless of the presence or absence of nearby fractures.

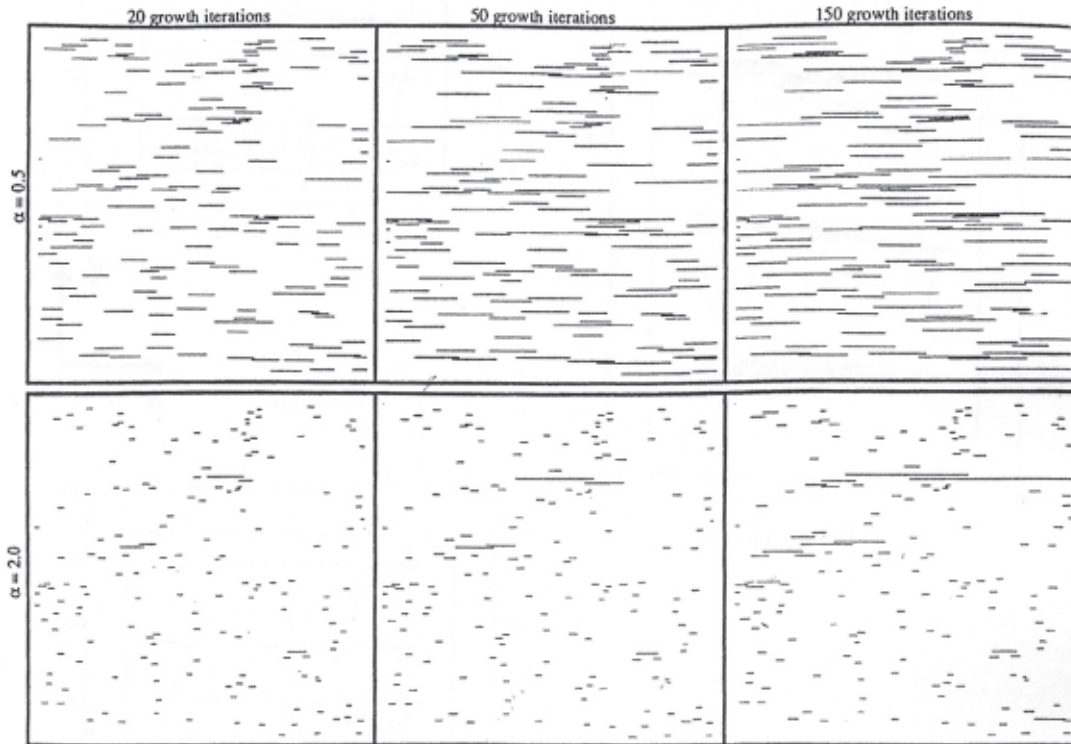


Figure 2-39. The evolution of typical fracture sets under two different velocity exponents α , indicated after 20, 50, and 100 growth iterations. The higher the velocity exponent, the greater the tendency of the fractures to form in clusters rather to be uniformly spaced /from Renshaw and Pollard 1994a/.

Thus any clustering present in the network tends to reflect the original clustering of the flaws rather than the selective growth of the clustered fractures. In contrast, as α is increased, only those fractures with the largest stress intensity factors will grow. Growth will be concentrated in those areas where the geometry of the fractures is such that the mechanical interaction of the flaws and fractures, leads to amplification of the energy release rates rather than to shielding. The restriction of growth to fewer and fewer fractures as α is increased leads to the development of fracture zones which are separated by zones of little or no fracture growth, $\alpha = 20$, Figure 2-37.

Similar results are presented by /Olson 1993/. He also investigated the sub-critical crack growth of a fracture set using numerical modelling techniques. The model calculates the mechanical interaction between simultaneously propagating fractures and uses the sub-critical crack propagation rule where propagation velocity during stable crack growth scales with the crack tip scale intensity factor K_I . The propagating velocity, v , is related to the opening-mode (extensional fracture) stress intensity factor K_I , with an empirically quantifiable, power-law relationship:

$$v = A \left(\frac{K_I}{K_{Ic}} \right)^n \quad \text{Equation 2-6}$$

where K_{Ic} is the critical fracture toughness, n is the sub-critical index and A is a proportionality constant. It is found that n is dependant on rock type and environmental conditions (such as wet v dry). Reported values vary from 20 or less for sandstones submerged in water /Atkinson 1984/ to values greater than 250 under dry conditions in carbonates /Olson et al. 2002/. The evolution of fracture sets in three models identical in all respects except for the value of the sub-critical indices, is shown in Figure 2-40a. It can be seen that the tendency for the fractures to cluster rather than form in a uniform distribution is directly related to the index value.

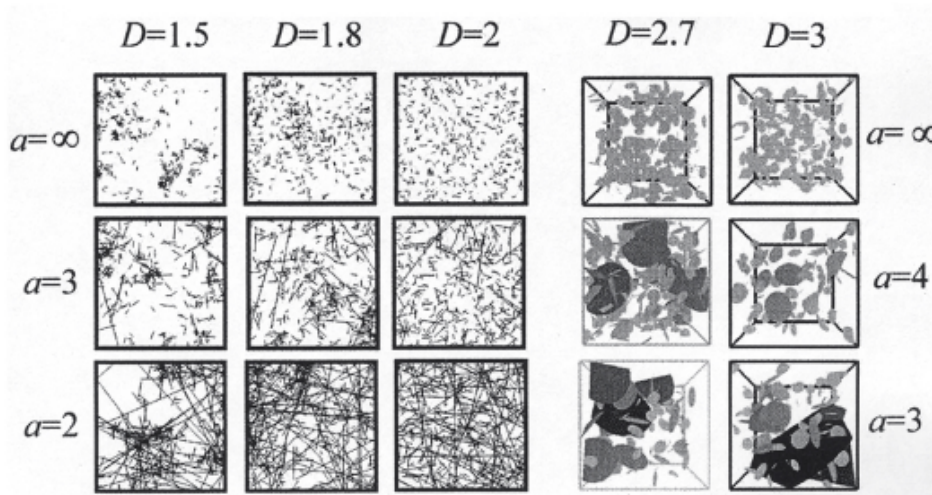
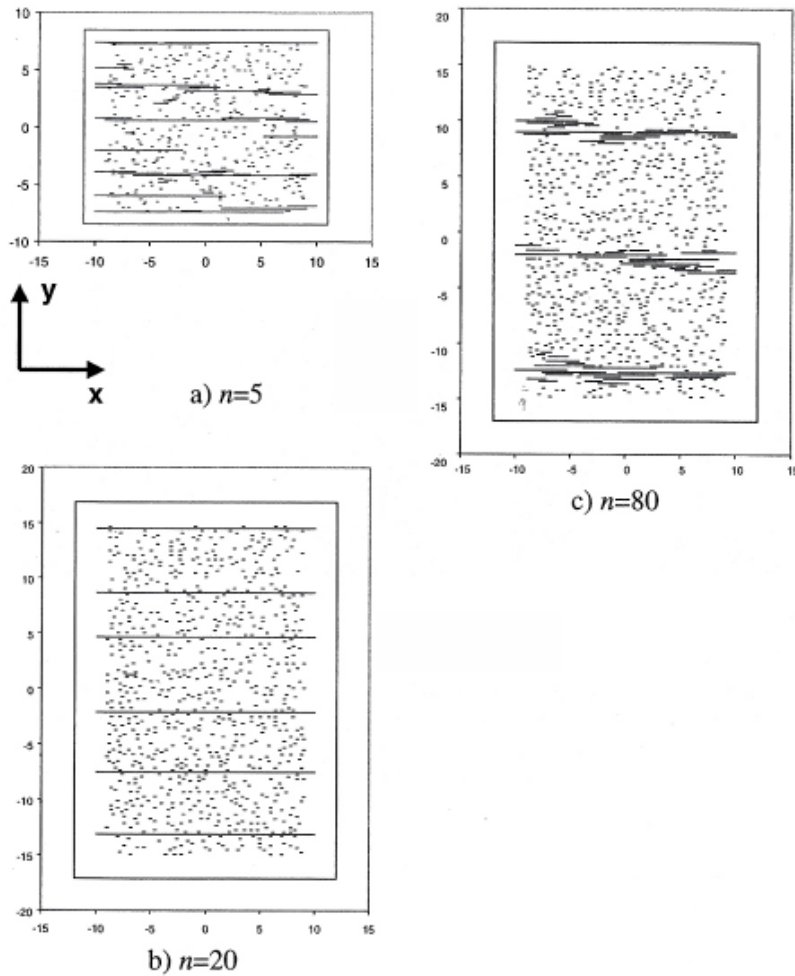


Figure 2-40. Examples of sub-critical fracture growth for sub-critical indices (n)* a) $n = 5$, b) $n = 20$ and c) $n = 80$. All simulations start with the same randomly located parallel flaws. An extensional strain was applied in the y direction at a constant strain rate. n is determined by rock type and environmental conditions and, as can be seen from the experimental results, has a dramatic influence of fracture spacing *It can be demonstrated empirically that $v = A (K_I/K_{Ic})^n$ where K_I is the stress intensity factor at the crack tip, K_{Ic} is the critical fracture toughness v is the sub-critical crack propagation velocity, A is a proportionality constant and the power n the sub-critical index. From /Olson 2004/. Bottom diagram shows examples of synthetic fracture networks generated from two fracture sets with power law length distributions, with varying values of the exponent α (top to bottom) and of the fractal dimension D (left to right). A decrease in α results in an increase in the proportion of large fractures. A decrease in D results in an increase of the clustering between fractures /from Darcel et al. 2003/.

Work by /Darcel et al. 2003/ on the stereological analysis of fractal fracture networks provides further insight into the clustering of fractures. They consider a 3D fracture network made up of two populations of fracture lengths l_1 and l_2 and consider the probability of intersection between the two populations. They derive the stereological function that gives the fracture distribution seen in 2D outcrops or 1D scan lines. They focus on the example of a fractal fracture network with a power law length distribution whose exponent α is independent of the fractal dimension, D . Figure 2-40 (lower diagram) shows examples of synthetic fracture networks generated with varying values of the exponent α (top to bottom) and of the fractal dimension D (left to right). A decrease in α implies an increase in the proportion of large fractures. A decrease in D implies an increase of the clustering between fractures. It follows that the degree of clustering can be quantified by the fractal dimension.

2.7.5 Conclusions

Understanding the distribution of fractures within a particular fracture set is essential if one wishes to predict the likely location of fractures within that set. A study of fracture distribution in natural rocks, analogue experiments and in numerical models has shown that the distribution is influenced by a variety of parameters and can vary from a random distribution, through a uniform spacing to the clustering of fractures. This depends primarily on the degree of development of the fracture set and upon the rock mechanics properties.

An understanding of this process is important when attempting to establish the likely position of adjacent fractures of a particular fracture set.

2.8 Frequency/size distribution patterns – issues of scale dependency and self similarity

2.8.1 Range of fracture size

As already noted in the Section 2.2 entitled “Missing Data” the principal task being addressed by the present study is that of determining a methodology of detecting critical “fractures” from tunnels, and deposition holes and an important part of such a study is to establish the range of fracture sizes that characterize the two study areas of Oskarshamn and Forsmark. These data have been collected for these areas using:

- Outcrop data of individual fractures.
- Interpretation of lineaments from the site scale.
- Intersections in cored boreholes.

There is a lack of data in the size range of some 10s of metres to 100s of metres as can be seen from Figure 2-1. A likely reason for this missing data relates to the size of typical outcrops in the study areas. These rarely exceed 50 m and put an upper limit on the size of fractures that can be detected from field studies. A study of aerial and satellite images provides fracture length data for fractures of a km length and over but few data are available for fractures in the range 10s to 100s of metres. Because these are the fractures that need to be detected during the construction of the repository it is important to establish whether these fractures are missing from the study areas or whether their absence on the graph of Figure 2-1 simply reflects the limitations of outcrop. There are two available ways of addressing this problem. The first is to draw on observations of fracture length/frequency distributions in areas not so constrained by lack of outcrops of the appropriate size and the second relates to exploiting the few relatively large outcrops in the study areas. These two approaches are discussed in the following sections.

2.8.2 Regional studies of fracture length/frequency

In this section the study of fracture length/frequency data from other regions where data collection is not hindered by lack of suitable sized outcrops is discussed. Three examples are briefly described below together with the resulting data sets.

/Van Dijk et al. 2000/ present fracture length/frequency data from the Monti Alpi region of the Southern Apennines of Italy. The range of data extends from thin section studies to the study of satellite images and involves both surface and subsurface data. The scale range is over 8 orders of magnitude and the resulting fracture frequency/length plot is shown in Figure 2-41. The diagram is composed of ~ 30,000 measurements and the data show that the small-scale and large-scale features form part of one, scale invariant system.

It is noted that if the length/frequency plot is exponential, then this is indicative of scale independence. If such data are plotted on a log/log plot they will produce a straight line (e.g. Figure 2-41). It follows that if only limited data are available but these plot on a distribution curve as an exponential, then by plotting the data on a log/log plot the graph can be extrapolated into regions of little or no data. Thus if it can be established that the limited length/frequency data from the study areas does form part of an exponential distribution it can be argued that the data can be extrapolated into the area where data are missing and can be used to predict the occurrence and density of the critical fractures.

Other studies of fracture length/ frequency distributions have been carried out by Odling et al. 1997, 1999/. In a detailed study of fracture systems on many scales these authors, reviewed the major controls and scaling behaviour of fracture systems expected in reservoir rocks. Lithological layering was found to be important and they identified two end-member fracture systems. In “strata-bound systems” fractures are often confined to single layers, sizes are scale restricted, and spacing is regular. In “non-strata-bound systems” (such as the crystalline basement of Scandinavia) fractures show a wide range of sizes (often power-law), are spatially clustered and vertically persistent.

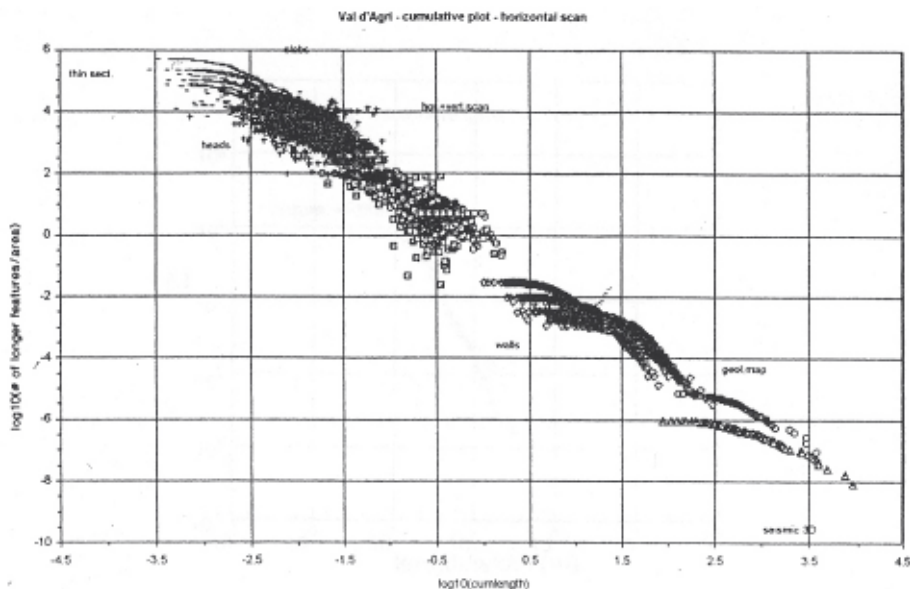


Figure 2-41. Results of a fracture length/frequency analysis. The diagram is constructed using all information regarding both surface and sub-surface data sets. The scale range is over 8 orders of magnitude and the diagram is composed of ~ 30,000 measurements. The data show that the small-scale and large-scale features form part of one, scale invariant system /from Van Dijk et al. 2000/.

These authors present data on cumulative frequency distribution for fracture length from Devonian sandstones of western Norway, Figure 2-42 which shows a striking linear relationship over two orders of magnitude. In a study of the fracture sets from the Tayma region of the Saudi Arabian platform, fractures ranging in length over five orders of magnitude were studied (Figure 2-43). Their cumulative frequency distributions are shown in this figure. Individually the data sets gathered from the various scales of observation (Figure 2-43a–c) show log-normal length distributions but collectively they show an overall power-law distribution.

However, it should not be assumed that there is always an exponential distribution of data on a frequency/length plot of fractures. For example in some parts of the Gulf of Suez rift, there are markedly less “medium-scale” faults than the exponential distribution would predict /Koestler et al. 1995/, and this is true in some North Sea oil fields /e.g. Fossen and Hesthammer 2000/. To the authors’ knowledge there are no reported examples of data falling *above* the straight line representing the exponential distribution. Thus we can take this line to give the maximum number of critical faults to be expected in any area. Based on this argument, an estimate of the maximum number of fractures in the range where the data are missing in Figure 1 can be obtained.

2.8.3 Fracture length/frequency plots from numerical models

Numerical modelling of fracture set formation, using a realistic criterion to account for fracture interaction, has been described in Section 2.7.4 (see e.g. Figures 2-39 and 2-40 and the associated text). The results of these experiments have been plotted on fracture length/frequency plots and these are shown in Figures 2-44 and 2-45. Figure 2-44 shows the length/frequency distribution for the three experiments shown in Figure 2-40a–c and it can be seen that each data set plots as a negative exponential curve. Data from similar experiments are presented in Figure 2-45 and a negative exponential distribution also characterises these results. It is noted that the field data and experimental data give the same fracture length/frequency distribution.

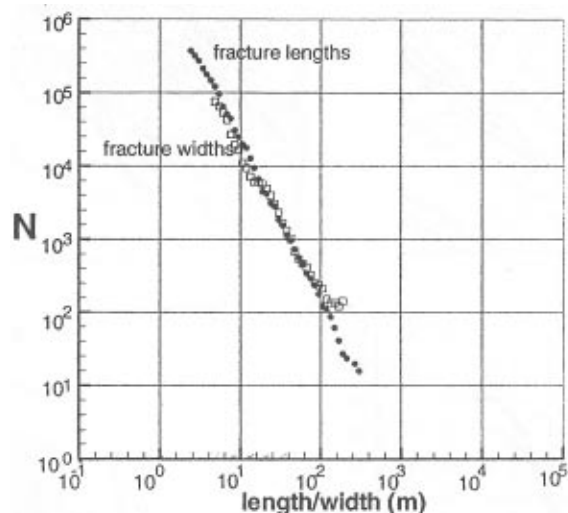


Figure 2-42. Cumulative distribution frequencies of fracture lengths (from bedding plane maps) and widths (from cliff sections). The points represent averages of the cumulative frequency plots from 7 maps and 8 cliff sections. The distributions are not significantly different /from Odling et al. 1999/.

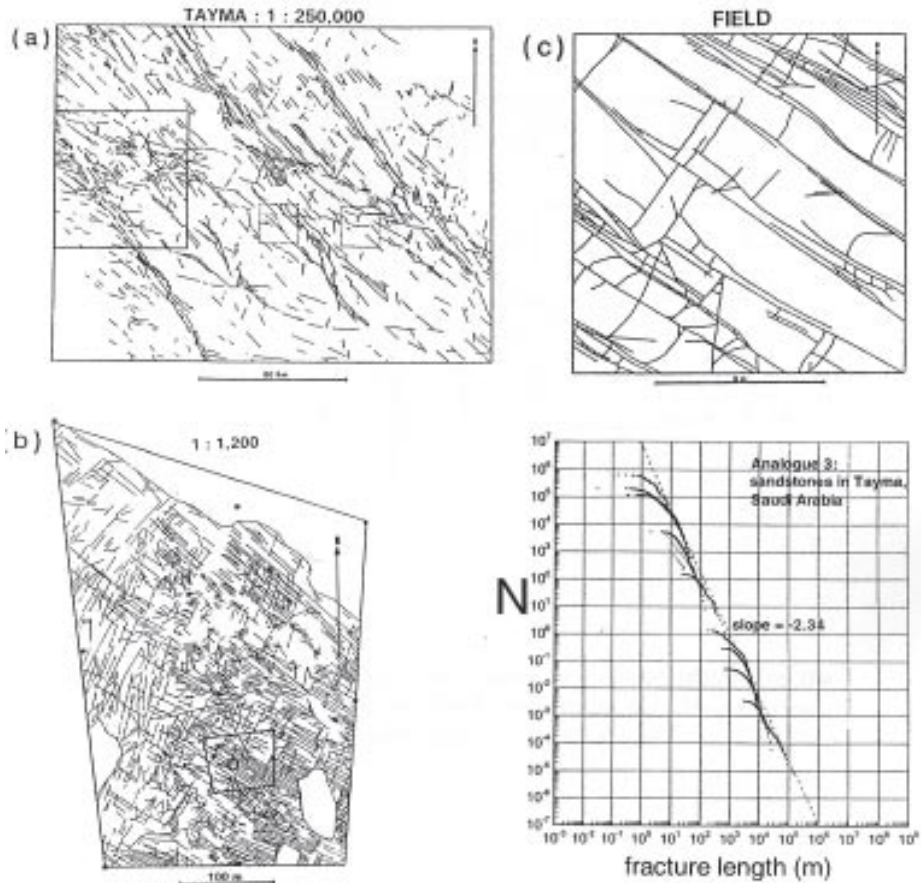


Figure 2-43. a)–c) Three examples of fracturing in the cover rocks of the Tayma region of Saudi Arabia at different scales and resolutions. a) Regional fault and graben system from an air photo mosaic b) low level aerial photo showing joints and c) field map of joints from outcrop surface. The graph shows the cumulative frequency distribution for fracture length constructed from data in a) to c). Individually the data show log-normal length distributions but collectively they show overall power-law behaviour (from Odling et al. 1999).

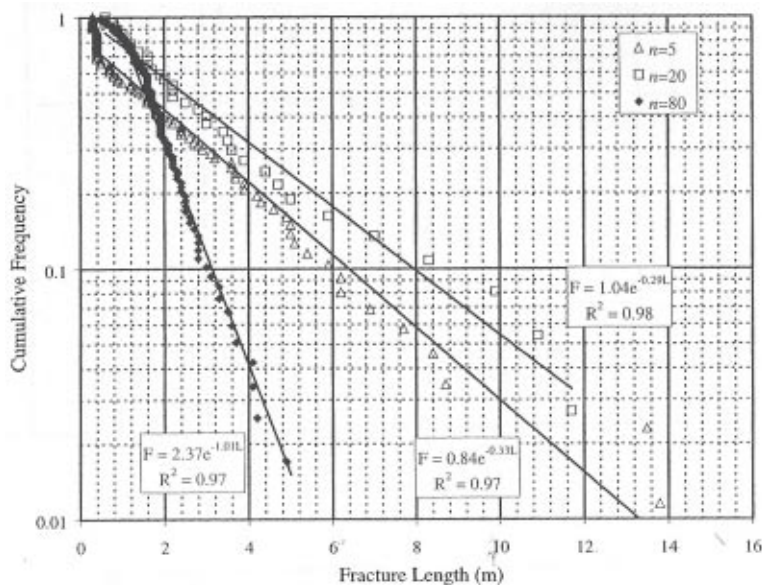


Figure 2-44. Cumulative frequency of fracture length for the patterns from Figure 2-40 a–c. Each case can be well described by a negative exponential curve (from Olson 2004).

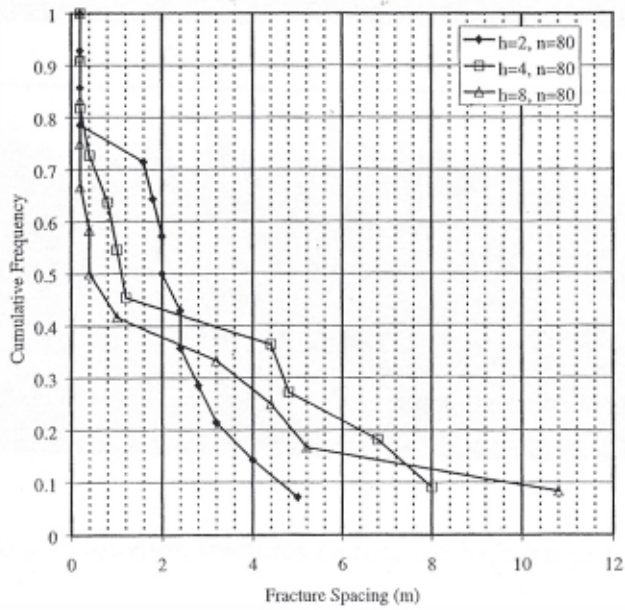
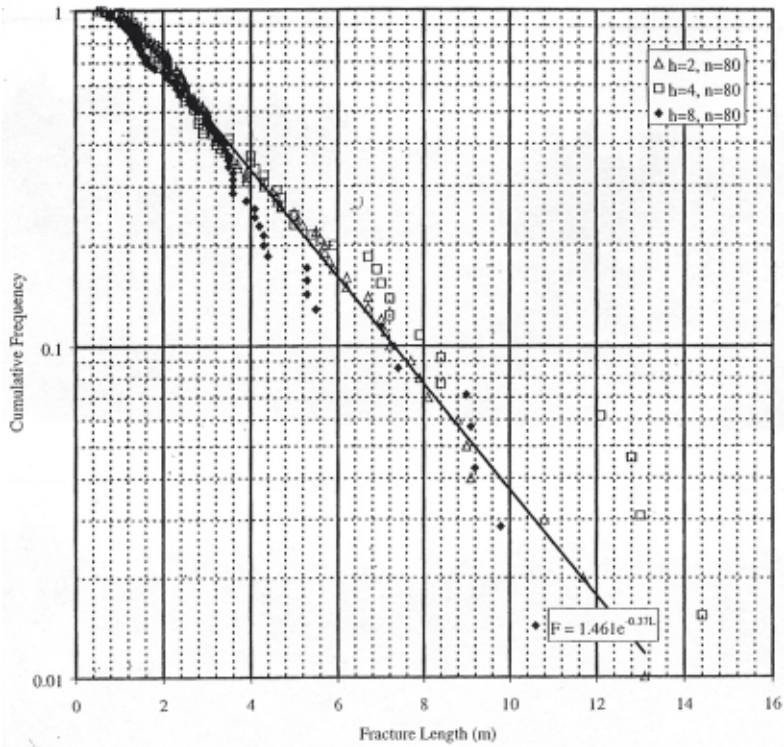


Figure 2-45. The upper diagram shows a plot of fracture length against log cumulative frequency for fractures in three numerical models. Note that all three patterns have markedly similar length distributions that follow a negative exponential curve. The bottom diagram shows the plot of fracture spacing against cumulative frequency for the same experiments [from Olson 2004/.

2.8.4 Direct observations of critical fractures in the study areas

It has been noted that the average size of outcrop in the study areas precludes the direct observation of fractures greater than ~ 50 m in diameter. However, quarrying in the Oskarshamn area has provided exposures large enough for these fractures to be observed. A study of these exposures confirms that fractures of this size exist and the outcrops are often dominated by single, discrete sub-horizontal exfoliation fractures several 100 m in length, Figure 2-46.

These fractures occur in the upper 150 m of the crust as a result of exhumation and removal of overburden stress and they are the result of the release of residual stresses. Below this depth the same residual stresses exist in the rock and there is the possibility that the local removal of the overburden linked to the excavation of the access tunnels and deposition holes may precipitate the formation of such fractures at depth.

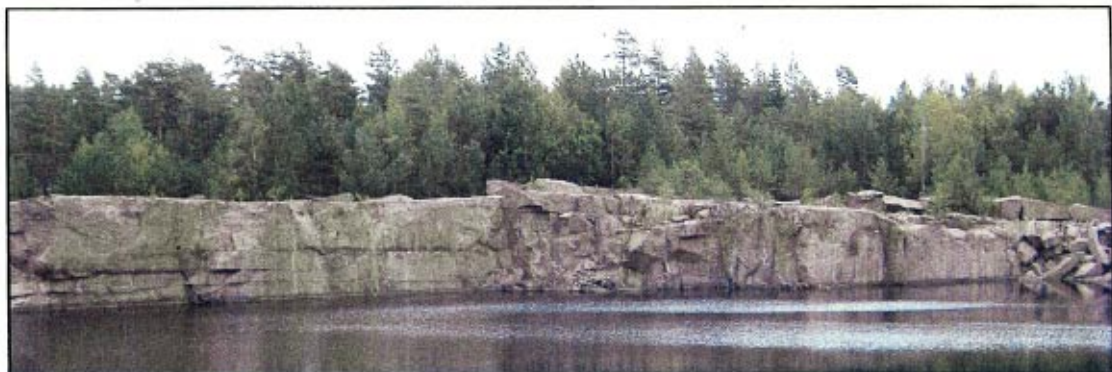
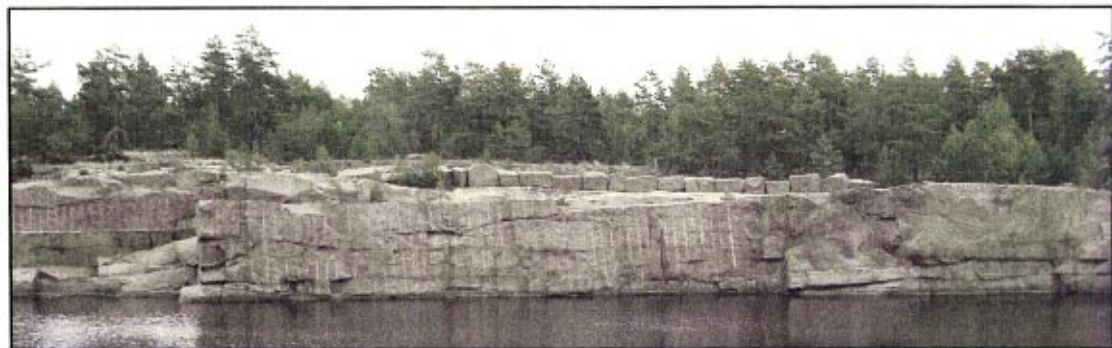
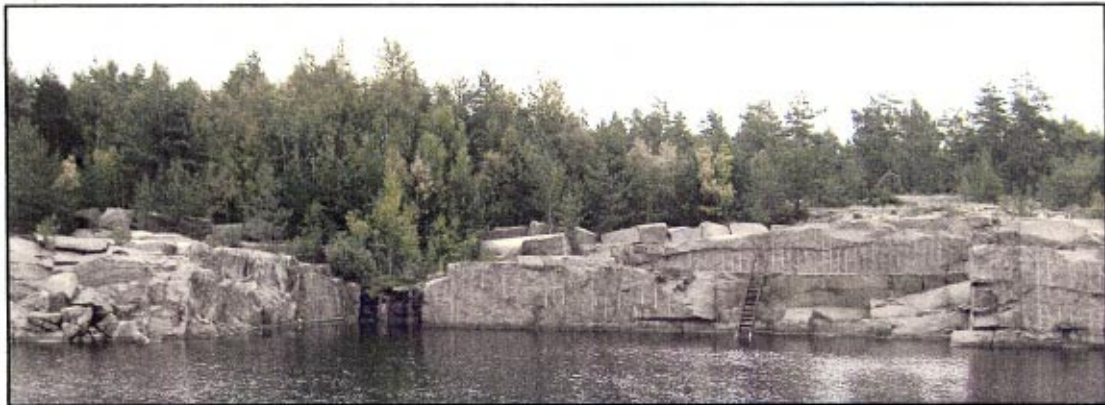


Figure 2-46. Long, continuous exfoliation fractures cutting the bedrock at the Kråkemåla quarry close to the Äspö laboratory. The rock is Gotemar granite which is 1,450 Ma, i.e. considerably younger than the bedrock at Äspö.

Work on fractures has shown that fracture patterns on different scales are often “self similar”. Figure 2-47 shows examples of fault segmentation on various scales ranging from 100 km to 100 mm. The self similar geometry of the various fracture patterns is apparent.

2.8.5 Conclusions

In this section the problem of the missing data in Figure 2-1 has been considered and an attempt made to determine if it represents a real lack of fracturing in the missing range or whether the omission reflects the lack of outcrops of an appropriate size to allow these fractures to be observed.

The two methods of determining this, namely a consideration of similar studies from other areas where fractures of all sizes can be observed (e.g. Figures 2-41 to 2-43) and observations of fractures in the occasional large outcrop in the study areas (Figure 2-46), both indicate that it is likely that the “missing fractures” in Figure 2-1 do occur. We must conclude therefore that there is no rationale for assuming that the missing fractures do not occur at the repository site and must ensure that we have a procedure in place to detect them.

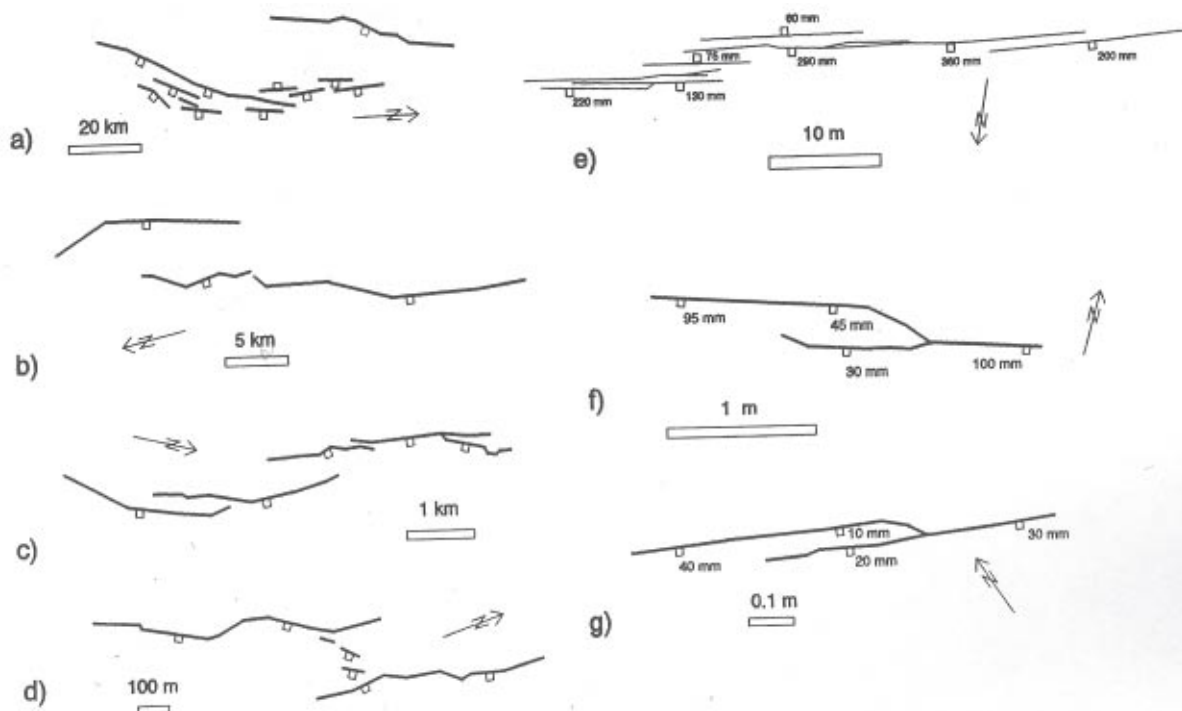


Figure 2-47. Examples of Fault Segmentation on varying scales: a) Beryl embayment, North Sea U.K.; b) active fault traces (Tobin and Pearce faults) in the Central Nevada /Jackson and Leeder 1994/, Figure 7/; c) faults in Volcanic Tableland, California /Dawers and Anders, 1995, Figure 4/; d) Lastros fault zone, Crete / Stewart and Hancock 1991, Figure 5c/; e) fault zone at Kilve, Somerset /Peacock and Sanderson 1994, Figures 7b and 7a respectively, Peacock and Sanderson 1997/.

2.9 Second-order structures linked to larger fractures – kinematic indicators

It was noted in Section 2.5 that because of the different modes of origin of shear fractures and extensional fractures the second order structures associated with them are different. These second order structures may characterise a particular deformation zone and as a result can be of great importance in correlating the zone between excavations (boreholes, tunnels and deposition holes). They can therefore be of first order importance when attempting to determine the length of a fracture (or other deformation zone) a task which is the principal aim of this report. The procedure for classifying the deformation zone intersections in boreholes and tunnels is discussed further in Section 10 and summarised in the table in Figure 2-59.

2.9.1 Second order structures

Extensional deformation can produce discrete extensional fractures and clusters of extensional fractures. Kinematic indicators associated with these structures include:

- Plumose structures, Figures 2-7 to 2-9.
- Fibrous minerals infilling these fractures at the time of their formation will grow with the fibres at right angles to the fracture wall, i.e. indicating opening of the fracture, Figure 2-10a.

Shear deformation can produce discrete shear fractures (Figure 2-2a), brittle deformation zones (Figures 2-2b and c) and ductile deformation zones (Figures 2-2d and 2-48). Kinematic indicators associated with these structures include:

- Slickensides, i.e. lineations formed on the fracture walls as a result of the shear movement along the fracture. They can indicate both the direction and sense of movement.
- Fibrous minerals infilling the fractures. If they form during the formation of the fractures they will grow with the fibres sub-parallel to the fracture wall, i.e. indicating movement parallel to the fracture walls, Figure 2-10b.
- Second order extensional fractures, en echelon tension gashes (Figure 2-11).
- Second order shear fractures, Riedel Shears
- Ductile deformation fabrics such as a shear induced cleavage (Figure 2-12).

2.9.2 Kinematic indicators

Many of these second order features are asymmetric and can be used to indicate the sense and direction of movement along a fracture, brittle deformation zone or ductile deformation zone. They are termed collectively “kinematic indicators” and many of the most commonly observed types are illustrated in Figure 2-48.

These kinematic indicators form at the same time as the major structures with which they are associated and therefore as a result of the same stress field. However, in most parts of the Earth’s crust the rocks have been subjected to a number of stress regimes which operated at different times during the geological history. Fracture networks in fractured rock masses are built up by the successive additions of individual fracture sets over geological time. Consequently the geometric features spatially associated with a particular fracture set may be related to the stress field operating during its formation or may be the result of a later stress field. The formation of kinematic indicators later than the major structures with which they are associated is discussed in the following paragraphs.

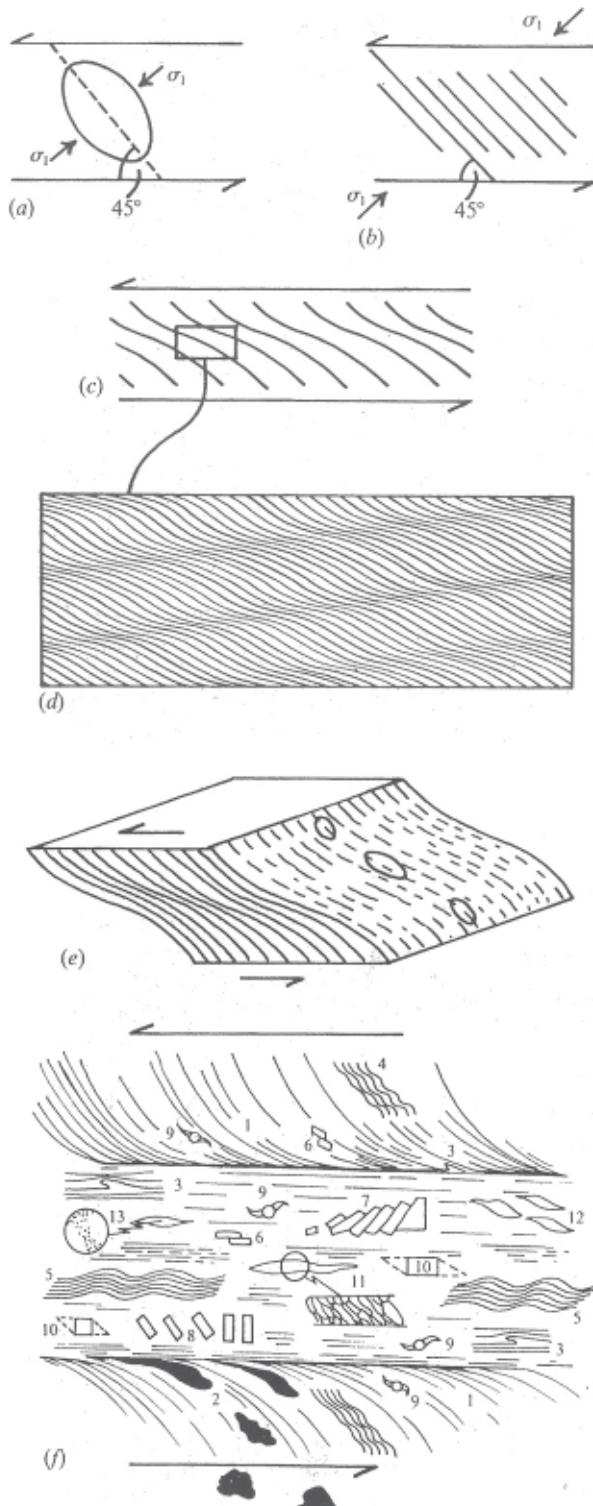


Figure 2-48. (a) The orientation of the maximum principal compressive stress associated with the first increment of shear deformation. (b) The compressive fabric produced by this stress. (c) Rotation of the shear zone fabric during shearing. (d) crenulation cleavage formed by the compression of the shear zone fabric. Block diagram showing the fabric as an S-L tectonite. Progressive deformation may result in the formation of mylonites in the central part of the shear zone (f) and these may contain a variety of kinematic indicators as shown /from Price and Cosgrove 1990, after White et al. 1986/.

The possibility of generating minor fractures around an earlier major fracture as a consequence of a later stress field has been considered by /Cruikshank et al. 1991/. In this paper the authors consider the use of fracture mechanics to interpret conditions responsible for the formation of secondary cracks that adorn joints and faulted joints. They recognise several types of minor cracks associated with the subsequent faulting (shearing) of joints. One is the kink, the crack that occurs at the termination of a straight joint and whose trend is abruptly different from that of the joint, Figure 2-49. They show that the sense of kinking indicates the sense of shear during faulting. A kink that turns clockwise with respect to the direction of the main joint is a result of right-lateral shear, and visa versa. Furthermore they show that the kink angle is related to the ratio of the shear stress responsible for the kinking to the normal stress responsible for the opening of the joint, Figure 2-49a.

The authors cite the work of /Olsen and Pollard 1989/ and show that the kink termination of the joint is part of a spectrum of possible crack tail geometries between the example where the far field stress field constrains the deflected fracture and guides it back into parallelism with the main fracture and the example where the local crack tip stress field dominates fracture propagation and the tail crack continues to diverge away from the parent fracture, Figure 2-50.

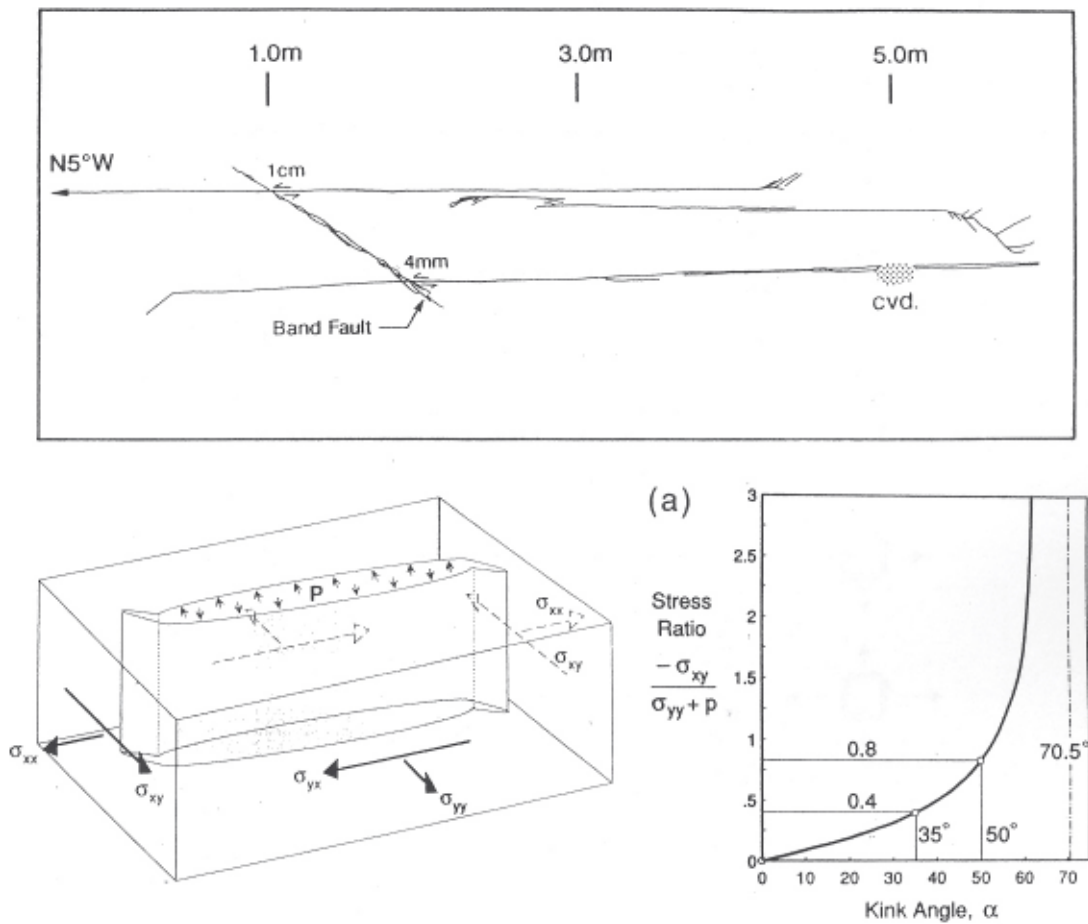


Figure 2-49. The upper diagram shows a map of several faulted joint segments and secondary fractures near their terminations. The amount of slip on the faulted joint is recorded by the offset of the “Band” fault. The joint at the bottom of the diagram ends in the north in a kink about 1 dm long that is oriented 35° counter-clockwise with respect to the trace of the joint. Bottom diagram shows a cartoon of a kinked crack with an internal fluid pressure P subjected to a far field stress field that imposes a shear parallel to the crack. The amount of opening is highly exaggerated. Graph a) shows the relationship between the ratio of far field stresses and the angle of kink or twist at the end of a mode I fracture /from Cruikshank et al. 1991/.

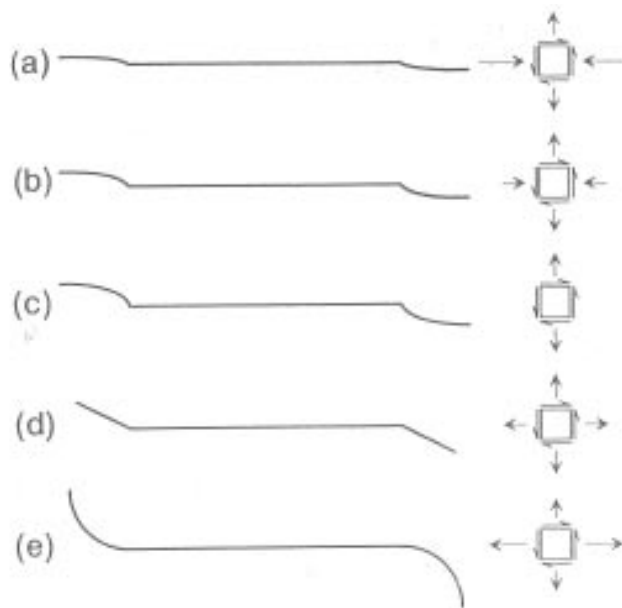


Figure 2-50. Examples of idealized curved tail cracks for various far-field loading conditions. In a) and b) the stress parallel to the fracture is compressive and in c) it is zero. In d) the stress parallel to the fracture is tensile and equal to that normal to the fracture. The fracture merely kinks. In e) the stress parallel to the fracture is a larger tensile stress than that normal to the fracture /from Cruikshank et al. 1991/.

/Cruikshank et al. 1991/, note that some of the fractures they observe in the field terminate in an array of en echelon fractures, e.g. Figure 2-51d. As a possible explanation for their formation they point to the work of /Pollard et al. 1982/ who analysed the condition of formation of en echelon cracks in front of a rectilinear crack and the degradation of a rectilinear crack front into a series of en echelon crack blades. The angle β between the en echelon crack blades and the host fracture is given by:

$$\tan(2\beta) = \frac{2\sigma_{xy}}{(\sigma_y + p)(1 - 2\nu)} \quad \text{Equation 2-7}$$

where ν is Poisson's ratio, τ the shear stress parallel to the parent fracture, σ_y the normal stress across the fracture and p the fluid pressure inside the fracture. The fundamental assumption is that the twist blade is normal to the direction of maximum tension immediately ahead of the crack front. This relationship is plotted in Figure 2-49a, and the way in which the en echelon fractures may link to the parent fracture is shown in Figure 2-52.

Other second order structures linked to shear movement along a fracture are shown in Figure 2-53. These structures may be linked to the initial stress regime under which the fracture formed or to a later stress field that was oriented in such a way as to impose a significant shear stress along it. The structures formed in a limestone from the Languedoc region of southern France. Veins and solution surfaces extend from near the tips of the fault in an antisymmetric arrangement. The fault is considered a Mode II crack (shear fracture) and the veins and solution surfaces mode I cracks of the opening and closing kind respectively. The theoretical stress distribution around the fracture shown in Figure 2-53 together with the predicted orientations of the compressional and extensional second-order structures that form, are shown in Figure 2-54.

It can be seen that it is possible to sub-divide kinematic indicators into those linked to the initial stress field which generated the parent fracture and those which relate to a later stress regime that caused movement on the early fracture and the formation of second order structures.

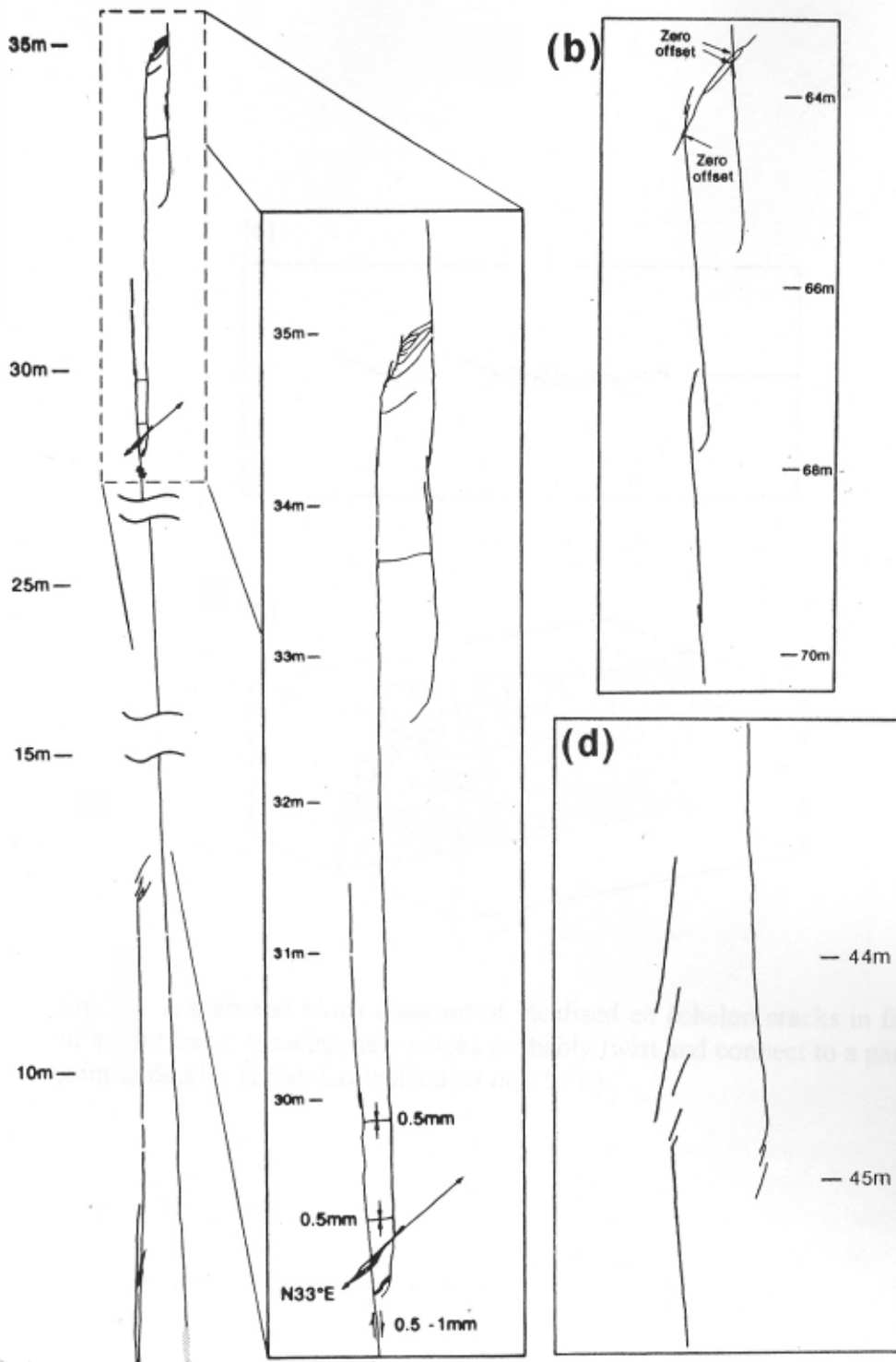


Figure 2-51. (left hand diagram) Horsetail fractures, bridge cracks and en echelon cracks along faulted joints. Horsetail fractures at 28 m and 35 m. Bridge cracks at 29 m, 29.8 m and 33.5 m. En echelon cracks at 13 m. The sense of slip is right lateral and the amount of slip at 28.5 m is 0.5–1.0 mm. b) Overlap and interaction of joints d) En echelon cracks at the tip of overlapping joint segments /from Cruikshank et al. 1991/.

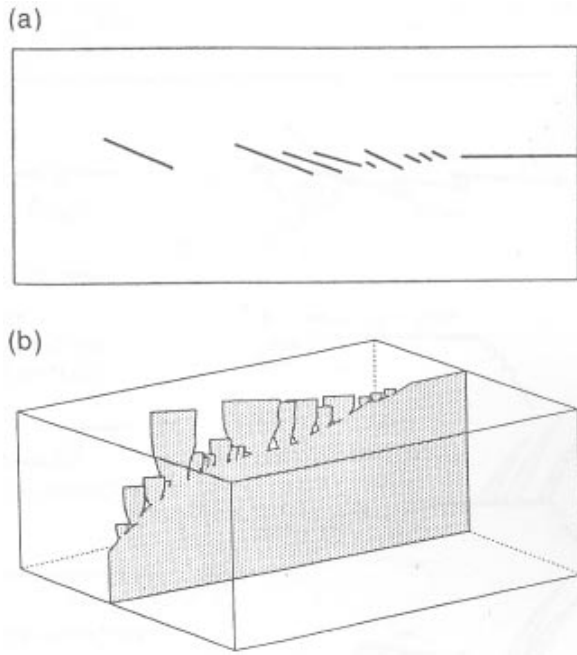


Figure 2-52. A map and block diagram of idealized en echelon cracks in front of a joint trace, showing how cracks probably twist and connect to a parent joint at depths /from Cruikshank et al. 1991/.

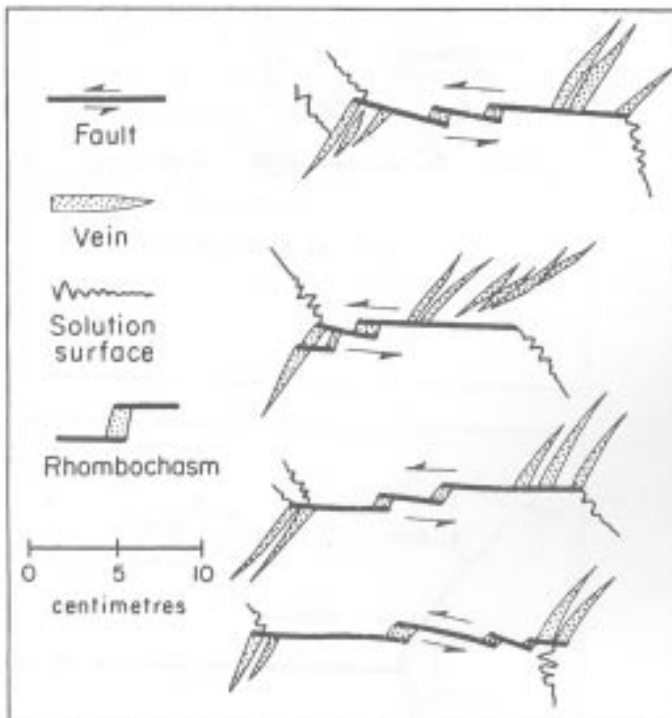


Figure 2-53. A map of small faults in limestone from the Languedoc region of southern France, /Rispoli 1981/. Veins and solution surfaces extend from near the tips of the fault in an antisymmetric arrangement. The fault is considered a Mode II crack and the veins and solution surfaces mode I cracks of the opening and closing kind respectively /from Pollard and Segall, in Atkinson 1987/.

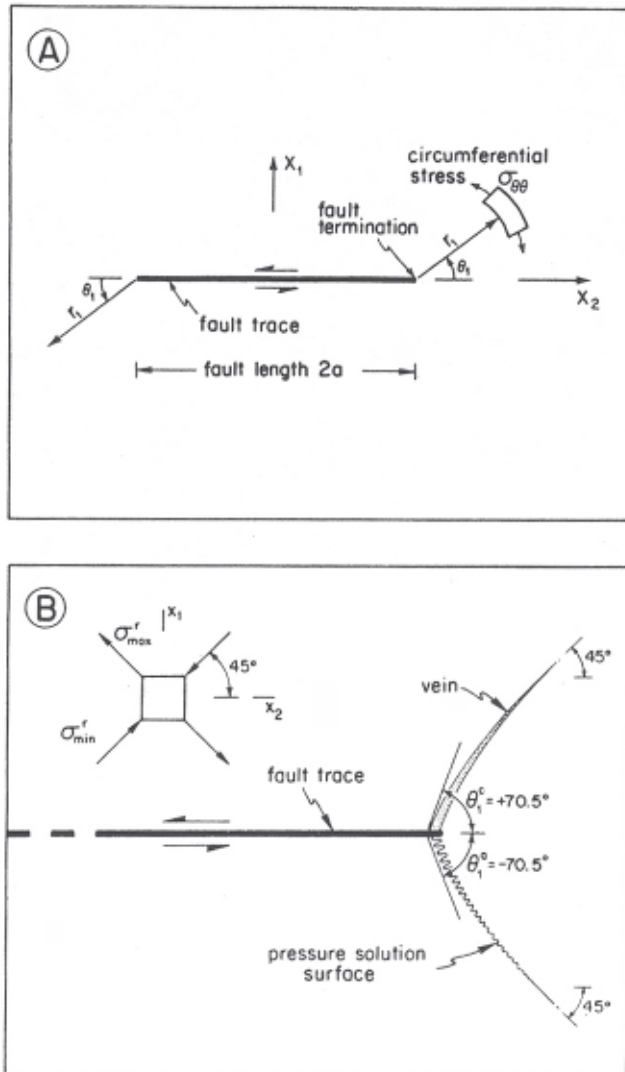


Figure 2-54. A) Idealized diagram of the small fault (Figure 2-53) represented as a Mode II crack. The circumferential stress, $\sigma_{\theta\theta}$, acting on an element near the crack tip is shown with polar coordinates r_1 , θ_1 , indicating its position. B) illustration of the initiation angle for a vein and solution surface extending from near the fault tip. The remote principal stresses are oriented at 45° to the fault trace /from Pollard and Segall, in Atkinson 1987/.

2.9.3 Conclusions

A variety of kinematic indicators form in association with the two types of fractures, (shear and extensional). In general these do not provide a direct criteria for detecting fracture length. They do however provide signatures that can be of considerable help when attempting to correlate fractures between boreholes and tunnels and in this way can be invaluable in helping to identify long fractures.

2.10 Conductivity

One of the most important signatures relating to the length of a fracture is its conductivity. Conductivity is related to geometric properties (length, aperture and continuity which is determined by the connectivity) and to the physical environment in which the fracture is situated (fluid pressure and current stress configuration). It is often assumed that the larger a fracture the greater its conductivity is likely to be.

However, it is possible that a large fracture has a low conductivity and the general statement that the larger the fracture the greater its conductivity needs to be tempered, particularly in view of the fact that the aim of this study is to detect critical deformation zones, i.e. any planar zone of weakness that might undergo shear displacements of greater than 10 cm in response to seismic events linked to post-glacial faulting. It is therefore important to consider the likely effect of the detailed differences of the various structures grouped under the heading of “critical structures” on conductivity.

2.10.1 Impact of fracture geometry on conductivity

Discontinuities include single, discrete, continuous breaks in the rock and arrays of small, sub-parallel fractures (fracture zones) often not apparently connected in the plane of observation. All things being equal, the more continuous a fracture the better its conductivity. However, many fracture zones are conductive and this may be because they are connected to a parent fracture as shown in Figure 2-52 or because they are linked by cross fractures. An example of two apparently isolated yet conducting fractures which form part of a brittle deformation zone cutting through a tunnel at the Äspö Hard Rock Laboratory is shown in Figure 2-55. The conductive fractures appear dark.



Figure 2-55. View of one of the bored tunnels at Äspö showing conductivity along discontinuous fractures. These fractures may be linked via a parent fracture (see Figure 2-53) or via small cross fractures which, in this example, do not outcrop on the tunnel wall.

2.10.2 Variation of fracture conductivity over geological time

A fracture may be currently conductive (see e.g. Figure 2-56b) or may have been originally conductive but subsequently infilled by mineralization linked to the flow of mineral charged fluids through the fracture (see e.g. Figure 2-56a). In addition to filling the fractures with minerals, mineralising fluids may also cause alteration of the wall rock. An example where the movement of fluids through a fracture has:

- precipitated minerals within the fracture,
- has caused alteration of the wall rock,
- but has not completely sealed the fracture so that it is still significantly conductive, is shown in Figure 2-57. These indicators of high fracture conductivity either in the past or currently can be used as a guide to fracture size, (see the conclusions of this section).

There is a considerable body of knowledge on the conductive properties of fracture networks and it has been shown that depending on the properties of a fracture network (specifically the density, length and orientation of the fractures making up the individual fracture sets that form the network) the network may have zero conductivity, channelized conductivity or pervasive conductivity. This is illustrated in the 2D model shown in Figure 2-58 /Jolly and Cosgrove 2003/. The fractures shown in this figure may represent the fractures of an extensive fracture set or, as indicated in the right-hand diagram may describe the fractures making up a fracture zone. When the parameters of the fracture set are such that the resulting conductivity is channelized (b), then the flow of fluid along a brittle deformation zone will be possible along an anastomosing system of channels of conductivity even though there will be areas within the deformation zone that are non-conductive. The model can be extended to three dimensions to generate a braided system of connected pathways enclosing isolated, non-conductive zones.

Thus a tunnel system such as the spiral tunnel at the Äspö Hard Rock Laboratory may intersect the same conductive zone at two levels but fail to identify it at a third location between the two conductive regions where projection of the structure from the two conducting sites predict that it should occur.

2.10.3 Fracture continuity, connectivity and conductivity

The tracing of diffuse fracture zones from one borehole to another can be more difficult than tracing a single discrete fracture. Clearly the more widely spaced the boreholes the less certainty there will be in the correlation of a fracture or deformation zone between the two. Posiva have attempted to improve the confidence level of cross-hole correlation by including a study of kinematic indicators of the fractures. These are primarily slickensides which give both the direction and sense of slip along the fracture. They have presented a new format for core and borehole log description, Figure 2-59.

The table shown in Figure 2-59 contains reference to cataclasites, pseudotachylites, welded crush rock etc all of which are fault products formed by brittle processes. It seems therefore anomalous to classify them as “semi-brittle” features. From the point of view of the task in hand, namely that of identifying planar or sub-planar zones of weakness along which slip might occur in response to seismicity linked to post-glacial faulting, all these features are important and need to be identified. They fall under the general heading of deformation zone or “critical structure”.



Figure 2-56. (a) A quartz filled fracture exposed in the wall of a bored tunnel at Äspö. (b) A currently conductive fracture exposed in the wall of a bored tunnel at Äspö, Iron minerals have been precipitated around the fracture on the tunnel wall as a result of the discharge of fluids from the fracture.



Figure 2-57. An example from the Äspö Hard Rock Laboratory where the movement of fluids through a fracture has precipitated minerals within the fracture, has caused alteration of the wall rock but has not completely sealed the fracture so that it is still significantly conductive.

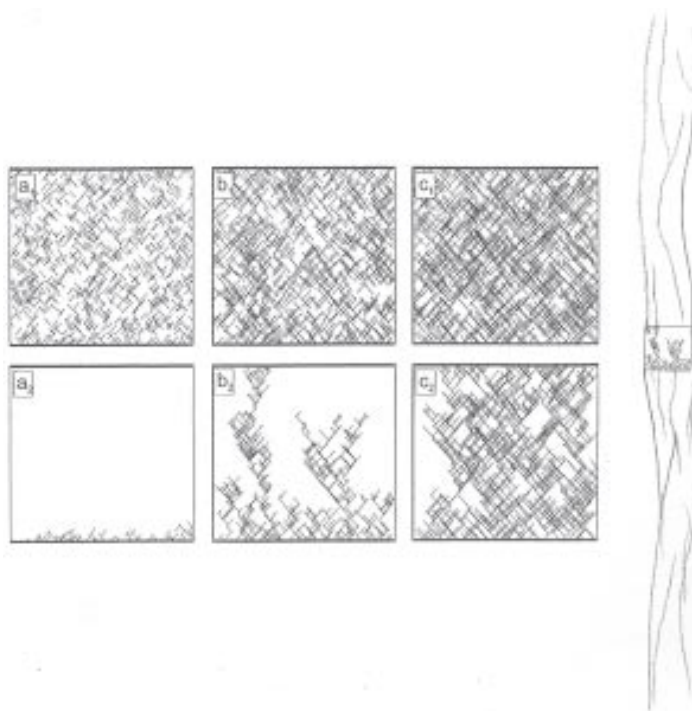


Figure 2-58. a₁) b₁) and c₁) show fracture networks made up of two orthogonal fracture sets. The orientation and density of the fracture sets in the three models are identical and they differ only in the length of the fractures which increases from models a₁) to c₁). In a₁) no connections occur between the upper and lower faces of the model (a₂). In b₁) channels of connectivity occur (b₂) and in c₁) the connectivity is pervasive, (c₂). The sketch on the right hand side of the diagram shows b₂ as part of a fracture zone. It contains an anastomosing channel system of conductive pathways containing regions that are non-conductive /Jolly and Cosgrove 2003/.

Classification procedure for deformation zone intersections at Olkiluoto

	Designation of a given intersection:		
Step 1	<p>Intersection shows intensive post-migmatitic/post-magmatic deformation (i.e. deformation which is lacking in the wall rocks on either side of the zone)</p> <p style="text-align: center;">Designation: Deformation zone intersection</p>		
Step 2	<p>Intersection shows cohesionless or low-cohesive deformation products: gouge, breccia, fractured rock and their partially mineralized equivalents*</p> <p style="text-align: center;">Designation: Brittle deformation zone intersection (BDI) (often called “fracture zone” or “R-structure”)</p>	<p>Intersection shows cohesive deformation products: cataclasites, pseudotachylite, welded crush rocks, etc. (all typically massive and structureless)</p> <p style="text-align: center;">Designation: Semi-brittle deformation zone, or semi-brittle fault zone intersection (SFI)</p>	<p>Intersection shows cohesive deformation products: mylonites, phyllonites, etc. (typically strongly foliated)</p> <p style="text-align: center;">Designation: Ductile deformation zone, or ductile shear zone intersection (DSI)</p>
Step 3	<p>Joint cluster intersection (BJI)</p> <p>Intersection shows <i>no clear</i> signs of lateral movement</p>	<p>Fault zone intersection (BFI)</p> <p>Intersection shows <i>clear</i> signs of lateral movement</p>	
Step 4	<p>Composite deformation zones (informal name)</p> <p>Treat as BDI +/- SFI +/- DSI zone, each component to be described separately</p>		

Figure 2-59. Classification scheme for describing deformation zone intersections in boreholes and tunnels at Olkiluoto /Milnes 2006, Paulamäki et al. 2006/.

Work at the Äspö Hard rock laboratory is described in Chapter 3 where an attempt has been made at cross correlation of deformation zones observed in tunnels and shafts with data on deformation zones obtained from boreholes drilled sub parallel to the tunnels and shafts. This study relies heavily on tracing conductive zones from one borehole or tunnel to the next. Other studies at Äspö, where attempts have been made to correlate fractures across the diameter of the spiral tunnel and over shorter distances between tunnels (Figure 2-60), have met with varying success. The position of the Laboratory with respect to the major fractures and fracture zones of the surrounding rock mass is shown in Figure 2-61. It is apparent from these studies that the cross-hole correlation confidence is inversely proportional to the separation of the boreholes. The proposed spacing of the deposition tunnels and deposition holes in the repository is shown in Figure 2-62, and is close enough for cross-hole correlation to be achieved with a high level of confidence particularly if the recommendations of Posiva are adopted and a record of kinematic indicators of the fractures and deformation zones is included in borehole descriptions.

In addition to the matching of kinematic indicators and conductive zones between boreholes, cross correlation can also be achieved by monitoring pressure response between boreholes where a detected deformation zone in one borehole is sealed above and below its outcrop on the borehole walls and a fluid pressure introduced to the sealed section. The location of any pressure response detected in adjacent boreholes enables a cross correlation to be made.

2.10.4 Influence of current stress regime on fracture conductivity

Another factor that influences the conductivity of fractures in addition to their length is their orientation with respect to the current stress field. This phenomenon has long been recognised in the hydrocarbon industry where it is often observed that similar fracture sets in a reservoir have very different conductivities and that these differences can be accounted for by considering the orientation of the different sets with respect to the present day stress field. Fractures oriented parallel to the maximum compression direction, σ_1 , and therefore at right angles to σ_3 , are the most conductive and those parallel to σ_3 i.e. normal to σ_1 , the least. This is well illustrated at the Äspö Hard Rock Laboratory where the conductive fractures are sub-vertical and striking NW-SE i.e. parallel to the current maximum principal compression and normal to minimum principal compression.

2.10.5 Conclusions

From the point of view of detecting large “fractures”, fracture infilling and wall rock alteration are extremely important features as they:

- Give an indication of fracture conductivity and therefore size.
- Act as clear and unique markers that facilitate cross-hole correlation of fractures.
- May provide the fracture with a clear geophysical signature that enables the extent of the fracture to be determined using geophysical techniques.

However, it is important to remember that it is possible to get long fractures which are not infilled and which do not display significant wall rock alteration. Examples of such fractures in the Oskarshamn area are the exfoliation fractures in the quarries at Kråkemålabrottet, Figure 2-39. These recently formed fractures, linked to exhumation and the release of residual stresses, are barren and there has not been sufficient time for percolation fluids to cause significant alteration of the wall rock.

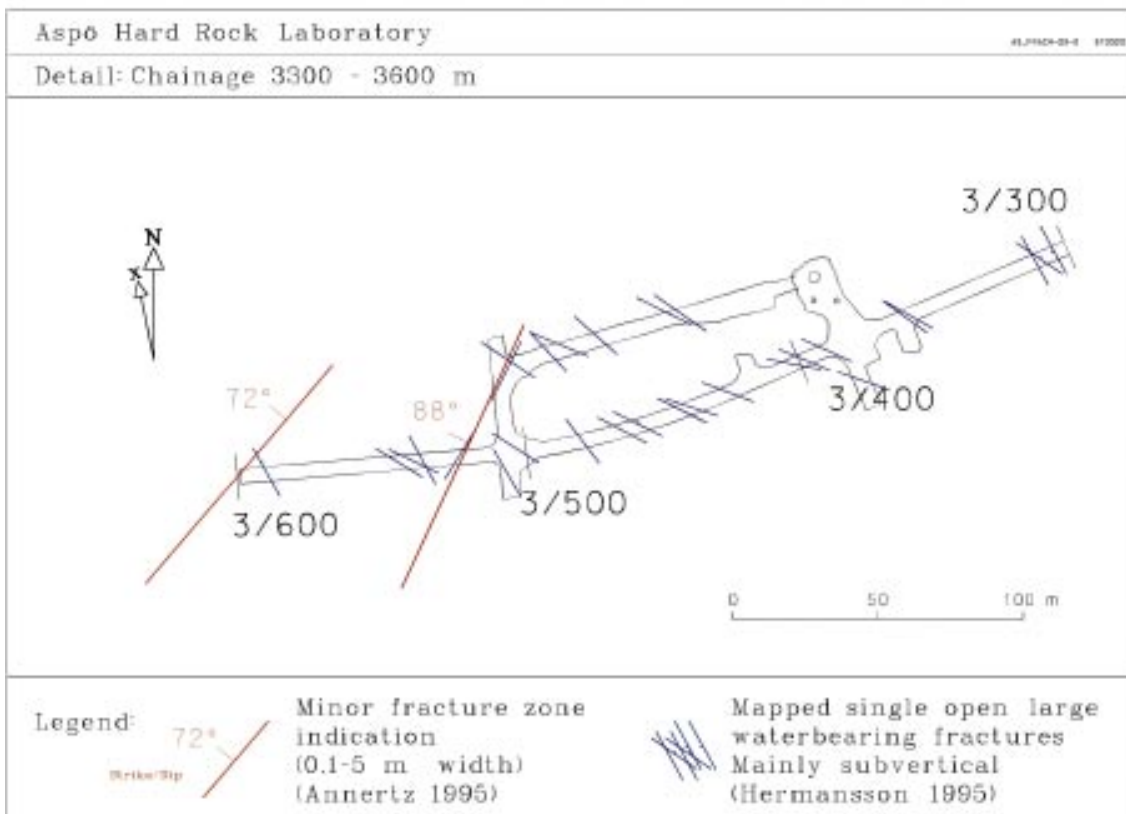
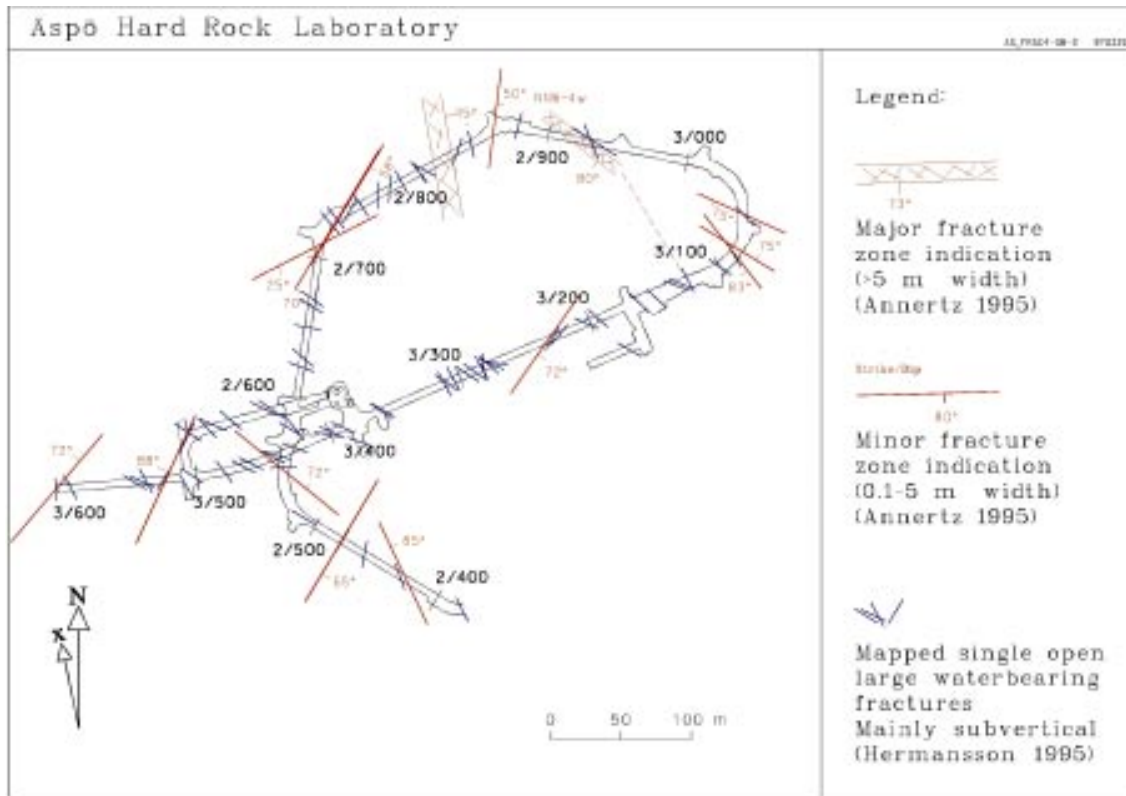


Figure 2-60. Plan view of the mapped fracture zones and single open large water bearing fractures in part of the Åspö HRL. The upper diagram is a detail of the lower diagram and the fractures are mainly sub-vertical /from Rhén et al. 1997/.

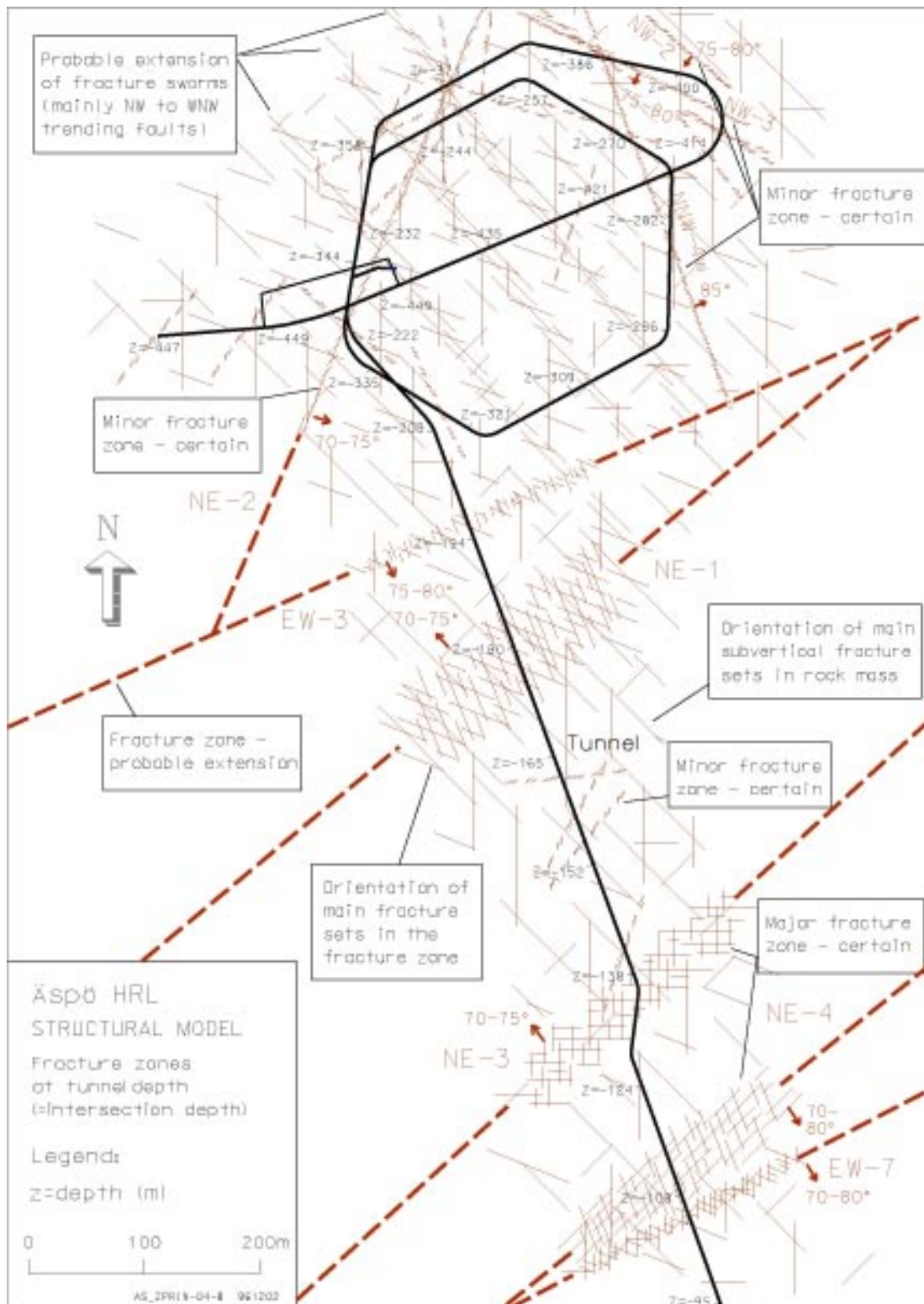


Figure 2-61. Plan view of the structural model of the rock mass surrounding the Äspö tunnel. The model shows the position and estimated extension of fracture zones (swarms) at tunnel level. The orientation of the main sub-vertical fracture set in the major fracture-zones in the intact rock mass is based on tunnel mapping data. "Fracture swarms" comprise concentrations of sub-parallel, often water bearing faults /from Rhén et al. 1997/.

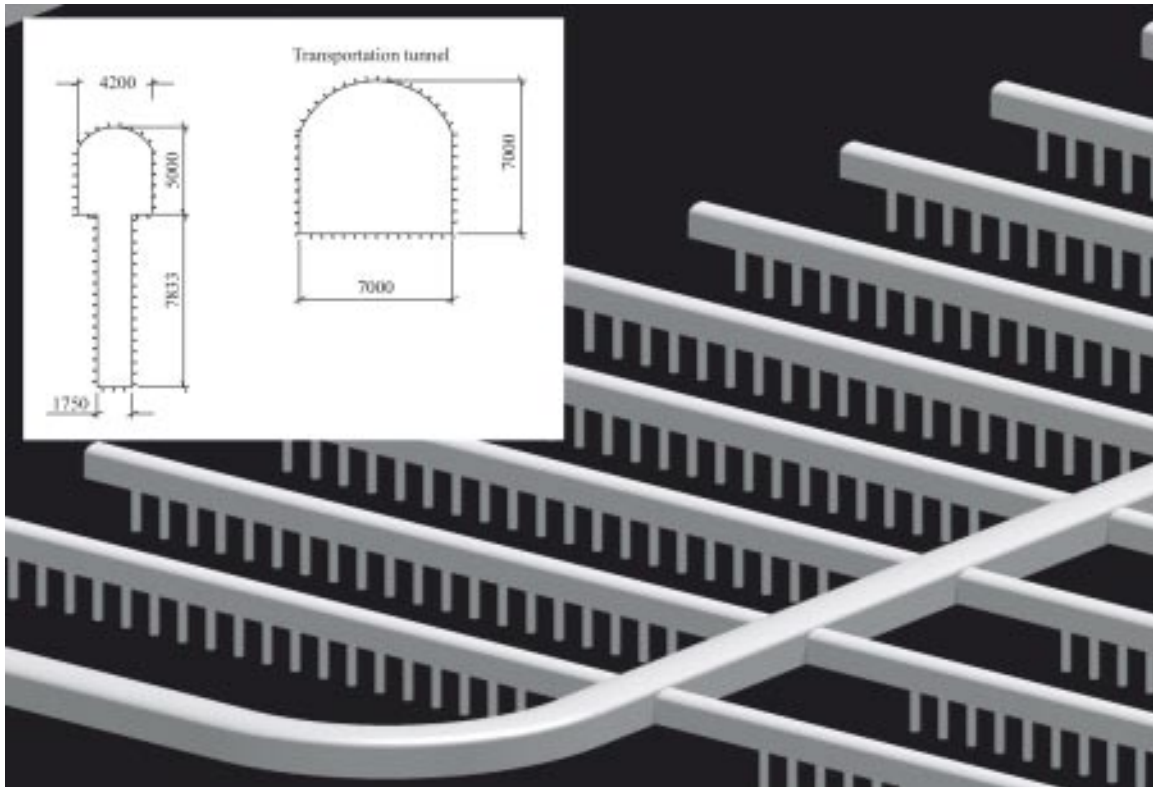


Figure 2-62. Tentative repository layout. The spacing of deposition tunnels and deposition holes spacing is currently 40 m and 6 m respectively. The insert shows the tunnel dimensions /from Munier and Hökmark 2004/.

One of the assumptions made in this discussion of the use of conductivity as an indicator of fracture length is that there is a direct relationship between fracture aperture (i.e. fracture normal displacement) and length in the same way as there is a relationship between fracture parallel displacement (slip) and length (see Figures 2-31 to 35). It must be noted however that relationship between aperture and length has not been demonstrated as convincingly as that between slip and length. Indeed, as is pointed out in Section 2.12.3 it is recognised that it is possible to have fractures with a large thickness which are not critical fractures. For example, many veins are found in rocks with a very large thickness to length ratio. In addition another important factor that influences the conductivity of a fracture is its orientation with respect to the current stress regime. This is discussed in Section 2.10.4 where it is pointed out that the most conductive fractures at Äspö are the vertical fractures striking NW-SE i.e. parallel to the current orientation of σ_1 and normal to σ_3 .

However, despite these various factors that influence conductivity, it is concluded that if a deformation zone displays a high conductivity it is appropriate to take this as an indication that the zone might be long and that its extent needs to be investigated. However, it is important to recognise that a low conductivity does not necessarily indicate a short fracture.

2.11 Site specific data

In this report the discussion of the problems of recognising critical deformation zones during the construction of a repository has been general. It could be made more site-specific for the Oskarshamn and Forsmark areas.

Both sites are situated in the Fennoscandian Shield and therefore have experienced a similar geological history after 1,800 million years. They are subjected to the same current stress regimes and will be subjected to similar changes in stress regime resulting from subsequent fluctuations in glaciation. The current stress regime and the likely impact of glacial movement on this are briefly outlined below.

2.11.1 Geological setting of the shield

The current stress regime of the Fennoscandian Shield is interpreted as the result of the Atlantic Ridge push combined with the Alpine collision between the African and European plates. However, the local stress regimes in the shield can vary significantly both in orientation and magnitude. For example the current stress state at the Äspö Hard Rock Laboratory is a horizontal, NW-SE trending σ_1 of 27 ± 2 MPa, with σ_2 and σ_3 being 12 ± 2 MPa and 11 ± 2 MPa respectively whereas the magnitudes of both σ_1 and σ_2 are considerably higher at Forsmark. The likely reasons for stress heterogeneity in the crust is linked to variations in lithology and the existence of fractures on all scales as discussed in Section 2.3.4. In addition there is a difference in the assumed ice thickness between Forsmark and Oskarshamn, and the latter may have been more affected by an end effect of the ice, being closer to an ice margin for a longer time.

2.11.2 Process of glacial loading

Work by /Lambeck and Purcell 2003/ on the process of glacial rebound and crustal stress in Finland and by /Lund 2005/ on the effects of deglaciation on the state of stress in the crust can be used to consider the impact of future glacial advances and retreats on the stress state in the crust at the proposed repository sites.

The current stress state will be modified by the advance and retreat of the Scandinavian ice cap. A preliminary study of this additional stress field has been carried out by assuming that the glacier represents a point load on the crust similar to the point load generated by the Hawaiian volcanoes on the Pacific floor, Figure 2-63. The upper diagram is a profile across the Hawaiian Archipelago showing morphology, free air gravity anomaly and refraction seismic velocity structure (in km/sec) beneath the ridge, the deep and the arch (peripheral bulge). The lower diagram shows two models (i) the flexure of a loaded elastic lithosphere of various effective elastic thicknesses and flexural rigidities (D) and (ii) the decay from flexural to Airy isostatic compensation for an 83 km visco-elastic lithosphere with a dissipation decay constant of 10^5 ma.

The effect of the thickness of the elastic plate on the distribution of deformation is apparent. For a thin plate (38 km thick) the peripheral bulge has its maximum height (100 m) approximately 500 km from the applied load. As the thickness of the elastic plate is increased so the bulge forms further away from the load and its height is reduced. In contrast to the static elastic model, the bottom diagram shows the effect of a load on a visco-elastic lithosphere. Here the deformation is not static and changes with time. The initial peripheral bulge migrates with time away from the site of loading and its height becomes progressively less until it is lost.

It follows from this brief discussion that if the deformation induced by a glacial load is to be determined (and it is this that determines the induced stresses that might cause seismic reactivation of existing fractures) then it is important to have the appropriate rheological model for the lithosphere.

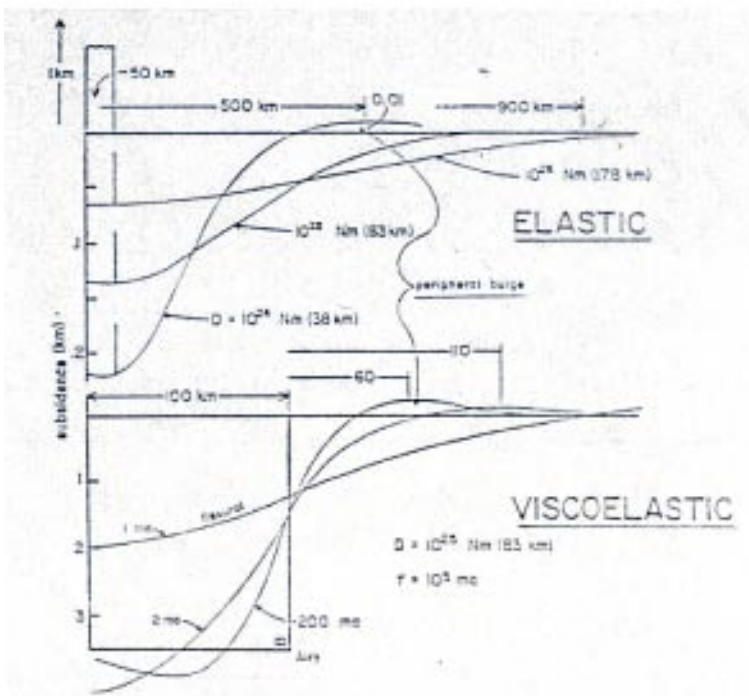
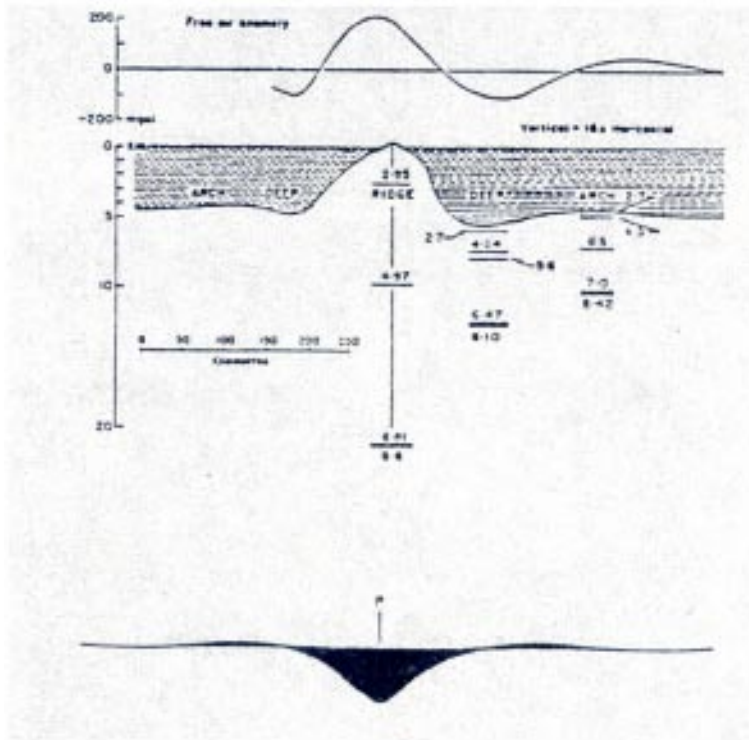


Figure 2-63. Upper diagram shows the profile across the Hawaiian Archipelago showing morphology, free air gravity anomaly and refraction seismic velocity structure (in km/sec) beneath the ridge, the deep and the arch. The lower diagram shows the flexure of a loaded elastic lithosphere of various effective elastic thicknesses and flexural rigidities (D) and decay from flexural to Airy isostatic compensation for an 83 km visco-elastic lithosphere with a dissipation decay constant of 10^5 ma.

2.11.3 Dynamic versus static glacial loading model

The static, point load analysis discussed above and represented in Figure 2-63, is not totally appropriate for the dynamic advance and retreat of an ice cap and will need to be modified. In this dynamic model, even the purely elastic analysis will involve a migrating peripheral bulge.

The response of the crust to glacial loading and unloading has been considered by /Price and Cosgrove 1990/ who point out that a simple analysis of parallel uplift or burial of the crust is inapplicable to the asymmetric loading that is linked to glacial movement. They argue that one sided loading leads to non-parallel burial and uplift of the crust and that this will impact on the fractures that might form and also on the fractures that are likely to be reactivated. The mechanics of crustal deformation linked to a migrating load has also been considered in the context of the formation of foreland basins which migrate with the induced peripheral bulge as the associated compressional thrust wedge migrates into the undeformed foreland.

It follows from the above discussion that the magnitude of the bulge and the related crustal stresses will be determined primarily by the thickness of the ice sheet, the rheology of the lithosphere and the local heterogeneities in the geology of the specific site, e.g. lithological variations, the presence of major fractures and pervasive fabrics etc. The better the understanding of these parameters, the more accurately the stress field likely to move through the crust during glacial advance and retreat can be predicted and, the greater the confidence one would have in identifying the orientation of the major fracture zones most likely to be reactivated seismically.

2.11.4 Conclusions

The arguments outlined above regarding the geological details of the proposed repository site emphasise the fact that the better the understanding of the fracture network, the structure and geological history of the site, the less the likelihood of missing critical deformation zones.

2.12 Discussion and conclusions

As stated in Section 1.2, the overall objective of the EXPECT project is:

To quantitatively estimate the likelihood of a deformation zone in the size range $50\text{ m} < r < 250\text{ m}$ intersecting a deposition tunnel or deposition hole, where r is the radius of the zone.

In an attempt to achieve this objective three tasks have been identified namely:

- To summarize the current state of knowledge on geological characteristics of deformation zones in the size range $50\text{ m} < r < 250\text{ m}$.
- To propose suitable investigation methods for identifying and localizing deformation zones in tunnels and boreholes and to give examples of their application. (The scope of work should mainly encompass investigative methods known to and used by SKB.)
- To examine the extent of the intersection of these zones with the repository tunnels and deposition holes, specifically to determine whether the zones intersect the full perimeter of the hole and to use the Full Perimeter Intersection (FPI) criterion to quantify the chances of a repository tunnel or deposition hole being intersected by a deformation zone in the size range $50\text{ m} < r < 250\text{ m}$. This quantification is achieved by DFN numerical modelling.

The present chapter addresses the first of these, Chapters 3 and 4 the second and the third approach is presented in an accompanying report /Munier 2006/.

2.12.1 The significance of conductivity as an indicator of fracture length

Despite the uncertainty regarding the relationship between the conductivity of a deformation zone and its size, empirical observations show that many long fractures are either currently or were in the past channels for fluid migration. Whilst acknowledging that not all large planar zones of weakness must be conductive (one could envisage some ductile shear zones along which continuity has not yet been lost having a low permeability) it is argued that when a fracture shows evidence of present or past conductivity, it should be regarded as being a critical fracture until proved otherwise.

Past movement of fluids through a fracture is often indicated by the alteration of the walls of the fracture by the fluids and/or by the precipitation of a mineral infill. The thickness of the infilling material and the thickness of the alteration zones are in many cases a good indicator of fracture length. Thus every effort should be made to establish whether a length/thickness correlation exists at each particular site. Examples from the Äspö Hard Rock Laboratory of an infilled fracture that is no longer conductive is shown in Figure 2-56a, an example of a currently conductive fracture is shown in Figure 2-56b and a fracture with intensely weathered wall rocks and containing a mineral infill, but which is still conductive, is shown in Figure 2-57. The different electrical and magnetic properties of the altered wall rock, the mineral infill and the fluid moving through the fractures compared to the intact, unaltered country rock and the drop in density of a brittle deformation zone resulting from the opening of voids, enable such fractures to be detected and their lateral extent determined by the use of various geophysical tools.

The reason why some long fractures do not display mineralization or alteration of the wall rocks probably relates to several factors including their age and their orientation with respect to the stress fields operation in the rock since their formation. Young fractures such as the exfoliation fractures at Kråkemålabrottet in Oskarshamn, Figure 2-46, may not have had sufficient time or there may have been no mineral charge fluids available, for them to become infilled with minerals. Alternatively, if the fractures are unfavourably oriented with respect to the stress regime in the rock (i.e. if they are oriented at a high angle to the maximum principal compression) then they are likely to have a relatively poor conductivity and are less likely to become infilled with minerals.

2.12.2 General versus site specific studies

This report addresses the general problem of identifying critical structures in a non-specified fractured rock mass. One of the key requirements is to determine the probability of such a critical deformation zone remaining undetected during the excavation of the tunnels and deposition holes during the construction of a repository. This probability can be reduced if the rock type of the proposed repository is known because the expression of fractures, their likely spatial organisation and continuity etc depends to some extent on the rock type. For example, fracture sets will tend to be less systematic and more continuous in a massive crystalline basement than in a foliated crystalline rock or bedded sedimentary succession. However, it is difficult to see how this probability can be precisely quantified. In this regard it is relevant to note that the rocks at Oskarshamn are very weakly foliated whereas the rocks at Forsmark contain a penetrative ductile deformation fabric that developed under amphibolite facies metamorphic conditions.

The understanding of the control on fracture orientation and propagation imposed by the mechanical anisotropy that characterizes a bedded succession and the impact of pre-existing fractures on the orientation of later fractures discussed in Section 2.3.4 (see Figure 2-5), can be used to consider the impact on fracturing of any mechanical anisotropy present in the crystalline rocks of the study areas. For example, at Oskarshamn the foliated crystalline basement is penetrated with granite plutons which are unfoliated, an important factor in accounting for the different expression of fractures in the two rock types. The weakly foliated rock is characterised by diffuse, fracture zones whereas the granites are cut by more discrete, clean-cut fractures.

It also follows that the probability of missing a critical deformation zone will be reduced if the fracture network existing in the rocks is established (i.e. if the orientation and spatial characteristics of the main fracture sets making up the fracture network are known) and if the location and orientation of the fracture likely to generate seismicity with respect to the repository area, are known.

An attempt has been made to establish the tectonic history of the main proposed repository sites in the Fennoscandian Shield (Oskarshamn, Forsmark, Olkiluoto etc) and to determine the orientation of the main fracture sets linked to the different episodes of tectonism. This information can be conveniently presented in table form as shown in Figure 2-64.

The concept of identifying a succession of regional stress fields that have affected an area is sound and an essential part of any study of a potential repository site. However, it is important to recognise that any regional stress field will be locally modified as a result of lithological heterogeneity and fractures (see the discussion in Sections 2.5.2. and 2.4 and Figure 2-5). Important changes in the current stress field occur in the Oskarshamn area. The stress regime in the north is different to that in the south and this is probably the result of lithological variations and important deformation zones /see Berglund et al. 2003/.

Thus the better the understanding of the repository site, the less the likelihood of missing critical deformation zones. However, the methodology of identifying these deformation zones is the same regardless of the state of knowledge of the bed rock and the key parameters that can be used to indicate fracture length are discussed in the following sections.

2.12.3 Fracture thickness and displacement

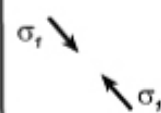
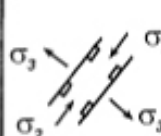
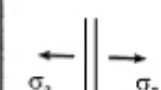
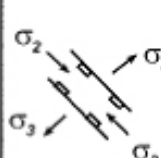
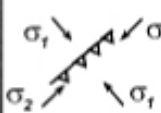
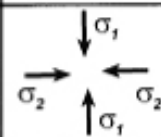
Two important parameters often linked to fracture or fracture zone length are “thickness” and “displacement”.

Thickness of a fracture or fracture zone.

It has been established that the thickness and continuity of a deformation zone will both increase as the zone increases in length (see Section 2.11, and Figures 2-55 to 2-57) and that this empirical link between length and thickness might be used to identify critical deformation zones. As discussed in the following section a similar link exists between length and displacement.

Displacement on a fracture (fracture parallel displacement)

Like the opening of extensional fractures, the displacement along shear fractures also varies predictably along its length. Maximum displacement frequently occurs in the central region of the fracture and decreases to zero at the fracture tips, (see Section 2.7 and Figure 2-31). Thus both fracture normal and fracture parallel displacements are sensitive indicators of fracture size and can be used to identify large fractures. It is recognised that it is possible to have fractures with a large thickness which are not critical fractures. For example, many veins are found in rocks with a very large thickness to length ratio. Never-the-less large thickness, thick border zones a hydrothermal alteration and fracturing (see Section 2.12.1), large displacements and high conductivity are features that are likely to characterise large fractures and other deformation zones and are some of the best indicators for detecting them. A policy of treating all fractures and deformation zones with a thickness, displacement or conductivity above a threshold value, as being critical deformation zones until the opposite is shown appears a rational policy. These threshold values are likely to be site specific and preliminary observations indicate that in crystalline rocks such as those that will house the repositories, the ratio of gouge thickness to fault length falls in the range 1:100 to 1:1,000.

Age (Ma)	Magmatism and volcanism	Sedimentation and deformation	Inferred causal stress state
<0.1, i.e., since last glaciation	None	No new fractures, but some significant reactivation of existing fractures	
<100	Current plate motion stresses dominated by ridge push + Alpine	Dominated NW-SE compression 25 MPa.	
<280	Hercynian orogeny (at 300 Ma) followed by the breakup of Pangea and the formation of the Atlantic Ocean and the related rifts including the Baltic rift	Development of the Baltic Rift Basin bounded by NE-SW trending normal faults	
<700		Development of fractures Block movements after sedimentation Vendian, Cambrian and Ordovician sandstones, siltstones and carbonates	
Planation of the Proterozoic bedrock			
1270-1260	Postjotnian diabase dykes (= feeder channels of the continental flood basalts)	Hydrothermal, illite-filled fractures in the migmatites Subsidence of the Satakunta sandstone graben (block movements)	
1400-1300		Deposition of the upper parts of the Satakunta sandstone	
1580-1550	Subjotnian diabase dykes Anorogenic rapakivi granites and associated felsic volcanics Söörmarkku felsic dyke	Hydrothermal fracture in the Palaeoproterozoic rocks Development of the sedimentary basin (graben) of the Satakunta sandstone Extensional tectonic regime: rifting of the crust, faulting	
1800-1770	Period of post-orogenic magmatism (not recorded in Satakunta)		
1850-1810	Late orogenic potassium granites (1840-1830Ma)	Pelitic migmatite belt: ductile deformation D ₃ related with the NW-SE-trending compression, overthrusting Ductile to semi-brittle, zonal deformation D ₄ Late-D ₃ in the psammitic migmatite belt: the Kynsikangas shear zone	
1885-1870	Lavia porphyritic granite ¹⁾ Pöytyä granodiorite ¹⁾	Ductile deformation D ₃ within the psammitic migmatite belt	
1890-1885	Synorogenic tonalities and granodiorites Ultramafic and mafic intrusions	N-S trending compression; Ductile, complex deformation D ₂ , thrust tectonics with the pelitic migmatite belt?	
<1910	Basic and intermediate volcanics	D ₁ -deformation: S ₁ -foliation Sedimentation: bedding S ₀	
>1910	Unknown pre-Svecofennian protocrust		

¹⁾ located outside the study area

Figure 2-64. Tentative chronological scheme summarizing the main lithological units and tectonic events affecting the Scandinavian Shield at Olkiluoto, Finland.

2.12.4 Further constraints on critical fractures

The aim of this study is to ensure that the movement along any deformation zone cutting the tunnel or borehole will not exceed 10 cm. The method chosen to ensure that such movements will not occur is to develop a methodology for detecting zones large enough to enable such slip magnitudes to occur. However, as noted in Section 2.6.3, it is possible to argue that many deformation zones encountered in the tunnels and deposition holes will not pose a threat to the integrity of the canisters, even if they are longer than the critical length.

A simple and uncontroversial indicator of a fracture being large, is whether or not its intersection with the tunnel can be traced around the full perimeter of the tunnel face. The use of Full Perimeter Intersection (FPI) as a method for identifying critical deformation zones is discussed in a separate, companion report by /Munier 2006/.

When a fracture that is larger than the tunnel or deposition hole diameter cuts the tunnel forming a complete elliptical intersection, Figure 2-65, it is necessary to assess its length to ensure that displacements exceeding the critical value cannot occur. However, any fracture that does not completely cut the tunnel or borehole as a continuous intersection line can be ignored because even if it represents the extremity of a critical fracture, movement along it at this location (i.e. at the end of the fracture) will fall well below the maximum permitted.

We might also argue that any critical deformation zone that does not cut the tunnel or deposition hole will not pose a threat to the integrity of the canisters even if it is in close proximity. This is because displacement along it will not significantly impact on the deposition hole.

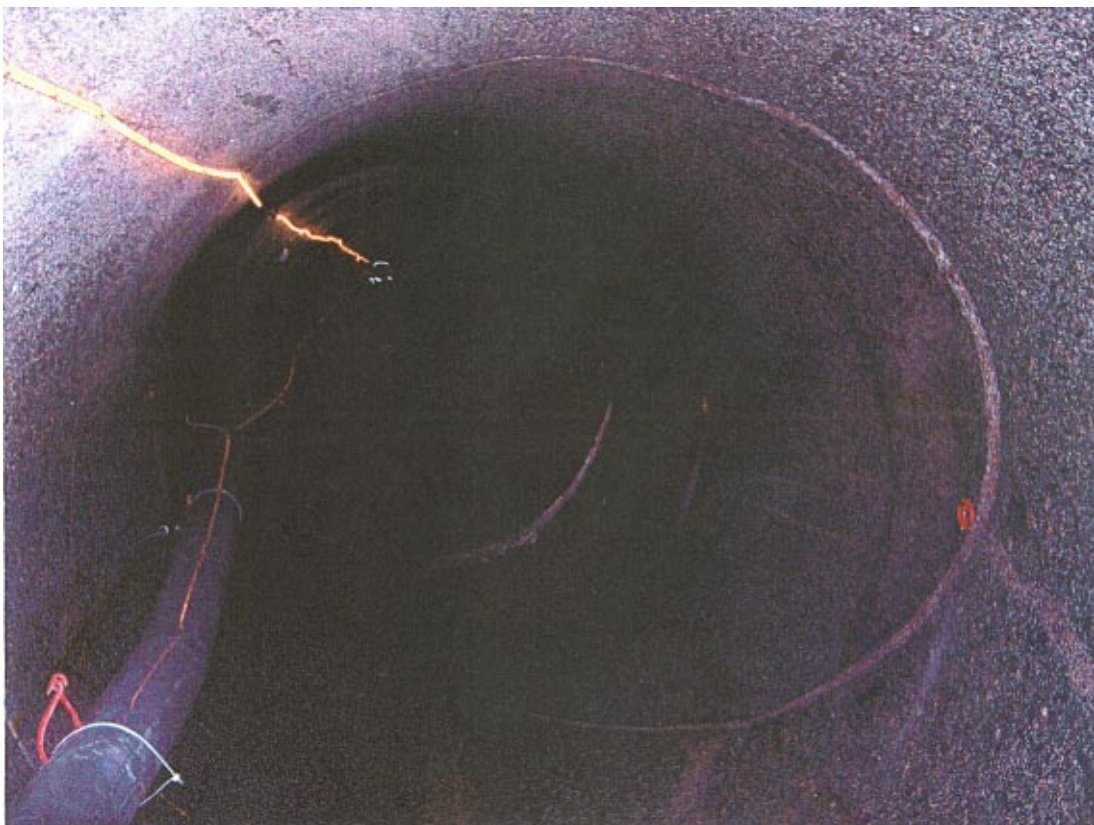


Figure 2-65. A pegmatite filled fracture cutting the tunnel. The fracture is longer than the tunnel diameter and as a result forms a complete ellipse as it intersects the tunnel wall. This is termed a "Full Perimeter Intersection" (FPI). Äspö Hard Rock Laboratory.

It should be pointed out that the arguments used above to determine that a fracture does not pose a threat to the integrity of the deposition hole relates only to the possibility of slip on that fracture damaging the canister. It does not imply that the fracture is not highly transmissive and is therefore of no threat to the buffer integrity.

2.12.5 Other techniques for determining the size of a critical structure

As a compliment the attempt to identify deformation zones with the likelihood of exceeding the critical length using geometric features of the type listed above, it is proposed that geophysical techniques be used. This is because fracture infilling (either by minerals or by water) and wall rock alteration that are the result of high fracture conductivity, a good indicator of fracture size, may provide the fracture with a clear geophysical signature that enables its extent to be determined using geophysical methods. These methods are discussed in detail in Chapter 3.

2.12.6 Identification of deformation zones using two or more boreholes

Another method of reducing the likelihood of missing critical deformation zones is to design the investigative probe holes that precede tunnel excavation so as to maximise the possibility of picking up long fractures by identifying them in more than one probe hole. This technique is currently being used by Posiva at Olkiluoto where the access ramp is being excavated.

The use of cross-hole correlation techniques to establish the extent and position of conductive fractures has been studied in the Äspö HRL during the TRUE Block Scale project and is described in the report /Andersson et al. 2002/. The study was carried to characterize a volume of rock (200×250×100 m in order to provide the basis for successful tracer experiments in a network of conductive fractures at the block scale. During this study, cross-hole correlation involving a variety of flow logging techniques was successfully used to trace the extent of conductive features. The report also describes the use of BIPS borehole television logs and BIPS-based BOREMAP corelog to correlate the hydraulic flow anomalies with geological features and highlights the difficulty that exists in determining the extent of the conductive structures outside the borehole array. As is discussed in Chapter 3 and in appendix A1, an attempt has been made at Äspö at cross correlation of deformation zones observed in tunnels and shafts with data on deformation zones obtained from boreholes drilled sub parallel to the tunnels and shafts.

Fracture recognition in more than one borehole or tunnel is one of the most important techniques for detecting large fractures. Consequently the reliability of the techniques used for matching fractures and fracture zones between two excavations (tunnels, deposition holes and boreholes) needs to be assessed.

It was pointed out in Section 2.11, that the level of confidence of fracture correlation goes down as the borehole separation increases and in addition is also decreased as:

- The irregularity of the fractures and fracture zones increases and,
- the continuity of the individual fractures making up a brittle deformation zone decreases. I.e. when traced along their length the individual fractures may pass into an echelon arrays of fractures with statistically the same strike but offset from each other either to the right or left.

This problem of correlation of deformation zones has received considerable attention recently by workers from Posiva and a new procedure for the recognition and classification of these zones in cored boreholes and tunnels has been introduced /Paulamäki et al. 2006/ Figure 2-59. It is based on the Sibson-Scholz fault zone model (/see Milnes 2006/ for an overview). For deformation zone correlation, data on the type of fracture, on the mineral infilling such as epidote, calcite and quartz, and on kinematic indicators, in particular slickensides and crystal fibres to get both a direction of movement and a sense of movement on the fractures are used.

This focused attempt to carefully classify the fractures and other deformation zones, making the maximum use of all features, will considerably reduce the possibility of miss-matching fractures and fracture zones between boreholes.

On the basis of the concepts discussed in this report an attempt has been made to identify the worse case scenario most likely to lead to a critical deformation zone remaining undetected and which could impact most adversely on the integrity of the deposition holes.

It is concluded that this would correspond to a sub-horizontal fracture, located just below the repository tunnel floor, which was infilled with weak material which rendered it non-conductive but gave it very little strength. Its non-conductive nature would result in none of the features that characterize long conductive fractures developing and the weak infill would mean that it was very susceptible to re-shear during post-glacial faulting

2.12.7 Conclusions

The task addressed by this chapter is that of identifying features of deformation zones' that relate to their length and which might be used either alone or in combination with other features or criteria to identify in tunnels and boreholes, deformation zones with a radius of > 50 m. It has been pointed out in Sections 1.4 and 2.1, that the term "deformation zone" includes a large spectrum of structures ranging from discrete brittle fractures through fracture zones to planar or sub-planar zones of intense ductile deformation known as shear zones. Different features and criteria for indicating length have been identified for the various structures included in the term "deformation zone". One of the most useful features that can be used to indicate the length of discrete fractures is whether or not they intersect the full perimeter of the tunnel or deposition hole. It is argued that only fractures that cut the whole tunnel or deposition hole need to be considered in size estimation.

The parameters most closely linked to fracture length that can be measured in a tunnel or deposition hole and which can be applied to the complete suite of structures included in the term "deformation zone" are:

- Aperture.
- Shear displacement.
- Conductivity.
- Deformation zone thickness.

Having established the parameters most likely to reflect the length of a deformation zone it is pertinent to ask whether the actual length can be established from any of them. The answer to this question appears to be no. However, these parameters, combined with the full perimeter intersection criteria, can be used to identify long fractures and other deformation zones and these can then be examined using other techniques to determine their extent.

These techniques include:

- Cross-hole correlation (exploiting kinematic indicators).
- Geophysical techniques.

It is suggested that the most effective way of ensuring that critical deformation zones are not overlooked is to combine a visual inspection of the fractures i.e. detailed characterization of the fractures in the tunnel, (where the focus will be on full perimeter intersection), deposition holes and exploratory bore holes and cores, using the main criteria listed above combined with geophysical scanning (see Chapter 3) and the employment of the improved geological data acquisition procedures similar to those now being employed by Posiva in connection with the ONKALO project, for establishing cross-hole fracture correlation which attempts to maximize

the use of structural data such as kinematic indicators to maximize the confidence level of correlation. It is noted that the use of kinematic indicators and other features in cross-hole correlation will require an appropriate core orientation technique.

In addition it is possible to argue that many deformation zones encountered in the tunnels and deposition holes will NOT pose a threat to the integrity of the canisters, even if they are longer than the critical length. For example, if any fracture does not completely cut the tunnel or borehole as a continuous intersection line it can be ignored because even if it represents the extremity of a critical fracture, movement along it at this location (i.e. at the end of the fracture) will fall well below the maximum permitted.

Finally it is noted that the better the understanding of the structure and geological history of the repository site and of the fracture network that pervades the rock mass, the less the likelihood of missing a critical deformation zone.

3 Investigation methods for the detection of deformation zones

3.1 Introduction

In this chapter the various borehole and core investigation techniques that can be used to obtain information about the location, type, orientation and extent of deformation zones are discussed. The usefulness of the various methods varies depending on the position within the repository structure. For example, destructive techniques, which can be used during the excavation of the ramp and possibly the access tunnels, must be avoided during the excavation of the deposition tunnels and deposition holes. The construction of the repository has been divided into 4 stages corresponding to the excavation of 4 zones, namely, 1) the ramp leading down to the repository level, 2) the tunnel face and trunk tunnel, 3) the deposition tunnels and 4) the deposition holes. The most appropriate methods for the detection of deformation zones during these 4 stages in the excavation of the repository site are summarised in Table 3-2 to 3-6. It is planned that the repository will be developed and constructed step by step within well defined subareas. In one subarea the excavation may be ongoing while the immediately adjacent subarea is in operation. This parallel development provides the opportunity and time to conduct detailed investigations of deformation zones (specifically their location, orientation and characterisation) at different places in the repository. This information can then be used to trace the deformation zones from one subarea to another. The search for these deformation zones (which include single fractures, fracture zones and brittle and ductile shear zones, see Section 1.4 and 2.1) at the repository level will mainly be conducted in parallel with the excavation and construction of the repository and will constitute an integrated part of the detailed site investigation. A similar layout of the Prediction/Outcome studies is being conducted within the ONKALO project in Finland by Posiva Oy (also see Section 2.12.7).

The results of the Complete Site Investigation provide a platform for the detailed underground investigations at the repository level. It is anticipated that the most important and specific results with respect to identifying critical deformation zones among other features will be obtained during the excavation of the ramp down to the repository level and during the excavation of the repository itself. The main aims of this investigation can be summarized as follows:

- To define the geological boundaries of the repository subareas.
- To select the position of the deposition tunnels.
- To select the position of the deposition holes in the deposition tunnel.
- To facilitate the safety acceptance of a deposition hole.

The programme of the detailed investigation during construction is of importance for both construction issues, and for providing input to future assessment of the long term safety. It is anticipated that a systematic strategy for the investigation and the documentation of the deformation zones will be developed within that framework, and will be implemented in parallel with the excavation work. The investigation strategy might vary in content and detail depending on the excavation stages.

In this section of the report, a combination of several investigation methods is suggested and discussed as a first strategic model for a systematic search for deformation zones. The combinations used will depend primarily on the stage of the excavation (i.e. whether it is the ramp, access tunnel or deposition holes that are being excavated) and on the rock type.

3.2 Sources of information

There are several possible methods of investigating a volume of rock. The main problem is always access. The repository can be divided into 4 subareas, Figure 3-1. The investigation strategy has to be developed on the basis of both the available access for investigations, and the suitability of methods. These may change at various stages in the excavation. The access available to the rock mass and the available techniques for detecting deformation zones (i.e. fractures, fracture zones etc) are considered for each subarea in Figure 3-1. This strategy will form part of the detailed investigation program that SKB will develop, and it will include:

1. Investigations from the ramp leading down to the repository.
2. Investigations at the repository level to decide on the position and orientation of (a) the trunk tunnels and (b) the deposition tunnels.
3. Investigations for each deposition tunnel to determining (a) the rock mass properties surrounding the deposition tunnel and (b) the appropriate positions for the deposition holes.
4. Investigations within the deposition holes drilled into the deposition tunnel floor to confirm deposition hole requirements are satisfied.

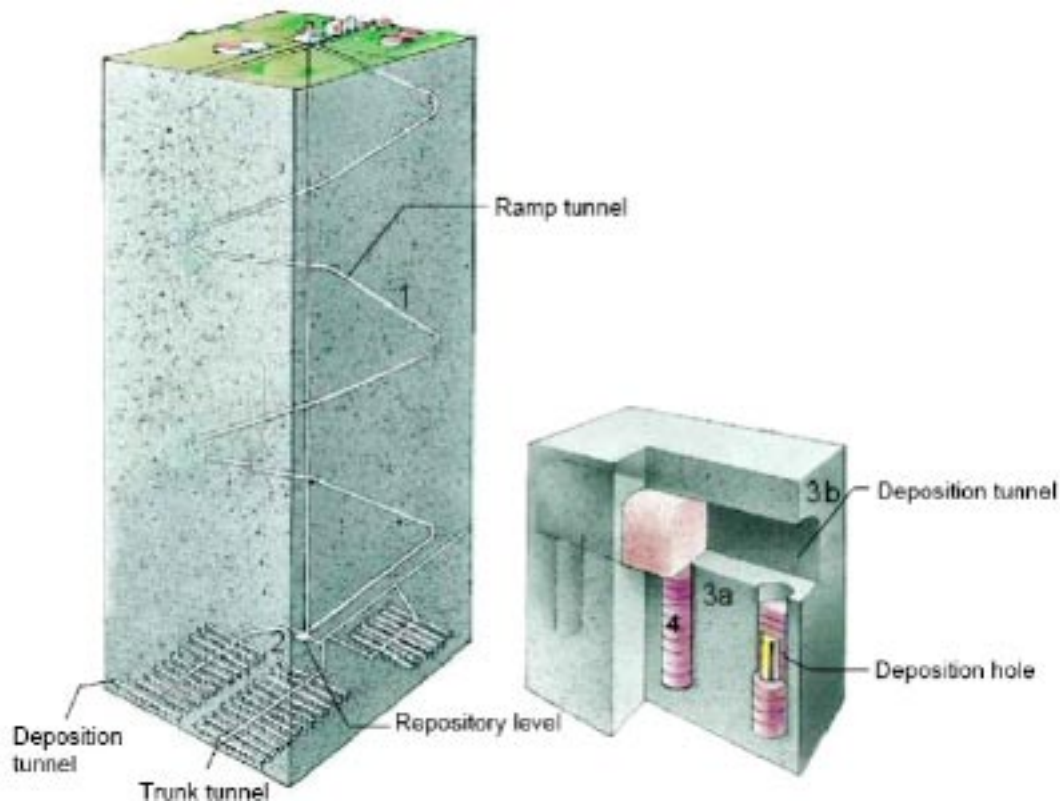


Figure 3-1. The areas of investigation in a rock mass in which a deep repository is located; 1) the ramp leading down into the rock, 2) the tunnel face and trunk tunnel, 3) the rock surrounding the deposition tunnel and 4) the rock mass surrounding the deposition holes.

The basic geometric conditions for the investigation of deformation zones will be dependent of the scale. The site investigation, which starts from the ground surface, considers structures that range from 100–1,000 m in length, a scale that will probably become reduced as the excavation proceeds and becomes progressively closer to the deposition hole site where the investigation will become more detailed. The excavation of the ramp forms a downwards going spiral and will therefore intersect existing fractures regardless of their orientation, an important factor when analysing fracture frequency and characteristics. At the level of the repository investigation techniques used in the deposition holes, position 3 in Figure 3-1, must be able to identify structures as small as a few metres in length. The bulk of the investigation phase and also the most important part with respect to the detection of critical deformation zones, will be conducted during the construction of the deposition areas.

3.3 Strategies for investigations

The strategy for the investigation aimed at the identification and location of deformation zones (i.e. fractures and fracture zones) is outlined in the flow diagram in Figure 3-2. The diagram includes a variety of data collected from ongoing, parallel investigations such as core mapping, geological mapping at the surface, hydrogeological investigation and others. Although, this discussion will concentrate on the detection of critical deformation zones, it is noted that an understanding of the general geology of the site will be necessary as this will provide an insight into the distribution and type of deformation zone that is likely to characterize the rock mass. The strategy adopted is such that the investigation is performed in a series of stages following the steps indicated in Figure 3-1. Different strategies must be developed depending on the site specific conditions and the thickness of the deformation zones (reference from Roy Stanfors).

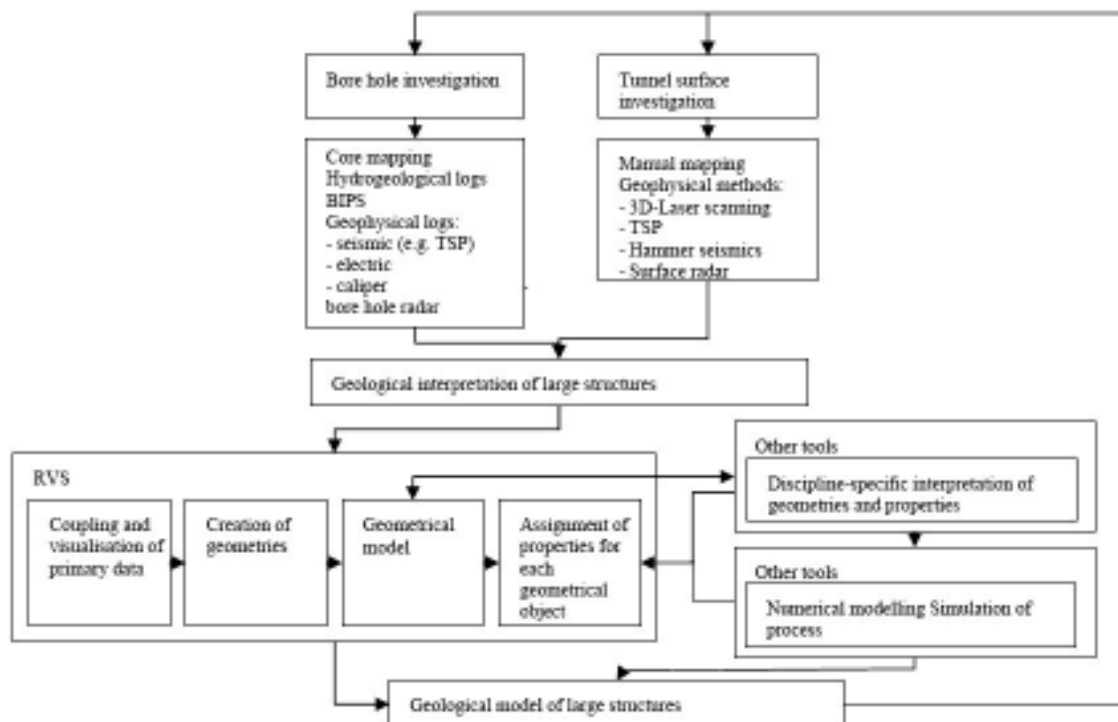


Figure 3-2. Strategic flow diagram showing the strategy for investigating, identifying and locating deformation zones which can then be integrated into the 3D geological model.

The step-wise investigation methodology from stages 1–4 will result in an increase in the knowledge of the deformation zones. The highest level of understanding of their orientation, frequency, geological appearance and rock mechanic characteristics will occur at stage 4 when a drilled deposition hole is characterized. The new geological information collected from the various stages will be added to the site geological 3D model, an interactive development process as shown in Figure 3-2.

This step-wise strategy will therefore gradually focus onto the main targets, i.e. each deposition hole at the repository level, working from a mainly statistical approach of data handling for the deformation zones at the surface to a deterministic approach in the deposition hole, as shown in Figure 3-3. As can be seen from this diagram most of the data will be retrieved at this level.

The understanding of the geometry and physical properties of the deformation zones which are encountered at each site is crucial for the development of a useful strategy. Fortunately fractures, fracture zones and shear zones, the main types of deformation zones, usually show a distinct signature in the geological and geophysical record, especially in crystalline rock. This is because fractures of large magnitude may currently conduct water or may have done so in the past with the result that the walls of the fractures have been altered either physically or chemically and/or minerals have been deposited along the fractures. Such features are easily identified from tunnels by direct observation and can be detected in boreholes using geophysical techniques. For example, water has a high electrical conductivity and can be discerned quite well using electric methods, especially in granites and similar rock types where the content of electrically conductive minerals is low. In contrast to the increase in electrical conductivity of a fracture resulting from the presence of water, there is a decrease in the magnetic response of a conductive fracture in rock types with a high content of magnetic minerals. The oxidation of the magnetic minerals in the fracture walls, which can result from their exposure to water, causes a diminishing of the magnetic response compared to that of the surrounding rock. This oxidation is often a result of an ancient fluid system in the rock, not related to the present fluids in the rock mass. In addition, the density of fractured rock is lower than the rock surrounding it as a result of the relatively larger number of voids filled either with water or air. This is reflected in seismic, gravity and density measurements. Thus, there are several geophysical methods available for identifying fractures and fracture zones and the task is to find techniques with a large enough detection volume and a high enough resolution to identify critical structures i.e. fractures, fracture zones and shear zones with a radius greater than 50 m. In addition, the systematic mapping of the tunnel walls will allow a continuous correlation between the geological observations from the tunnels and the geophysical data from nearby boreholes. Good exposures of the deformation zones in the tunnels allows a detailed characterization of the zones which will indicate the most suitable borehole investigation method(s) for their detection. These various methods are listed and discussed in Section 3.4.

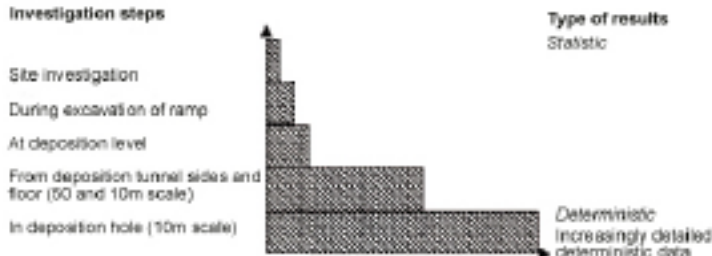


Figure 3-3. Step-wise strategy used to focus the search for critical deformation zones around the main target areas i.e. the deposition holes. It involves working from a statistical approach at the surface to a deterministic approach in the deposition tunnel.

3.3.1 Correlation and identification of deformation zones

It is recognised that it is a difficult matter to detect and define the boundaries of deformation zones and that there is unlikely to be one unique method for observing them in the rock mass. Their geological signatures are likely to vary and are probably site specific. In addition, very few of the currently available methods have both the long range and very high resolution needed. Therefore, combined investigation methods are necessary.

SKB has performed several borehole tests in order to determine the most successful combinations. These are discussed briefly in Section 3.5 and in more detail in appendices A1 and A2 and in /Carlsten et al. 2001/. It is concluded that deformation zones can be detected in boreholes using BIPS and the combined flow-, resistivity and calliper logs. From other investigations of boreholes, correlations between different geophysical signatures and fracture frequency have been established and from these results so called “pseudo fracture frequencies” can be estimated.

In contrast to borehole logs which have a high resolution (i.e. in the cm to mm range) the borehole radar has a much lower resolution. However, it has a longer range which can be exploited to provide information on the length of a deformation zone. Thus by combining borehole radar results with the higher resolution logs, the location and extension of a deformation zone into the rock around the borehole can be determined. Radar can trace fractures up to a distance of 25 m from the borehole. In this way structures with a length of up to ~ 50 m can be measured and larger structures identified.

The geological and geometric characteristics that can be used to indicate the length of a deformation zone are discussed in Chapter 2 where it is concluded that the main features that can be used directly or indirectly to help recognized critical deformation zones are:

- Aperture.
- Shear displacement.
- Deformation zone thickness.
- Kinematic indications.

Although contentious, conductivity may, in some examples, be related to the length of the deformation zone.

3.3.2 Implementation and training

It is necessary to further develop a strategic working procedure for detecting deformation zones during the construction of the repository as there are no specific non-destructive methodologies existing at present that will both identify the deformation zone and define the limit of its extent. The detailed information that can be captured during the excavation of the ramp will therefore provide an excellent data base for the development of such an investigation model (see Figure 3-4). The tunnel walls will offer possibilities for accurate mapping and detailed studies of the “geological signatures” of deformation zones, as well as for accurate measurement of the orientation of these structures by for example 3D laser scanning. Using the results of these investigations in combination with radar measurement on the surface and in boreholes, the extent of possible critical structures can be traced within the rock mass.

As the excavation of the repository proceeds through the 4 stages shown in Figure 3-1, a strategic methodology for the capturing of data linked to critical structures will successively be developed and the geological model SDM 2.3, developed from the detailed investigations at the surface and in boreholes, will be continuously upgraded using the data base built up during excavation.

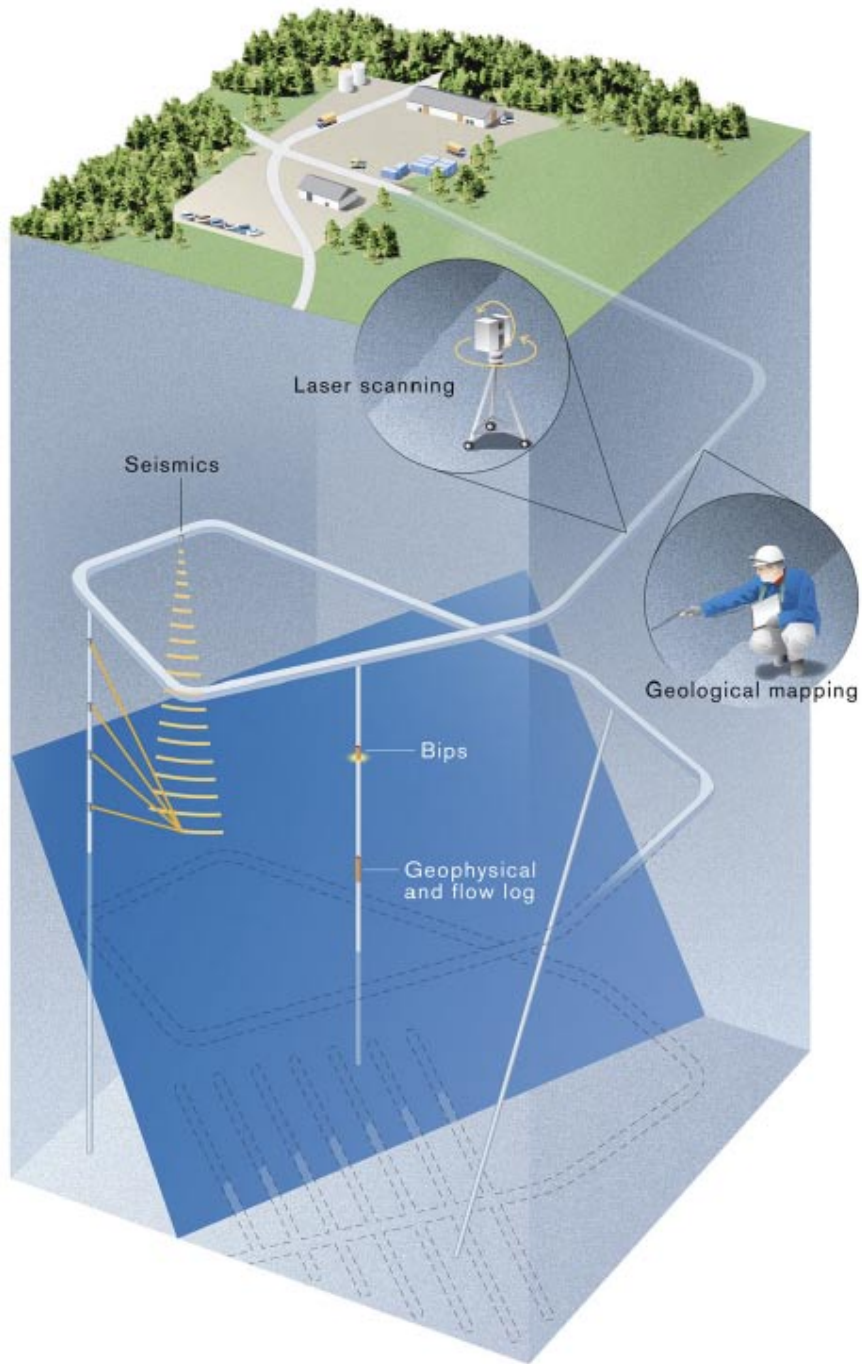


Figure 3-4. Investigations from the ramp leading down to the repository to detect deformation zones.

Suggested methods to be used for “the search” for critical deformation zones are presented in Table 3-1.

A possible procedure for the use of the techniques listed in Table 3-1 for identifying deformation zones during the construction of a repository might be as follows:

1. Geological mapping according to SKB methodology, both at the surface prior to the excavation and within the tunnels and boreholes during excavation.
2. Processing of the geological data to search for the geological signatures for critical deformation zones.
3. 3D laser scanning of the tunnel will be used to compliment the geological investigation by providing an accurate documentation of the position, orientation and width of deformation zones intersecting the tunnel.
4. Combined analysis of geological information and measured laser data to determine the orientation of the potentially critical deformation zones and evaluation of the geological signatures.
5. Development of the 3D geological model.
6. Generate a plan to search for critical deformation zones using data from point 4 and 5.
7. Core drilling in selected directions to intersect the deformation zones.
8. Combine borehole data such as flow, resistivity and calliper logs. See also Appendix 1 for a description of studies of the correlations of deformation zones between tunnels and boreholes at the Äspö HRL”.
9. Use borehole radar measurements to determine the extent of critical deformation zones.
10. Processing of the information obtained from 1–9.
11. Updating the 3D geological model with the new data.

It is likely that any site investigation will be site specific. The development of the strategic model for the detection of critical deformation zones will gradually evolve as new data becomes available as steps 1 to 9 are carried out.

The strategic model is based on the hypothesis that there is a correlation between geological characteristic parameters of deformation zones as described in Chapter 2 and their extent. It is crucial that the research carried out during the construction of the repository is carefully executed so that the model is tested, modified and evaluated to the point where it is sufficiently accurate to be used with confidence at the level of the repository. The milestones in this process are:

- Finding the critical geological characteristics of the deformation zones.
- Finding suitable technical tools to define their extent.
- Determining if there is a spatial variation of the geological characteristics with depth.
- Defining uncertainties, limitations, and establishing the most suitable methods to use at the various stages of repository construction.

3.3.3 Investigations of a deposition area

A major issue when the repository level is reached will be that of determining the optimum layout of the repository subarea, which will involve a number of parallel deposition tunnels. At this stage knowledge of major lithological boundaries and important deformation zones will be essential.

This phase is represented by position 2 in Figure 3-1. The central trunk tunnels to the deposition tunnels have been fixed in place, but the boundaries for the deposition subarea have yet to be defined. The accessible geological data at that position will be the upgraded geological model SDM 2.3 plus data obtained from investigations conducted at the level of the repository (Figure 3-5). Geophysical and horizontal borehole logging is made from position 2 in Figure 3-1 in order to investigate the rock mass ahead of the tunnel face. Possible investigations methods suitable for use in this position are presented in Table 3-3.

3.3.4 Investigations for the positioning of the deposition tunnels

Closely related to investigations for defining the deposition subareas is the determination of the orientation and location of the deposition tunnels, position 3 in Figure 3-1. Investigations are made from the central trunk tunnel into the surrounding rock mass. The tunnel walls are mapped according the methodology developed during the construction of the Äspö HRL, with possible site specific modifications based on information gathered during the excavation of the ramp. When the location and orientation of the deposition tunnels has been decided, core drilling is carried out along the entire length of the proposed tunnel and various borehole methods such as radar, seismic methods and logs are used to locate possible critical deformation zones,

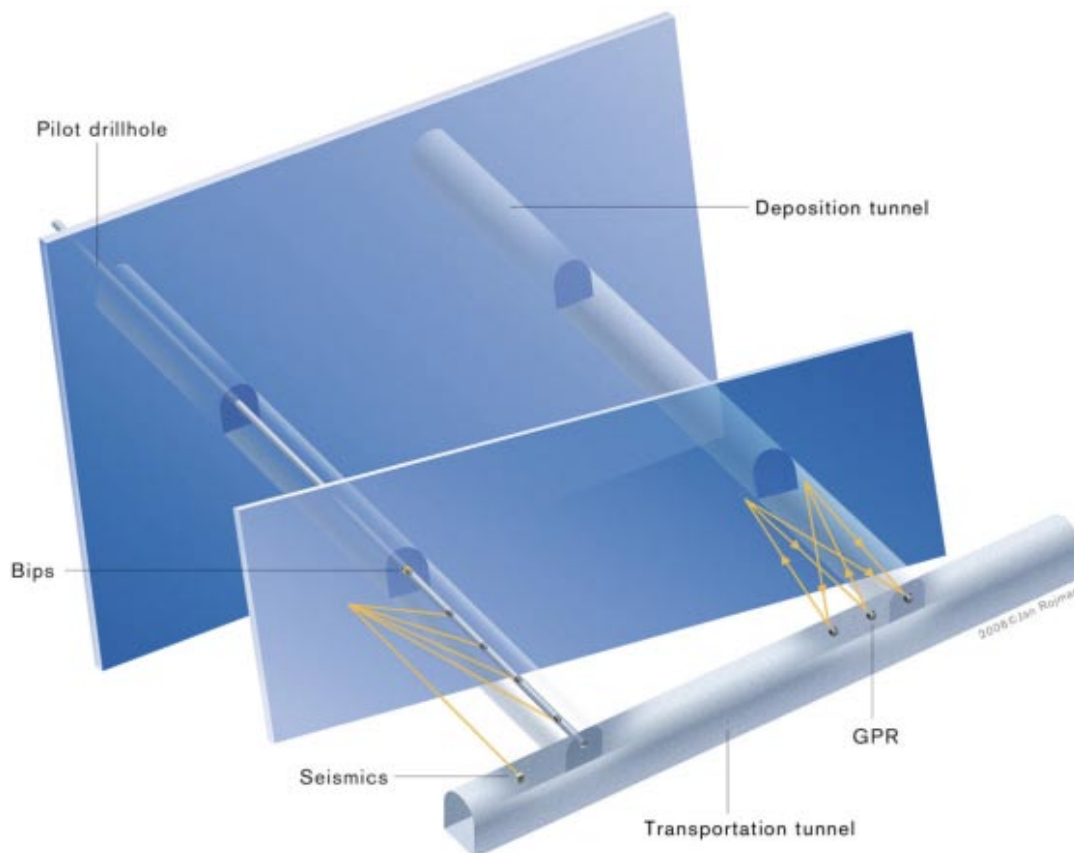


Figure 3-5. Investigation procedures at the repository level (position 2 in Figure 3-1) to detect deformation zones and to determine the optimum location for the deposition tunnels and holes.

Figure 3-5. Tomographic technique may be used between boreholes in rock volumes that need special attention. The results of the investigations are used to determine the final position of the deposition tunnels, and to determine their lengths. Possible investigation methods are presented in Table 3-4.

At this point the 3-D geological model is upgraded with the newly acquired borehole and geological information.

3.3.5 Investigations for the placement of the deposition holes

Very detailed investigations are needed to determine the placing of each deposition hole along the deposition tunnels, position 4 in Figure 3-1. The range for the search will be in the order of 10 m into the rock mass surrounding the deposition tunnel.

The surface investigation of the deposition tunnel walls and especially the floor of the tunnel will be very important. This requires that the tunnel floor must be completely cleaned. Surface mapping using 3D laser scanning will accurately position the fractures in space. Surface radar will be a complement as a non-destructive method that can be used to “look” into the rock mass. Pilot core drilling will be carried out in the proposed positions of the depositions holes. Borehole investigations with radar and logs and especially hydraulic logs will be of great help in detecting large fractures and smaller, interlinked fractures (i.e. fracture zones).

It is also possible to use hydraulic pressure build-up tests to find out if fractures in adjacent boreholes are linked together as presented in /Andersson et al. 2002/. Possible investigation methods are presented in Table 3-5.

The excavation of a number of parallel deposition tunnels at the same time will facilitate the development of a detailed geological model of the construction area. This will provide the basis for the planning of further detailed investigations for the positioning of the deposition holes.

At this point in the development of the site the information from the 3D geological model will be used in the planning of the drilling program for the vertical boreholes which are likely to be drilled within the volume of the proposed deposition holes. The drilling program will be wholly based in the geological model. It will be important to use non-destructive methods when working on the surface of the deposition tunnels and holes.

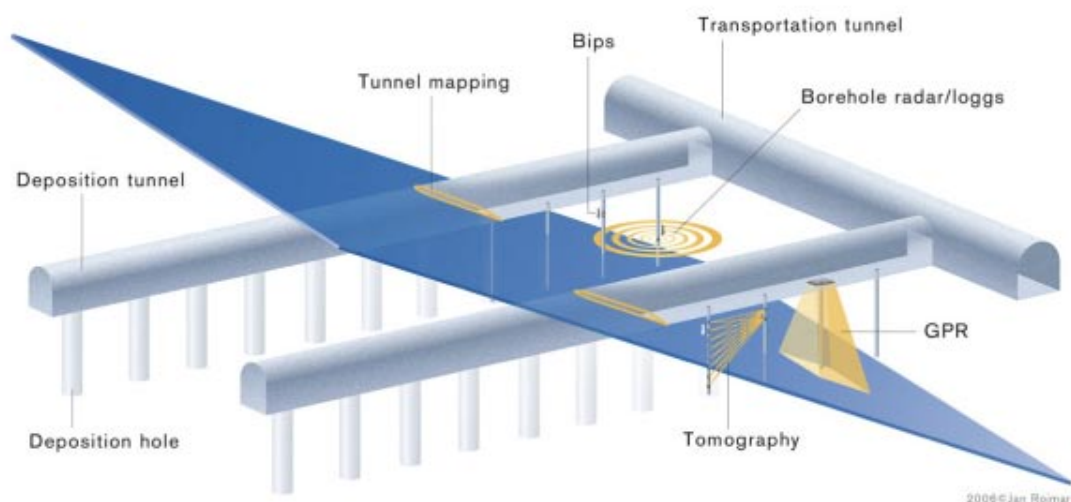


Figure 3-6. The surface investigation of the deposition tunnel walls and floor.

3.3.6 Acceptance of deposition holes

The criteria used for accepting a deposition hole will guide the strategy for detecting the critical deformation zones. The methods to be used are primarily surface mapping of the walls of the deposition hole. This could be achieved by 3D laser-scanning in combination with manual mapping. The scanning will also provide information on the surface roughness of the walls as well as the tolerance of the circular shape along the entire length of the hole. If fractures occur on the surface of the deposition hole, radar or surface seismics might be used to determine their extent into the rock mass. This procedure is illustrated in Figure 3-7 and the possible investigation methods are presented in Table 3-6.

Geological data from the different deposition holes will be used to update the detailed 3D geological model and for the correlation of fractures and fracture zones between the holes. This will result in a very accurate 3D geological model.

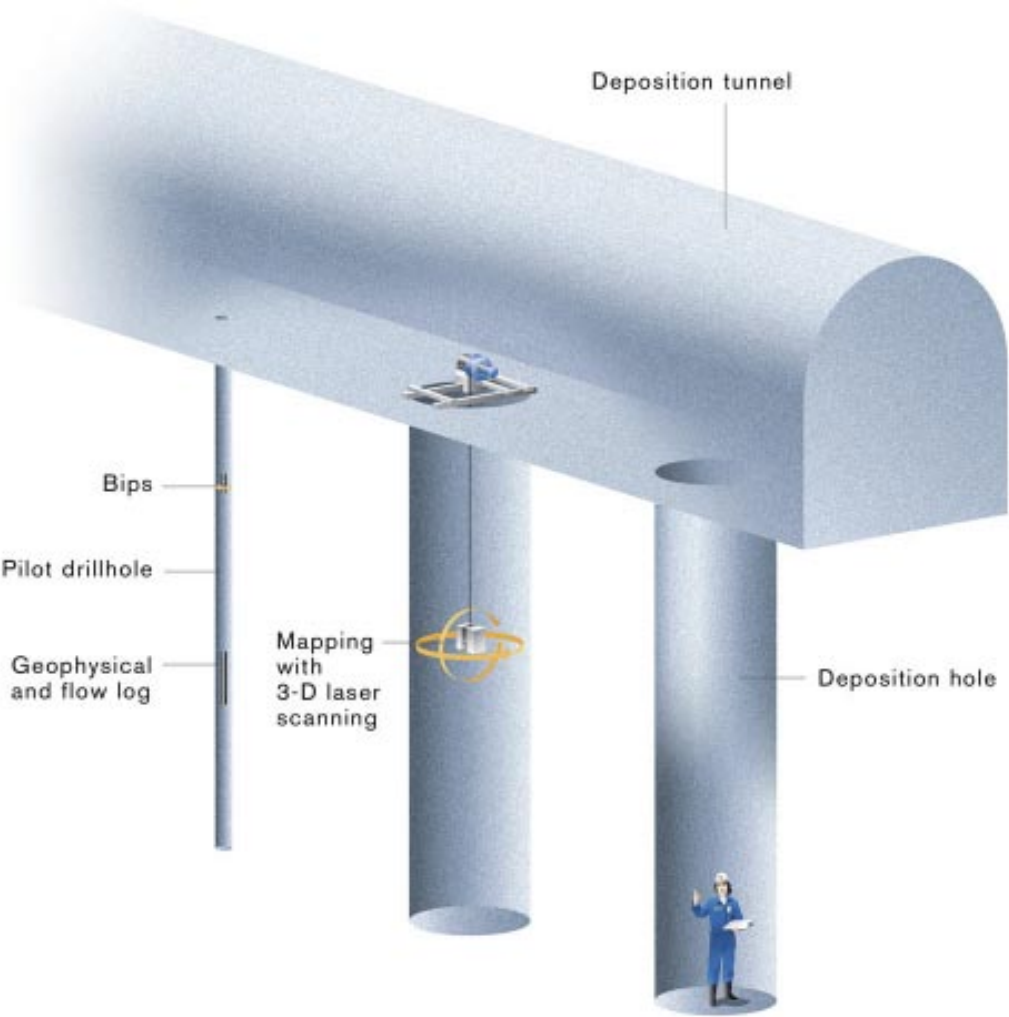


Figure 3-7. Investigations within the deposition holes drilled into the deposition tunnel floor.

3.4 Overview of available methods

The selected potential investigation methods for the detection of the deformation zones during the construction of the different parts of the repository are presented in Table 3-2 to 3-6. The selection of each method is based mainly on references from other investigations performed for SKB, especially from the construction phase of the Äspö HRL (Table 3-1) /Almén and Stenberg 2005, Winberg et al. 1996/, and the main parameters used in the selection has been the potential contribution that the method can make to the detection of deformation zones.

During the work on the site descriptive model made by SKB four geometrical scales has been defined /Rhén et al. 1997/. In the classification table (Table 3-1) three of these are used. These are the; site scale (100–1,000 m), the block scale (10–100 m) and detailed scale (0–10 m). It is necessary that in one or more tests the zone can be identified down to the mm-cm scale.

A short summary of selected investigation methods for detecting deformation zones are presented in the following sections. They include both borehole investigations and methods useful on tunnel surfaces.

Table 3-1. A classification of useful geological methods for detecting “deformation zones”. From /Almén and Stenberg 2005/.

Subject	Method	Usefulness			Notes
		Site scale	Block scale	Detailed scale	
Lithological units	Geological tunnel mapping	3	3	3	
Rock composition	Probe boreholes and percussion holes	–	1	1	
Rock boundaries	TV-logging	–	2	2	
	Core logging	3	3	3	
	Geophysical borehole logging	1	1	1	
Rock type characteristics	Geological tunnel mapping	3	3	3	
	Core logging	3	3	3	
	Geological analysis of rock samples	–	–	2	
	Mineralogical analysis of fracture fillings	–	–	3	
Small scale fractures	Geological tunnel mapping	3	3	3	
	Core logging	2	2	2	
	TV-logging	3	3	3	
	Geophysical borehole logging	2	2	2	
Major fracture zones and minor fracture zones	Geological tunnel mapping	3	3	3	
	Core logging	3	3	3	Minor zones
	Percussion boreholes	–	2	2	
	TV-logging	–	–	–	
	Geophysical borehole logging	2	2	2	
	Radar methods	2	2	2	Minor zones
	Seismic methods	2	2	2	
Single open fractures	Geological tunnel mapping	–	3	3	
	Core logging	–	3	3	
	TV-logging	–	2	2	
	Radar methods	–	2	2	

Very useful = 3, Useful = 2, Less useful = 1, Not applicable or used = –.

3.4.1 Tunnel mapping

Geological mapping complemented with laser scanning of the tunnel surfaces during the excavation of the ramp will increase the knowledge of the location, orientation and geometry of deformation zones and will provide a good description of their characteristic features. Investigations in boreholes drilled from the ramp can be used for detailed analyses of the long fractures and fracture zones located in the tunnel at depth (Table 3-2). The same borehole measurement techniques will be used as those used in boreholes drilled from the ground surface.

After the drilling of the deposition holes, mapping of the surface of the holes will be achieved by careful manual examination and by laser scanning (Table 3-5). The mapping will be performed according to a methodology developed by SKB. The documentation is made after each drilling in order to verify and confirm the occurrence and location of any predicted deformation zones.

The deposition tunnel will also be used as a base tunnel for further investigations of the surrounding rock mass (Table 3-6). This investigation will be mainly focused on determining the extent of potential long deformation zone found in the deposition holes. The investigation techniques will be tomography using seismic and radar technology and Tunnel Seismic Prediction (TSP). Complementary detailed analyses will be made from data from borehole logging and logs.

3D laser scanning

A high resolution, three dimensionally correct model of a surface or object can be obtained from full coverage 3-D laser scanning. Pulses of infra-red light with a specific wavelength are produced and the reflected intensity of the pulse as well as the length and amplitude is tuned to the height, divergence and the properties of the receiver. The laser scanning data are usually combined with digital photos /Mettenleiter et al. 2000, Langer et al. 2000/. A three-dimensional model based on point information (point cloud) is produced and, with a scanner that can rotate 360° horizontally and 310° vertically, results in real 3D measurements. Depending on the equipment, different resolutions can be achieved, but point-distances of 1-3 mm are needed for the detection of fractures. The highly accurate spatial information (position and orientation) of geological structures such as fractures that this technique provides is the main advantage of this method /Feng and Röshoff 2004/. Together with ortho-photographs this method can be used to provide an excellent basis for geological mapping (Figure 3-8).

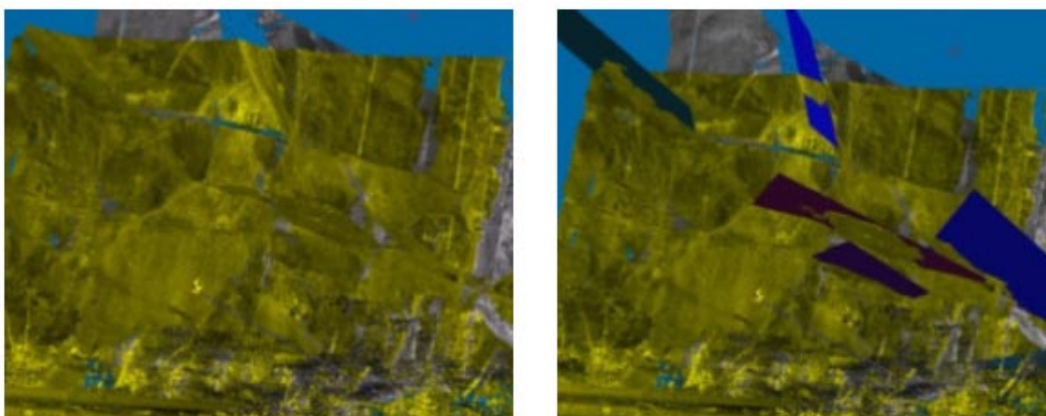


Figure 3-8. Fracture mapping from laser scanning data. Left: tunnel wall with fracture traces. Right: tunnel wall with best-fit surfaces to the fractures.

3.4.2 Borehole methods

The methods presented here are those used by SKB to identify deformation zones.

Core analysis

The main source of primary geological data in boreholes comes from the mapping of the rock core, and is acquired according to the methodology called BOREMAP, used by SKB and described in SKB MD 143.006 version 2.0. Together with core mapping the image logging system (BIPS, see following section) is used to infer the orientation and kinematic indications from the core and borehole information.

Image logging, BIPS (Borehole Image Processing System)

BIPS is a borehole TV system used to produce a rolled out image that covers the entire 360° of the inside of the borehole. From BIPS images the orientation and a simple characterization of each fracture along the borehole can be obtained as shown in A2-5 to A2-12. Knowing the orientation of the borehole, the orientation of each fracture might be deduced. The interpretation is dependent on the quality of the image and the lithology and structure of the rock mass. This can be used in combination with other methods such as radar images and differential flow to identify and trace deformation zones between boreholes /Carlsten et al. 2001/.

A combination of data from different methods for measuring changes of physical properties along a borehole is used to identify deformation zones. Several of the measurements must be corrected to allow for the environmental conditions during the measurement (pressure, temperature etc) and instrument characteristics. For example:

- Fluid temperature is used to correct resistivity logs. It yields information on inflow and outflow of fluids in the borehole. It is also used when calculating salinity from the fluid resistivity.
- Fluid inflow yields information on the inflow of fluids into the borehole.
- Calliper measurements (mm) give information of the borehole diameter and are used to correct the other logs.

Techniques for single hole investigations of the bedrock have been developed during different projects within the SKB research program. Not surprisingly, several studies show that a combination of geophysical techniques is the most efficient method for predicting deformation zones (fractures and fracture zones) in the bedrock surrounding the borehole. Several of these techniques are presented below.

Hydro-geological tests

Fluid flow in fractures is investigated using; pressure monitoring, flow meter logging and interference tests. These methods give general information on the effect of underground activities on the hydraulic system within the rock mass /Almén and Stenberg 2005, Rhén and Forsmark 2000, Hermansson et al. 1996/. Methods which will give information on the scale of deformation zones are pressure build up tests and especially tests using multi-packer systems. In these tests an investigation of the hydraulic properties of deformation zones can be used to identify and trace their extent between boreholes. By isolating conductive features in boreholes and monitoring their hydraulic properties the influence of a borehole or tunnel can be discerned, and thus give information of the extent and the orientation of the fluid conductive feature /Andersson et al. 2002/.

Geophysical logging

A combined interpretation of the different logging methods (in this case density, magnetic susceptibility and natural gamma radiation), together with petrophysical data and/or data from geological core logging, make it possible to estimate the physical signature of different rock types.

In addition it is possible to identify the position of fractures and to determine the “pseudo fracture frequency” (classification of pseudo fracture logging and pseudo fracture frequency logging) based on the analysis of the short normal resistivity, calliper and single point resistance, sonic and focused resistivity (300 cm) loggings.

The position of deformation zones is estimated by applying a second derivative filter to the logging data and the location of maxima or minima in the filtered logging (depending on the logging method).

Electric logs

The electric resistivity, which is the inverse of the electric conductivity, is usually measured in these methods. They also need to be corrected for borehole diameter and borehole fluid resistivity.

Generally several different methods such as Short normal resistivity (N16 (inch)), Long normal resistivity (N64 (inch)), Focused guard log resistivity (140 cm), Lateral resistivity and Single Point Resistance (SPR) are used in combination.

The Short normal and Long normal resistivity measurements have a penetration into the surrounding rock that is dependent on the distance between the transmitter and receiver. The measurements from the Long normal method are not as exact as the measurements from the Short normal method, but it can detect anomalies in resistivity further away from the borehole. From these measurements it is possible to detect deformation zones and the apparent porosity can be calculated using Archie's law /Parasnis 1973/.

Radar

In this technique a transmitter located in the borehole emits an electro-magnetic pulse into the surrounding bedrock. Structures with divergent electrical properties act as reflectors for the radar waves and the reflected energy is registered by a receiver in the borehole. Variations in the radar waves can reveal deformation zones within the studied rock volume /Lowrie 1997/.

One-hole interpretations are used for locating and determining the orientation of deformation zones such as fractures and crush zones in the bedrock, and lithological contacts, which are penetrated by, or occur in the vicinity of the borehole /Serzu et al. 2004/.

Seismic logs

The waveform from a seismic source can be divided into two motions; the longitudinal wave or P-wave and the transverse wave or S-wave. The S-waves are dependent on the elastic properties of the media whereas the P-waves are not, this difference is manifested in different ways as the waves travel through the media. The S-waves do not travel through water or gas whereas P-waves do, thus increasing the importance for this method as a detection method of discrete fractures or fracture zones. Seismic waves travel more slowly in damaged rock than in undamaged rock. In water saturated rock containing permeable fractures and fracture zones the shear wave cannot travel or will be very much delayed by these structures. The S-wave velocity can also be used together with P-wave velocity and density measurements to calculate elastic parameters of the rock mass /Telford et al. 1976/.

Vertical seismic profiling (VSP) (borehole measurements)

This method is used in boreholes to identify the source reflections registered in surface-based seismic surveys. The method can also detect and localise gently dipping reflectors lying beneath the borehole, as well as steeply dipping reflectors close to but not cut by the borehole.

Tomographic investigations

Several studies using Radar and Seismic tomography have been carried out to determine the properties of the rock mass between boreholes. The distance between the boreholes depends on the method used.

Seismic tomography is used for two or three-dimensional investigations of rock masses and is based on the variations in velocities of seismic waves. P- and S-wave velocities and velocity variations are calculated between two or more boreholes. The position of the source of the wave is continuously altered and the receivers of the wave are spread over an area. An image of the rock mass through which the seismic wave has been transmitted can be obtained. The difference in distance and thus travel time for the wave from the different source positions enables this image to be deduced. The seismic velocity is influenced by discontinuities in the rock such as fractures, fault zones, their infilling materials e.g. water or gas, lenses of material with different densities as well as by the rock stress conditions. Structural anisotropies such as foliations or layering can also influence the velocities and external sources such as excavation work can create noise, which can disturb the measurements.

During an investigation using seismic tomography in the Gotthard Base Tunnel, in Switzerland on a profile 417 m in length, fractures as small as 10 m long were detected as well as larger-scale features such as the foliation. The seismograms produced presented P- and S-wave profiles from distances up to 380 m away from the tunnel /Giese et al. 2005, in press/.

In the ZEDEX project performed at the Äspö hard rock laboratory, the seismic tomographic experiment was performed to examine the excavation disturbed zone (EDZ) between two deposition holes. The results from this project indicate that the method is useful for detecting fractures ranging over several scales /Emsley et al. 1997/.

In radar tomography, measurement of electrical resistivity of the rock mass is used to detect changes in the fracture geometry and the hydraulic properties of a rock mass. Measurements are made between multiple boreholes, or between borehole and ground surface.

In a study of Radar tomography at AECL's Underground Research Laboratory in Canada, the distance between the two 210 m long boreholes used in the experiment was 108 m at the collar and 78 m at their ends /Serzu et al. 2004/. The results obtained from this study, were compared to a geological model constructed from core logs and hydro-geologic data from the drill holes. A good correlation between the model and the radar results was found, even though the transmissivity values of the fractures detected were found to vary over a large range.

In this study it was found that the radar reflector data from single-hole radar using frequencies of 22 and 60 MHz, could detect reflectors up to 50 m away from the borehole. The identity of this reflector could not be established, as it did not cross any drill hole. However, reflectors at a distance of about 30–40 m could be directly linked to fractures crossing the borehole. These deformation zones were water saturated and a few centimetres thick. Other boreholes with a radius of 48 mm could also be detected using this method.

3.4.3 The use of geophysical techniques in tunnels

At the level of the repository investigations are performed from the tunnel face. In order to locate deformation zones within 100 m of the tunnel, the narrow range Tunnel seismic Prediction (TSP) method is used and to detect zones up to 500 m from the tunnel, the long range TSP-technique is applied. The resolution at the 500 m range is in the order of about 2–5 m

and in order to make detailed investigations, borehole methods are needed (Table 3-3). The holes must be horizontal or slightly inclined. In order to increase the detail knowledge of the structures it might be necessary to use tomographic technology, i.e. measurements between two or more boreholes. One main aim at this stage in the excavation will be to tune the orientation of the deposition tunnels of the repository.

Investigations carried out along the floor of the deposition tunnel will include surface methods, specifically geological mapping, laser scanning, surface radar and hammer seismics. The range for the investigation is up to approximately 10 m into the rock mass and the aim is to use the results for the positioning of the deposition holes in relation to existing deformation zones, Table 3-4. It is assumed that a pilot core drill hole will be drilled in the centre of each proposed deposition hole. These holes are used for various techniques of borehole investigations including logs and borehole radar. The combined, very detailed analyses of the rock mass will probably make it possible to fully detect all deformation zones along the floor of the deposition tunnel.

Surface based investigations involve measurements from the ground or tunnel surface. The surface based methods will normally only detect potentially deformation zones and their resolution makes them unsuitable for detecting single fractures at depth. For small-scale analysis, up to a range of 100 m, Hammer seismic and TSP (Tunnel Seismic Prediction) are suitable methods.

Reflection seismic profiling

Reflection seismic profiling is a surface based geophysical method in which the travel pattern of seismic waves in the bedrock is used to interpret the subsurface structures. The method is used by SKB to determine the occurrence of deformation zones, and (to some extent) lithological boundaries.

It can pick up reflections down to depths of 1–3 km and is used, together with geological information from surface mapping, drilling and VSP (Vertical Seismic Profiling) data to determine the lateral extent and position of rock boundaries, and deformation zones.

Refraction seismics

In this technique, the travel time and pattern of acoustic waves are used to determine the thickness of unconsolidated deposits. The technique is also used to determine the seismic velocities of different soils and rocks. The resulting velocity profiles are used to identify different types of sediments in the soils and to evaluate rock quality in the bedrock. The groundwater level can sometimes be obtained from these measurements.

Tunnel Seismic Prediction (TSP)

This technique is used to detect features in the rock mass beyond the tunnel face, (Figure 3-9). The deformation zones crossing the tunnel axis ahead of the tunnel face will be detected with the greatest accuracy using this equipment. This system does not have to be in contact with the actual tunnel face. Using TSP either from the tunnel or in boreholes, many of the deformation zones surrounding the tunnel can be located. The seismic signal can be produced by several detonations and then detected by dual triaxial sensors located perpendicular to each other, which would be contained in casings firmly cemented into boreholes in both sidewalls of the tunnel.

The full wave form of both the compression and shear wave are detected. A 2-D or 3-D model of the deformation zones in the rock mass in front of the tunnel face is then produced.

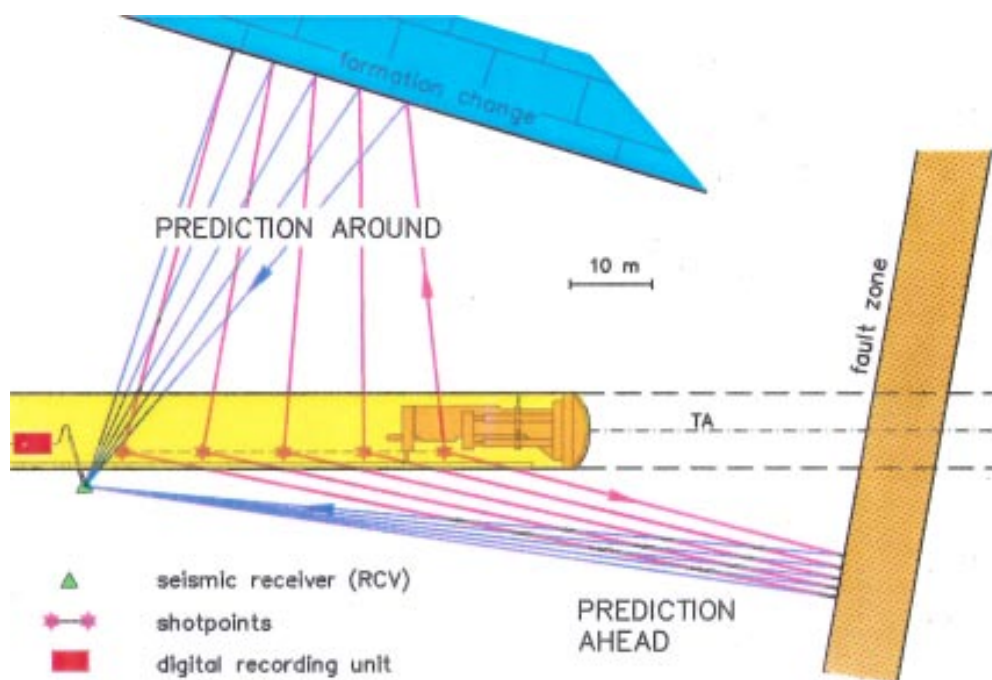


Figure 3-9. Tunnel Seismic Prediction (TSP) detection of fractures inside the rock mass in front of the tunnel.

Resistivity measurements

The resistivity of a rock mass can be determined by transmitting electricity through the rock and measure the resulting potential field. There are different methods and configurations used to measure this. The type of minerals and the amount of water in the rock volume change the resistivity, which makes it a good method for identifying deformation zones which contain a larger amount of water than the main body of the rock and which are sometimes the source structure of conductive minerals such as sulphides and graphite. Certain rock types contain these minerals disseminated throughout the rock mass, which make them undesirable for the location of a repository from SKB's point of view. Resistivity measurements can be used to detect these rock masses. In addition, an indication of the depth to highly saline waters (deep brine) can be determined from these measurements. They can also provide information on the presence and thickness of soils which have a strong response in resistivity compared to the surrounding materials, such as silts or clay.

Ground Penetrating Radar (GPR)

This method uses travel patterns and the velocity of electro-magnetic waves to determine the depth and geometry of a structure and is commonly used to identify the electric conductivity of unconsolidated deposits and the position of the groundwater table. The method can also be used in tunnels to detect near-surface fractures and deformation zones in the rock mass. The applicability of the technique is strongly dependant on the fracturing of the rock mass and the clay content in the deformation zones, since high contents of fine grained members, reduces the penetration distance. The penetration depth varies depending on the radar probing frequencies but is generally about 15–30 m (for crystalline rock). At radar probing frequencies of 10–10,000 MHz the lithology and structural characteristics of fractures in near surface granitic

rock can be detected to a depth of tens of metres. In some of the methods used for tunnel measurements several antennas are used to increase the accuracy of the measurements and the antennas are directed to receive the electro-magnetic signals from the surface at which they are aimed. This decrease the noise from other surfaces in the tunnel that otherwise would disturb the results (Sträng Thomas, 2006, Personal communication, Geosigma AB, geosigma@geosigma.se, Post Box 894, 75108 Uppsala, Sweden).

3.5 The recognition of deformation zones in boreholes and tunnels – case studies from Äspö

The problem of recognising deformation zones from borehole data, cores and tunnel observations has been addressed by several studies at Äspö. It is clear from these and other studies that there are two important aspects that bear on the recognition of these zones from such limited data sets. The first relates to the effect of scale of observation (borehole versus tunnel) on the ease with which deformation zones can be identified and the second relates to the correlation of the deformation zones from one borehole or tunnel to another.

The impact of the scale of observation on the task of recognising deformation zones and the difficulty of correlating these zones between boreholes can be illustrated with reference to three studies carried out at the Äspö HRL. These involve;

1. The correlation of data from a borehole (KBH02) drilled in advance of and sub-parallel to the ramp tunnel in the region before its spiral descent to the repository depths, and data from the tunnel.
2. Correlation of data from the cored borehole KA3191F which was drilled along the centre line of the TBM tunnel at Äspö prior to the excavation of the tunnel, and data from the tunnel
3. The correlation of data from the elevator shaft at Äspö and two sub-parallel boreholes (KAS 02 and KAS 05) approximately 40 m either side of the shaft.

The results of these studies are summarised in Appendix A1.2, A1.3 and A1.4 respectively.

Other studies have been carried out with the specific task of identifying deformation zones from borehole data. This is best achieved by the use of several different types of borehole and core studies and SKB have performed several borehole tests to determine the most useful combination of data gathering techniques to detect these zones. One such test, which is described in detail in Appendix 2, was carried out on the cored borehole KLX03 from Laxemar. The borehole is a kilometre long and 8 important deformation zones were detected as well as a minor zone at a depth of ~ 720 m (Figure 3-10).

The position along the borehole of flowing fractures are deduced primarily from the difference flow logging data and the result of difference flow logging of part of borehole KLX03 is shown in Figure 3-11. The geological characterisation (rock type, degree of fracturing etc) is achieved mainly from the Boremap-mapping which is based on BIPS-images and the core. From the Boremap-mapping the orientation (strike/dip) and the intersection angle (α) between the fracture and borehole together with the intersection length can also be obtained.

An indication of the extension of the fractures can be determined from radar images. The degree of detail depends strongly on the resolution (frequency) of the radar measurements. The resolution in the dipole 250 MHz images is higher than in the 100 MHz and 20 MHz images. However, the penetration range in the dipole 250 MHz is less compared to 100 MHz and 20 MHz. The best penetration range is achieved with dipole 20 MHz, but the resolution is the lowest. Large-scale structures (deformation zones) are best viewed in the 20 MHz images, while small-scale structures (single fractures, minor zones etc) are best viewed in the 250 MHz or 100 MHz images. The frequency of the directional antenna is 60 MHz. Examples of radar images obtained from the same section of borehole KLX03 using frequencies of 20, 100 and 250 MHz are shown in Figure 3-12.

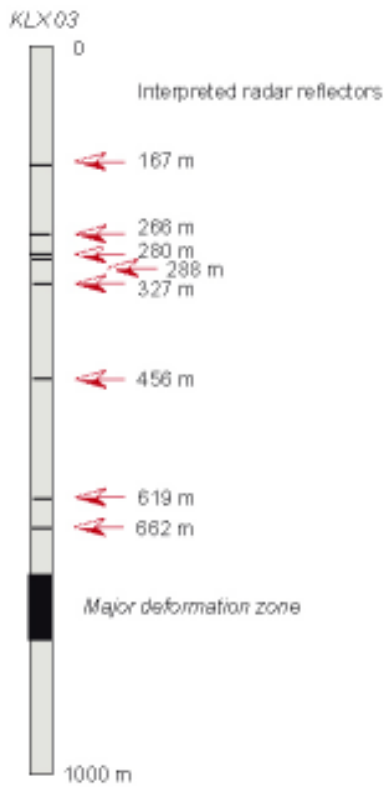


Figure 3-10. Interpreted radar reflector intervals in borehole KLX03 used for the correlation study.

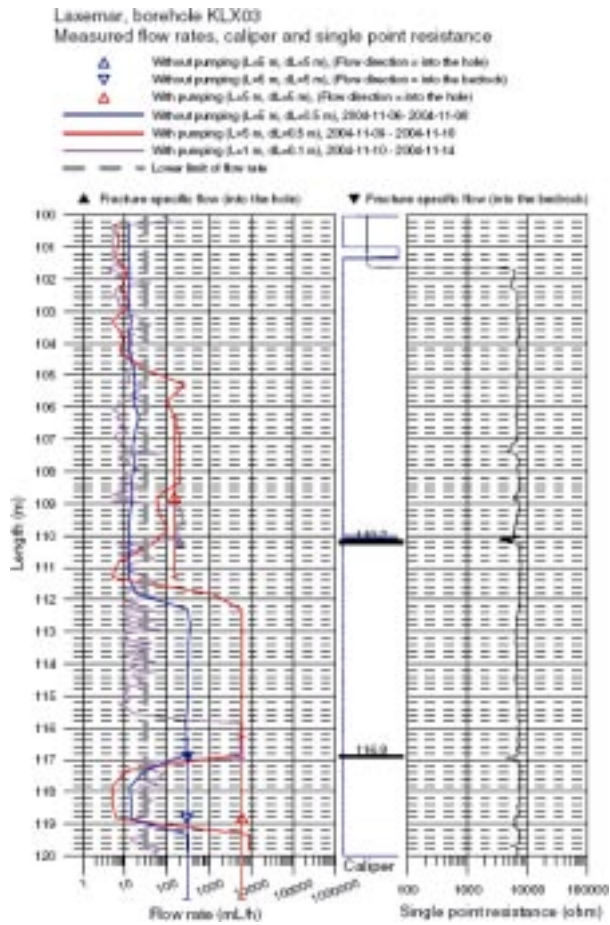


Figure 3-11. Difference flow logging and key for a section of the borehole KLX03 from Laxemar /Rouhiainen et al. 2005/.

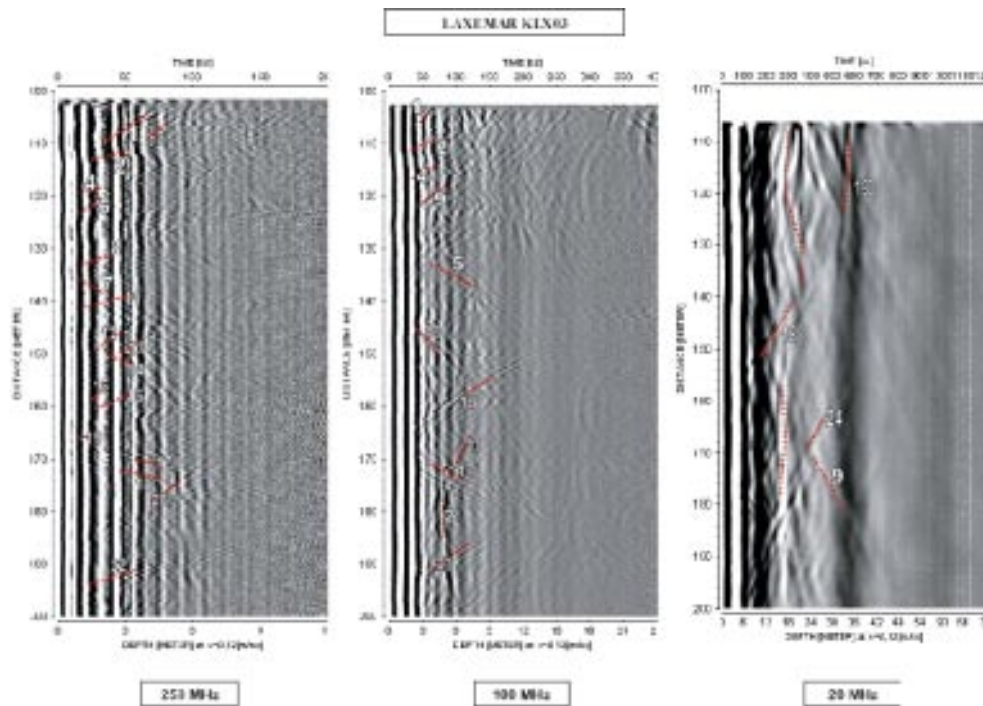


Figure 3-12. Example of radar images from dipole antenna measurements, 20 MHz, 100 MHz and 250 MHz for the borehole KLX03 from Laxemar /Gustafsson and Gustafsson 2004/.

In these images the borehole corresponds to the left hand side of the diagram and consequently the deformation zone is shown on one side of the hole only. It is assumed that the persistence of a radar detected structure will be the same on both sides of the borehole. For example, if a radar reflector (structure) can be traced up to 12 m from the hole on the radar image, it is assumed that the structure has a minimum length of $12+12 = 24$ m.

3.6 Modelling updates

As indicated in Chapter 2, the geological signatures of critical deformation zone (fractures, fracture zones or shear zones) are likely to be site specific. These signatures must be identified for each site by developing experience gained initially from the early investigations of the site area and gradually built up during the excavation of the repository from the ramp to the final depth for the repository.

The geological team at the site must carefully develop a methodology based on the specific site conditions in order to observe and identify the special features linked to the deformation zones. The geological characteristics of these structures must be integrated into the routine geological mapping of cores and tunnel surfaces.

The strategy must be to use a combination of geological and geophysical methods for the identification of the critical structures and it is recommended that the process starts by using techniques that make observations on the mm-dm scale and is then extended to techniques capable of imaging progressively larger and larger portions of the structure.

A strategy based on the experience of characterization methods gained from the construction of the Äspö HRL is regarded as a base-line for the investigation strategy. The first goals for the research and development works during construction of the Äspö HRL were:

1. To verify the pre-investigation methodology developed at the Äspö HRL and,
2. to finalise detailed characterization methodologies.

The approach for the verification of pre-investigations is summarised in Figure 3-13. Further information can be found in /Almén and Stenberg 2005/.

As can be seen an understanding of the types and orientations of the critical deformation zones is gradually developed during the step-wise investigations of the site starting with the data collected from the ground and finishing with a detail investigation of each deposition hole.

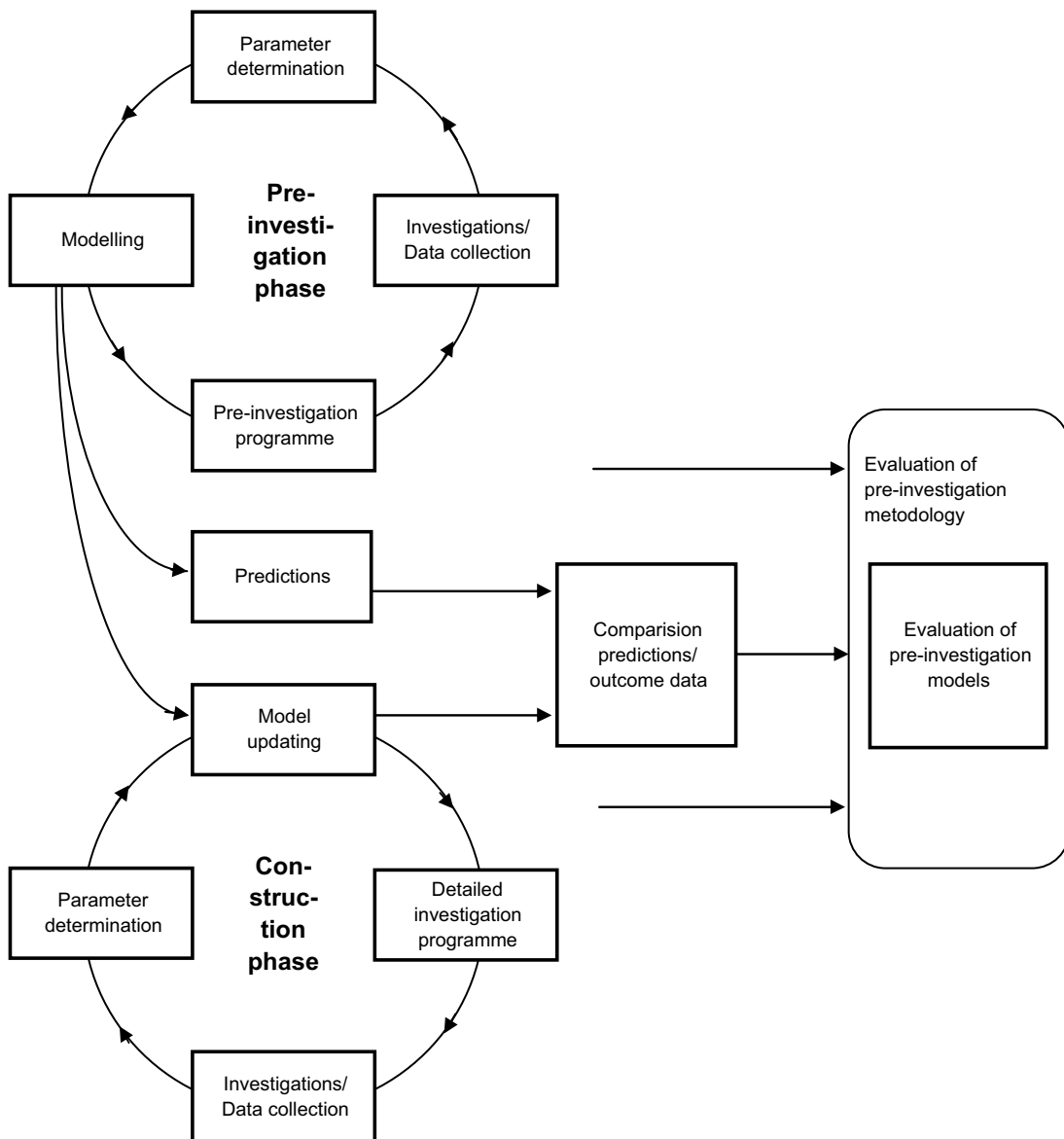


Figure 3-13. The procedure for verification of the pre-investigation methodology /from Almén and Stenberg 2005/.

The strategies for integrated site modelling are developed during the ongoing site investigations and the experience and data obtained during the evolution of the site are continuously incorporated into the modelling strategies as described in Section 3.3.2. It is anticipated that further modelling strategies will be developed during the last years of the site investigations, and that there will be substantial time available before the construction works starts for the further development of modelling tools, if required.

3.7 Discussion and summary

3.7.1 The learning and application process

It is emphasised that the investigation strategy discussed in this chapter consists of two phases, a learning phase and an application of the learning phase.

The learning phase is linked to the excavation of the ramp down to the level of the repository. This phase comprises of:

- The construction of an accurate 3-D geological model.
- The accurate documentation of specific geological parameters (e.g. deformation zone aperture, shear displacement, conductivity and thickness).
- The processing of the geological information.
- The testing of the data.
- The testing of techniques.
- The validation of the data and techniques.
- Updating of the modelling approach to meet the needs from the underground construction.
- Establishing the strategic investigation model.

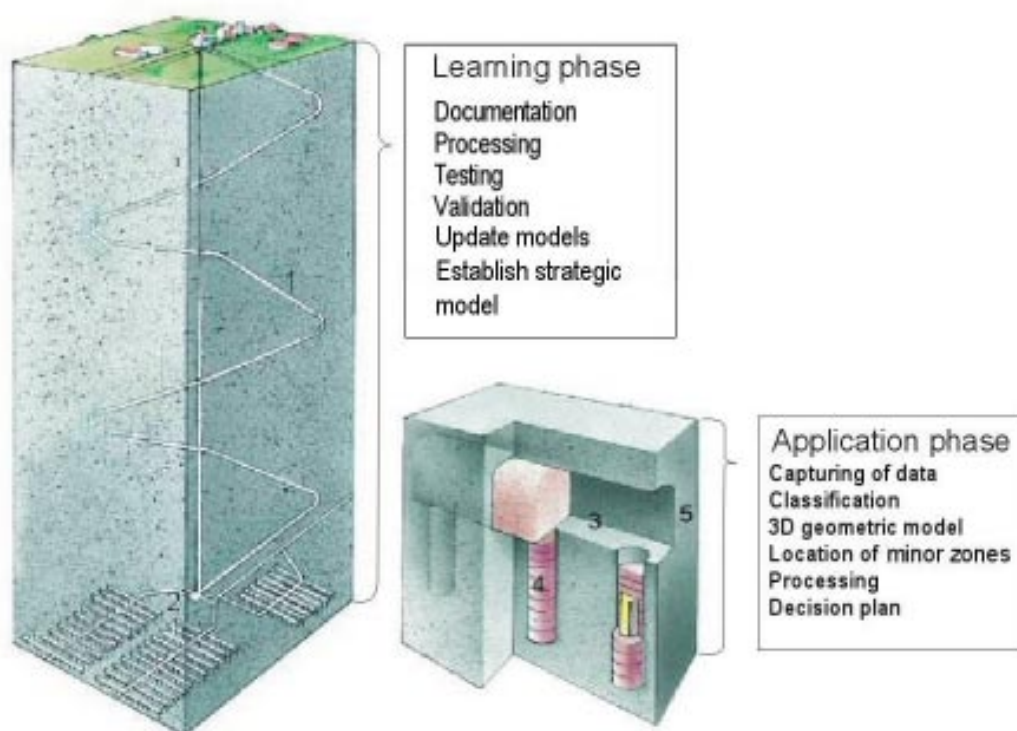


Figure 3-14. The schematic picture of the learning and application process.

The learning process will focus on finding the critical features linked to the long fractures and fracture zones and of establishing the most appropriate techniques for detecting them. These are likely to be site specific. Data must be processed, tested and validated so that one can be sure that the critical features are linked to deformation zones that are of importance. The result will be a tool box which will include investigation methods which in combination with a knowledge base generated during the site investigation will enable the detection and classification of deformation zones. It is also important to determine whether the deformation zones will (i) occur in a certain geological environment (e.g. clustered in a particular rock type), (ii) be randomly spaced, or (iii) vary with depth.

The learning phase is necessary in order to be able to detect, interpret and classify the deformation zones that characterize the site. It will provide a major input into the knowledge base and will enable the risk of missing deformation zones to be minimized.

The application phase includes the identification and selection of the critical rock volume for the repository and the selection of the positions for the deposition tunnels and the deposition holes. The tool box developed in the learning phase will be applied to determine the location, and examine and classify the deformation zones in a specific rock volume. When a potential structure is found and classified as large the next important step is to determine its extent. This phase may include the following steps:

- The geological documentation of the rock surfaces.
- The application of various geophysical methods according to the tool box.
- The inspection and processing of the geological data.
- The classification of the data for finding critical structures.
- The development of the 3D geological model with new data.
- Selecting the appropriate investigation processes for finding the extent of critical structures.
- Generating a decision plan for the location and orientation of the deposition tunnels and deposition holes.

3.7.2 Risk evaluation

It is important to consider whether a risk evaluation, similar to the one performed by /Hökmark 2003/, could be made for the layout of a tunnel with a deposition hole designed according to KBS-3V, to evaluate the minimum distance between the deposition hole and a detected critical structure. Any deformation zone striking at an angle between 0 and about 80° to the trend of the deposition tunnel, that cuts a deposition hole may cause shear displacement of the hole during an earthquake, see Figure 3-15.

It will be recalled from the discussion in Chapter 2 that because the shear displacement that occurs along a fracture varies from a maximum close to the centre to zero at the fracture tips, not all parts of a critical deformation zone will have potential slip values greater than the permitted upper limit of 10 cm. Thus even if a critical structure cuts the deposition hole, if the intersection is close to the fracture edge, large displacements (i.e. greater than 100 mm) will not occur.

The most critical situations are likely to be associated with horizontal and sub-horizontal long structures located just below the repository; hence the detection of these is particularly important. If there are clusters of horizontal/sub-horizontal long fractures just below the selected repository that level should be avoided from the start. Unfortunately it will be difficult to identify such clusters from ground surface investigations, and it is for this reason that it is recommended that further investigations for locating them from the ramp are carried out. From the location at the end of the ramp at the level of the repository at a time prior to the excavation of the centre tunnels for a subarea, i.e. at position 2 in Figure 3-1, it is difficult to detect any large horizontal structures some hundred metres away. Further technical development is needed to address this problem.

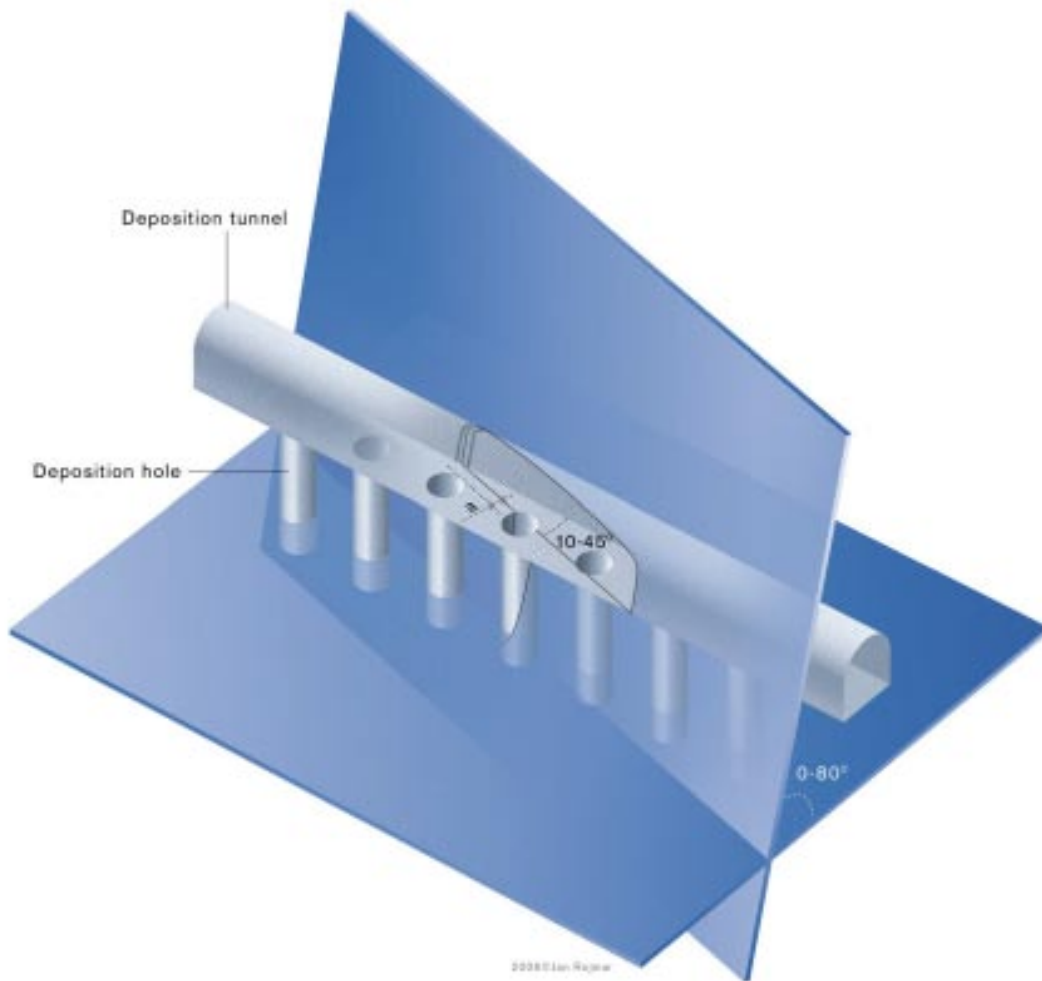


Figure 3-15. The minimum distance between the deposition hole and the deformation zone found in the tunnel wall and an unfavourable orientation of a deformation zone with respect to the deposition holes.

3.8 Conclusions

It is a difficult task to observe and identify deformation zones remotely in a rock mass and no single or unique method is currently available with the precision, resolution and range needed.

However, based on previous experience from SKB site investigations and the construction of the Äspö HRL, it is concluded that it is possible to locate critical deformation zones if:

- An accurate 3-D geological model is developed.
- The site specific characteristics of such zones are established.
- A site specific strategy is developed and implemented before, and modified on the basis of data obtained during the construction of the repository.
- Suitable technical methods are combined and used at the various stages of the excavation.
- The strategy and methods are verified.

The outcome of the work has a high probability of:

- Locating the deformation zones in the repository tunnels and deposition holes.
- Providing guidance for the “decision model” used for the construction of the repository.

At this stage no specific method or combination of methods can be recommended because the optimal “tool box” for the investigations may have to be established based on site specific characteristics which determine the types of deformation zones that are likely to develop. However, the suggested methods in Table 3-2 to Table 3-6 can be used to provide an initial order of selection.

It is necessary that further work be carried out and tests made in order to establish the appropriate “tool box” of known, tested and calibrated methods best suited to the task of detecting critical deformation zones. During the excavation of any specific repository, the experience and data gathered by using the techniques included in the “tool box” during the excavation of the ramp and tunnels will be critical in the development of a 3-D geological model on which the layout and position of the deposition holes can be planned with confidence.

Table 3-2. Investigation methods during the excavation of the ramp (access tunnel).

Position in excavation	Scale of structural geological object	Tunnel surface methods			Borehole methods ¹⁾			Pseudo fracture logs	Seismics VSP ³⁾
		Mapping ²⁾	Laser scanner	Seismic	Core logging and BIPS	Electric	Radar ³⁾		
Investigation during excavation of ramp	> 1 m	Y	Y	Y	Y	Y	Y	Y	Y
	ca 1 m	Y	Y	Y	Y	Y	Y	Y	Y
	dm-scale	Y	Y	Y	Y?	Y?	Y	Y?	Y
	cm-scale	Y	Y	Y	Y	Y?	Y?	Y?	Y?
	mm-scale	Y	Y	Y	Y	Y	Y	Y	Y

¹⁾ Inclined or horizontal holes.

²⁾ Structural and geological mapping.

³⁾ Affected by saline water.

Table 3-3. Investigation methods in trunk tunnels (i.e. non-deposition tunnels) at the repository level.

Position in excavation	Scale of structural geological object	Tunnel surface methods			Borehole methods ⁴⁾			Flow	Pseudo fracture logs	Seismics VSP ⁶⁾
		Mapping ⁵⁾	Laser scanner	Seismic	Seismics	Seismics	Core logging and BIPS			
Investigation at deposition level	> 1 m	Y	Y	Y	Y	Y	Y	Y	Y	Y
	ca 1 m	Y	Y	Y	Y	Y	Y	Y	Y	Y
	dm-scale	Y	Y	Y	Y	Y?	Y?	Y?	Y?	Y
	cm-scale	Y	Y	Y	Y	Y	Y	Y?	Y?	Y
	mm-scale	Y	Y	Y	Y	Y	Y	Y?	Y?	Y?

⁴⁾ Mainly horizontal holes.

⁵⁾ Structural and geological mapping.

⁶⁾ Can not be used in horizontal holes.

Table 3-4. Investigation methods in deposition tunnels for the positioning of deposition holes.

Position in excavation	Scale of structural geological object	Tunnel surface methods				Borehole methods ⁷⁾				Pseudo fracture logs	Seismic VSP			
		Mapping ⁸⁾		Radars	Laser scanner	Seismics	Seismics	Seismics	Seismics			Core logging and BIPS	Electric Radar ⁹⁾	Hydraulic logs
		Manual	Surface radar	3-D with laser photo	3-D with laser photo	Hammer seismics	Tomography	Manual Image	Single point			Borehole	Hydraulic and flow logs	Calliper, diff. resistivity, sonic
Investigation from deposition tunnel for canister positions (10 m scale)	> 1 m ca 1 m dm- scale cm-scale mm-scale	Y Y Y Y Y	Y Y Y Y Y?	Y Y Y Y Y	Y Y Y Y?	Y Y Y Y?	Y Y Y Y	Y Y Y?	Y Y Y?	Y Y Y?	Y Y Y Y?	Y Y Y Y?		

⁷⁾ Vertical holes in areas of possible long fractures. Drilled at canister positions. Max length 10 m.

⁸⁾ Structural and geological mapping.

⁹⁾ Affected by saline water.

Table 3-5. Investigation methods within the deposition holes drilled into the deposition tunnel floor.

Position in excavation	Scale of structural geological object	Tunnel surface methods ¹⁰⁾				Bore hole methods ¹¹⁾				Pseudo fracture logs	Seismic VSP			
		Mapping ¹²⁾		Radars	Laser scanner	Seismics ¹³⁾	Seismics	Seismics	Seismics			Core logging and BIPS	Electric Radar ¹⁴⁾	Flow
		Manual	Surface radar	Surface radar	3-D with laser photo	Tomography	Tomography	Manual Image	Single point			Borehole	Flow Diff	Flow Diff
Investigation in deposition hole (10 m scale)	> 1 m ca 1 m dm-scale cm-scale mm-scale	Y Y Y Y Y	Y Y Y Y Y?	Y Y Y Y Y	Y Y Y Y?	Y Y Y Y	Y Y Y Y	Y Y Y?	Y Y Y?	Y Y Y Y?	Y Y Y Y?	Y Y Y Y?		

¹⁰⁾ Investigations after drilling of the deposition hole.

¹¹⁾ Investigations from the pilot drill hole of the deposition hole.

¹²⁾ Structural and geological mapping.

¹³⁾ Tomographic investigations between two or more pilot holes.

¹⁴⁾ Maybe affected by saline water. Including tomographic analysis between two or more pilot holes.

Table 3-6. Investigation methods for the rock mass around the deposition tunnel (50 m scale).

Position in excavation	Scale of structural geological object	Tunnel surface methods		Borehole methods ¹⁵⁾					Flow	Pseudo fracture logs	Seismic VSP ¹⁷⁾	
		Radar	Seismic	Seismic	Seismic	Seismic	Seismic	Seismic				Core logging and BIPS
Investigation from the deposition tunnel of the surrounding rock mass (50 m scale)	> 1 m	Y	Y	Y	Y	Y	Y	Y	Y	Y	Y	Y
	ca 1 m	Y	Y	Y	Y	Y	Y	Y	Y	Y	Y	Y
	dm-scale	Y	Y	Y?	Y	Y	Y?	Y?	Y	Y?	Y	Y
	cm-scale	Y?	Y?				Y?	Y	Y?	Y?	Y?	Y?
	mm-scale							Y	Y			

¹⁵⁾ Horizontal boreholes.

¹⁶⁾ Affected by saline water.

¹⁷⁾ May not be used in horizontal holes.

4 Method for the detection of minor deformation zones using new characterization data

4.1 Introduction

The terminology used in Chapter 4 is referring to the current use for pre-investigations in the Äspö project at Laxemar. The terminology is comprehensively described in Section 1.4.

4.2 Field investigations

Recent field investigations at the Laxemar subarea aimed at identifying minor deformation zones has involved aerial photography, laser scanning, geological mapping and geophysical surveys. Seven 400×400 m quadrants were targeted for detailed field examination (Figure 4-1).

High resolution Lidar data provided a very high level of detail regarding topographical lineaments (Figure 4-2).

The aim of this investigation is the identification and characterisation of some Minor Deformation Zones (MDZ) in one of the well-exposed quadrants in the Laxemar investigation area. The term MDZ is used to designate an essentially 2-dimensional structure whose lateral extent is < 1,000 m and thickness < 5 m. MDZs commonly show evidence of both brittle and ductile deformation in the form of brittle, relatively low-cohesive products such as fractures, breccias and gouge material, and ductile products i.e. cohesive, strongly foliated or mylonitic rock.

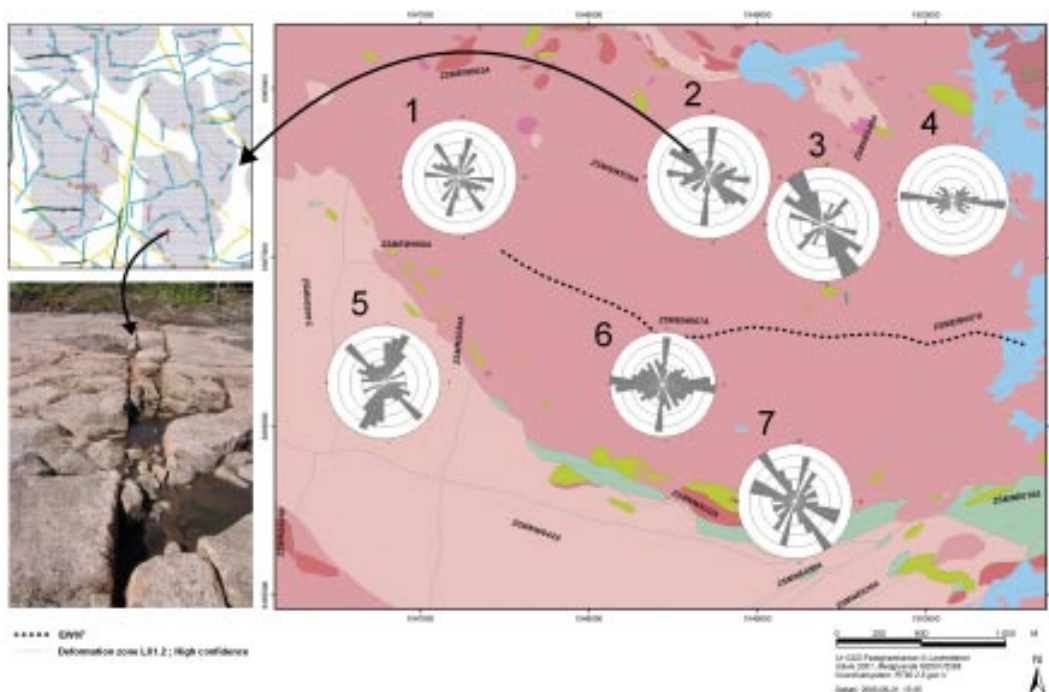


Figure 4-1. Location of the seven quadrants with Rosette-diagrams in the Laxemar area in which detailed fieldwork was carried out. The quadrant no. 2 represents the area around KLX09 in Figure 4-2.

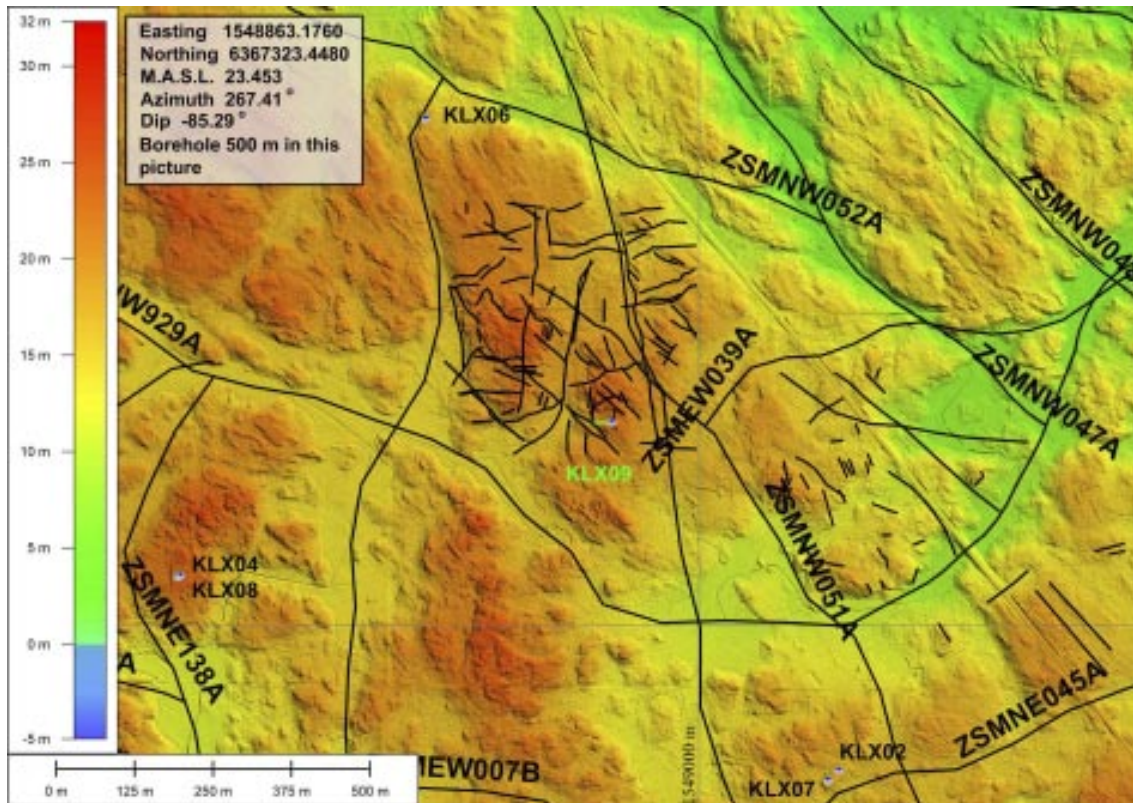


Figure 4-2. High resolution Lidar data of part of the study area showing some interpreted lineaments. Investigated area is close to borehole KLX09.

In this section preliminary data are presented that have been obtained from investigations in a quadrant close to borehole KLX09 which is approximately 1,000 m deep. Three lineaments (magnetic and topographic) have been partly uncovered and can be followed for approximately 50–100 m. at the surface (Figure 4-3).

The investigation has been focused on the following activities:

- The integrated evaluation of available detailed geophysical data and laser scanning results.
- The field investigation used to localise specific MDZs.
- The digging out and cleaning up of the surface features detected by the Lidar technique in order to trace out some of the localised MDZs.
- The drilling of boreholes in order to geologically and hydraulically verify and characterise some of these MDZs at depth.

After cleaning, lineament no. 2 can be followed at the surface for 30–40 m. Over this distance it changes from a minor fracture zone to a single fracture (Figure 4-4 and Figure 4-5). Two cored boreholes verify the existence and position of this fracture zone at depth (Figure 4-6, Figure 4-7 and Figure 4-8).

Detailed characterisation of this zone using both the surface and borehole data is planned and will be carried out in June 2006.

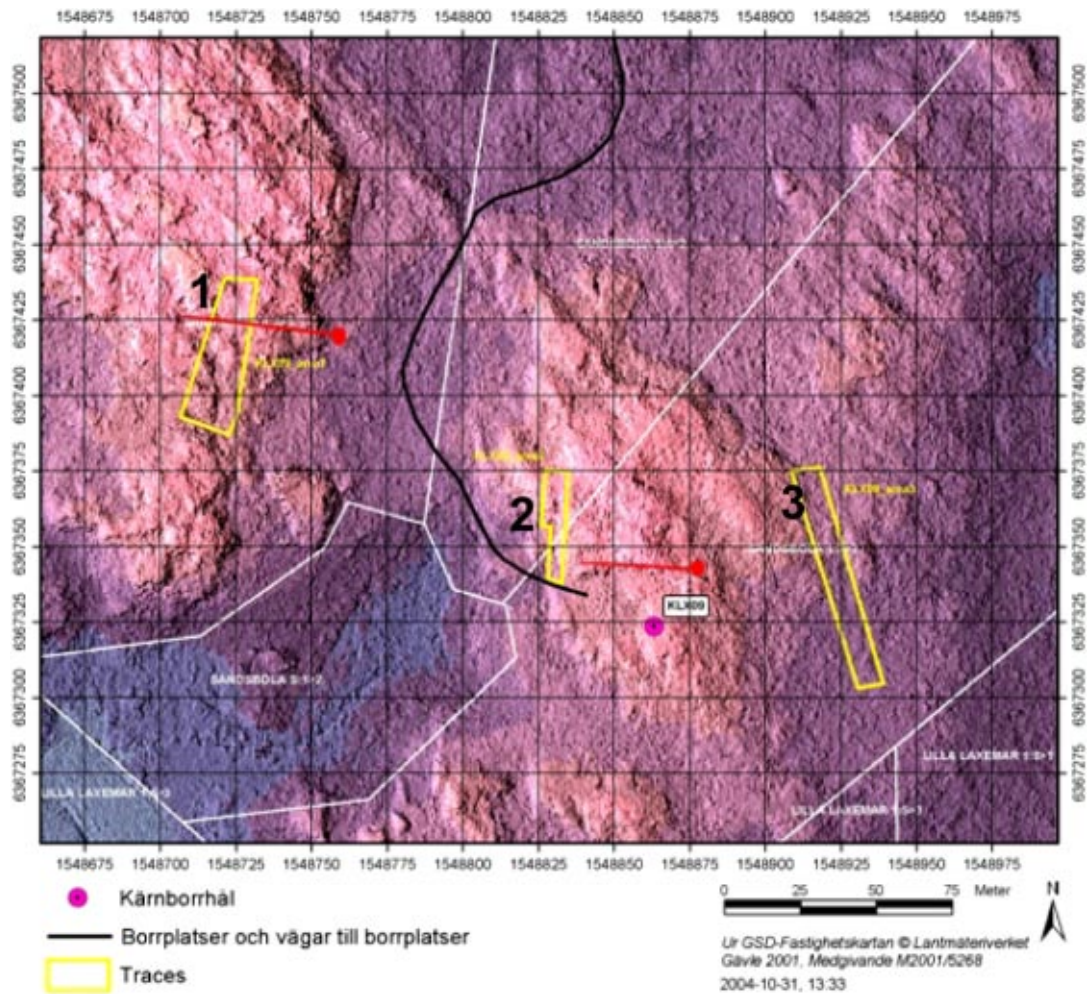


Figure 4-3. Map showing the location of the three partly uncovered lineaments (nos. 1 to 3) situated close to borehole KLX09. Data from KLX09D is included in this study. Data from KLX09F was not available when compiling this report.



Figure 4-4. Part of lineament 2 exposed at the surface by cleaning of the outcrop (see Figure 4-3).



Figure 4-5. Part of lineament 2 exposed at the surface by cleaning of the outcrop (see Figure 4-3).

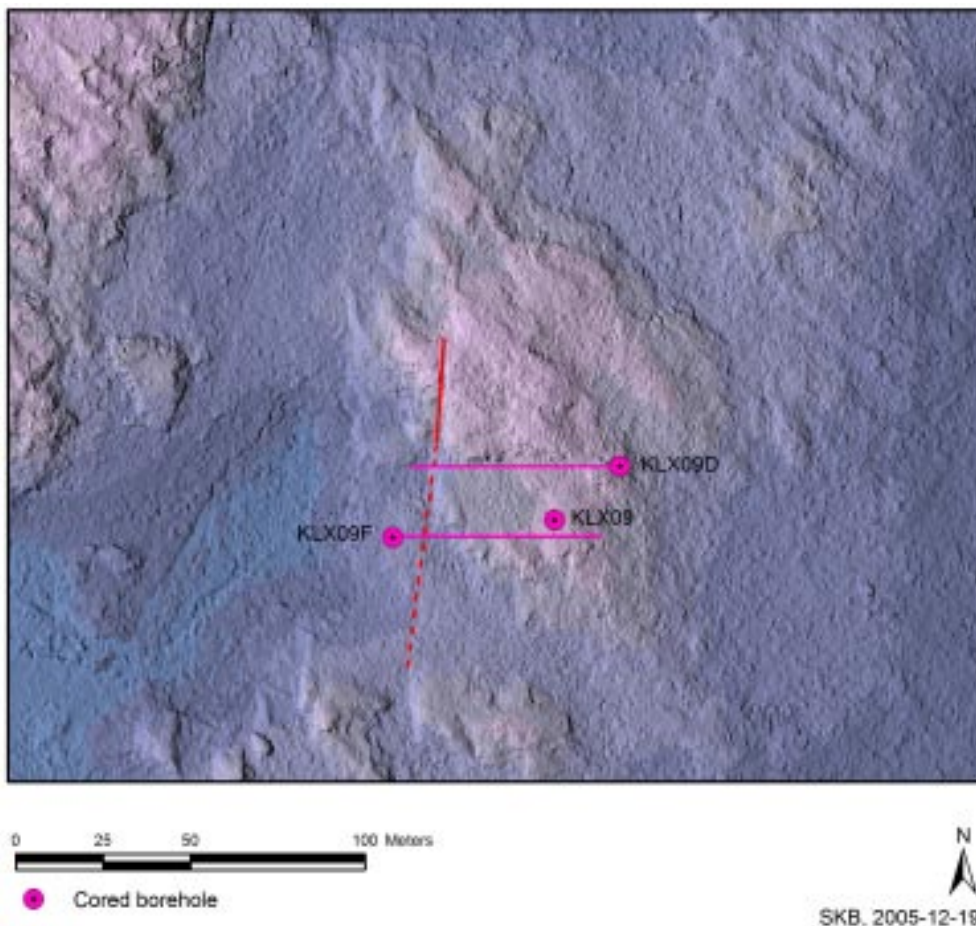


Figure 4-6. The location and direction of the two boreholes KLX09D and KLX09F. They plunge at 60° and were drilled to locate and characterise (at depths) the deformation zone that causes lineament 2 shown by the ~N-S trending solid and dashed line.

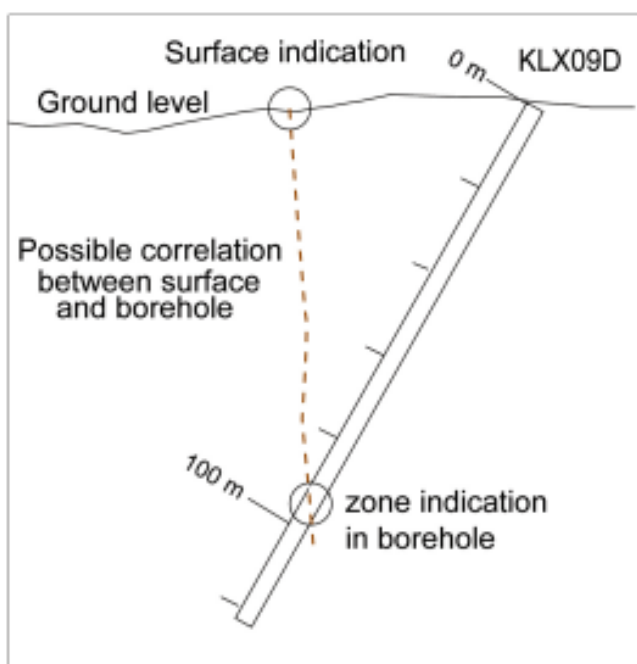


Figure 4-7. Preliminary cross-section showing borehole KLX09D and its intersection with the minor deformation zone which occurs at approximately 85 m down the borehole.



Figure 4-8. Cores from borehole KLX09D for the interval 78.74–94.11 m. The most intensively fractured part of the supposed MDZ occurs at c 82.50–85.0 m.

4.3 Conclusions

- A new and ongoing study at Laxemar involving detailed surface investigations, based on geophysics and high resolution Lidar data, has been used to identify lineaments at the surface caused by minor deformation zones.
- These lineaments have been exposed by cleaning of the outcrop and have been shown to be minor deformation zones/long fractures with an extension in the range 10–100 m.
- It is interesting to note the changes in thickness and character along these short structures. They vary from “single fractures” to “fracture zones”.
- These studies in the Laxemar area indicate clearly that the “missing fractures” which range in size between 10 and 100 m do occur in this study area.

5 Summary and conclusions

The displacement of glacial striations by faults in northern Scandinavia provides irrefutable evidence of post-glacial faulting. One of these faults, the Pävie fault Figure 1-1, extends for approximately 200 km and has a maximum displacement of ~ 10 m. Evidence in the form of extensive liquifaction of glacial sediments indicates that most of these faults grew by a series of seismic pulses rather than by aseismic creep. As a consequence of these observations it has become necessary to consider the possibility that these seismic events might reactivate, i.e. cause slip along other fractures in the vicinity of these faults.

Movement on fractures cutting a deposition hole has been considered and studied using numerical modelling and it has been established that movement in excess of 10 cm. is likely to affect the integrity of the canister (Section 1.1). The movement on a fault is usually maximum in the central region of the fracture and reduces to zero at the fracture tips and the magnitude of the slip is directly related to the fault length. Based on this relation it can be argued that there is the possibility that fractures longer than 100 m can move by 10 cm. or more as a result of a seismic stimulus from a post-glacial fault. It is therefore essential to ensure that fractures with a radius $r > 50$ m (known as critical structures) do not cut the deposition hole.

It is recognised that in addition to discrete fractures there exists in rocks a number of other types of planar and sub-planar zones of weakness along which slip might occur. These include fracture zones and ductile shear zones and these, together with discrete fractures, have been termed collectively “deformation zones”. Thus any study aimed at detecting these critical structures has to consider all types of deformation zones and identify the features and properties which can reveal their length.

The aim of this report is to determine what properties and natural features a deformation zone has that reflect its length and that can be detected in tunnels and boreholes. Its principal goal is to establish the probability of detecting critical structures that intersect the deposition holes and this task has been broken down into two objectives namely:

- To summarize the current state of knowledge on geological characteristics of large structures ($50 \text{ m} < r < 250 \text{ m}$).
- To propose suitable investigation methods for identifying and localizing such large structures and to give examples of their application.

In order to meet these objectives a survey of published literature on fracture and deformation zone morphology has been undertaken and is presented in Chapter 2. In addition a strategy for selecting suitable investigation methods to search for deformation zones at different stages in the construction of a repository has been developed and is discussed in Chapter 3. This is followed by a survey of studies for the Äspö HRL on the correlation of deformation zones between tunnels and boreholes using geological signatures and geophysical techniques (Chapters 3 and 4 and Appendices A1 and A2).

5.1 Project Findings

5.1.1 Geological indicators of deformation zone (fracture) size

The survey of published literature on deformation zone morphology clearly indicates that there are several local indicators of their size. However, none of these indicators which are listed below, are by themselves sufficient for assessing the sizes of these features:

- The displacement along shear fractures varies predictably along their length. Maximum displacement frequently occurs in the central region of the fracture and decreases to zero at the fracture tips.
- It has also been established that the thickness and continuity of fractures and of deformation zones in general will both increase with increases in length and that this empirical link between length and thickness might be used to identify critical deformation zones. However, it is also recognised that it is possible to have fractures with a large thickness, which are not critical fractures. For example, many veins are found in rocks with a very large thickness to length ratio. Thus both fracture normal and fracture parallel displacements are sensitive indicators of fracture size and can be used to help identify large fractures.
- Observations show that many long fractures are either currently or were in the past channels for fluid migration. Clearly, there is great uncertainty and variability in any relationship between the conductivity of a deformation zone and its size and not all large planar zones of weakness will be conductive. (For example, shear zones along which continuity has not yet been lost are likely to have a lower permeability than a fracture or fracture zone of the same size). However, it is argued that when a deformation zone shows evidence of present or past conductivity, it should be regarded as being a critical zone until proved otherwise. Indicators of high fracture conductivity either in the past or currently, include mineralization along the fracture, significant alteration of the wall rock and sometimes a high current conductivity can all be used as a guide to fracture size.

The uncertainty in the probability of a critical deformation zone remaining undetected during the construction of the tunnels and deposition holes can be reduced if the rock type of the proposed repository is known because the expression of the deformation zones, their likely spatial organisation and continuity, etc, depends to some extent on the rock type. For example, fracture sets will tend to be less systematic and more continuous in a crystalline basement than in a bedded succession of sedimentary rocks. It is difficult to see how this probability can be precisely quantified using only geological characteristics. However, the better the understanding of the repository site, the less the likelihood of missing critical deformation zones. The methodology of identifying these deformation zones is the same regardless of the state of knowledge of the bed rock and the key parameters that can be used to indicate fracture length are discussed in Chapter 2. These are:

- Fracture apertures.
- Shear displacement.
- Deformation zone thickness.
- Conductivity.

5.1.2 Experience from the SKB sites

The general findings discussed above are also supported by results from investigations conducted at the Äspö HRL and at the Laxemar site investigation site Chapter 4 and Appendices A1 and A2:

- At the Äspö HRL there is a good correspondence between minor deformation zone indications at the surface, in the tunnel and in cored boreholes, concerning estimated frequency and spacing. However, identifying a specific minor structure in parallel boreholes or in a borehole and a parallel tunnel or shaft more than 10–20 m apart has proved to be

very uncertain except when one can obtain a very good signature of the structure such as a kinematic indicator, characteristic mineralization or wall rock alteration. In few cases it has been possible to estimate the size of a deformation zone at Äspö. Although it has not been possible to define any relationship between size, width, hydraulic and geological properties, it has been possible to follow some deformation zones in the range of 100–500 m using their kinematic signatures or hydraulic conductivity.

- A useful method for identifying and estimating the extension and orientation of clay-filled and especially water-bearing fractures is to correlate data from BIPS, borehole radar and hydraulic difference logs with parameters in the borehole logs. Thus, correlation between difference flow meter, BIPS, SPR-log and borehole radar with 20, 100 and 250 MHz antenna has provided valuable information concerning the characterisation of minor deformation zones. Under normal conditions radar techniques can be used to trace a fracture zones up to 10–40 m from the borehole and under favourable conditions, up to 60 m.
- New and ongoing studies in Laxemar have provided exposures large enough to study structures with surface traces larger than 50 m. Detailed surface investigations, based on detailed geophysics and high resolution Lidar data, provide information for localising lineaments, which after uncovering proved to be minor deformation zones/long fractures with an extension in the range of 10–100 m. These correspond to critical deformation zones, i.e. zones with radii larger than 50 m. At this particular study site, magnetic and topographical lineaments are often good indicators of deformation zones. It was also noted that the width and characteristics vary along these short structures from being essentially “single fractures” to “fracture zone”.
- The trace length/frequency plot from the Forsmark area (Figure 2-1) shows a gap in the data concerning fractures in the length range 10–1,000 m. The detailed exposure study at Laxemar discussed above combined with observations in the few large exposures provided by quarries (Figure 2-46), confirm that this lack of data reflects the limited size of outcrop in the region rather than a real absence of critical fractures (i.e. radius > 50 m).

5.1.3 Suitable investigation methods

It is a difficult task to observe and identify deformation zones remotely in a rock mass from the limited exposure provided by a tunnel or borehole and no single or unique method is currently available with the precision, resolution and range needed. However, based on previous experience from SKB’s site investigations and the construction of the Äspö HRL it is concluded that it will be possible to locate critical deformation zones if:

- The site specific characteristics of such deformation zones, particularly those related to their length are established.
- A staged, site specific strategy for the detection of deformation zones is developed and implemented during the detailed investigation program that accompanies the stepwise construction of the repository.
- Suitable technical methods are combined and used at the various stages of the excavation to detect deformation zones.
- The strategy and methods are verified.

The techniques already tested at the Äspö HRL or during the ongoing site investigations are judged essentially sufficient, but at this stage no specific method or combination of methods can be recommended because the optimal “tool box” for the investigations based on the site specific characteristics of the critical deformation zones, has yet to be established. Thus for any site, a study must be made to establish the appropriate “tool box” of methods suitable for detecting deformation zones and these methods need to be tested and calibrated. This “tool box” of techniques will enable the effective and efficient accumulation of data during the construction of the various stages of the repository and this will enable a detailed 3D geological model of the site to be built up and refined as discussed in Chapter 3. The selected techniques will be site

specific and controlled primarily by rock type and the types of deformation zones cutting the rock mass.

The testing and calibration of the selected techniques can only be seriously undertaken during the underground excavations. Plans for such activities therefore need to be implemented in the detailed characterisation programme.

Improved geological data acquisition procedures are now being employed by Posiva in connection with the ONKALO project, for establishing cross-hole fracture correlation which attempts to maximize the use of structural data such as kinematic indicators to maximize the confidence level of correlation.

5.2 Implications for the site characterisation programme

The strategy for ensuring that all critical deformation zones cutting the deposition holes will be detected will involve the following:

The geological mapping of the tunnels and boreholes and the search for critical deformation zones using the geometric features and other criteria established in Chapter 2. This visual survey will be complemented by the geophysical techniques described in Chapter 3. This is possible because fracture infilling (either minerals or water) and wall rock alteration, both resulting from high fracture conductivity, are considered to be good indicators of fracture size, and often provide the fracture with a clear geophysical signature that enables its extent to be determined using geophysical methods. However, as noted in Section 2.10, it is possible that a large fracture may have a low conductivity and the general statement that the larger the fracture the greater its conductivity needs to be tempered, particularly in view of the fact that the aim of this study is to detect critical deformation zones, i.e. any planar zone of weakness that might undergo shear displacements of greater than 10 cm in response to seismic events linked to post-glacial faulting. It cannot be assumed that all conductive structures are long and that non-conductive deformation zones are short. However, field experience indicates that many large deformation zones are conductive and it is argued that when a conductive zone is located, then it should be assumed to be long until proved otherwise.

- Another method of reducing the likelihood of missing critical deformation zones is to design the investigative probe holes that precede tunnel excavation so as to maximise the possibility of picking up long fractures for example by cross hole correlation between the probe holes. The recognition of a deformation zone in more than one borehole or tunnel is one of the most important techniques available for detecting large fractures and other critical structures. Consequently the reliability of the techniques used for matching fractures and fracture zones between two excavations (tunnels and boreholes) needs to be assessed. This problem of fracture correlation, using geological signatures and kinematic indicators has received considerable attention recently by workers from Posiva and a new procedure for the recognition and classification of deformation zones in boreholes and cores and tunnels has been introduced, (Figure 2-59).
- The use of the Full Perimeter Intersection (FPI) criteria for the detection of deformation zones has been discussed in a companion report /Munier 2006/ in which it is pointed out that any deformation zone that does not completely cut the tunnel, as a continuous intersection line can be ignored. Even if it represents the extremity of a critical fracture, movement along it at this location (i.e. at tip of the fracture) will fall well below the maximum permitted. However, while the (extended) FPC provides a feasible method of detecting critical deformation zones it may not represent the best method for qualifying potential deposition holes. Its efficiency could be improved, and it also over-predicts (i.e. it includes fractures which are shorter than the critical value of radius > 50 m) resulting in the degree of utilisation of the deposition holes being unnecessarily low. However, it remains a powerful criterion for conservatively identifying critical deformation zones. Any zone with a FPI in the deposition tunnels must be examined to determine whether or not it is a critical zone.

Thus a combination of the geological signatures, geophysical investigation techniques and the FPI criterion provides the basis for ensuring that all critical deformation zones cutting the repository holes will be detected.

As discussed above a specific investigation programme for identifying the critical deformation zones needs to be established for each site. The programme should explore the feasibility and implications of the methods suggested in this reports within the site specific context (Chapter 3).

A plan for testing the methods, verification and the training of the staff needs to be established. This programme could be initiated immediately during the remaining parts of the ongoing surface based investigations at Laxemar (see Chapter 4), but this early (i.e. surface) phase of the site investigation would not provide sufficient data to enable the final selection of the verification method to be made. The selection would only be possible after further experience and data have been acquired during the excavation of the access routes (shafts, ramps and tunnels) i.e. after the first phase of the repository construction, (Figure 3-1).

5.3 Quantification of the probability of missing a critical deformation zone in a deposition hole

The aim of this report is to quantify the confidence level of detecting critical deformation zones, i.e. structures with a radius > 50 m, cutting a deposition hole. These structures include individual fractures, fracture zones and ductile shear zones, i.e. any planar or sub-planar feature along which slip in excess of 10 cm might occur as a result of seismic movement along nearby faults.

In order to achieve this goal three different approaches have been used. The first was to identify features which can be observed in tunnels and boreholes which are related to the length of a structure. The second was to select appropriate geophysical techniques for determining the distance away from the borehole or tunnel that the detected structure extends and the third, using DFN modelling, was to examine the extent of the intersection of the structure with the deposition tunnel, specifically to determine whether the structure intersects the full tunnel perimeter.

It is concluded that the most important parameters linked to fracture and fracture zone length are fracture aperture, shear displacement, deformation zone thickness and conductivity (see Chapter 2). There is some controversy regarding the reliability of these criteria, for example, it has been pointed out that many relatively short fractures and fracture zones have a large thickness and that short fractures and fracture zones can be conductive. Nevertheless, there is considerable geological evidence to indicate that in many examples these parameters are linked to the length of a structure. Consequently a pragmatic approach has been adopted, namely that of assuming that all thick and/or conductive structures are critical until proven otherwise.

A variety of geophysical techniques have been identified that can be used to indicate the length of a structure that intersects a borehole or tunnel (Chapter 3). One of the most important is borehole radar which gives a good indication of the extent of the fracture zone into the rock around the hole.

The third approach that can be used to identify potentially critical structures relates to the identification of critical fractures that intersect the full perimeter of the deposition tunnel. This is discussed in a separate report /Munier 2006/ and these structures can be identified by geological mapping of the deposition tunnel complimented by the use of laser scanning.

A further technique that can be used to determine the length of a structure is that of “Cross-hole correlation”. Before any deposition hole is excavated a pilot hole is drilled along its centre. Core and borehole logging of this provide information on the location and orientation of fractures

and fracture zones. Any structure whose extrapolation would intersect an adjacent borehole, deposition hole or tunnel if the structure were sufficiently long, can be investigated using the procedure of cross-hole correlation (see Chapter 2, Figure 2-58).

It is therefore recommended that any deformation zones (fractures, fracture zones etc) in the repository tunnels or deposition holes that display the characteristics of long structures and/or which show a full perimeter intersection, be investigated using appropriate geophysical techniques and the technique of cross-hole correlation to determine whether or not they are critical structures. In this way the chances of missing a critical deformation zone cutting a deposition hole is reduced to a minimum.

On the basis of the above discussion, and bearing in mind that SKB has an experienced and well trained team with access to the geophysical tools needed to complete their investigation, it can be argued that by following this procedure, the chances of missing any critical deformation zone can be reduced to a minimum and that the best available site specific 3D geological data base can be obtained i.e. one which is focused on describing the size, type, orientation, location etc of deformation zones within a proposed repository site. This data base will then provide the input for the DFN modelling (presented in an accompanying report /Munier 2006/) that can be used to quantify the probability of a repository tunnel or deposition hole at a specific repository site, being intersected by a deformation zone in the size range $50 \text{ m} < r < 250 \text{ m}$.

6 References

- Almén K-E, Stenberg L, 2005.** Äspö Hard Rock Laboratory. Characterisation methods and instruments. Experiences from the construction phase. SKB TR-05-11, Svensk Kärnbränslehantering AB.
- Andersson J, Ström A, Svemar C, Almén K-E, Ericsson L O, 2000.** What requirements does the KBS-3 repository make on the host rock? Geoscientific suitability indicators and criteria for siting and site evaluation. SKB TR-00-12, Svensk Kärnbränslehantering AB.
- Andersson P, Byegård J, Dershowitz B, Doe T, Hermansson J, Meir P, Tullborg E-L, Winberg A, 2002.** Final report of the TRUE Block Scale project 1. Characterisation and model development. SKB TR 02-13.
- Arvidsson R, 1996.** Fennoscandian earthquakes; whole crustal rupturing related to postglacial rebound. *Science* 274(5288): 744–746.
- Atkinson B K, 1984.** Subcritical crack growth in geological materials. Chemical effects of water on the strength and deformation of crustal rocks. H. Kirby Stephen and C. H. Scholz. Washington, DC, United States, American Geophysical Union. 89; 6: 4077–4114.
- Atkinson B K (ed.), 1987.** Fracture mechanics of rock. London, United Kingdom, Academic Press.
- Bai T, Pollard D D, 2000a.** Closely spaced fractures in layered rocks; initiation mechanism and propagation kinematics. *Journal of Structural Geology* 22(10): 1409–1425.
- Bai T, Pollard D D, 2000b.** Fracture spacing in layered rocks; a new explanation based on the stress transition. *Journal of Structural Geology* 22(1): 43–57.
- Bankwitz P, Bankwitz E, Thomas R, Wemmer K, Kaempfer H, 2004.** Age and depth evidence for pre-exhumation joints in granite plutons; fracturing during the early cooling stage of felsic rock. *Geological Society Special Publications* 231: 25–47.
- Berglund J, Curtis P, Eliasson T, Olsson T, Starzec P, Tullborg E-L, 2003.** Äspö Hard Rock Laboratory. Update of the geological model 2002. SKB IPR-03-34, Svensk Kärnbränslehantering AB.
- Bogdanov A A, 1947.** The intensity of cleavage as related to the thickness of the bed. *Soviet Geology* 16.
- Buergmann R, Pollard D D, Martel S J, 1994.** Slip distributions on faults; effects of stress gradients, inelastic deformation, heterogeneous host-rock stiffness, and fault interaction. *Journal of Structural Geology* 16(12): 1675–1690.
- Burford, R O, Harsh P W, 1980.** Slip on the San Andreas Fault in central California from alignment array surveys. *Bulletin of the Seismological Society of America* 70(4): 1233–1261.
- Bäckblom G, 1989.** Guide-Lines for use of nomenclature on fractures, fracture zones and other topics. SKB HRL-96-18
- Börgesson L, Johannesson L-E, Hernelind J, 2003.** Earthquake induced rock shear through a deposition hole. Effect on the canister and the buffer. SKB TR-04-02, Svensk Kärnbränslehantering AB.
- Carlsten S, Lindqvist L, O Olsson, 1989.** Comparison between radar data and geophysical, geological, and hydrological borehole parameters by multivariate analysis of data. SKB TR 89-15.

- Carlsten S, Stråhle A, Ludvigson J-E, 2001.** Conductive fracture mapping A study on the correlation between borehole TV- and radar images and difference flow logging results in borehole KLX02. SKB Rapport R-01-48, Svensk Kärnbränslehantering AB.
- Cartwright J A, Mansfield C, Trudgill B D, 1996.** The growth of normal faults by segment linkage. Modern developments in structural interpretation, validation and modelling. P. G. Buchanan and D. A. Nieuwland. London, United Kingdom, Geological Society of London. 99: 163–177.
- Cartwright J A, Trudgill B D, Mansfield C S, 1995.** Fault growth by segment linkage; an explanation for scatter in maximum displacement and trace length data from the Canyonlands Grabens of SE Utah. *Journal of Structural Geology* 17(9): 1319–1326.
- Cotterell B, Rice J R, 1980.** Slightly curved or kinked cracks. *International journal of fracture* 16: 155–169.
- Cruikshank K M, Zhao G, Johnson A M, 1991.** Analysis of minor fractures associated with joints and faulted joints. *Journal of Structural Geology* 13(8): 865–886.
- Darcel C, Bour O, P Davy, 2003.** Stereological analysis of fractal fracture networks. *J. Geophys. Res.*
- Eichhubl P, 2004.** Growth of ductile opening-mode fractures in geomaterials. *Geological Society Special Publications* 231: 11–24.
- Emsley S, Olsson O, Stenberg L, Alheid H-J, Falls, 1997.** ZEDEX – A study of damage and disturbance from tunnel excavation by blasting and tunnel boring. SKB TR 97-30, Svensk Kärnbränslehantering AB.
- Evans A G, Blumenthal W, 1984.** High temperature failure mechanisms in ceramic polycrystals., Plenum Press. New York.
- Feng Q, Röshoff K, 2004.** In-situ mapping and documentation of rock faces using full-coverage 3D laser scanning technique. *International Journal of Rock Mechanics & Mining Sciences* (41) p. 379.
- Fossen H, Hesthammer J, 2000.** Possible absence of small faults in the Gullfaks Field, northern North Sea; implications for downscaling of faults in some porous sandstones. *Journal of Structural Geology* 22(7): 851–863.
- Friedman M, 1972.** X-ray analysis of residual elastic strain in quartzose rocks. *Basic and applied rock mechanics*. [location varies], United States, A.A. Balkema. 10: 573–595.
- Gash S P J, 1971.** A study of surface features relating to brittle and semi-brittle fracture. *Tectonophysics* 12(5): 349–391.
- Giese R, Dickmann T, Eppler T, Lüth S, 2005.** In press Seismic tomography to investigate the tunnel surroundings of the Side Gallery West of the multifunctional station Faido. *Symposium Geology Alptransit, Zurich*.
- Griffith A A, 1925.** Theory of Rupture. *Proceedings of the First International Conference of Applied Mechanics, Delft*.
- Griggs D T, Handin J, 1960.** Observations on fracture and a hypothesis of earthquakes. In *Rock Deformation*. Memoir 79 of the Geological Society of America. Eds. D. Griggs & J.Handin. pp. 347–73.
- Gustafsson J, Gustafsson C, 2004.** RAMAC and BIPS logging in boreholes KLX03, HAV11 to HAV13 and HLX21 to HLX25. Oskarshamn site investigation. Revised April 2006. SKB P-04-275. Svensk Kärnbränslehantering AB.
- Hedin A, 2005.** An analytic method for estimating the probability of canister/fracture intersections in a KBS-3 repository. SKB R-05-29, Svensk Kärnbränslehantering AB.

- Hermansson J, Follin S, Nilsson P, Nyberg G, Winberg A, 1996.** Äspö Hard Rock Laboratory- TRUE Block Scale update of the structural-hydraulic model and compilation of scoping data set. Internal progress report IPR-02-13. Svensk Kärnbränslehantering AB.
- Hoagland R G, Hahn G T, Rosenfield A R, 1973.** Influence of Microstructure on Fracture Propagation in Rock. *Rock Mechanics. Supplementum = Felsmechanik. Supplementum = Mecanique des Roches. Supplementum 5(2): 77–106.*
- Hodgson R A, 1961.** Classification of structures on joint surfaces. *American Journal of Science 259(7): 493–502.*
- Hoshino K, Koide H, Inami K, Iwamura S, Mitsui S, 1972.** Mechanical Properties of Japanese Tertiary Sedimentary Rocks under High confining Pressures. Report 244, Geological Survey of Japan.
- Hökmark H, 2003.** Canister positioning. Influence of fracture system on deposition hole stability. SKB R-03-19, Svensk Kärnbränslehantering AB.
- Jackson J, Leeder M, 1994.** Drainage systems and the development of normal faults; an example from Pleasant Valley, Nevada. *Journal of Structural Geology 16(8): 1041–1059.*
- Jolly R J H, Cosgrove J W, 2003.** Geological evidence of patterns of fluid flow through fracture network; examination using random realizations and connectivity and analysis. *Geological Society Special Publications 209: 177–186.*
- Koestler A G, Milnes A G, Keller P, 1995.** Quantification of fault/fracture systems for reservoir simulation – use of systematic data from field analogues. In: *Project Summary Reports on Reservoir Characterisation and Near Well Flow (PROFIT).* Norwegian Petroleum Directorate.
- La Pointe P, Cladouhos T, 1999.** An overview of a possible approach to calculate rock movements due to earthquakes at Finnish nuclear waste repository sites. POSIVA 99-02, Posiva Oy Helsinki Finland.
- La Pointe, P, Wallmann P, Thomas A, Follin S, 1997.** A methodology to estimate earthquake effects on fractures intersecting canister holes. SKB TR 97-07, Svensk Kärnbränslehantering AB.
- La Pointe, P, Cladouhos R T, Follin S, 2002.** Development, application, and evaluation of a methodology to estimate distributed slip on fractures due to future earthquakes for nuclear waste repository performance assessment. *Bulletin of the Seismological Society of America 92(3): 923–944.*
- La Pointe, P R, Cladouhos T T, Outters N, Follin S, 2000.** Evaluation of the conservativeness of the methodology for estimating earthquake-induced movements of fractures intersecting canisters. SKB TR-00-08, Svensk Kärnbränslehantering AB.
- La Pointe, P R, Olofsson I, Hermanson J, 2005.** Statistical model of fractures and deformation zones for Forsmark. Preliminary site description Forsmark area – version 1.2. SKB R-05-26, Svensk Kärnbränslehantering AB.
- Lagerbäck R S, 1991.** Seismically deformed sediments in the Lansjärv area, Northern Sweden. SKB TR 91-17, Svensk Kärnbränslehantering AB.
- Lambeck K, Purcell A, 2003.** Glacial rebound and crustal stress in Finland. Posiva 2003-10, Posiva Oy Olkiluoto Finland.
- Langer D, Mettenleiter M, Härtl F, Fröhlich C, 2000.** Imaging lidar for 3-D surveying and CAD modelling of real world environments. *Int J Robotics Res 19: pp. 1075–1088.*
- Li V C, 1987.** Mechanics of shear rupture applied to earthquake zones. *Fracture mechanics of rock.* K. Atkinson Barry. London, United Kingdom, Acad. Press: 351–428.

- Lowrie W, 1997.** Fundamentals of Geophysics. University press, Cambridge, p. 354.
- Lund B, 2005.** Effects of deglaciation on the crustal stress field and implications for endglacial faulting: a parametric study of simple Earth and ice models. SKB TR-05-04, Svensk Kärnbränslehantering AB.
- Mandl G, 2005.** Rock joints. The mechanical genesis, Springer.
- Mazurek M, P Bossart, T Eliasson, 1996.** Classification and characterization of water-conducting features at Äspö: Results of investigations on the outcrop scale. SKB HRL International Cooperation Report ICR 97-01, SKB.
- Mettenleiter M, Härtl F, Fröhlich C, Langer D, 2000.** Imaging laser for 3-D modelling of real world environments. Proceedings of the IASTED International Conference Modelling, Identification and Control, Innsbruck, Austria.
- Munier R, 1995.** Studies of geological structures at Äspö. Comprehensive summary of results. SKB HRL Progress Report 25-95-21, SKB.
- Munier R, 2004.** Statistical analysis of fracture data, adapted for modelling Discrete Fracture Networks-Version 2. SKB R-04-66, Svensk Kärnbränslehantering AB.
- Munier R, 2006.** Using observations in deposition tunnels to avoid intersections with critical fractures in deposition holes. SKB R-06-54, Svensk Kärnbränslehantering AB.
- Munier R, H Hökmark, 2004.** Respect distances. Rationale and means of computation. SKB R-04-17, Svensk Kärnbränslehantering AB.
- Munier R, Stenberg L, Stanfors R, Milnes A G, Hermanson J, Triumf C-A, 2003.** Geological Site Descriptive Model. A strategy for the model development during site investigations. SKB R-03-07, Svensk Kärnbränslehantering AB.
- Mörner N-A, 1996.** Liquefaction and varve deformation as evidence of paleoseismic events and tsunamis; the autumn 10,430 BP case in Sweden. Quaternary Science Reviews 15(8–9): 939–948.
- Mörner N-A, 2004.** Active faults and paleoseismicity in Fennoscandia, especially Sweden; primary structures and secondary effects. Tectonophysics 380(3–4): 139–157.
- Mörner N-A, Tröften P E, Sjöberg R, Grant D, Dawson S, Bronge C, Kvamsdal O, Sidén A, 2000.** Deglacial paleoseismicity in Sweden: the 9663 BP Iggesund event. Paleogeophysics and Geodynamics, Stockholm University, Stockholm, Sweden, In: Quaternary Science Reviews 19 (2000) pp. 1461–1468.
- Odling N E, 1997.** Scaling and Connectivity of joint systems in sandstones from western Norway. J. Struct. Geol. 19(10): 1257–1271.
- Odling N E, Gillespie P, Bourguine B, Castaing C, Chiles J P, Christensen N. P, Fillion E, Genter A, Olsen C, Thrane L, Trice R, Aarseth E, Walsh J J, Watterson J, 1999.** Variations in fracture system geometry and their implications for fluid flow in fractures hydrocarbon reservoirs. Petroleum Geoscience 5(4): 373–384.
- Olson, J, Pollard D D, 1988.** Inferring stress states from detailed joint geometry, A. A. Balkema, Rotterdam, Netherlands (NLD). ISBN 9061918359.
- Olson, J, Pollard D D, 1989.** Inferring paleostresses from natural fracture patterns; a new method. Geology (Boulder) 17(4): 345–348.
- Olson, J E, 1993.** Joint pattern development; effects of subcritical crack growth and mechanical crack interaction. Journal of Geophysical Research, B, Solid Earth and Planets 98(7): 12,251–12,265.

- Olson, J E, 2004.** Predicting fracture swarms; the influence of subcritical crack growth and the crack-tip process zone on joint spacing in rock. Geological Society Special Publications 231: 73–88.
- Parasnis D S, 1973.** Mining Geophysics. Elsevier Scientific publishing company. p. 395.
- Paulamäki S, Paananen M, Gehör S, Kärki A, Front K, Aaltonen I, Ahokas T, Kempainen K, Mattila J, Wikström L, 2006.** Geological model of the Olkiluoto site version 0. Posiva Working Report 2006-37, Posiva Oy Olkiluoto Finland.
- Peacock D C P, Sanderson D J, 1994.** Geometry and development of relay ramps in normal fault systems. AAPG Bulletin 78(2): 147–165.
- Peacock D C P, Sanderson D J, 1997.** Geometry and development of normal faults. Evolution of geological structures in micro- and macroscales. (Ed.) S. Sengupta. London, Chapman & Hall.
- Pollard D D, Fletcher R C, 2005.** Fundamentals of structural geology, Cambridge University Press.
- Pollard D D, Segall P, Delaney P T, 1982.** Formation and interpretation of dilatant echelon cracks. Geological Society of America Bulletin 93(12): 1291–1303.
- Price N J, 1966.** Fault and Joint Development in Brittle and Semi-Brittle Rock, Pergamon Press. London.
- Price, N J, Cosgrove J W, 1990.** Analysis of geological structures, Cambridge University Press. Cambridge, ISBN 0-521-31958-7.
- Ramsay J G, Graham R H, 1970.** Strain variation in shear belts. Canadian Journal of Earth Sciences = Journal Canadien des Sciences de la Terre 7(3): 786–813.
- Renshaw, C E, Pollard D D, 1994a.** Are large differential stresses required for straight fracture propagation paths? Journal of Structural Geology 16(6): 817–822.
- Renshaw C E, Pollard D D, 1994b.** Numerical simulation of fracture set formation; a fracture mechanics model consistent with experimental observations. Journal of Geophysical Research, B, Solid Earth and Planets 99(5): 9359–9372.
- Rhén I, Forsmark T, 2000.** Äspö Hard Rock laboratory- High Permeability features (HPF). SKB Internal progress report IPR-00-02. Svensk Kärnbränslehantering AB.
- Rhén I, Gustafson G, Stanfors R, Wikberg P, 1997.** Äspö HRL – Geoscientific evaluation 1997/5. Models based on site characterization 1986–1995. SKB TR 97-06, Svensk Kärnbränslehantering AB.
- Rhén I, Stanfors R, Wikberg P, Forsmark T, 1995.** Comparative study between the cored test borehole KA3191F and the first 200 m extension of the TBM tunnel. SKB Progress Report 95-12, Svensk Kärnbränslehantering AB.
- Rispoli, R, 1981.** Stress fields about strike-slip faults inferred from stylolites and tension gashes. Tectonophysics 75(3–4): T29-T36.
- Rives T, Razack M, Petit J P, Rawnsley K D, 1992.** Joint spacing; analogue and numerical simulations. Mechanical instabilities in rocks and tectonics; a selection of papers. P. Burg Jean, D. Mainprice and P. Petit Jean. Oxford-New York, International, Pergamon. 14; 8–9: 925–937.
- Rouhiainen P, Pöllänen J, Sokolnicki M, 2005.** Difference flow logging of borehole KLX 03. Subarea Laxemar. Oskarshamn site investigation. SKB P-05-67. Svensk Kärnbränslehantering AB.
- Savage J C, Prescott W H, Lisowski M, King N E, 1981.** Strain on the San Andreas Fault near Palmdale, California; rapid, aseismic change. Science 211(4477): 56–58.

Sengupta, S (ed.), 1997. Evolution of geological structures in micro- and macroscales. London, Chapman & Hall.

Serzu M H, Kozak E T, Lodha G S, Everitt R A, Woodcock D R, 2004. Use of borehole radar techniques to characterize fractured granitic bedrock at AECL's Underground Research Laboratory. *Journal of Applied Geophysics* 55(1–2): 137–150.

Stråhle A, 2001. Definition och beskrivning av parametrar för geologisk, geofysisk och bergmekanisk kartering av berg. SKB Rapport R-01-19, Svensk Kärnbränslehantering AB.

Talbot C, Munier R, 1989. Faults and fracture zones in Äspö. SKB HRL Progress report 25-89-11

Telford W M, Geldart L P, Sheriff R E, Keys D A, 1976. Applied Geophysics. Cambridge Univeristy Press, p. 860.

Trudgill B, Cartwright J, 1994. Relay-ramp forms and normal-fault linkages, Canyonlands National Park, Utah. *Geological Society of America Bulletin* 106(9): 1143–1157.

Walsh J, Nicol J A, Childs C, 2002. An alternative model for the growth of faults. *Journal of Structural Geology* 24(11): 1669–1675.

Walsh, J J, Watterson J, 1987. Distributions of cumulative displacement and seismic slip on a single normal fault surface. *Journal of Structural Geology* 9(8): 1039–1046.

van Dijk, J P, Bello M, Toscano C, Bersani A, Nardon S, 2000. Tectonic model and three-dimensional fracture network analysis of Monte Alpi (Southern Apennines).

Watterson J, 1986. Fault dimensions; displacements and growth. International structure of fault zones. Wang, Chi and yuen. Basel, Switzerland, Birkhaeuser Verlag. 124: 365–373.

White S H, Bretan P G, Rutter E H, 1986. Fault-zone reactivation; kinematics and mechanisms. Major crustal lineaments and their influence on the geological history of the continental lithosphere. H. G. Reading, J. Watterson and S. H. White. London, United Kingdom, Royal Society of London. 317; 1539: 81–92.

Winberg A, Andersson P, Hermansson J, Stenberg L, 1996. Results of the Select Project. SKB HRL-96-01.

Winberg A, Hermansson J, 1996. Äspö Hard Rock Laboratory- TRUE Block Scale Experiment Allocaton of Experimental volume. SKB Internal progress report IPR-02-14. Svensk Kärnbränslehantering AB.

Wu H, Pollard D D, 1995. An experimental study of the relationship between joint spacing and layer thickness. *Journal of Structural Geology* 17(6): 887–905.

Example of minor deformation zone characteristics from Äspö HRL and their cross correlation between boreholes and tunnels

A1.1 Introduction

During the pre-investigations for the Äspö HRL a great number of narrow (dm to a few metres thick), minor deformation zones (MDZ) and longer, single fractures were mapped on outcrops on Äspö. Only a few of them are topographically significant but too narrow to be geologically unambiguously indicated /Talbot and Munier 1989/.

The term MDZ (minor deformation zone) is used to designate an essentially 2-dimensional structure whose lateral extent is < 1,000 m and width < 5 m. MDZ commonly show evidence of both brittle and ductile deformation. They can be characterised by brittle, low-cohesive products such as fractures, breccias and gouge or by cohesive strongly foliated or mylonitic rock the product of ductile deformation.

Many examples of MDZ identification and characterisation at Äspö are reported from projects such as the TRUE Block Scale Project /Andersson et al. 2002/ and the Select Project /Winberg et al. 1996/.

Mapping in the tunnel indicated several MDZ not thicker than ca 4 m. Most consist of a single or up to a handful of faults that often contain gouge and most of them are important hydraulic conductors /Markström and Erlström 1996/.

All the structures mapped are longer than 5 m, and some faults were traced over distances of at least 20 m. Mapping on the surface at Äspö suggests that faults similar to those mapped in the tunnel have extents in the order of tens to hundreds of metres /Mazurek et al. 1996/.

In the following section three examples of attempted correlation of MDZs between boreholes and tunnels are presented from an ongoing study concerning MDZ evaluation at the Äspö HRL. In addition this comparison of data from investigation boreholes and tunnels, demonstrates the possibility of identifying MDZs prior to the excavation of the tunnel.

A third example is discussed where an attempt has been made to use radar data from boreholes and the direct mapping of a shaft wall, to correlate MDZs between the two.

The main aim of this study is to identify techniques that can be used to recognise MDZs with lengths in the range 50–1,000 m and to establish the relationship between deformation zone size (length, thickness), and their hydraulic and geologic properties.

A1.2 ÄSPÖ HRL – Example 1

A1.2.1 Comparison between ramp tunnel and KBH02

The sub-horizontal cored borehole KBH02 was drilled during pre-investigations i.e. prior to tunnel excavation, part of the ramp leading down to the spiral section of the HRL. The main aim of the borehole was to locate and investigate geophysically indicated deformation zones. The borehole is close to and almost parallel to the tunnel for about 900 m, Figure A1-1.

A comparison between tunnel mapping data and data obtained from the borehole investigations, especially concerning deformation zones and longer fractures, is presented in Figure A1-2 and Table 3-1.

Tunnel mapping data is taken mainly from Äspö TMS (Tunnel Mapping System) and /Mazurek et al. 1996/. It is important to note that the borehole mapping of KBH02 was performed without BIPS TV.

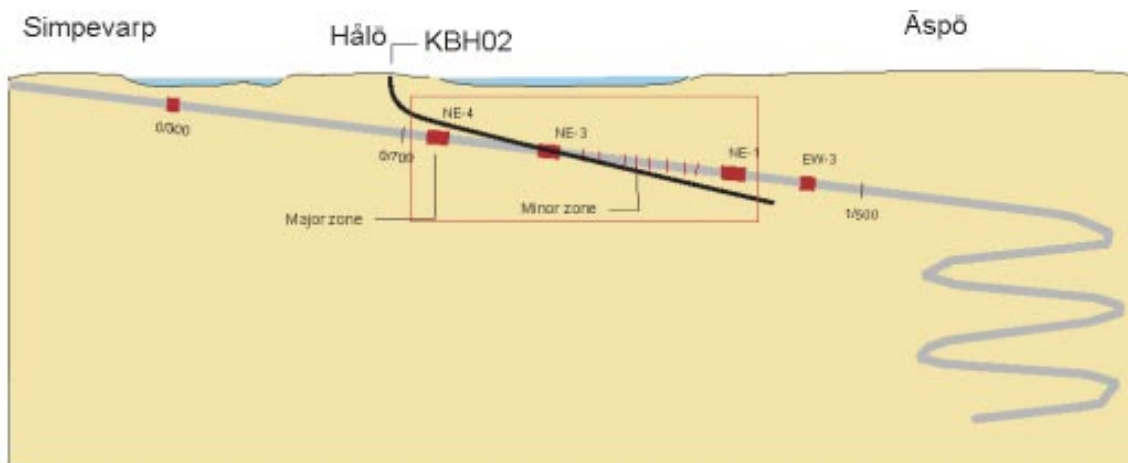


Figure A1-1. Position of KBH02 in the Äspö HRL.

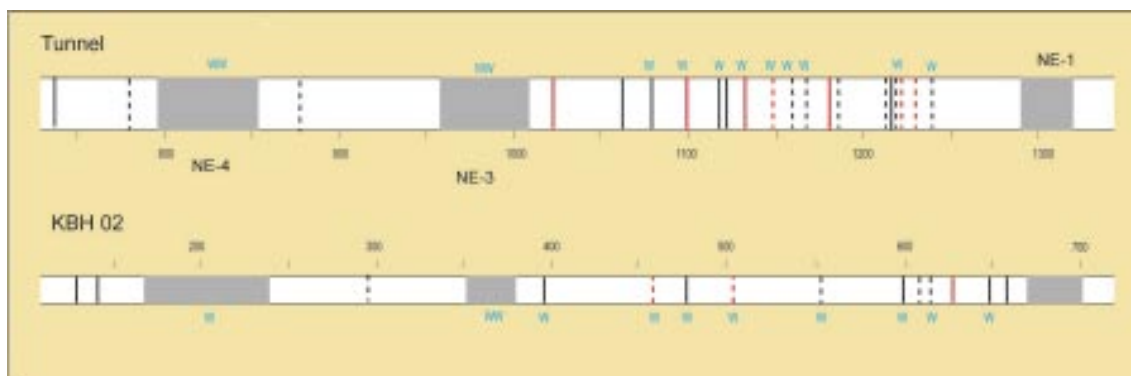


Figure A1-2. Comparison between the Äspö Tunnel section (750–1,350 m) and KBH02 (100–700 m).

Table A1-1. Comparison of mapping data in tunnel section (650–1,350 m) and core borehole KBH02 (100–700 m). Observed length in KBH02 translated to tunnel length.

Tunnel Length	Zone	Water inflow	KBH02 Length	Zone	Water inflow
735	MZ	–	750	MZ	–
780	LF	–	762	MZ	–
796–858	NE–4	ww	785–860	NE–4	w
875	LF	–	–	–	–
–	–	–	915	LF	–
958–1,009	NE–3	ww	955–1,005	NE–3	ww
1,020	MZ*	–	1,015	MZ	w
1,060	MZ	–	–	–	–
1,080	MZ	w	1,080	LF*	w
1,100	MZ*	w	1,095	MZ	w
1,120	MZ	w	–	–	–
1,125	MZ	–	1,125	LF*	w
1,135	MZ*	w	–	–	–
1,148	LF* (r)	w	–	–	–
1,156	LF	w	–	–	–
1,165	LF (r)	w	–	–	–
1,180	MZ*	–	1,175	LF	w
1,185	LF	–	–	–	–
1,210–1,220	MZ+ LF (r)	w	1,220	MZ	w
1,230	LF*	–	1,230	LF	–
1,240	LF	w	1,240	LF	w
–	–	–	1,250	MZ*	–
–	–	–	1,270	MZ	w
–	–	–	1,280	MZ	–
1,290–1,320	NE–1	ww	1,295–1,330	NE–1	ww

MZ: minor zone, LF: long fracture, NE-1, NE-3, NE-4: major zones, *: associated with fine-grained granite, (r): radar indicator.

A1.2.2 Main results

- There is a good correlation between the major fracture zones detected in borehole KBH02 and those recorded in the tunnel mapping data regarding both position and zone width.
- The number of minor zones is almost the same in borehole and tunnel but it is often very difficult to correlate a particular zone in the borehole with a specific zone in the tunnel.
- The lower number of long fractures detected in KBH02 compared to the tunnel can be explained by the difficulty in detecting fractures in a borehole, without radar and BIPS.
- In both KBH02 and in the tunnel it was noted that most of the structures are water bearing.
- There was no radar measurements in KBH02 but such measurements were taken in the two boreholes (KA1061A and KA1131B) drilled from niches in the tunnel (Figure A1-3) /Olsson 1992/.
- There is a likely correlation between three radar indications of fracture zones in the boreholes and in the tunnel, but to be certain it is necessary to demonstrate that the structures in the tunnel have the same geological signatures as the fracture zones thought to correlate with them in the cores.

A1.3 ÄSPÖ HRL – Example 2

A1.3.1 Comparative study of the cored borehole KA3191F and the first 200 m of the TBM tunnel

The last 400 m of the ÄHRL were excavated by a Tunnel Boring Machine (TBM) with a diameter of 5 m /Rhén et al. 1995/.

In order to make a good characterisation of the TBM rock volume a cored borehole (KA3191F) was drilled in advance of the TBM boring. One aim was to compare data from the cored borehole KA3191F with the documentation data from the TBM-tunnel.

The borehole KA3191F was drilled from the TBM assembly hall along the centre line of the planned TBM tunnel down to the lowest position of the excavation at a depth of 450 m below ground surface in the vicinity of the shafts. The borehole is 210 m long (7-4).

A comparison of the data from borehole KA3191F and the TBM-tunnel is presented in A1-5 and Table A1-2.

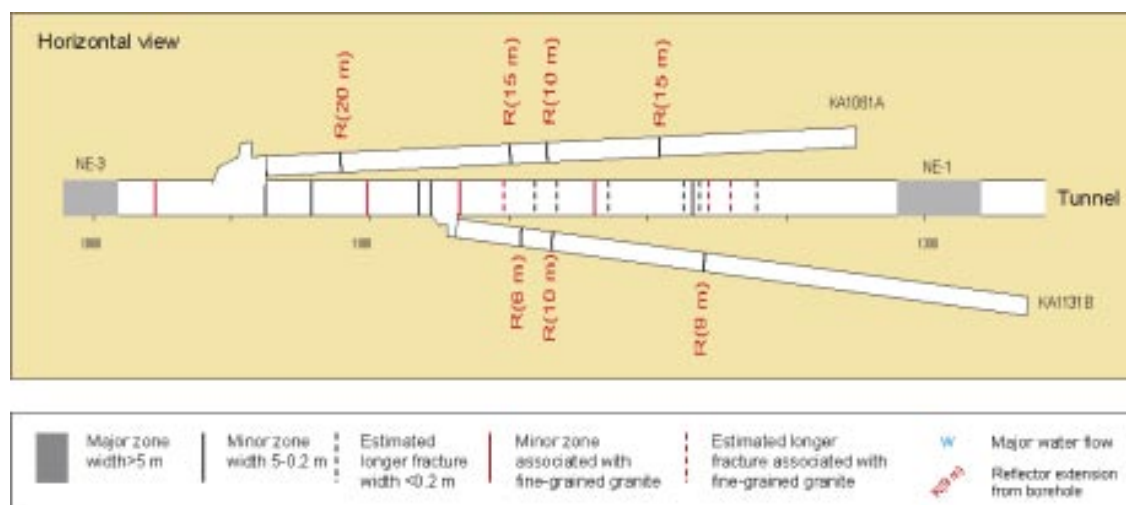


Figure A1-3. Radar reflectors in boreholes drilled from the ramp (KA1061A and KA1131B).

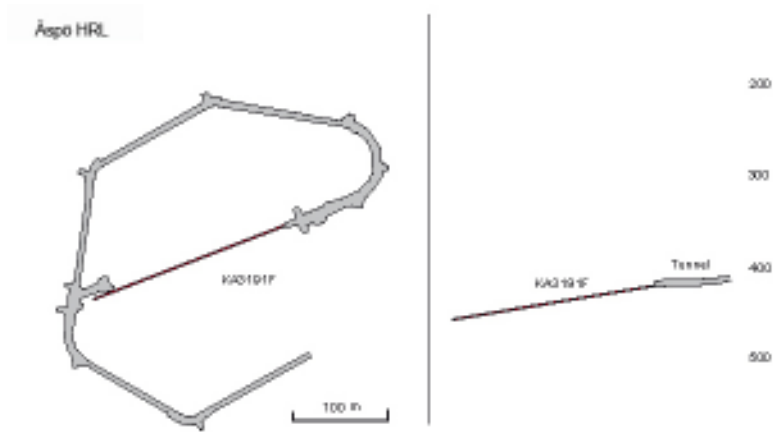


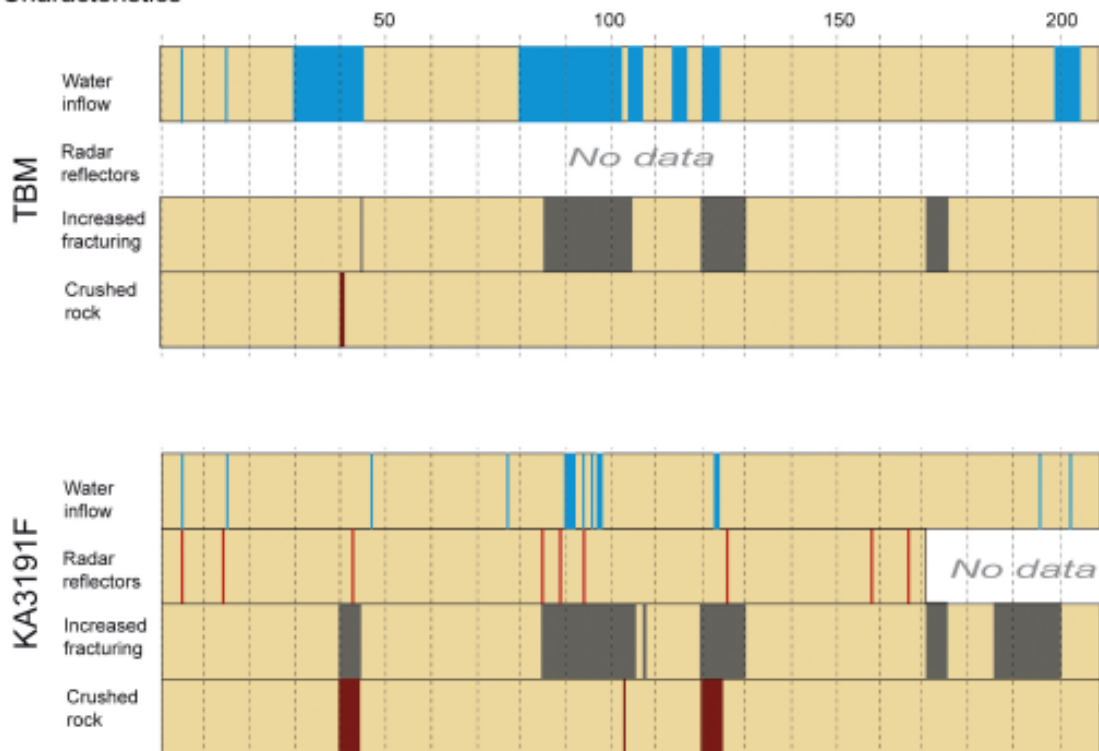
Figure A1-4. Position of KA3191F and the TBM tunnel.

A1.3.2 Main results

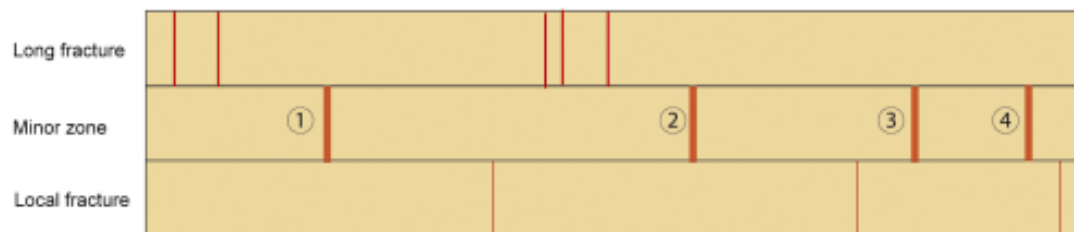
- It was possible to make accurate predictions from the borehole data regarding the major rocks and major conductive sections encountered in the tunnel.
- A correlation was also found between some but not all radar reflectors detected in the borehole and geological and hydraulic structures within the tunnel.
- There is normally a good correlation between geophysical logging data and increased fracturing/alteration of the rock in the tunnel.
- There is a direct correlation between the results of flow mapping during drilling and hydraulic tests, and the parts of the tunnel that have or have not been grouted.

Comparison between TBM and pilot hole (KA3191F)

Characteristics



Interpretation



Interpretation data - Minor zones	
① Mylonite, increased fracturing, water (geophysical logs, radar)	③ Increased fracturing (geophysical logs, radar)
② Increased fracturing, water (geophysical logs, radar)	④ Increased fracturing, greenstone, water (geophysical logs)

Figure A1-5. Comparison of data from borehole KA3191F and the TBM tunnel.

Table A1-2. Comparison between characteristics mapped in TBM-tunnel and borehole data in KA3191F.

Characteristics	TBM Tunnel investigations	KA3191F Borehole investigations	Borehole radar
Increased fracturing	45 m	40–43 m	42 m
	80–105	85–105	85.88
	–	108	–
	120–130	120–130	126
	–	–	158
	171–175	171–175	166
Crushed rock	–	188–200	–
	40–41 m	40–43 m	42 m
	–	102	–
Water inflow	–	120–125	126
	5 m	5 m	5 m
	15	15	14
	30–45	48	42
	–	78	
	80–102	90–92	88
		94	94
		96	
		98	
	104–106	–	
	113–116	–	
120–123	120–123	126	
198–203	195	No data	
	202	No data	

A1.4 ÄSPÖ HRL – Example 3

A1.4.1 Comparative study between geological mapping data of the elevator shaft and the cored boreholes KAS05 and KAS02.

During the construction of the Äspö HRL two vertical ventilation shafts (diameter 1.5 m) and one elevator shaft (diameter 3.8 m) were excavated using the raise-boring technique. The elevator shaft was mapped from 0–440 m depth. The ventilation shafts were only partly available for mapping /Munier 1995/.

Data from the sub-vertical cored boreholes KAS05 and KAS02 can be compared with geological shaft data Figure A1-6 /Sehlstedt et al. 1989, Ståhle 1989/. KAS05 and KAS02 were drilled at an early phase of the pre-investigations for Äspö HRL. Their position with respect to the shaft are shown in A1-6.

The only prominent structure in the elevator shaft is an approximately 10 m thick mylonite zone at a depth of between 150–170 m that locally strike N–NNE and dips 75° NW. The mylonite contains a thin fault zone with a measured flow rate in the range of 1–5 l/min. It is noteworthy that only a handful of fractures carry water in the elevator shaft /Munier 1995/.

A1.4.2 Main results

- The distribution of rocks in the shaft and the boreholes (Småland granite with fine-grained granite and greenstone) is quite similar.
- The frequency of MDZ and longer fractures mapped in the shaft is in the same order as that estimated in the boreholes. However, it seems to be very difficult to make a correlation between certain structures in a shaft and boreholes ca 50 m from the shaft.
- The relatively large separation between the boreholes and the shaft (between 40–50 m, see A1-6) has resulted in an element of uncertainty in tracing a specific structure in the shaft to the adjacent boreholes. However, probable correlations based on radar data from the boreholes and oriented data from the shaft are given in this figure. Radar can normally be used to trace fractures from the borehole into the surrounding country rock for distances between 10–40 m /Carlsten 1989/.

The possible extension of structures based on radar data from the boreholes and orientation data measured in the shaft is shown in A1-7.

A1.5 Conclusions

- In the Äspö HRL there is a good correspondence between minor deformation zone indications on the surface, in the tunnel and in cored boreholes concerning estimated fracture frequency and spacing.
- Considerable uncertainty is associated with attempting to correlate a specific minor structure between parallel boreholes or between a borehole and a parallel tunnel or shaft when separated by more than 10–20 m unless they are characterised by a good hydraulic or geological signature.
- Based on exHydraulic conductivity can be an important signature of long fractures.
- In the few cases where we have been able to estimate the length of the MDZ at Äspö, it is not possible to define any relationship between length, thickness, hydraulic and geological properties. However, it has been possible to follow some MDZs in the range of 100–500 m using their kinematic signatures or hydraulic conductivity.

Based on experience from Äspö HRL it is found that a good geological understanding of the actual site, based on the following methods is useful in estimating the length and character of MDZs.

- Surface studies focused on MDZs comprising detailed geological, magnetic and resistivity investigations.
- Core borehole investigations comprising mapping of MDZs using primarily kinematic indicators, radar data and the comparison between estimated MDZs in boreholes and surface observations.

Comparison between elevator shaft and core boreholes KAS 02 and KAS 05

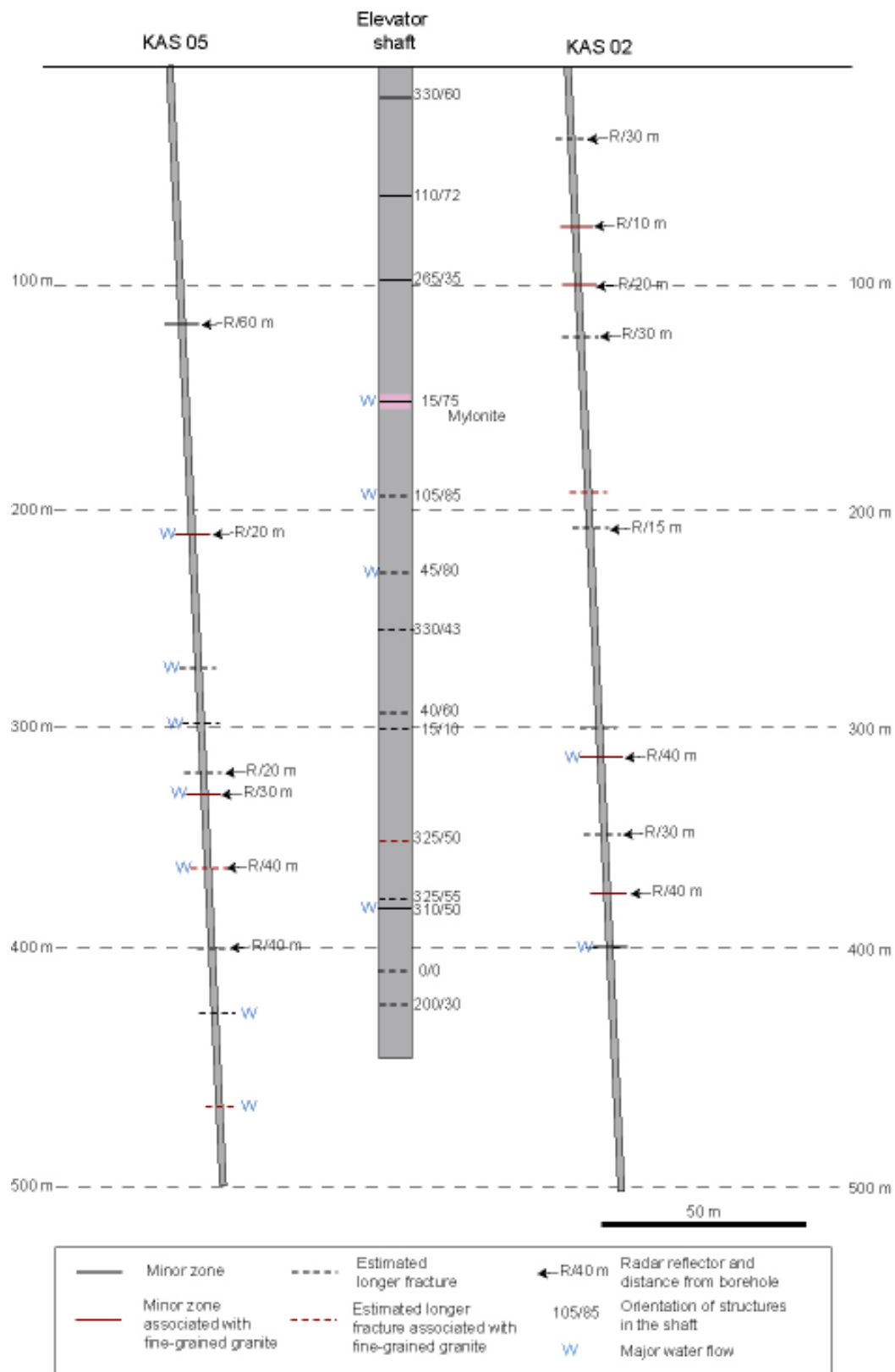
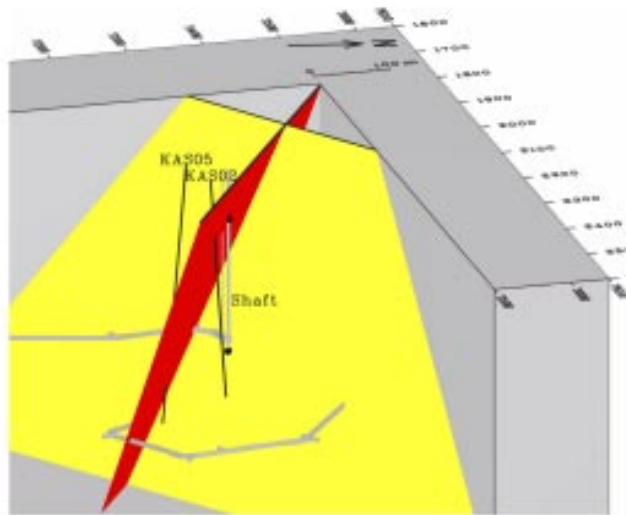


Figure A1-6. Comparison of the boreholes and shaft.



Shaft Depth (m)	Orientation (strike/dip)	Character	KAS02 Calculated intersection	Calculated angle	Reflector intersection	Reflector angle	KAS05 Calculated intersection	Calculated angle	Reflector intersection	Reflector angle
240 m	110/72	Minor zone	76 m	21°	72 m	20°	292 m	14°	316 m	28°
	045/33	Minor zone	294 m	42°	316 m	35°	340 m	31°	330 m	30°

Figure A1-7. Possible extension of structures based on radar data from the boreholes and orientation data measured in the shaft.

Identification of minor deformation zones by the analysis of borehole data including radar images

A2.1 General

Extensive fracture analyses are normally performed within the framework of the geological site investigations. Characterisations are typically focused on either large-scale deformation zones or fractures in outcrops and boreholes. Analyses of deformation zones in the interval (50 m < r < 250 m) are scarce. However, it is possible to obtain additional knowledge of fractures and deformation zones in this size range by reworking borehole data with the specific aim of recognising these zones.

One method that can be useful in attempting to estimate the length of fractures intersected by boreholes is to correlate data from BIPS, borehole radar and hydraulic difference logs with parameters in the borehole logs such as anomalous mineral clustering, hydraulic anomalies and kinematic indicators. We anticipate that some, perhaps most, of correlated anomalies would correspond to flowing structures. A correlation study in the KLX03 borehole (from Laxemar) is presented below. Borehole KLX03 was selected for this study as a borehole representative for the geological conditions in Laxemar.

A2.2 Correlation between difference flow logging results, BIPS borehole-TV and borehole radar images in KLX03

A2.2.1 Introduction

The main purpose of this study is to correlate the interpreted flowing fractures from difference flow logging with BIPS borehole TV and radar images.

The positions of flowing fractures are primarily deduced from the difference flow logging, A2-1. The geological characterisation (rock type, degree of fracturing etc) is mainly collected from the Boremap-mapping which is based on BIPS-images and the core. From the Boremap-mapping the orientation (strike/dip) and the intersection angle (α) between the fracture and borehole together with the intersection length is also obtained.

The radar measurements provide geometrical information of the fractures up to a certain distance (extension) from the borehole. Thus, an estimation of the minimum extension of the fractures into the rock mass. The interpretation process of borehole radar results in the distance (extension) from the borehole being given on only one side of the borehole. The minimum length of the fracture can probably be doubled by assuming that the structure continues on the opposite side of the borehole. The extension of radar reflectors has generally not been reported and consequently a special study has been carried out concerning the extension of radar reflectors because of their usefulness in determining the length of fractures and fracture zones. The degree of detail depends strongly on the resolution (frequency) of the radar measurements. The intersection angle (α) between the reflector and borehole together with the intersection length are important parameters in the correlation process.

The ultimate goal of this study is to detect minor deformation zones and to determine their persistence.

Interpretations of radar images from eight locations in borehole KLX03 are presented below.

A2.2.2 Explanations

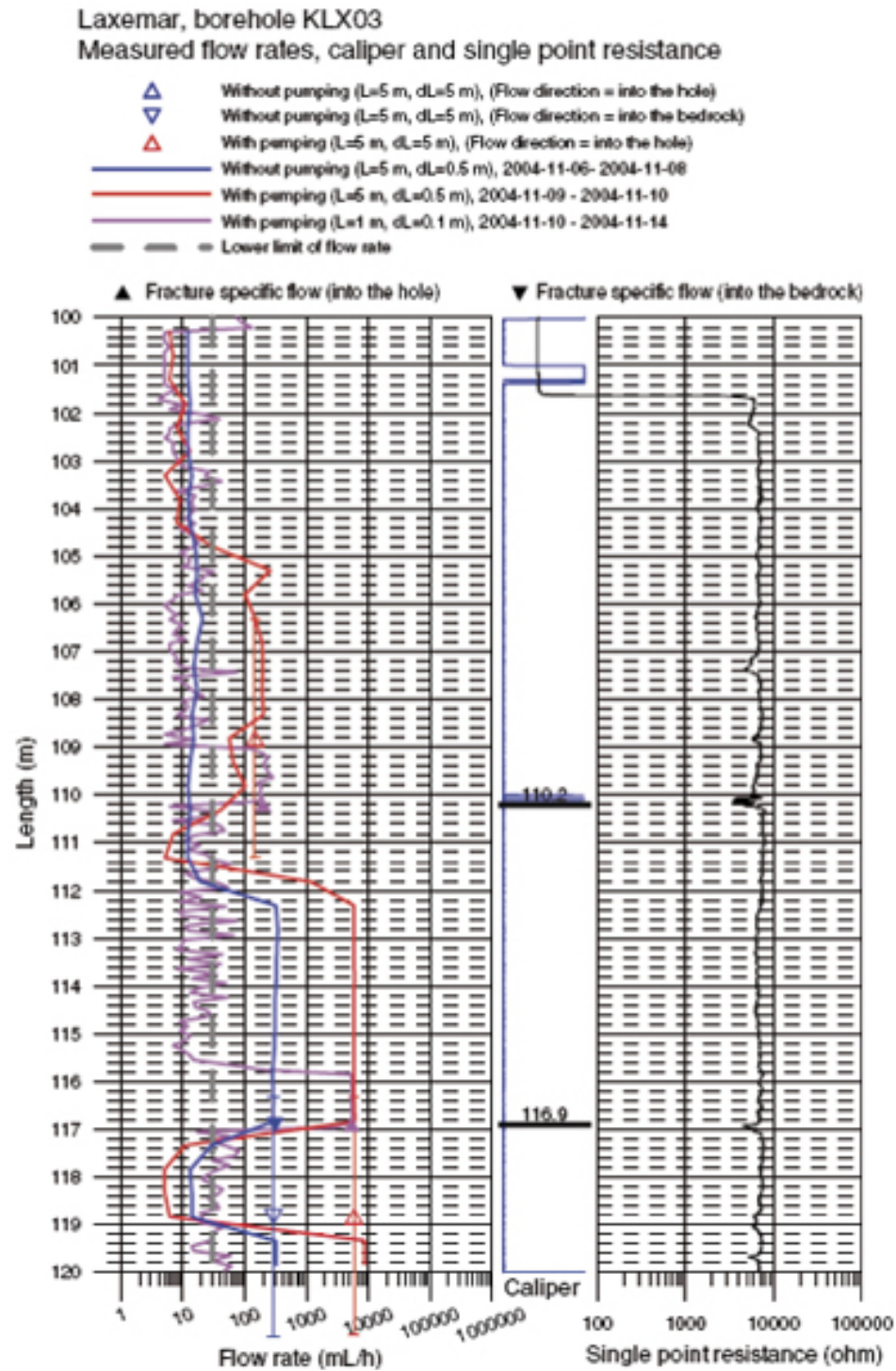


Figure A2-1. Difference flow logging and key for the borehole KLX03 from Laxemar /Rouhiainen et al. 2005/.

All presented orientations are using the right-hand rule (SKB nomenclature). The α -angle is the angle between the borehole axis and the intersecting plane.

The distance from the borehole has been interpreted from the radar map and is given in one direction from the borehole. It is assumed that the persistence of a radar interpreted structure will be the same on both sides of the borehole. For example, if a radar reflector (structure) can be traced to a distance of 12 m on the radar map, it is assumed that the structure has a minimum length of $12+12 = 24$ m.

The resolution in the dipole 250 MHz images is higher than in the 100 MHz and 20 MHz images. However, the penetration range in the dipole 250 MHz is less compared to 100 MHz and 20 MHz. The best penetration range is achieved with dipole 20 MHz, but the resolution is the lowest see A2-2. Large-scale structures (deformation zones) are best viewed in the 20 MHz images, while small-scale structures (single fractures, minor zones etc) are best viewed in the 250 MHz or 100 MHz images. The frequency of the directional antenna is 60 MHz.

From the single-hole interpretation there is one Possible Deformation Zone identified between 722–1,000 m. This part of the borehole was omitted during the correlation process.

A2.2.3 Interpretations

It is possible to carry out the correlation at eight locations in borehole KLX03 and a general view of these locations is shown in A2-4. The section within the minor deformation zone has been excluded in this correlation study.

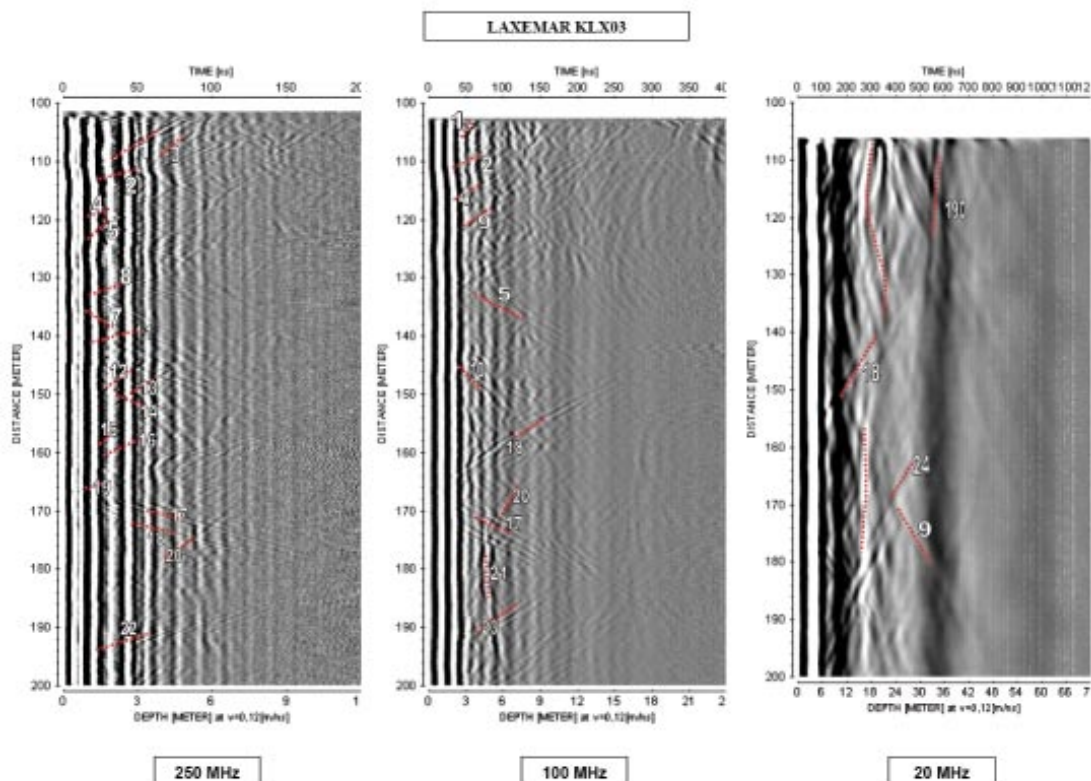


Figure A2-2. Example of radar images from dipole antenna measurements, 20 MHz, 100 MHz and 250 MHz for the borehole KLX03 from Laxemar /Gustafsson and Gustafsson 2004/.

Table 5-10. Interpretation of radar reflectors from dipole antennas 20, 100 and 250 MHz and the directional antenna in borehole KLX03.

RADINTER MODEL INFORMATION (20, 100 and 250 MHz Dipole Antennas and directional antenna)							
Site:		Oskarshamn					
Borehole name:		KLX03					
Nominal velocity (m/µs):		120.0					
Name	Intersection depth	Intersection angle	Direction to object (gravity roll)	Interpreted Dip 1	Interpreted Strike 1	Interpreted Dip 2	Interpreted Strike 2
21	16.50	2	279	89	212		
1	116.00	28					
2	117.10	64					
4	122.90	52					
5	124.10	19					
3	124.30	21					
7	127.30	30					
9	128.30	52	348	55	280		
6	130.80	19					
8	135.40	55					

Figure A2-3. Example of presentation of results from borehole radar interpretation /Gustafsson and Gustafsson 2004/.

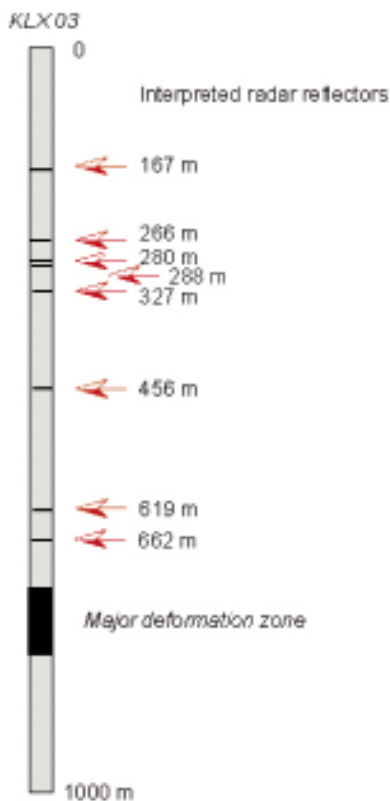


Figure A2-4. Interpreted radar reflector intervals in borehole KLX03 used for the correlation study.

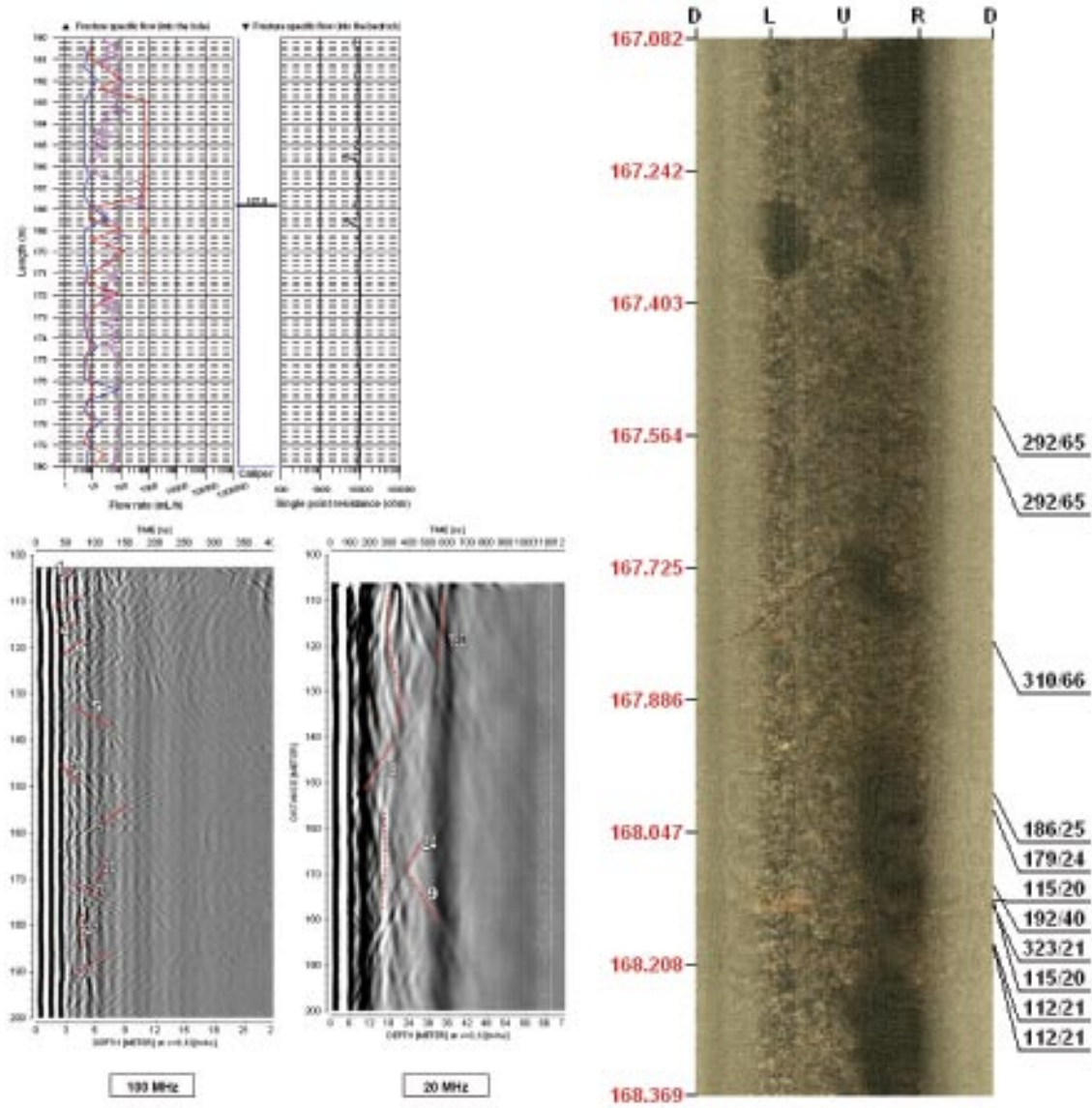


Figure A2-5. Characteristics of location KLX03-167 m.

KLX03 167 m

Difference flow:

Inflow or outflow occurs at the fracture at 167.8 m.

Borehole radar:

Reflector 18 occurs at 167.7 m. The angle α between the reflector and the borehole axis is 64° . The reflector can be observed up to a distance of 18 m away from the borehole in dipole 20 MHz and in dipole 100 MHz.

BIPS and Boremap:

A fracture orientated 310/66 occurs at 167.8 m. ($\alpha = 39^\circ$).

Host rock

Granite to quartz-monzodiorite (501044), light pinkish grey, massive, medium grained, porphyritic.

Alteration

No alteration of the host rock is observed except for local oxidation adjacent to the fracture.

Fractures

Open fracture striking 310/66 ($\alpha = 39^\circ$) with no mineral infill but with oxidized walls. The fracture is planar with rough surfaces and it has a possible aperture of 0.5 mm.

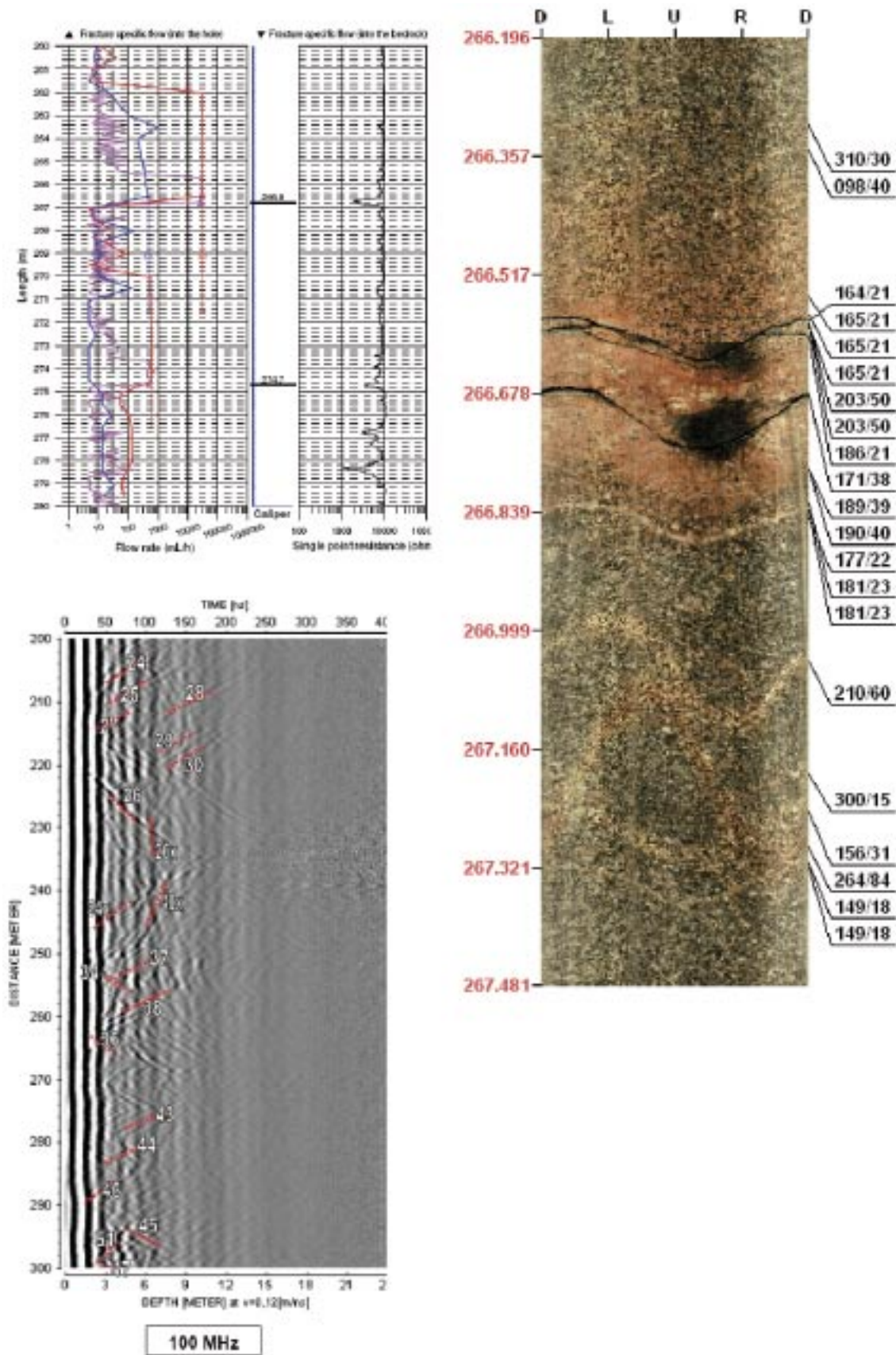


Figure A2-6. Characteristics of location KLX03-266 m.

KLX03 266 m

Difference flow:

Inflow or outflow occurs at a fracture at 266.8 m.

Borehole radar:

Reflector 38 occurs at 266.9 m. The angle α between the reflector and the borehole axis is 64° . The reflector can be observed up to a distance of 16 m away from the borehole in dipole 100 MHz.

BIPS and Boremap:

A fracture orientated 164/21 occurs at 266.6 m, ($\alpha = 57^\circ$). Best agreement with radar reflector ($\alpha = 64^\circ$).

A fracture orientated 186/21 occurs at 266.62 m, ($\alpha = 60^\circ$). Best agreement with radar reflector ($\alpha = 64^\circ$).

A fracture orientated 171/38 occurs at 266.7 m, ($\alpha = 41^\circ$).

Host rock

A 20 cm wide pegmatite vein occurs at 266.66–266.81 m in weakly oxidized granite to quartz-monzodiorite (501044). The upper contact of the pegmatite strikes 203/50 ($\alpha = 37^\circ$) and the lower contact strikes 190/40 ($\alpha = 44^\circ$). The pegmatite is light reddish green and weakly brecciated in the section 266.66–266.61 m. The breccia is epidote-sealed. A 1 cm thick fine grained granitic (511058) vein is also observed at 266.85 m striking 180/23.

Fractures

In the BIPS-image three clearly visible fractures can be observed. The first occurs at 266.60 m and strikes 164/21 ($\alpha = 57^\circ$). It is mapped as having a thickness of 0.5 mm and a probable aperture of 0.5 mm, which means that the core pieces do not fit. The fracture mineralogy is chlorite, calcite and pyrite, and the wall rock is oxidized. The fracture is planar with rough surfaces and a joint alteration number of 1.5.

The second fracture occurs at 266.62 m striking 186/21 ($\alpha = 60^\circ$). It shows the same mineralogy and oxidation as the former but it is tighter with an estimated aperture of 0.5 mm, which means that the core pieces do fit well, but the aperture cannot be estimated from BIPS. The joint alteration value is set at 1.5.

The third fracture is observed at 266.71 m striking 171/39 ($\alpha = 41^\circ$) and shows the same properties as the fractures above it, except that it is a slightly thicker, 1 mm, and has a probable aperture of 0.5 mm.

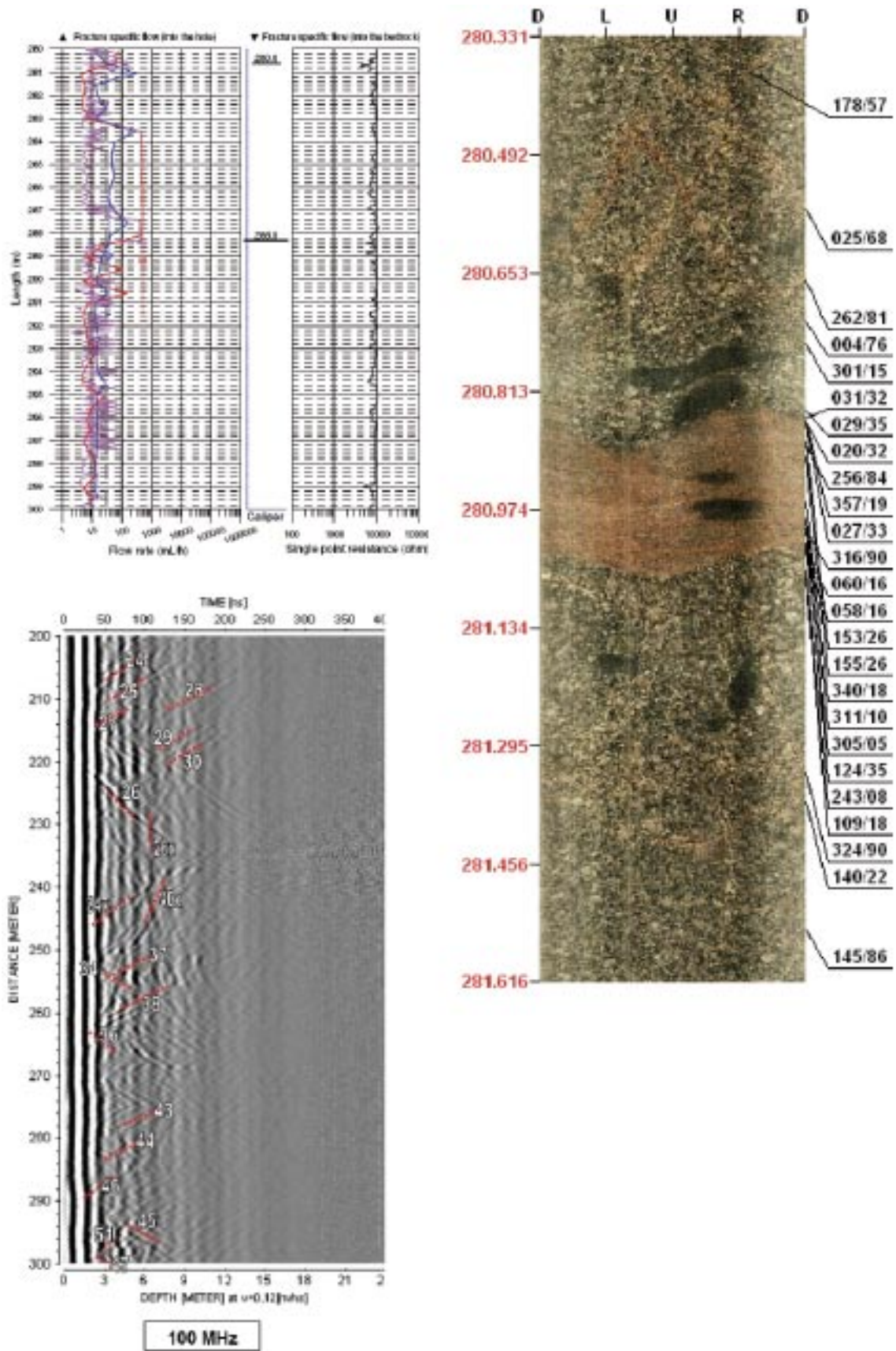


Figure A2-7. Characteristics of location KLX03-280 m.

KLX03 280 m

Difference flow:

Inflow or outflow occurs at a fracture at 280.6 m.

Borehole radar:

Reflector 43 occurs at 279.9 m. The angle α between the reflector and the borehole axis is 66° . The reflector can be observed up to a distance of 8 m away from the borehole in dipole 100 MHz.

BIPS and Boremap:

A fracture orientated 025/68 occurs at 280.57 m. ($\alpha = 22^\circ$).

A fracture orientated 029/35 occurs at 280.8 m. ($\alpha = 53^\circ$). Best agreement with radar reflector ($\alpha = 66^\circ$).

Host rock

Granite to quartz-monzodiorite (501044), light reddish grey, massive, medium grained, porphyritic. It is faintly foliated in the section 280.75–280.86 m at the contact with the granitic vein.

Vein

At 280.86–281.05 m a light brownish red fine to medium grained weakly foliated granite vein occurs (511058). The upper contact strikes 031/32 ($\alpha = 55^\circ$) and the lower strikes 060/16 ($\alpha = 63^\circ$). At the upper contact the host rock shows weak foliation.

Sealed fractures

Three very thin calcite sealed fractures are mapped within the granitic vein. Their orientation is approximately 150/30 ($\alpha = 50^\circ$ or 40°). Two sealed fractures with oxidized walls are also observed in the granitic vein and their orientation is approximately 320/10 ($\alpha = 80^\circ$).

Fractures

At 280.57 m there is a 1 mm wide, open fracture oriented 025/68 ($\alpha = 22^\circ$). It has a possible aperture of 0.5 mm and oxidized walls. It is planar with rough surfaces and it is filled with chlorite, pyrite and calcite. This fracture is cross-cut by a laumontite-calcite-sealed fracture with oxidized walls at 280.58 m. The orientation is 262/81 ($\alpha = 20^\circ$) and it is only 0.5 mm wide.

A broken fracture with no fracture minerals is observed at 280.85 m. The orientation is 029/35 ($\alpha = 53^\circ$) and it is planar with rough surfaces and a joint alteration value of 1. It has a possible aperture of 0.5 mm.

Another broken fracture is observed at 280.99 m striking 311/10 ($\alpha = 85^\circ$). It is planar with rough surfaces and is chlorite and calcite fill. It has a low joint alteration number (1.5). The thickness is 0.5 mm and it has a possible aperture of 0.5 mm. This fracture is not visible in BIPS.

An open fracture with no visible mineral fill is observed at 281.06 m striking 243/08 ($\alpha = 78^\circ$). It is planar with rough surfaces and the aperture is mapped as 0 mm (certain).

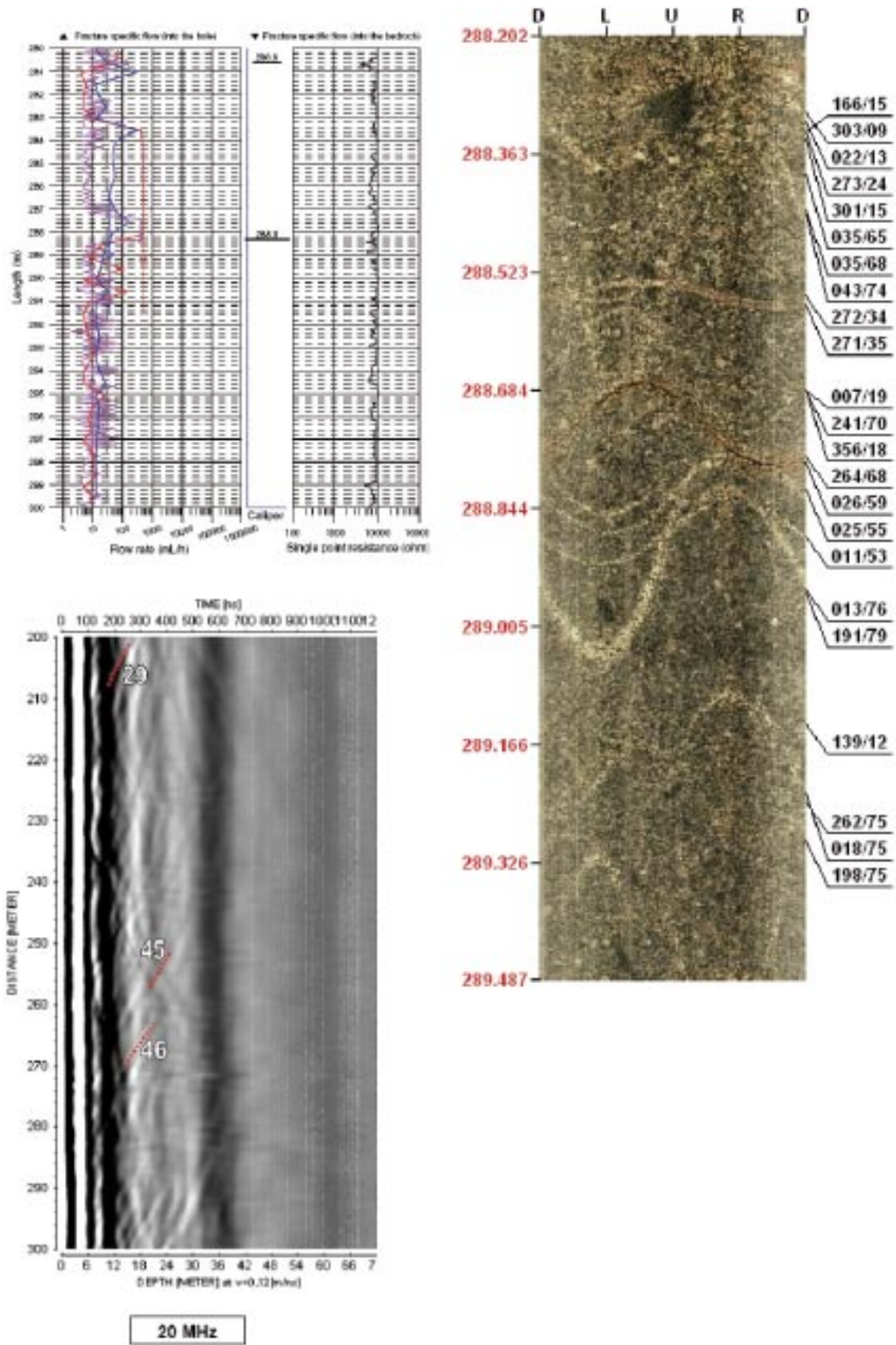


Figure A2-8. Characteristics of location KLX03-288 m.

KLX03 288 m

Difference flow:

Inflow or outflow occur at a fracture at 288.3 m.

Borehole radar:

Reflector 45 occurs at 288.7 m. The angle α between the reflector and the borehole axis is 60° . The reflector can be observed up to a distance of 30 m away from the borehole in dipole 20 MHz.

BIPS and Boremap:

A fracture orientated 022/13 occurs at 288.3 m. ($\alpha = 72^\circ$). Best agreement with α -angle for radar reflector (60°).

A fracture orientated 264/68 occurs at 288.7 m. ($\alpha = 34^\circ$).

Host rock

Granite to quartz-monzodiorite (501044), light reddish grey, massive, medium grained, porphyritic.

Fractures

Two broken fractures are mapped at 288.33 m and 288.34 m. The first one is pyrite bearing, irregular with rough surfaces and strikes roughly 022/13 ($\alpha = 72^\circ$). It has a possible aperture of 0.5 mm and a thickness of 0.5 mm. The second is interpreted as being broken during drilling or the handling of the core. It is calcite filled. No orientations are given.

Several sealed fractures occur between 288.31 and 288.50 m. Fracture mineralogy varies: calcite, chlorite, quartz or the fractures may be barren and only indicated by oxidized walls. Their orientation varies but they are mostly sub-horizontal (303/09, 273/24 and 166/15 with α -angles 84° , 77° and 63°), except for the fractures only indicated by oxidized walls which strike approximately 038/68 ($\alpha = 20^\circ$).

A chlorite-calcite filled fracture with oxidized walls occur at 288.73 m. Its orientation is 264/68 ($\alpha = 34^\circ$) and it has an aperture of 1 mm. It is planar with rough surfaces and has a joint alteration number = 1.5.

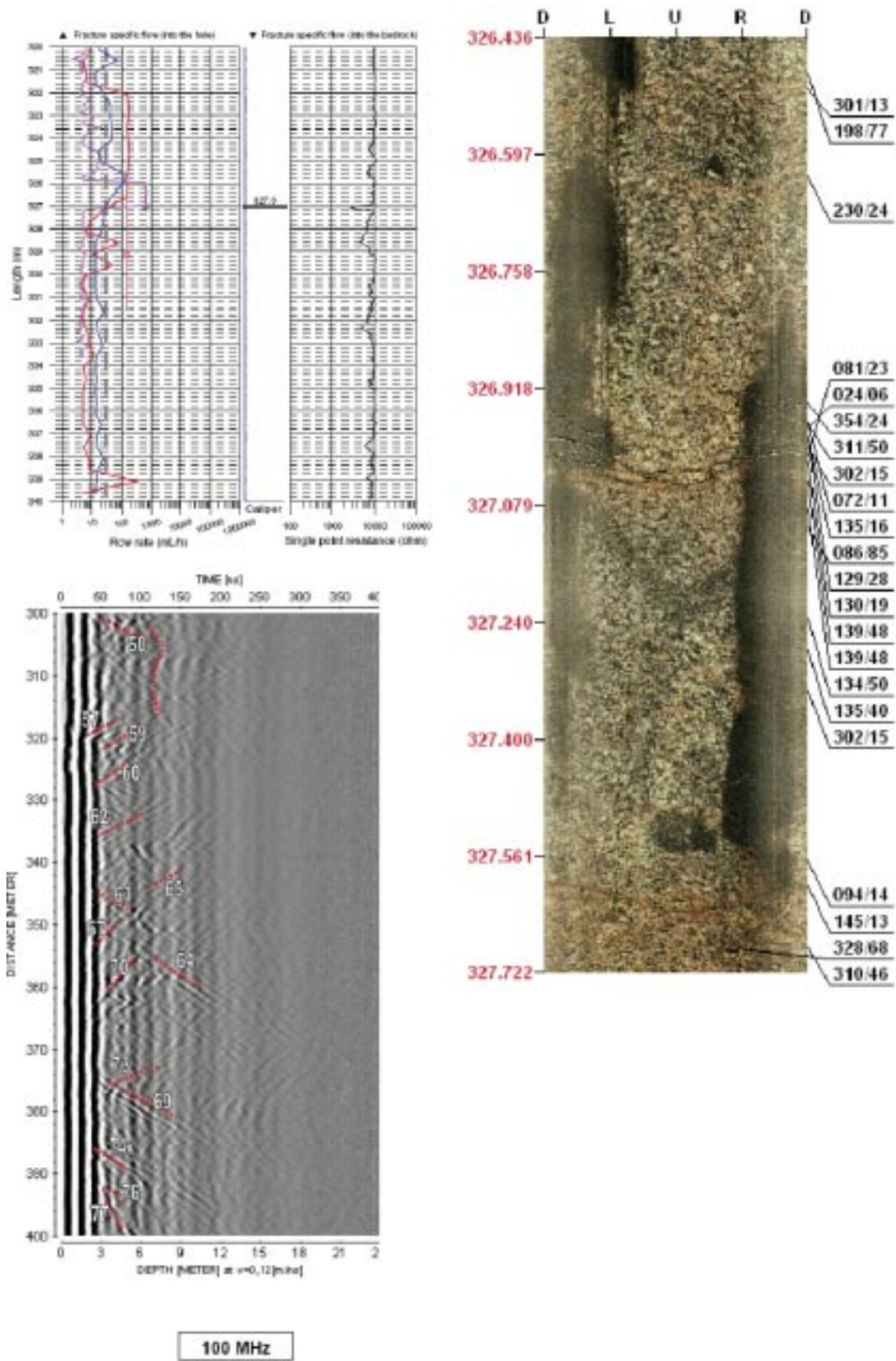


Figure A2-9. Characteristics of location KLX03-327 m.

KLX03 327 m

Difference flow:

Inflow or outflow occurs at 327.0 m.

Borehole radar:

Reflector 59 occurs at 327.5 m. The angle α between the reflector and the borehole axis is 60° . The reflector can be observed up to a distance of 12 m away from the borehole in dipole 100 MHz. Not found with directional antenna.

BIPS and Boremap:

A fracture orientated 135/16 occurs at 327.0 m. ($\alpha = 60^\circ$).

Host rock

Granite to quartz-monzodiorite (501044), light pinkish grey, massive, medium grained, porphyritic.

Alteration

The host rock is weakly saussuritized in the section 326.33–327.00 m. The saussuritization does not seem to be related to this fractured section, since it has a greater intensity higher up in the borehole.

Open fractures

Broken fractures occur at 326.94 m, 326.98 m, 327.01 m, 327.02 m, and 327.04 m. The fracture mineralogy is chlorite, calcite and pyrite. Pyrite is not observed in the fractures at 326.94 and 326.98 m. They are all sub-horizontal, planar with rough surfaces and a joint alteration number of 1.5. The measured orientations are: 354/24, 072/11, 135/16, 129/28 and 081/23 respectively and the fractures have α values of ($\alpha = 71^\circ, 67^\circ, 60^\circ, 48^\circ$ and 55°). All are mapped as having possible apertures, but as with the fractures in section 266.60–266.80 m, apertures of fractures infilled with dark chlorite are usually difficult to determine because almost black chlorite and apertures cannot be differentiated in BIPS.

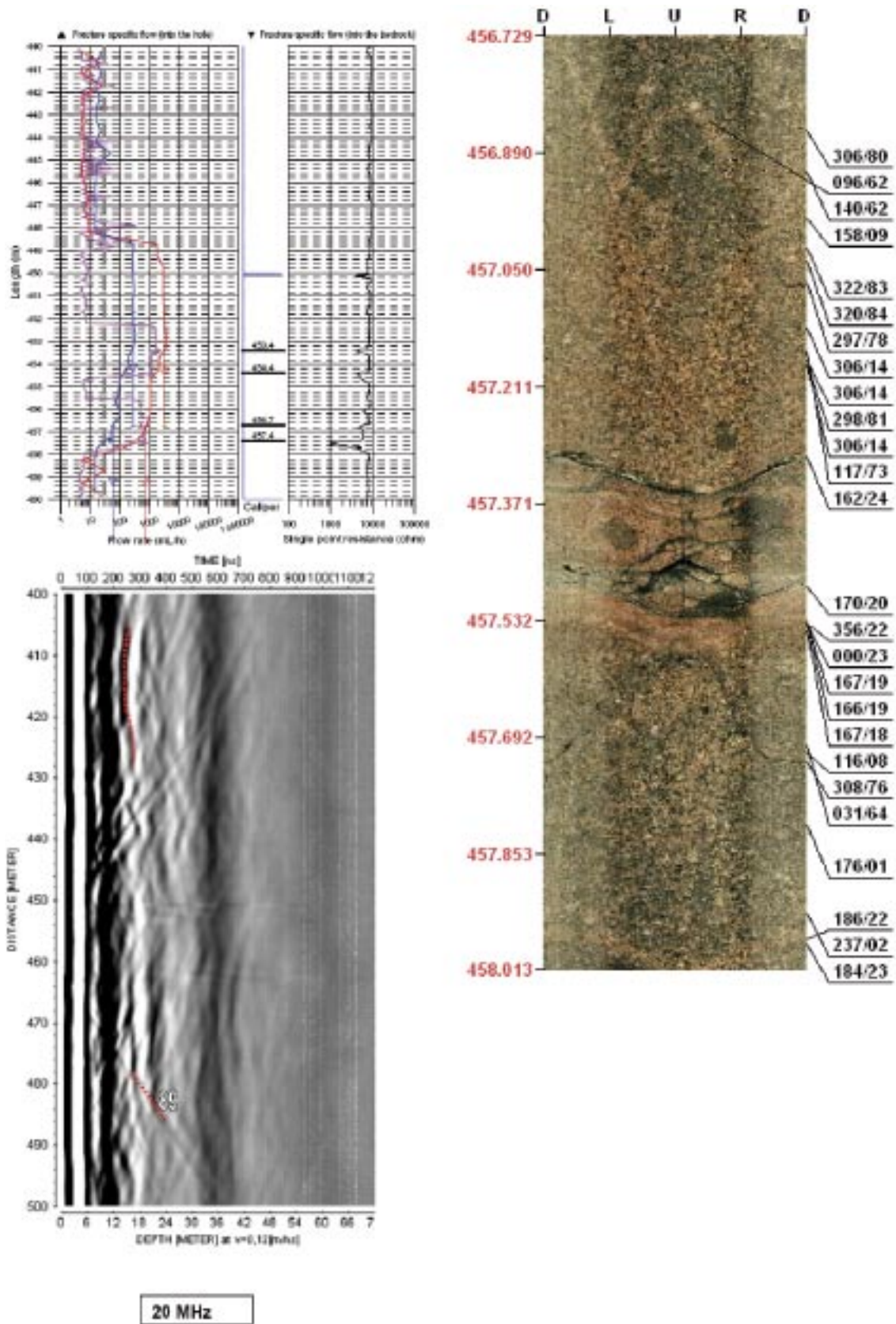


Figure A2-10. Characteristics of location KLX03-45 m.

KLX03 456 m

Difference flow:

Inflow or outflow occurs at fractures at 453.4, 454.4, 456.7 and 457.4 m.

Borehole radar:

Reflector 89 occurs at 456.5 m. The angle α between the reflector and the borehole axis is 70° . The reflector can be observed up to a distance of 35–40 m away from the borehole in dipole 20 MHz.

Reflector 90 occurs at 458.6 m. The angle α between the reflector and the borehole axis is 74° . The reflector can be observed up to a distance of 18 m away from the borehole in dipole 100 MHz.

BIPS and Boremap:

A fracture orientated 164/24 occurs at 457.3 m. ($\alpha = 54^\circ$). Acceptable agreement with radar reflector 89 ($\alpha = 70^\circ$).

A fracture orientated 170/20 occurs at 457.5 m. ($\alpha = 59^\circ$). Good agreement with radar reflector 89 ($\alpha = 70^\circ$).

Orientation of upper border of crush zone is 162/24 ($\alpha = 54^\circ$).

Host rock

Granite to quartz-monzodiorite (501044), light reddish grey, massive, medium grained, porphyritic.

Alteration

Weak oxidation between 457.181 m and 457.560 m. Above and below this weak oxidized section the rock is only faintly oxidized, indicating that this section is more oxidized than the surrounding rock.

Crush zone

At 457.332–457.537 m a crush zone is documented having a piece length of 40 mm. Mineralogy: chlorite, clay minerals, calcite and quartz, which are altered. The strike and dip of the upper border are 162.1/24.2 ($\alpha = 54^\circ$).

Sealed fracture network

A sealed fracture network is mapped at 457.130–457.538 m. The fracture mineralogy of this is as follows: calcite, pyrite, chlorite and epidote. The piece length is approximately 20 mm. No orientations are given.

Vein

A thin granitic vein (511058) occurs next to the zone at 457.507–457.556 m. It is fine- to medium grained, light reddish brown, massive and equigranular. The upper contact strikes 170.2/19.7 ($\alpha = 59^\circ$) and the lower contact strikes 166/19.3 ($\alpha = 59^\circ$).

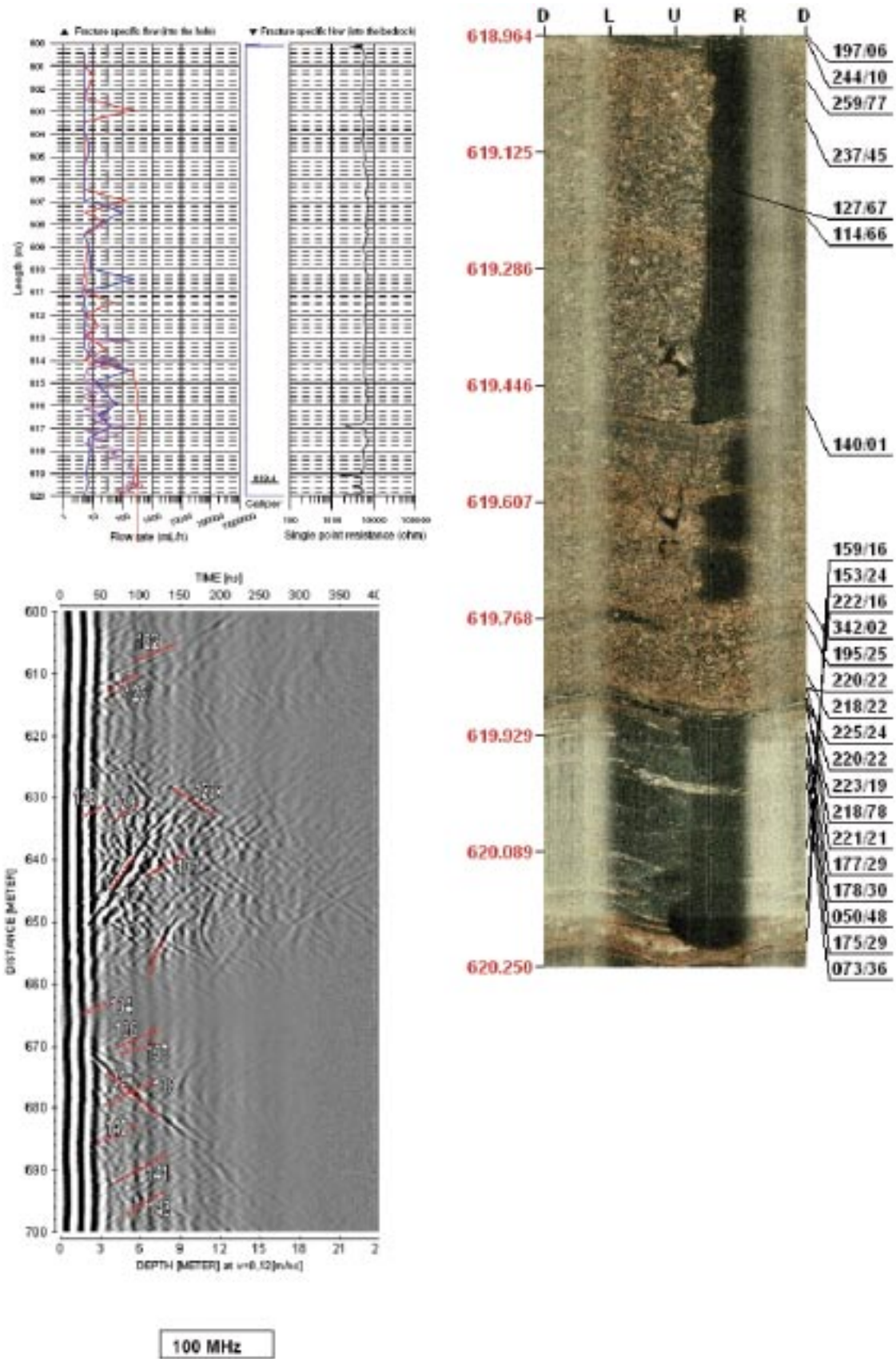


Figure A2-11a. Characteristics of location KLX03-619 m.

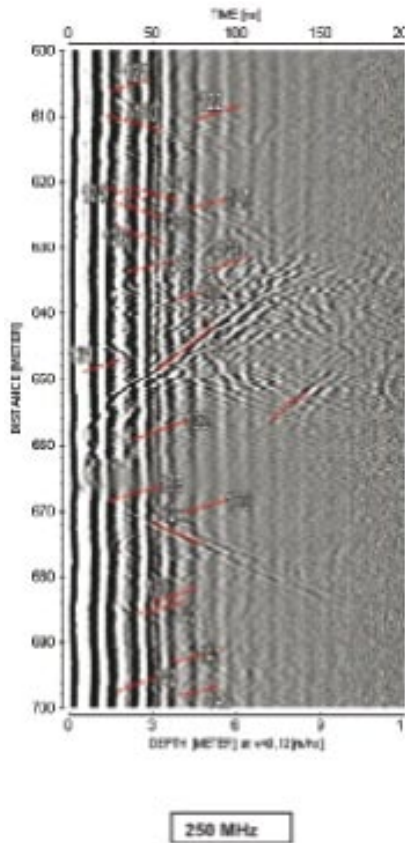


Figure A2-11b. Characteristics of location KLX03–61 m.

KLX03 619 m

Difference flow:

Inflow or outflow occurs at fractures at 619.4 m and 620.1 m.

Borehole radar:

Reflector 123 at 618.7 m, angle to borehole axis is 77° . The reflector can be observed to a distance of 12 m away from the borehole in dipole 100 MHz.

Reflector 124 at 620.0 m, angle to borehole axis is 80° . The reflector can be observed to a distance of 6 m away from the borehole in dipole 250 MHz.

BIPS and Boremap:

A fracture orientated 140/01 occurs at 619.49 m. ($\alpha = 75^\circ$). Good agreement with α for radar reflector (77° or 80°).

A fracture orientated 195/25 occurs at 619.79 m. ($\alpha = 58^\circ$).

Host rock

Hybrid rock of diorite/gabbro and Ävrögranite. It is dark pinkish grey and weakly foliated, medium grained and porphyritic.

Alteration

The host rock is faintly oxidized.

Fracture

619.49 m is a possibly open, 0.5 mm thick fracture with chlorite, calcite, pyrite and an undefined transparent medium-soft mineral which does not react with hydrochloric acid. The fracture has also oxidized walls. It strikes 140/01 ($\alpha = 75^\circ$) and is planar with a rough surface. At the contact with a mafic rock which strikes 220/22 ($\alpha = 66^\circ$), there is another open planar fracture at 619.79 m striking 195/25 ($\alpha = 58^\circ$) with chlorite and epidote and rough surfaces.

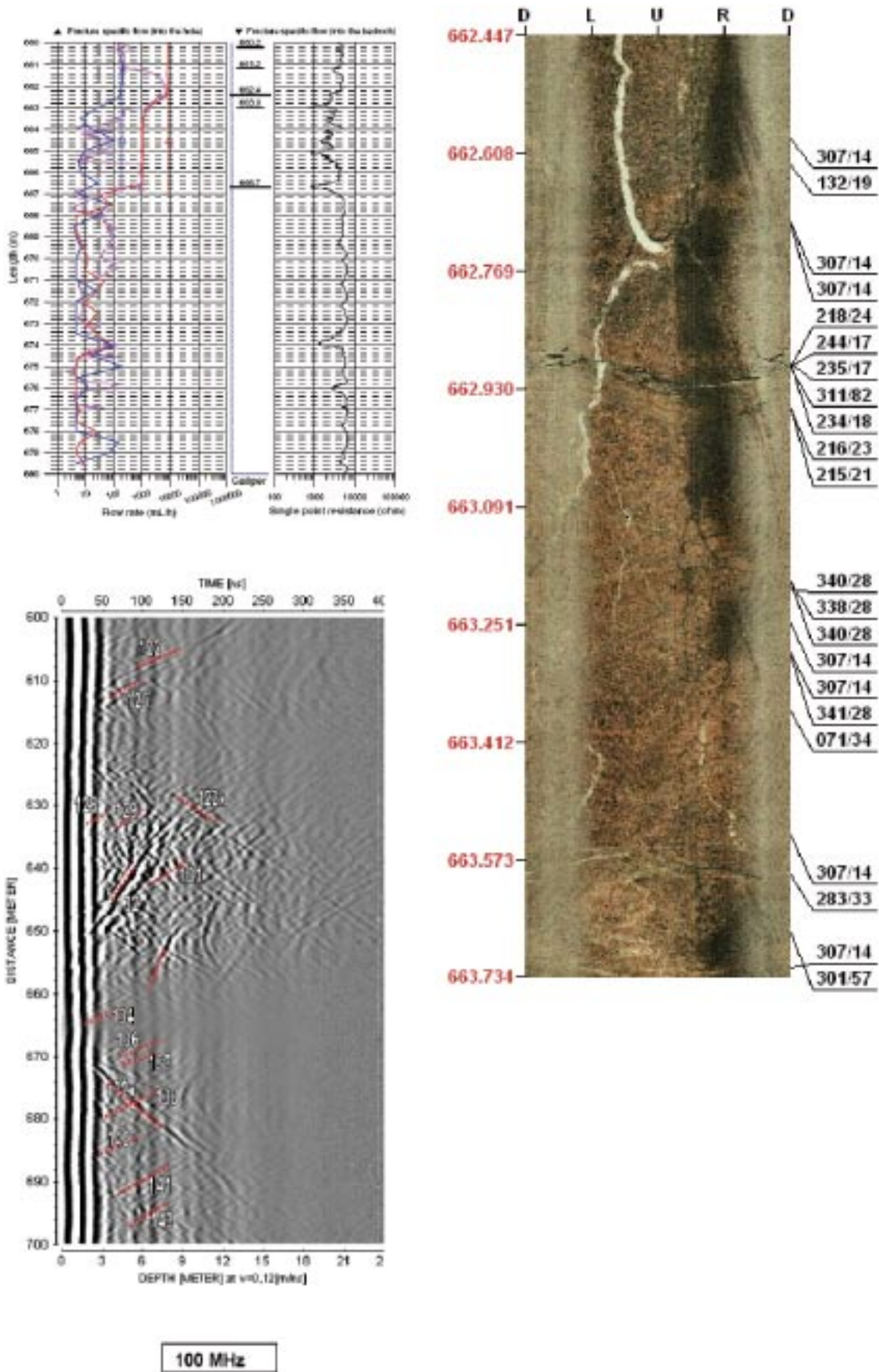


Figure A2-12a. Characteristics of location KLX03-662 m.

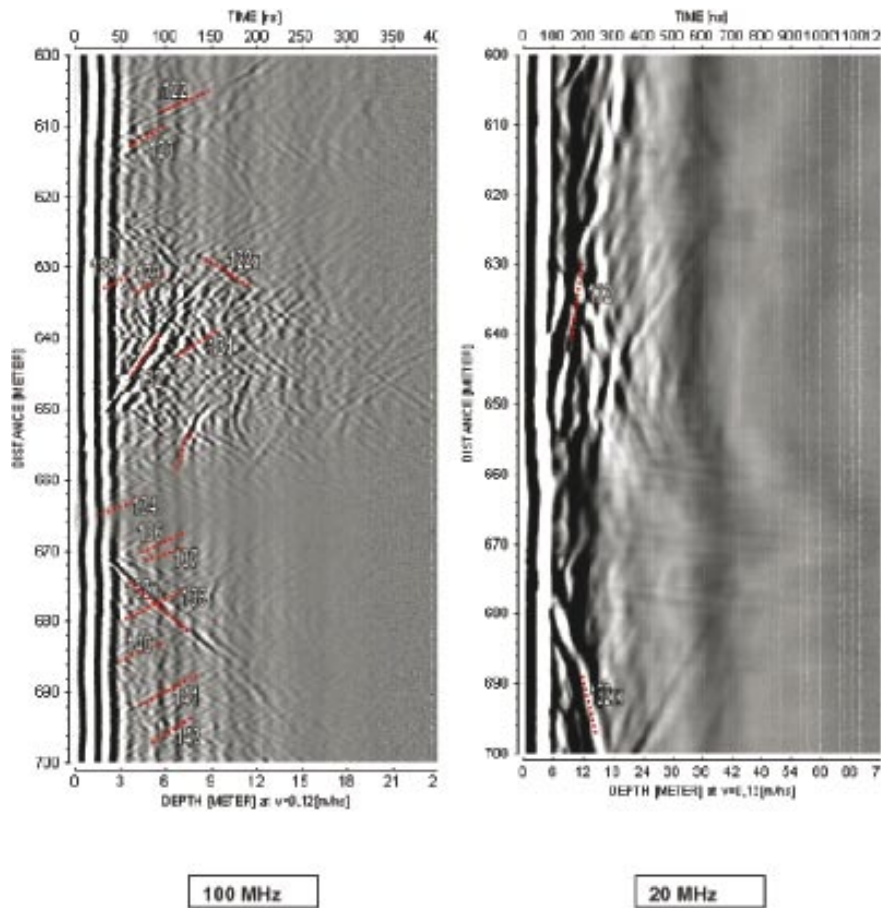


Figure A2-12b. Characteristics of location KLX03–662 m.

KLX03 662 m

Difference flow:

Inflow or outflow occurs at fractures at 662.4 m. and 663.0 m.

Borehole radar:

Reflector 133 at 661.2 m. The angle α between the reflector and the borehole axis is 62° . The reflector can be observed up to a distance of 6 m away from the borehole in dipole 250 MHz.

Reflector 132x at 662.3 m. The angle α between the reflector and the borehole axis is 31° . The reflector can be observed up to a distance of 15 m away from the borehole in dipole 100 MHz.

BIPS and Boremap:

A fracture orientated 234/18 occurs at 662.9 m. ($\alpha = 71^\circ$) and another oriented 216/23 occurs at 662.97 m. ($\alpha = 63^\circ$). Good agreement with α -angle for radar reflector 133 at 661.2 m (62°).

Host rock

A fine-grained granitic vein occurs at 662.90–662.97 m. It is light greyish red, faintly foliated and equigranular. The contacts strike approximately 225/19 ($\alpha \sim 68^\circ$). The surrounding rock is a quartz monzonite to monzodiorite (501036) which is dark grey, medium grained, equigranular and massive.

Alteration

Medium oxidation occurs between 662.71 and 663.95 m. The oxidation intensity is higher relative to the surrounding.

Deformation

A weak brittle-ductile shear zone occurs between 662.90 and 662.97 m. The orientation is 225/20 (the upper boundary strikes 234/18, $\alpha = 71^\circ$, and the lower 216/23, $\alpha = 63^\circ$).

On the lower side of the brittle-ductile shear zone the rock is weakly to faintly brecciated between 663.19 and 663.291 m and faintly brecciated from 663.54 to 663.72 m.

Fractures

Broken fractures occur at 662.905 and 662.91 m. They are clay-filled and mapped as having 0.5 mm thickness and 0.5 mm possible and 1 mm certain apertures respectively. They are both planar with rough surfaces. Their orientations are 244/17 ($\alpha = 74^\circ$) and 219/24 ($\alpha = 63^\circ$) respectively.

Calcite filled fractures that are interpreted as having been broken during drilling or core handling occur at 662.81, 663.19 and 663.29 m and their orientations are 311/82, 338/28 and 341/28 respectively ($\alpha = 22^\circ$, 72° and 72°). The first also contains chlorite and pyrite.

A2.2.4 Conclusion

- A useful method of identifying water and clay filled fractures and fracture zones, and of estimating their extension and orientation is to correlate data from BIPS, borehole radar and hydraulic difference logs with parameters in the borehole logs.
- Correlation between results from difference flow meter, BIPS, SPR-log and borehole radar with 20, 100 and 250 MHz antenna has been shown to give valuable information concerning the characterisation of Minor Deformation Zones. The radar technique can be used to determine how far away from the borehole the fracture extends. It can normally trace fractures over distances between 10–40 m away from the borehole and under favourable conditions up to 60 m away.
- It should be noted that borehole radar may give high amount of reflectors, which are not related to any fractures, i.e. they can be related to lithological contacts, veins, dykes etc. However, by correlating data from BIPS, borehole radar and hydraulic difference logs, such reflectors can be excluded.